N° d'ordre 2013ISAL0102
Année 2013

Thèse

Vertical-flow constructed wetlands for the treatment of wastewater and stormwater from combined sewer systems

Traitement des eaux résiduaires de temps sec et temps de pluie en réseau unitaire par filtres plantés de roseaux

Présentée devant
L'Institut National des Sciences Appliquées de Lyon

Pour obtenir
Le grade de docteur

Formation doctorale
Génie Civil

École doctorale
Mécanique, Energétique, Génie Civil, Acoustique (MEGA)

Par
José Luis ARIAS LOPEZ

Soutenue le 30 septembre 2013 devant la Commission d'examen

Jury

Jean-Luc BERTRAND-KRAJEWSKI	Professeur	Directeur de thèse
Pascal MOLLE	Docteur	Co-directeur de thèse
Sylvie BARRAUD	Professeur	Présidente
Joan GARCIA SERRANO	Professeur	Rapporteur
Ghassan CHEBBO	Professeur	Rapporteur
Fabio MASI	Docteur	Examinateur
Florent CHAZARENC	Docteur - HDR	Examinateur

Laboratoire de Génie Civil et d'Ingénierie Environnementale (LGCIE)

N° d'ordre 2013ISAL0102
Année 2013

Thèse

Vertical-flow constructed wetlands for the treatment of wastewater and stormwater from combined sewer systems

Traitement des eaux résiduaires de temps sec et temps de pluie en réseau unitaire par filtres plantés de roseaux

Présentée devant
L'Institut National des Sciences Appliquées de Lyon

Pour obtenir
Le grade de docteur

Formation doctorale
Génie Civil

École doctorale
Mécanique, Energétique, Génie Civil, Acoustique (MEGA)

Par
José Luis ARIAS LOPEZ

Soutenue le 30 septembre 2013 devant la Commission d'examen

Jury

Jean-Luc BERTRAND-KRAJEWSKI	Professeur	Directeur de thèse
Pascal MOLLE	Docteur	Co-directeur de thèse
Sylvie BARRAUD	Professeur	Présidente
Joan GARCIA SERRANO	Professeur	Rapporteur
Ghassan CHEBBO	Professeur	Rapporteur
Fabio MASI	Docteur	Examinateur
Florent CHAZARENC	Docteur - HDR	Examinateur

Institut national de Recherche en Sciences et Technologies pour l'Environnement et l'Agriculture (IRSTEA)

Laboratoire de Génie Civil et d'Ingénierie Environnementale (LGCIE)

SIGLE	ECOLE DOCTORALE	NOM ET COORDONNEES DU RESPONSABLE
CHIMIE	**CHIMIE DE LYON** **http://www.edchimie-lyon.fr** Insa : R. GOURDON	M. Jean Marc LANCELIN Université de Lyon – Collège Doctoral Bât ESCPE 43 bd du 11 novembre 1918 69622 VILLEURBANNE Cedex Tél : 04.72.43 13 95 **directeur@edchimie-lyon.fr**
E.E.A.	ELECTRONIQUE, ELECTROTECHNIQUE, AUTOMATIQUE http://edeea.ec-lyon.fr Secrétariat : M.C. HAVGOUDOUKIAN eea@ec-lyon.fr	M. Gérard SCORLETTI Ecole Centrale de Lyon 36 avenue Guy de Collongue 69134 ECULLY Tél : 04.72.18 60 97 Fax : 04 78 43 37 17 **Gerard.scorletti@ec-lyon.fr**
E2M2	EVOLUTION, ECOSYSTEME, MICROBIOLOGIE, MODELISATION http://e2m2.universite-lyon.fr **Insa : H. CHARLES**	Mme Gudrun BORNETTE CNRS UMR 5023 LEHNA Université Claude Bernard Lyon 1 Bât Forel 43 bd du 11 novembre 1918 69622 VILLEURBANNE Cédex Tél : 04.72.43.12.94 **e2m2@biomserv.univ-lyon1.fr**
EDISS	**INTERDISCIPLINAIRE SCIENCES-SANTE** **http://ww2.ibcp.fr/ediss** Sec : Safia AIT CHALAL Insa : M. LAGARDE	M. Didier REVEL Hôpital Louis Pradel Bâtiment Central 28 Avenue Doyen Lépine 69677 BRON Tél : 04.72.68 49 09 Fax :04 72 35 49 16 **Didier.revel@creatis.uni-lyon1.fr**
INFOMATHS	INFORMATIQUE ET MATHEMATIQUES http://infomaths.univ-lyon1.fr	M. Johannes KELLENDONK Université Claude Bernard Lyon 1 LIRIS - INFOMATHS Bâtiment Nautibus 43 bd du 11 novembre 1918 69622 VILLEURBANNE Cedex Tél : 04.72. 43.19.05 Fax 04 72 43 13 10 **infomaths@bat710.univ-lyon1.fr**
Matériaux	**MATERIAUX DE LYON**	M. Jean-Yves BUFFIERE Secrétaire : Mériem LABOUNE INSA de Lyon École Doctorale Matériaux Mériem LABOUNE Bâtiment Antoine de Saint-Exupéry 25bis Avenue Jean Capelle 69621 VILLEURBANNE Tel : 04 72 43 71 70 Fax : 04 72 43 72 37 **ed.materiaux@insa-lyon.fr**
MEGA	**MECANIQUE, ENERGETIQUE, GENIE CIVIL, ACOUSTIQUE (ED n°162)**	M. Philippe BOISSE Secrétaire : Mériem LABOUNE Adresse : INSA de Lyon École Doctorale MEGA Mériem LABOUNE Bâtiment Antoine de Saint-Exupéry 25bis Avenue Jean Capelle 69621 VILLEURBANNE Tel : 04 72 43 71 70 Fax : 04 72 43 72 37 **mega@insa-lyon.fr** Site web : **http://www.ed-mega.com**
ScSo	**ScSo*** M. OBADIA Lionel	M. OBADIA Lionel Université Lyon 2

A mis viejos

Remerciements

La réalisation de cette thèse CIFRE a été possible grâce à la collaboration de l'IRSTEA de Lyon, l'INSA de Lyon, la société SAFEGE et SCIRPE, l'Agence de l'eau Rhône Méditerranée Corse et la Communauté de Communes du Pays de Gex. Je leur adresse toute ma reconnaissance.

First of all, I would like to take this opportunity to thank Mr. GARCIA and Mr. CHEBBO for accepting to be the reporters of this thesis. Also, I would like to thank Mr. MASI, Mr. CHAZARENC and Mrs. BARRAUD who agreed to be part of the jury.

Toute ma gratitude, ensuite, envers mon Directeur de thèse, M. Pascal MOLLE, personne très humaine, d'une bonne humeur et d'une patience précieuses.. Il a su partager ses connaissances avec moi. Sans lui ce travail n'aurait pas été possible. Pascal, je pense que tu représentes vraiment l'esprit de notre équipe « Epuration » à l'IRSTEA : qualités scientifiques et personnelles. J'y ai reçu un accueil chaleureux et je n'aurai pas pu trouver mieux.

Je voudrais également remercier M. Jean-Luc BERTRAND-KRAJEWSKI, mon deuxième Directeur de thèse, pour ses nombreux conseils scientifiques, qui ont réellement enrichi ce travail de recherche.

Au sein de la super équipe Epuration de l'IRSTEA, je souhaite mentionner plus spécialement M. Nicolas FORQUET : un autre atout de l'équipe, intelligent, humble, rigolo et toujours prêt à donner un coup de main. Je te remercie Nico pour ton aide précieuse avec le modèle simplifié, les TDR, sonde s::can, etc. Merci de m'avoir épargné de nombreuses migraines.

Je tiens aussi remercier Olivier GARCIA pour son enthousiasme et sa bonne/mauvaise humeur pendant le travail de terrain à Challex Plage ainsi que pour sa disponibilité y compris les week-ends, sous la neige, la pluie, la chaleur extrême. Avoir travaillé avec toi a toujours été un plaisir.

Je remercie aussi Patrice VERNAY pour les trajets vers Challex avec le son de la radio à fond, son aide sur le terrain et sa bonne humeur. Merci à M. Jean-Luc BERCKERT pour sa disponibilité et son aide avec l'installation de l'équipement métrologique à Challex. Merci aussi à M. Clément CRETOLLIER et M. Jean-Marc PERRET pour leur aide et leurs conseils lors du travail de terrain.

Merci à l'équipe CANOE du laboratoire LGCIE pour son aide mieux comprendre ce logiciel.
Merci au laboratoire de chimie de l'IRSTEA pour sa disponibilité, malgré la difficulté de programmer des campagnes de temps de pluie, quand on ne sait pas exactement quand elles vont arriver. Un grand merci au secrétariat de l'IRSTEA pour son aide dans la logistique de plusieurs comités de pilotages, congrès etc., plus particulièrement Noëlle MORAND et Edwige NAPPEY.

Merci aux stagiaires qui m'ont aidé avec ce travail de recherche, Amélie DASRE et une mention spéciale à Sandrine PAPIAS, pour son aide avec le travail de terrain et la sonde s::can.

Merci aussi à mes "potos" de l'équipe : Alex, mon "coloc" de bureau pendant ses années de thèse marquées par nos cris de défoulement, nos chants spontanés, nos conversations théolo-

socio-presspeoplelogiques, et surtout, merci de m’avoir initié à la pétanque. Merci à Ugolin pour son amitié, Maxou et ses chiots, Claudia (Chipolatas avec les potos !), Juanito Nuage, Anianette (et son rire aigu mais contagieux eh), JuJu-bling-bling-Fournel, Paul Picole, Stéph, Claire, Julie, Daniel, Chochotte et le reste de l’équipe. Je vous remercie tous pour les séances pétanque à la Place Colbert jusqu’à minuit, les apéros, les restos chinois, les barbeucs, les séances ping-pong, baby-foot, bref, pour la super bonne ambiance qu’on a dans cette équipe.

Enfin, merci aussi à mes amis en dehors du boulot, Carolinette pour son aide et sa patience pour supporter mes plaintes, Seb, Marinette, Lores, Flor, Chavi, Pample, Mirims, Nati, Pupu… qui m’ont aidé à me changer les idées quand j’en avais besoin par de nombreuses sorties, week-ends, diners. Merci les gars d’avoir été là.

Y el agradecimiento más importante… a mi familia, en especial a ustedes mis viejitos, que siempre han estado a mi lado, apoyándome, regañándome, queriéndome; nunca imaginé que al salir de casa llegaría aquí.

Résumé étendu

Introduction

La filière de filtres plantés de roseaux à écoulement vertical pour le traitement des eaux usées domestiques est relativement bien développée en France (plus de 2500 stations à ce jour) et permet un traitement poussé de la matière carbonée et la nitrification. Bien que dimensionnée initialement pour des réseaux séparatifs d'eaux usées, les travaux menés par Molle (2003) ont montré la robustesse de cette filière pour accepter des surcharges hydrauliques importantes en temps de pluie. Des conditions limites hydrauliques de temps de pluie ont été alors établies et reprises dans le guide « Macrophytes » (2005). Ces nouvelles bases de dimensionnement permettent déjà aux collectivités des économies non négligeables en termes de gestion de temps de pluie en réseau unitaire (sur-dimensionnement de la station d'épuration et gestion séparée des eaux pluviales non nécessaires). Cependant ces limites ne sont pas optimisées et demandent à être validées sur une station spécialement conçue dans cet objectif. Afin de généraliser le dimensionnement de ce type de station aux réseaux unitaires, il convient également d'étudier l'influence du contexte climatique et des caractéristiques du réseau sur les flux à traiter.

Dans ce contexte, une station d'épuration (STEP) de 2000 EH située à Challex (01) a été mise en eau en avril 2010. Son dimensionnement a été conçu de manière à intégrer les eaux de temps de pluie dans des proportions adaptables suivant l'évolution de l'étude. Une approche particulière a été mise en œuvre dans son dimensionnement de manière à optimiser le travail de recherche (changement possible de nombreux paramètres de fonctionnement) et le suivi métrologique.

Les principales questions sur l'acceptation des surcharges hydrauliques (SH) par les filtres plantés de roseaux à écoulement vertical (FPR-V) qui nous ont intéressée sont les suivantes :

1. Quel est le temps de noyage maximal qui peut être accepté sans mettre en péril le bon fonctionnement biologique des FPR-V ?
2. Quels sont les contextes locaux (coefficient d'imperméabilisation du bassin versant, pente du réseau...) qui influencent le plus l'acceptation des SH par les FPR-V ?
3. Quel type de climat est le plus problématique pour l'acceptation des SH par les FPR-V ?
4. Quelles sont les conceptions de FPR-V les plus adaptées pour les SH ?

Par conséquent, pour tenter de répondre aux questions précédentes, notre étude vise à :

1. Développer un modèle hydraulique simplifié, simulant le comportement hydraulique du premier étage d'un FPR-V (qui est le plus limitant hydrauliquement). Le modèle se focalise sur le temps de noyage et analyse l'impact des saisons, jours d'alimentation et charges hydrauliques sur les taux d'infiltration.
2. Relier l'hydraulique du FPR-V aux traitements épuratoires, par l'établissement de relations temps-de-noyage/dynamique-de-nitrification et par conséquent, fixer des seuils de sécurité (alertes des dysfonctionnements).

3. Déterminer l'impact du contexte local (le type de climat, les saisons, les caractéristiques du réseau d'assainissement et du bassin versant) sur les performances du FPR-V.
4. Fournir des indices pour adapter les FPR-V à traiter de manière optimale les surcharges hydrauliques en fonction du contexte local.

Comme objectif principal, cette étude cherche à améliorer les connaissances sur l'acceptation des surcharges hydrauliques par le système français du FPR-V, sans compromettre ses performances de traitement. En outre, le projet prévoit d'assister les concepteurs des FPR-V avec un modèle hydraulique facile à gérer, qui pourrait les aider à prendre des décisions pour le dimensionnement des nouveaux FPR-V, en fonction du contexte local spécifique.

Bibliographie

Il existe deux types principaux de filtres plantés de macrophytes à écoulement souterrain, selon les critères hydrologiques, ils sont classés comme suit :

1. Filtre planté à **écoulement horizontal**, cette filière est caractérisée par un flux horizontal et saturé traversant le filtre à gravier.

2. Filtre planté à **écoulement vertical**, composée de gravier ou de sable, comme matériel filtrant. L'eau est répartie de manière homogène à la surface et s'écoule verticalement dans un milieu non saturé.

Les premiers filtres plantés de roseaux (FPR) construits en France ont été installés à Saint Bohaire par le Cemagref (Lienard 1987). La filière a connu une expansion dans le pays pendant les années 1990, depuis ils ont acquis une bonne réputation pour les petites collectivités (Molle *et al.* 2005a). Le système est également populaire en raison de ses besoins et coûts d'exploitation faibles, qui les rendent attractifs pour les petites collectivités, où seuls les coûts d'investissement sont subventionnés.

Filtre planté de roseaux à écoulement vertical

Le filtre étant non saturé la plupart du temps, l'épuration est réalisée dans un milieu aérobie, grâce à la biomasse qui se développe dans le milieu poreux. Le filtre est une excavation étanchée par une geomembrane imperméable, remplie de différents matériaux (sable ou gravier) de granulométries différentes, qui augmentent avec la profondeur. Dans la couche la plus profonde, des tuyaux de drainage reliés à l'atmosphère sont installés, afin de promouvoir l'aération en profondeur du système (Cooper *et al.* 1996). Le système a été développé pour fournir de hauts niveau de transfert d'oxygène par convection, (dû à l'alimentation par bâchées) et par diffusion, permettant la nitrification.

Au niveau international, le système est usuellement alimenté par des eaux usées prétraitées par décantation (Brix & Arias 2005), et par conséquent le matériau filtrant est composé de sable (Brix 1994a). Cependant, en France le système a été adapté pour traiter des eaux usées brutes (Lienard 1987, 1990), en montrant de très bonnes performances épuratoires. Dans cette adaptation un deuxième étage est nécessaire pour obtenir de meilleurs rendements de dégradation de la matière organique et de nitrification (Molle *et al.* 2005a).

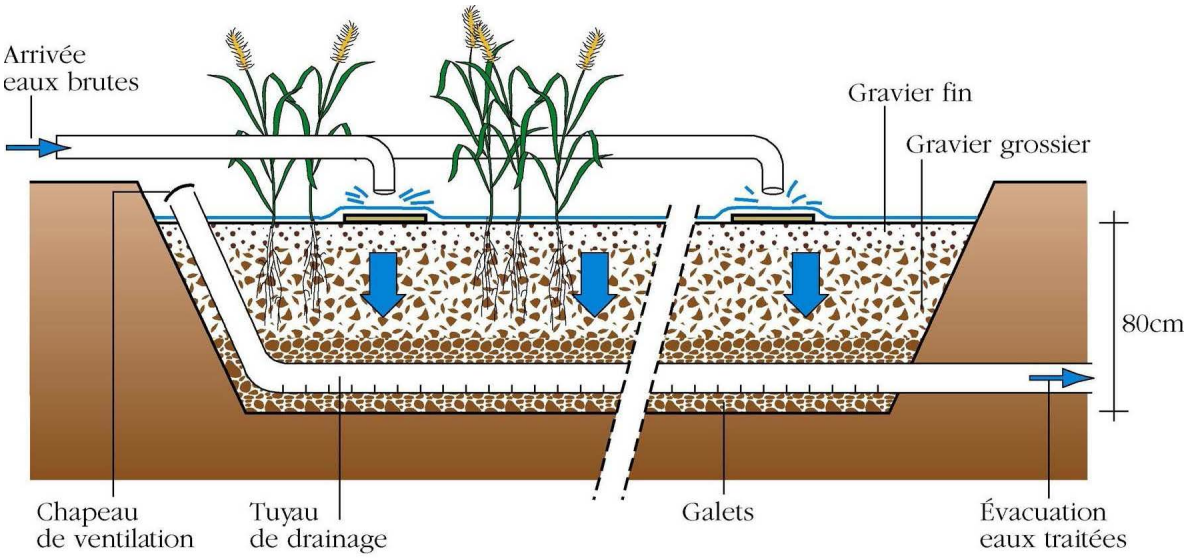

Figure 1: Illustration schématique transversale d'un filtre planté de roseaux à écoulement vertical (Iwema *et al.* 2005)

Le système français est composé de 2 étages verticaux, dont le premier possède 3 cellules en parallèle qui sont alimentées alternativement pendant 3.5 jours (1 semaine de repos) et le deuxième étage possède 2 cellules en parallèle, alimentées aussi pendant 3.5 jours (avec 3.5 jours de repos), comme le recommande l'état de l'art français (Molle *et al.* 2005a). Ces périodes d'alternance sont essentiels pour (i) contrôler la croissance de la biomasse dans le milieu poreux, (ii) minimiser le colmatage dû à la minéralisation des dépôts organiques provoqués par les matières en suspension (MES) contenues dans les eaux usées brutes, qui sont retenues à la surface du filtre du première étage (Lienard 1990), ainsi que pour (iii) maintenir des conditions aérobies dans le filtre. Alors que le premier étage est plutôt dédié à un traitement élevé des MES et de la matière carbonée (et seulement 50 à 60 % de la nitrification), le deuxième étage vient affiner les rendements obtenus et complète la nitrification.

Traitement des périodes de temps sec et de temps de pluie par les filtres plantés de roseaux

Pendant les périodes de temps sec, le système français montre des rendements épuratoires de l'ordre de 95 %, 91 % et >85 % pour les MES, la demande chimique en oxygène (DCO) et l'azote Kjeldahl (NK) respectivement, à charge nominale, selon une étude menée sur plus de 80 filtres plantés de roseaux à écoulement vertical en France (Molle *et al.* 2005a). Si le traitement des MES et DCO semble stable, on observe une décroissance de la nitrification avec l'augmentation de la charge en NK. Cela est dû à plusieurs facteurs. En premier lieu la forme principalement dissoute (environ 70% sous forme de NH_4-N) rend l'azote ammoniacal fortement dépendant des écoulements et notamment des passages préférentiels, et d'autre part une proportion non négligeable de l'azote ammoniacal est adsorbée sur la matière organique puis nitrifiée entre les bâchées et en période de repos. En conséquence de quoi, l'augmentation de la charge induit une proportion plus importante d'azote qui passe directement en sortie ainsi qu'une saturation accélérée des sites d'adsorption. Ces deux facteurs font que l'augmentation de la charge en NK tend à réduire les performances de nitrification. En dessous de charges de 10 et 15 NK $g.m^{-2}.j^{-1}$ pour le premier et deuxième étage

les rendements sont presque complets et diminuent progressivement avec l'augmentation de charge (Molle et al., 2005, 2008).

Les charges polluantes en période de temps de pluie sont d'une grande variabilité, selon les caractéristiques propres des pluies (intensité, durée), du bassin versant, de la pollution du sol et de la pollution atmosphérique locale, de la période de temps sec avant la pluie, etc. L'ensemble de ces facteurs rend très complexe la caractérisation des eaux de temps de pluie. Parmi les impacts sur le filtre, dus aux caractéristiques des eaux de pluie et des variations de débit, on peut mentionner que les événements pluvieux :

- Induisent un plus grand nombre de bâchées et, par conséquent, un temps de séjour plus court de l'eau dans le réacteur biologique, ainsi qu'une diminution des transferts d'oxygène par diffusion.
- Apportent sur le filtre une charge plus importante de MES, ce qui peut favoriser le colmatage à long terme.

Compte tenu de la sensibilité de la nitrification aux conditions d'oxygénation et de l'hydraulique du système, elle est un bon paramètre pour évaluer les limites épuratoires des filtre par temps de pluie. L'enjeu sera de trouver l'optimum entre les capacités hydrauliques des filtres et la limite d'oxygénation qui affecte la nitrification. En effet, si de fortes surcharges hydrauliques sont physiquement acceptables, un noyage prolongé de la surface du filtre peut être défavorable à l'activité biologique, en raison d'un manque de renouvellement de l'oxygène.

Forquet *et al.* (2009) affirment que le renouvellement convectif de l'oxygène dans un filtre à écoulement vertical est dépendant de la charge hydraulique (CH) et du nombre de bâchées par jour. Leur étude montre qu'au-dessus d'une valeur seuil (jusqu'à 170 $gO2/m^2$/jour environ), la relation linéaire entre CH et oxygène entrant par convection se rompt. Cette valeur dépend du nombre de bâchées par jour, et au-delà cette valeur, le renouvellement d'oxygène par convection devient limité. Si la filière peut accepter de grandes charges hydrauliques, les limites d'acceptation doivent être définies.

Charge hydraulique et limites de performances

Selon Cooper (2005), les facteurs les plus importants à prendre en compte dans la conception des filtres plantés de roseaux à écoulement vertical sont :

- Concevoir un milieu poreux du filtre qui permet le passage des eaux usées à travers le lit avant que la bâchée suivante arrive, et en même temps retenir les effluents assez longtemps pour permettre un temps de contact avec la biomasse qui se développe dans le milieu poreux, pour atteindre le niveau de traitement requis.
- Fournir une superficie suffisante pour promouvoir les transferts d'oxygène et la croissance de la biomasse.

En raison des différentes conceptions et utilisations des FPR-V, il est complexe de trouver un consensus sur leur limites hydrauliques dans la littérature. Kadlec & Wallace (2009) indiquent que des CH allant à plus de 1 $m.j^{-1}$ ont été employées dans des FPR-V montrant de bonnes performances pour DBO/DCO et NH_4. Molle *et al.* (2006) ont démontré que la version française des FPR-V peut accepter une CH allant jusqu'à 4 $m.j^{-1}$ (>10 fois la CH nominale).

De plus, ils ont montré que des CH en continu de 1.8 $m.j^{-1}$ pendant 5 mois peuvent être traitées et respecter les concentrations maximales établies (DCO : 125 mg/L, DBO_5 : 25 mg/L, NK < 10 mg/L). Des premières limites pour la filière française (Tableau 1) ont été établies par Molle (2003) selon la profondeur du dépôt organique, la récurrence et la dynamique des surcharges hydrauliques :

Tableau 1: Limites hydrauliques proposées par Molle (2003)

Dépôt organique (cm)	*0-10*		*10-25*	
Surcharge hydraulique	**Hebdomadaire**	**Mensuelle**	**Hebdomadaire**	**Mensuelle**
$m.j^{-1}$	1.80	3.50	0.90	1.80
$m.h^{-1}$	0.25	0.25	0.11	0.11

Cependant, la réponse biologique n'a pas été précisément définie pour ces premières limites d'acceptation des temps de pluie. Bien que de nombreux FPR-V soient alimentés par des réseaux unitaires, les limites d'acceptation des eaux pluviales n'ont pas été bien définies, car elles dépendent d'une multitude de facteurs tels que l'âge du système, la saison, les caractéristiques du réseau d'assainissement, et bien sûr, les conditions climatiques (intensité, durée et fréquence des pluies). Par conséquent, la conception du filtre doit non seulement accepter la surcharge hydraulique, mais il doit aussi minimiser le temps de noyage à la surface, pour assurer un renouvellement suffisant d'oxygène nécessaire pour le traitement. A cet effet, il faut (i) étudier la dynamique des performances épuratoires du premier étage (le plus limitant hydrauliquement), selon les surcharges hydrauliques reçues. Cependant, comme les contextes locaux influencent la CH arrivant au système, il est essentiel (ii) d'étudier l'impact de la dynamique des précipitations locales (durée, fréquence et intensité), ainsi que l'impact des caractéristiques du système d'assainissement (pente, taille du bassin versant et pourcentage d'imperméabilisation) sur le comportement du filtre. En plus, (iii) la conception du FPR-V (surface, hauteur de revanche...) aura un impact sur l'acceptation des surcharges hydrauliques. L'ensemble de ces trois facteurs est essentiel pour la définition des limites d'acceptation des CH. Tout cela rend très complexe le design des FRP-V pour l'acceptation des eaux de pluie. Par conséquent, des modèles dynamiques (mécanistes et simplifiés) peuvent être des outils indispensables pour décrire l'hydraulique du système. L'application des modèles semble une condition nécessaire pour mieux comprendre hydraulique des FPR et pour leur conception dans de tels scenarios.

Modélisation

La plupart des modèles numériques des FPR sont principalement utilisés pour d l'écoulement horizontal (Pastor *et al.* 2003; García *et al.* 2004; Małoszewski *et al.* 2006; Tomenko *et al.* 2007). Seules quelques études sont réalisées pour des FPR à écoulement vertical, où les modèles mécanistes sont les plus fréquents (Wanko *et al.* 2006; Forquet *et al.* 2009; Freire *et al.* 2009; Šimůnek *et al.* 2009; Giraldi *et al.* 2010). Parmi les modèles mécanistes, le code le plus populaire est Hydrus (Šimůnek *et al.* 2009).

Cependant, si les modèles mécanistes sont des outils puissants pour décrire en détail la dynamique du FPR-V, ils sont généralement trop compliqués à caler, en raison de nombreux paramètres de calage, aussi bien pour l'hydraulique que pour les processus biochimiques. Ces modèles sont à l'origine conçus et utilisés pour la recherche, par conséquent, leur

manipulation reste difficile pour des utilisateurs non experts. Choisir entre une description détaillée et une manipulation facile dépendra des objectifs de modélisation. Quand un objectif de dimensionnement global par les concepteurs est visé, l'utilisation de modèles simplifiés semble une bonne alternative.

Si les modèles hydrauliques mécanistes destinés à étudier la dynamique des FPR-V sont peu nombreux, les modèles simplifiés adaptés aux FPR le sont encore moins. On peut compter parmi eux : Meyer *et al.* (2008) et Ross *et al.*(2011). Ils reposent sur des bilans de masse entre chaque compartiment des filtres. Ces modèles sont faciles à utiliser pour la conception des FPR, cependant ils sont adaptés à des configurations spécifiques liées au traitement des surverses de déversoirs d'orage. Or, le régime d'alimentation et les objectifs de traitement sont différents du contexte du traitement des eaux usées domestiques qui reçoivent une charge hydraulique et organique constamment. Il apparait donc nécessaire d'adapter ces types de modèles simplifiés de FPR-V, basés sur des données d'une station en taille réelle, afin de caractériser de manière fiable l'hydraulique des FPR-V à long terme. De même, il est nécessaire de déterminer dans quelles conditions hydrauliques la partie biologique du filtre est affectée afin de bien préciser les limites hydrauliques tant sur un point physique que biologique.

Matériels et méthodes

Station d'épuration expérimentale

L'étude a été réalisée sur un système français de FRP-V, situé à Challex, Ain (01). La station a été mise en service en avril du 2010, pour une capacité de 2 000 équivalent habitants (EH). Elle est conçue pour traiter les eaux résiduaires brutes de temps sec et de temps de pluie d'un bassin versant de 60-ha. Avec une surface totale de 2 m²/EH, la station d'épuration (STEP) est composée de deux étages, constitués de 3 et 2 cellules en parallèle pour le premier et le deuxième étage respectivement, selon les recommandations françaises (Molle *et al.* 2005a).
L'eau provenant du réseau unitaire entrent dans la STEP via un répartiteur de débit. Les débits <= 100 m³/h sont acheminés par la filière de temps sec vers une chasse hydraulique, qui alimente par bâchées la cellule en fonctionnement du 1er étage. Pour des débits supérieurs, allant jusqu'à 3600 m^3/h, l'eau excédentaire est acheminée par la filière de temps de pluie à la cellule alimentée, sans distribution homogène. Pour des débits supérieurs à 3600 m^3/h, un déversoir d'orage (DO) protège la station contre les pluies extrêmes.

De plus, une hauteur de revanche, à 0.5 m au-dessus de la surface du filtre, protège le filtre du 1er étage contre des temps de noyages excessifs (manque d'oxygène dans le milieu poreux) en by-passant les eaux vers la sortie station. Une fois l'eau filtrée par le 1er étage, elle est drainée vers la 2ème chasse hydraulique, puis envoyée sur le 2ème étage de traitement. Une fois l'eau traitée par l'ensemble de la STEP, elle est déversée dans le milieu récepteur (le Rhône).

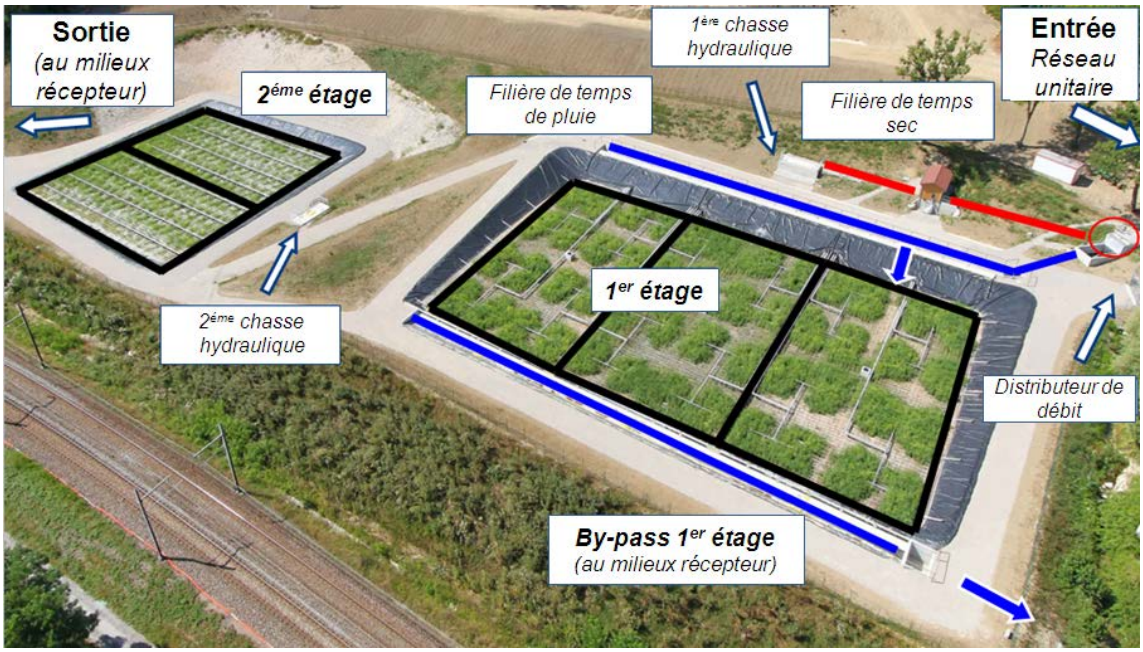

Figure 2 : Illustration schématique de la STEP de Challex

En temps sec, chaque cellule du premier étage est alimentée pendant 3.5 jours, avec 7 jours de période de repos, pendant que le deuxième étage est alimenté pendant 3.5 jours avec 3.5 jours de repos. Pendant les événements de temps de pluie, la rotation de cellules est faite après 100 bâchées (1.81 m d'eau), dont l'objectif est de protéger les cellules des longues périodes de noyage. Les objectifs de traitement ont été définis en période de temps sec et visent à respecter les concentrations suivantes à la sortie de la STEP :

Tableau 2 : Objectif de traitement en période de temps sec

Polluant	Concentration maximale (moyenne sur 24h)
DBO_5	25 mg/L
DCO	90 mg/L
MES	35 mg/L
NK	20 mg/L

L'étude du comportement des filtres âgés a été réalisée sur les données recueillies sur une station comportant 20 cm de dépôt organique lors de la thèse d'Ania Morvannou (Morvannou 2012). Il s'agit de la station d'Evieu (01, 200 EH).

Suivi hydraulique

L'étude a porté sur l'impact des surcharges hydrauliques sur les performances de traitement des FPR sur une période de suivi de deux ans. Ainsi, un équipement spécifique a été mis en place dans la STEP expérimentale pour suivre l'hydrodynamique du système à chaque étage (débit entré par la filière de temps sec et la filière de temps de pluie, débit sortie 1er et 2éme étage, et by-pass 1er étage). Toutes les mesures hydrauliques ont été contrôlées et enregistrées sur un enregistreur de données (Gartner ®) sur un pas de temps d'une minute. L'évolution de la teneur en eau pendant les périodes d'alimentation a été mesurée dans deux cellules du 1er étage par un ensemble de 15 sondes TDR (time-domain reflectometry), couvrant 5 profils sur trois profondeurs différentes (10 cm, 25 cm et 40 cm).

Suivi des performances épuratoires

Les performances épuratoires du filtre ont été évaluées en utilisant des approches différentes :

- Douze campagnes d'échantillonnage classiques (7 de temps sec et 5 de temps de pluie), de type bilan 24 h proportionnel au débit, ont été réalisées pour évaluer les performances de chaque étage pour différentes charges et saisons.

  Les paramètres qui ont été analysés par le laboratoire Irstea sont MES, DCO total et dissoute, DBO_5, NK, $N\text{-}NH_4$, $N\text{-}NO_3$, $N\text{-}NO_2$ et $P\text{-}PO_4$ conformément aux standards internationaux (APHA 2005).

- Des mesures en continu de certains paramètres à la sortie du 1er étage ont permis d'observer le comportement dynamique du filtre par temps de pluie.

  Ces mesures en continu se sont focalisées spécialement sur les concentrations en NO_x-N pour suivre précisément le comportement de l'azote sur le premier étage de traitement. En plus des mesures de conductivité électrique à chaque étage de traitement (sondes WTW LF 470), de MES, DCO (totale et dissoute) et NO_x-N ont été déterminées avec une sonde UV-Visible (s::can Messtechnik GmbH, Vienne, Autriche) au pas de temps d'une minute (Rieger *et al.* 2004; De Bénédittis & Bertrand-Krajewski 2006).

  L'étalonnage de la sonde s ::can a été basée sur la méthode de régression des moindres carrés partiels (PLS, Partial Least Squares) (Aji et al. 2003), qui est l'étalonnage le plus robuste, en particulier pour les relations concentration-spectre. L'étalonnage a été réalisé à partir d'échantillons prélevés au cours de l'étude (97 pour les MES, 99 pour les NO_x-N, 97 pour la DCO totale et 75 pour la DCO dissoute) dans des périodes de temps sec et de temps de pluie pour balayer une large gamme de concentrations. L'étalonnage PLS montre des résultats très satisfaisants pour NO_x-N, DCO totale et MES, avec des coefficients de régression de 0,99, 0,91 et 0,84 respectivement. Pour la DCO dissoute, la corrélation n'est pas suffisamment précise pour être utilisée pour la prédiction.

- Une campagne intensive pour étudier les performances sur de longues périodes d'alimentation.

  Au cours de cette campagne (du 27 aout au 7 septembre 2012), une cellule du premier étage a été alimentée pendant 11,5 jours consécutifs. L'objectif principal était d'observer la relation entre l'appauvrissement en oxygène et la baisse des performances épuratoires. En plus des mesures hydrauliques et des sondes en continu, des mesures supplémentaires ont été réalisées :

  - Mesures en continu de NH_4-N à l'entrée et à la sortie du premier étage (VARiON ® Plus sondes, WTW).
  - Cinq bilans 24 heures à chaque étage de traitement tous les deux jours.
  - Prélèvements à l'entrée du premier étage au cours des jours sans bilan 24 h.
  - Mesures de concentration d'oxygène gazeux dans le sol du 1er étage profil (Dräger capteur XS © analyseur de gaz).

- Quatre traçages à la fluorescéine (fluorimètre GGUN-FL22) entre les bilans 24 h.

Modélisation hydraulique

Le modèle hydraulique simplifié

Le modèle hydraulique simplifié est construit avec différents composants à partir desquels le débit d'eau est calculé par un bilan massique (Figure 3). Le premier composant est un volume de stockage d'eau au-dessus de la surface du filtre. Il reçoit les eaux usées en provenance de la chasse hydraulique et l'infiltration est gouvernée par les vitesses d'infiltration. Les variations de charge hydraulique (CH) jouent un rôle important dans le processus d'infiltration (Beach *et al.* 2005). L'infiltration du volume stocké en surface du filtre a été modélisée par une loi d'infiltration simplifiée (Equation 1), où la conductivité hydraulique (*K*) de la loi de Darcy est remplacée par un paramètre représentant la capacité d'infiltration (*ICP*) proportionnelle à la vitesse d'infiltration et *h* est la hauteur d'eau à la surface du filtre (charge hydraulique). En alimentation par bâchées, cette simple équation suppose que le dépôt de boues est saturé. Par conséquent, le gradient hydraulique de la loi de Darcy peut être approché par la hauteur d'eau à la surface du filtre pour une faible hauteur de dépôt comme cela est le cas sur la station de Challex.

$$IV = ICP \cdot h \qquad \textbf{Équation 1}$$

où:

IV = vitesse d'infiltration, en m/s^{-1}

ICP = paramètre de capacité d'infiltration, en s^{-1}

h = charge hydraulique, en m

La seconde composante est le filtre, qui est simplement représenté par le délai (time-lag) représentant le temps de passage apparent à travers le filtre.

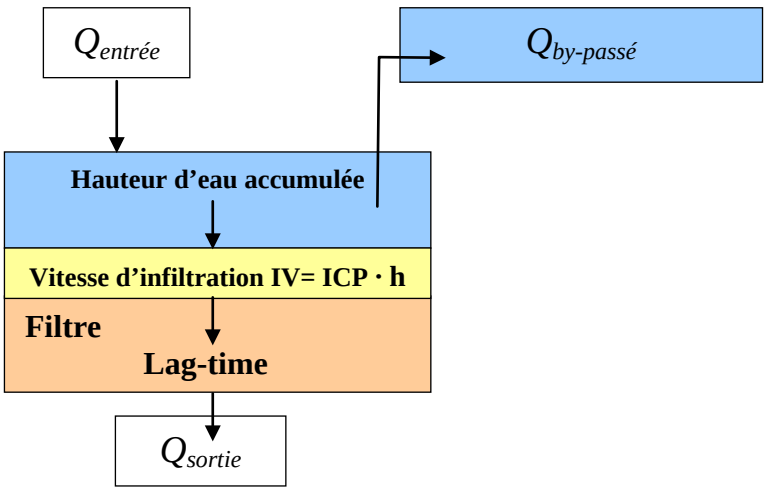

Figure 3 : Diagramme schématique du modèle hydraulique simplifié

Calage du modèle hydraulique simplifié

Ce calage doit d'abord définir (i) le lag-time qui représente le filtre lui-même, (ii) le stockage de l'eau sur le milieu poreux et iii) le paramètre *ICP*. Le lag-time a été défini pour un filtre jeune (STEP Challex) et un filtre mature (STEP Evieu) grâce à l'ensemble des événements (journées de temps sec et de temps de pluie) en 8 et 11 minutes pour des filtres jeunes et matures respectivement. Ensuite, ces valeurs ont été introduites dans le modèle pour caler le paramètre *ICP*. Le stockage de l'eau dans le filtre a été calculé à l'aide des sondes TDR et des relations temps/stockage d'eau, en faisant l'hypothèse d'une répartition homogène de la teneur en eau. Un maximum d'environ 25 m^3 est stocké dans le filtre de Challex, ce qui ne représente que 10 % des flux d'entrée. En période estivale, l'eau est stockée plus lentement qu'en hiver. Ces équations ont été introduites dans le modèle pour comprendre l'impact du stockage de l'eau sur le débit de sortie et les valeurs d'*ICP*.

Pour étudier la sensibilité du paramètre *ICP* et son évolution au fil du temps, le modèle a été calé sur des débits de sortie en fonction : (i) de la charge hydraulique (de 0.20 à 2.53 $m.j^{-1}$), (ii) du jour d'alimentation, (iii) de la saison (tous les mois de l'année) et (iv) de l'âge du système (filtres avec 2 -Challex- et 8 -Evieu- ans de fonctionnement). Pour l'ensemble des scénarios, le paramètre *ICP* a été calé en trois étapes :

- Compte tenu de la non homogénéité de la planéité de la surface du filtre (non homogénéité des dépôts organiques), le paramètre *ICP* a été calé sur le débit de sortie du 1er étage par la méthode des moindres carrés.
- La hauteur d'eau modélisée a été comparée aux valeurs mesurées, pour vérifier la cohérence du modèle.
- Enfin, le modèle simplifié a été comparé au modèle mécanique, Hydrus 1D (seulement pour le filtre jeune -Challex-).

  Pour le calage du modèle Hydrus-1D, une caractérisation hydrodynamique du matériau d'infiltration a été réalisée. Cela produit un ensemble de paramètres (valeurs initiales) qui ont été utilisés dans le module d'optimisation inverse inclus dans Hydrus-1D. Les paramètres ont été (i) la conductivité hydraulique à saturation K_s, (ii) la teneur en eau résiduelle θr, (iii) la teneur en eau à saturation θs, (iv) alpha α et (v) le paramètre *n*.

  Cette méthodologie de calage, mise en œuvre par Morvannou et al. (2013), limite le risque de non-convergence du modèle, car les valeurs obtenues sont susceptibles d'être proches des valeurs optimales. Certaines données du site expérimental (teneur en eau et débits de sortie du 1er étage) ont été parallèlement utilisées pour la modélisation inverse.

Modèle simplifié et les facteurs d'influence sur l'acceptation hydraulique

Le modèle simplifié est utilisé pour la modélisation hydraulique à long terme. Les principaux objectifs de cette modélisation sont: (i) analyser l'impact du contexte local et de la conception du filtre sur l'acceptation des temps de pluie et (ii) établir une limite d'acceptation de charges hydrauliques selon les différents contextes. La méthodologie développée pour cette partie de la modélisation est la suivante :

- Définir le contexte local (bassin versant et réseau d'assainissement)
- Définir les variables climatiques (types de pluies)
- Calcul des débits arrivant à la STEP (transformation pluie-débit et transport exécuté dans le logiciel d'hydraulique urbaine CANOE)
- Calcul du temps et de la hauteur du noyage (fonctionnement du filtre)
- Calcul du nombre d'alertes de dysfonctionnement et des volumes by-passés à la surface du 1er étage (alertes définies à partir des mesures de performances épuratoires sur le site expérimental)
- Réduire les dysfonctionnements et rejets (établir un dimensionnement optimal pour chaque scenario)

Le Tableau 3 montre les paramètres modélisés pour aboutir aux objectifs de la modélisation à long terme.

Tableau 3 : Résumé des grandeurs modélisés

Configurations modélisées		**Valeurs**
Climat	*Bretagne*	-
	Rhône-Alpes	
Caractéristiques du réseau d'assainissement	*Coefficient d'imperméabilisation*	10% 17% 23% 30%
	Pente	1% 4% 7% 10%
	Déversoir d'orage	5 QN TS* 12 QN TS 20 QN TS 40 QN TS Aucune limite
Conception du filtre	*Surface*	0.9 m^2 p.e 1 m^2 p.e 1.2 m^2 p.e 1.5 m^2 p.e
	Hauteur de revanche du by-pass du 1er étage	0.1 m 0.3 m 0.5 m 0.7 m
Age du filtre	*Filtre jeune*	1 an
	Filtre vieux	8 ans

** Note: QN TS = Débit nominal de temps sec*

Comportement hydraulique du filtre

Hydraulique du filtre

Au cours des deux ans de suivi de la STEP de Challex, les pluies ont représenté 33,8 % des jours, et 16,6 % des jours ont produit des débits supérieurs au débit accepté par la filière de temps sec (100 m^3/h). Pendant les pluies, la STEP a traité des surcharges hydrauliques allant jusqu'à 5,31 $m.j^{-1}$ (> 14 fois le débit de temps sec) comme le montre la Figure 4. En raison de l'intrusion des eaux claires parasites en hiver (décembre à février), la STEP traite souvent des CH supérieures à la CH nominale (CHN). En période estivale, la CH traitée est souvent inférieure à la CHN.

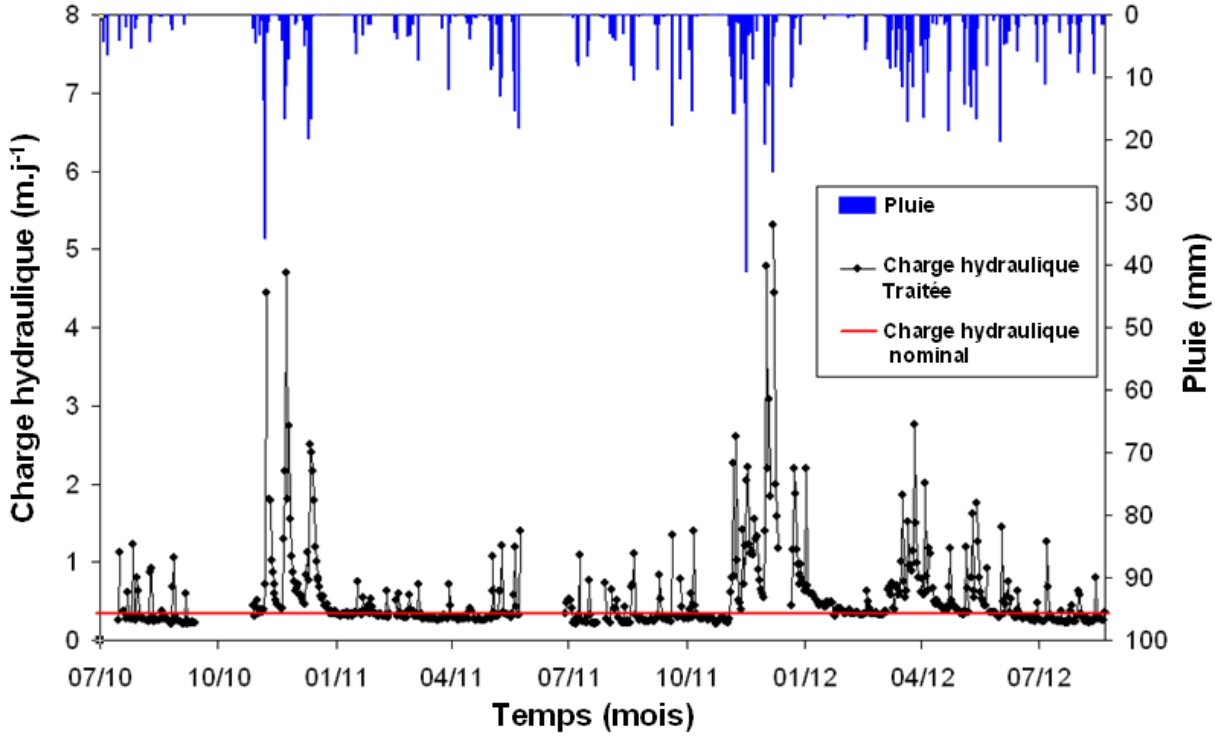

Figure 4 : Pluies et charges hydrauliques traitées pendant les deux ans de suivi de la STEP

Environ 51 % des CH traitées sont inférieures à la CHN et moins de 1% des événements observés ont été supérieurs à 10 fois la CHN (avec un maximum à 14.35 fois la CHN). Cela démontre que les vitesses d'infiltration du 1er étage sont suffisamment élevées pour accepter de grandes surcharges hydrauliques pendant les premières années de fonctionnement du filtre.

Campagnes TDR

Afin d'améliorer les connaissances sur la distribution d'eau à la surface du filtre, onze campagnes TDR ont été effectuées au cours des deux ans du suivi de la STEP. Compte tenu du faible débit d'alimentation des bâchées, toutes les mesures des profils TDR n'ont pas évoluées de manière similaire, suivant leur distance par rapport au point d'alimentation. Le front de distribution d'eau au cours d'une période d'alimentation est affecté par la saison et la charge hydraulique. En hiver le front d'eau avance plus rapidement en raison d'une plus faible

perméabilité liée à l'absence de roseaux et à la faible minéralisation de la couche de dépôt sur le filtre. Suivant la CH, quand une pluie arrive au filtre, le front de la distribution d'eau évolue rapidement. La Figure 5 présente l'évolution du front de distribution d'eau en fonction des CH. Il est clair que la saison hivernale est fortement différente des autres. Les campagnes TDR ont confirmé la non-homogénéité de la distribution de l'eau sur les filtres.

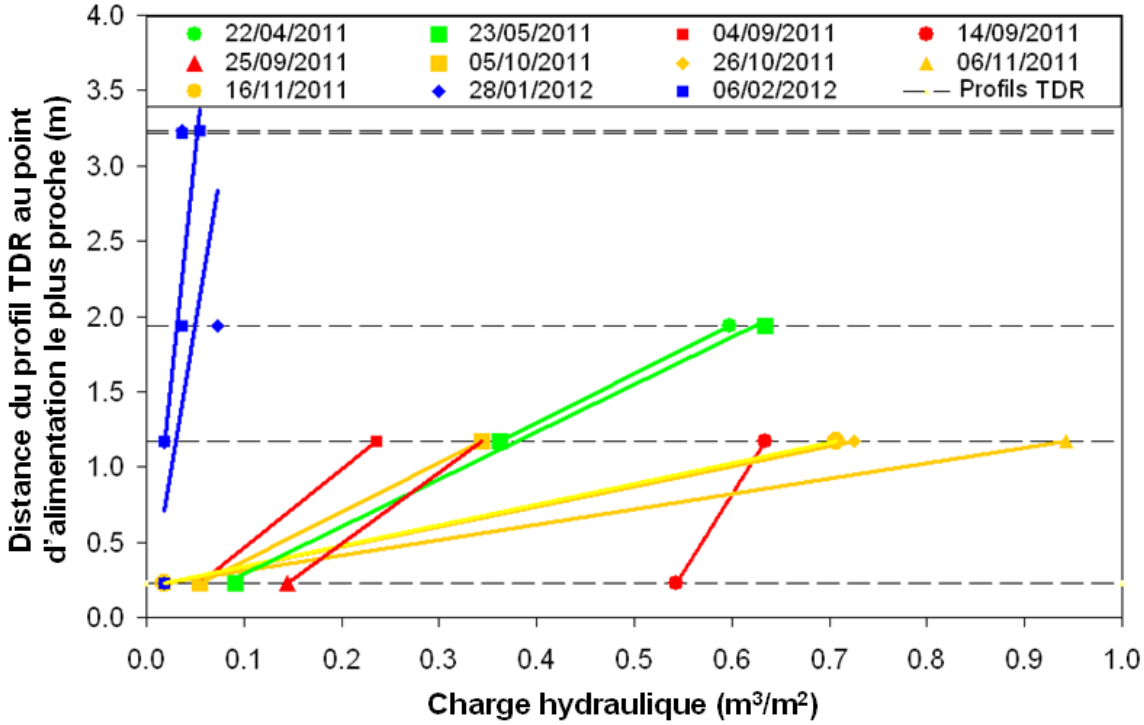

Figure 5 : Charge hydraulique requise pour atteindre les profils TDR, par campagne et par saisons

En conséquence, suivant la distribution de l'eau en surface du filtre, la surface inactive est d'environ de 51 % pour les campagnes où l'eau arrive jusqu'au profil TDR #2 (débit de temps sec quand les roseaux sont présents), et 20 % pour les campagnes où l'eau a été mesurée au profil #3 (débit de temps sec en début du printemps). Cette sous-exploitation du filtre génère une surcharge organique et hydraulique là ou l'eau s'infiltre. Cela pourrait avoir un impact ultérieur sur les performances épuratoires au début d'une période d'alimentation.

Modélisation hydraulique simplifiée

Le modèle hydraulique simplifié du filtre a été conçu en utilisant un coefficient d'infiltration empirique *ICP*, qui est le principal facteur gouvernant l'infiltration dans le modèle simplifié. Il permet de représenter l'évolution dans le temps du débit à la sortie du filtre et, plus important, la hauteur d'eau et le temps de noyage à la surface du filtre. Un total de 92 événements, soit 33 épisodes pluvieux de différentes durées et intensités et 59 périodes de temps sec, répartis sur les deux ans de suivi (pour le filtre jeune) et deux campagnes de mesures sur un filtre mature (Evieu) ont permis de caler le paramètre *ICP*. Le modèle simplifié a révélé une évolution saisonnière du paramètre *ICP* qui s'explique par la présence ou non des roseaux ainsi que par le degré de minéralisation du dépôt organique (Figure 6).

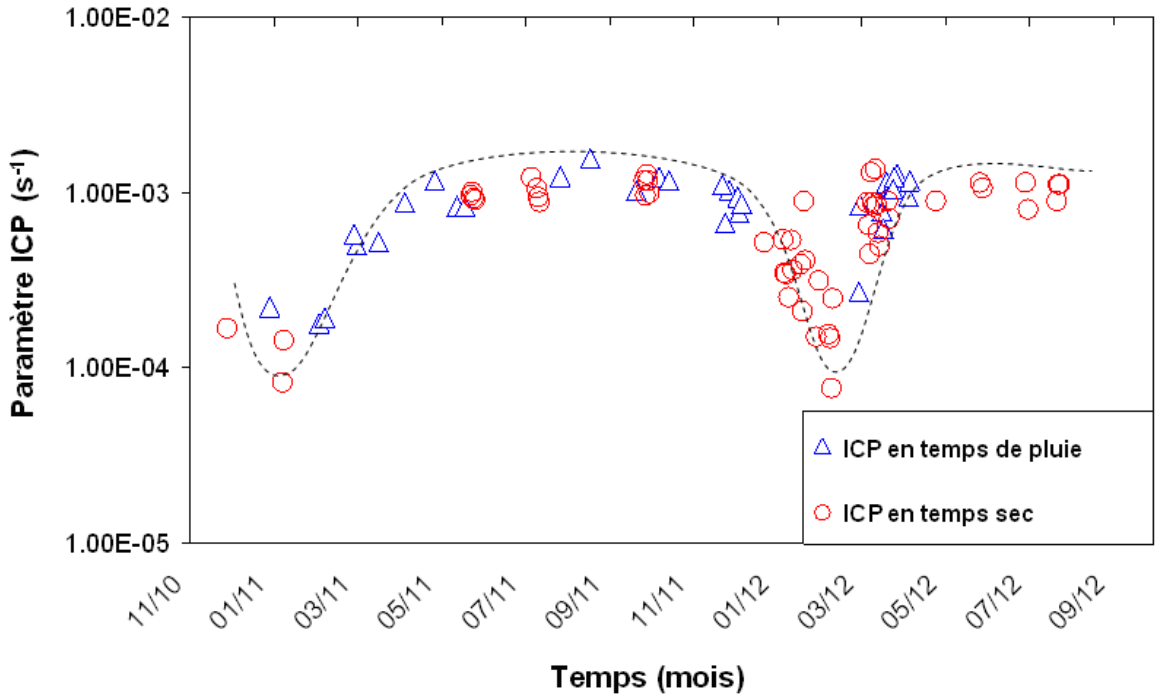

Figure 6 : Evolution du paramètre ICP pendant les deux ans de suivi de la STEP de Challex

Malgré les données limitées du filtre mature (Evieu), les valeurs du paramètre *ICP* sont inférieures à celles d'une station jeune quelle que soient les saisons. Ce fait montre l'influence de la couche de dépôt organique sur la perméabilité du milieu. Les valeurs moyennes mensuelles d'*ICP* ont été utilisées pour la modélisation à long terme.

Comparaison avec Hydrus-1D

Pour avoir une meilleure confiance dans le modèle simplifié, une comparaison a été faite avec le logiciel hydrodynamique Hydrus-1D. Étant donné que la saison est l'un des facteurs les plus influant sur l'hydrodynamique du filtre, la procédure de modélisation inverse a été faite pour deux saisons différentes (hiver et été) pour des périodes de temps sec.

Les paramètres de calage obtenus avec Hydrus reproduisent correctement les débits à la sortie et la teneur en eau dans le filtre. Des débits mesurés à la sortie du 1er étage ont été comparés aux données simulées par Hydrus et par le modèle simplifié. Selon la Figure 7, le modèle simplifié montre une bonne similarité avec les résultats d'Hydrus, et des deux modèles avec les données mesurées.

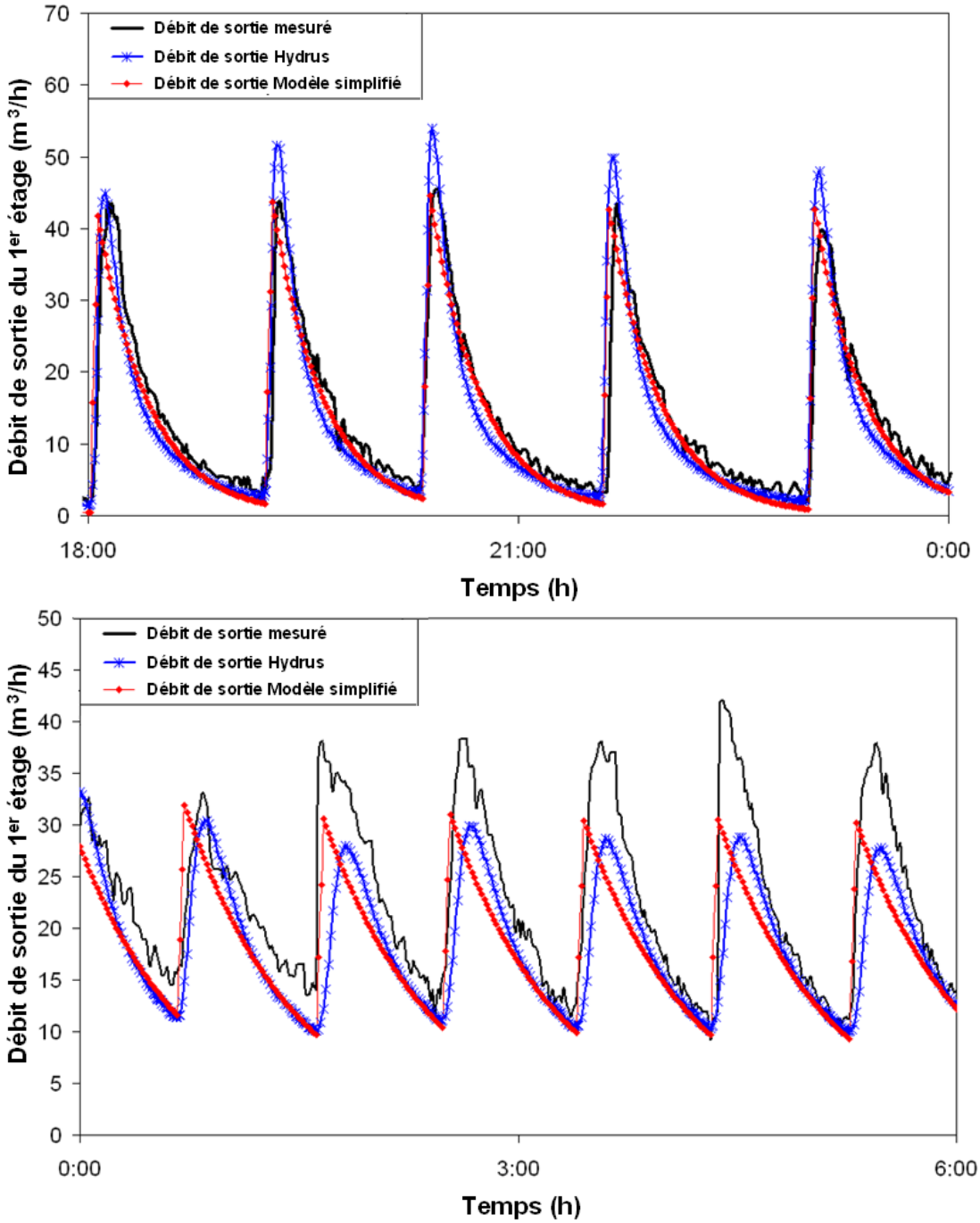

Figure 7 : Débit de sortie du 1er étage mesuré, simulé par Hydrus et par le modèle simplifié pour l'été (*en haut*) et l'hiver (*en bas*)

Le coefficient de Nash-Sutcliffe montre une différence négligeable entre les deux modèles par rapport aux données mesurées, obtenant pour l'événement d'été 0.86 et 0.9 pour le modèle simplifié et le modèle Hydrus respectivement. En hiver, les coefficients de Nash-Sutcliffe sont plus faibles mais toujours acceptables, de 0,51 pour le modèle simplifié et 0.515 pour le modèle Hydrus. Globalement, nous arrivons à de meilleurs résultats de modélisation en été qu'en hiver. En ce qui concerne les hauteurs de flaquage, les simulations sont en accord avec les valeurs mesurées, compte tenu des faibles hauteurs observées (Figure 8).

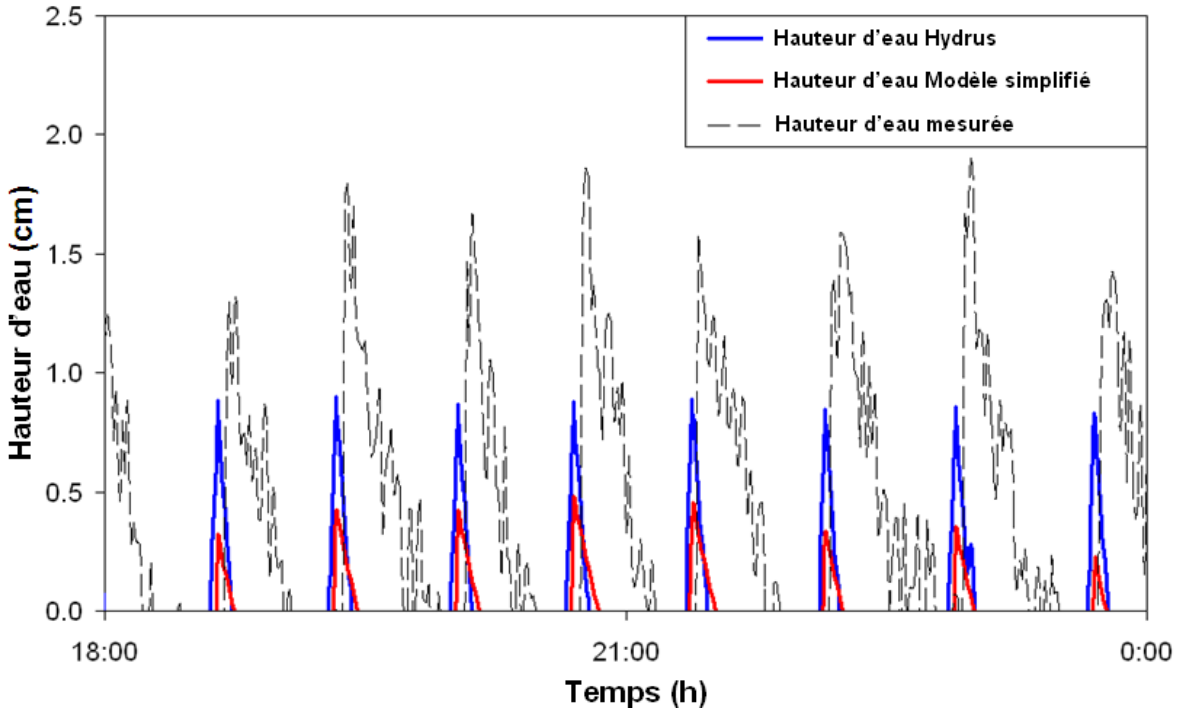

Figure 8 : Hauteur d'eau mesurée, simulée par Hydrus et par le modèle simplifie pour un événement en hiver

Il y a généralement un bon accord entre les deux modèles en termes de temps de flaquage. Il faut remarquer que les hauteurs d'eau mesurées sont utilisées comme indication compte tenu des problèmes de planéité de la surface du filtre. La bonne similarité du modèle simplifié avec Hydrus nous conforte sur la capacité du modèle simplifié à reproduire l'hydraulique d'un filtre planté de roseaux.

Performances du filtre

Caractéristiques des eaux usées

Les caractéristiques des eaux usées entrant à la STEP dépendent (i) de la saison (présence des eaux claires parasites), (ii) de l'activité humaine (week-end et vacances scolaires pour les eaux usées domestiques) et (iii) des conditions météorologiques (en fonction de l'historique des temps sec, les pluies peuvent créer un effet de dilution ou un événement à effet de rinçage avec des teneurs en polluant élevées), qui produisent des variations de charges hydrauliques et organiques entrant à la STEP de Challex. Le Tableau 4 présente les caractéristiques de charge hydraulique et organique à l'entrée de la STEP au cours des campagnes classiques d'échantillonnage sur le site expérimental.

Tableau 4 : Caractéristiques des eaux usées arrivant à la STEP de Challex, des charges organiques et hydrauliques sur le filtre du 1er étage pendant les campagnes (les charges de temps de pluie ont été ramenées à une base journalière)

	Charge hydraulique (m/j)	**Charges Polluantes (g/m²/j)**							
		MES	***DCO totale***	***DCO dissoute***	***NK***	***NH_4-N***	***NO_x-N***	***PO_4-P***	***DBO_5***
Périodes de temps sec (nombre de données)									
Charges moyennes									
Max.	0.29(7)	85(7)	136(7)	20(7)	14(7)	8.2(7)	0.25(7)	0.79(7)	56(4)
Min.	0.42	128	164	27	18	8.9	0.47	0.89	76
	0.23	52	115	17	12	7	0.11	0.67	40
Ecart-type									
	0.06	24	19	3.7	1.8	0.64	0.17	0.08	18
Concentrations moyennes (mg/L)		289	477	71	48	29	0.85	2.8	175
Evénements de temps de pluie (nombre de données)									
Charges moyennes	1.27(5)	236(5)	319(5)	63(5)	25(4)	12(5)	4.01(5)	1.58(5)	169(2)
Max.	2.26	624	890	76	49	19	7.41	2.65	288
Min.	0.68	79	49	49	13	7	0.75	0.92	49
Écart-type	0.64	226	336	13	17	4.7	2.62	0.78	169
Concentrations moyennes (mg/L)		179	257	40	18	8	2.4	1.11	148
Charges nominales	**0.35**	**139**	**279**		**28**	**21**		**5**	**111**
Pourcentage									
Selon la charge moyenne en périodes de temps sec	83 %	61%	49%		50%	39%		16%	50%
Selon la charge *moyenne* et *maximale* en événements de temps de pluie	363% 646%	170% 449%	114% 319%		89% 175 %	57% 90%		32% 53%	152% 259%

La STEP est globalement sous-chargée (environ 49 % de la charge organique et 83 % de la CH selon la valeur nominale) par temps sec mais peut recevoir des charges élevées lors d'événements de temps de pluie (319 % de la charge organique et 646 % de la charge hydraulique en moyenne). Les concentrations mesurées en périodes de temps sec soulignent que les eaux usées sont légèrement diluées. Le rapport NH_4/NK, de 0.6 et 0.51 avec un écart-type de 0.06 et 0.09 pour les événements de temps sec et de temps de pluie respectivement, montre le caractère particulaire des eaux usées. En effet, ces ratios sont légèrement inférieures à ceux habituellement observés pour les petites collectivités en France [environ 0.75 (Molle et al. 2005)]. Comme une partie importante des performances épuratoires s'appuie sur la filtration, les eaux usées plutôt particulaires de Challex favorisent l'efficacité du traitement épuratoire. Le rapport DCO/DBO_5 de 2.7 et 1.7, pour les événements de temps sec et de temps de pluie respectivement, montrent que les eaux usées sont parfaitement biodégradables.

Performances épuratoires

MES et DCO

Pour l'analyse des performances épuratoires, tous les bilans ont été calculés sur une base journalière, afin de faciliter la comparaison et obtenir des données représentant l'intensité des événements. Au premier étage, les niveaux de performance de temps sec et temps de pluie restent très proches, 91 % et 86 % pour les MES et la DCO respectivement. Ces niveaux de performances sont comparables à ceux observés sur ce type de procédés en temps sec (Molle et al. 2005). Les concentrations à la sortie du premier étage sont généralement en accord avec les objectifs globaux de traitement de la STEP de Challex, ce qui démontre la robustesse du système. La STEP a montré des performances épuratoires globales très élevées, indépendamment des charges hydrauliques, malgré les fortes variations des charges organiques que les pluies peuvent apporter. On a obtenu des performances globales (temps sec et temps de pluie) de 98 % et 93 % pour les MES et la DCO respectivement.

Azote Kjeldahl (NK)

En temps sec, les performances du 1er étage suivent les niveaux d'élimination classique observés dans les différents filtres plantés de roseaux français (Molle et al. 2008). Comme des charges en azote relativement faibles ont été appliquées (environ 50 % de la charge nominale), l'efficacité d'élimination de NK est élevée, de l'ordre de 76 % et 70 % pour le premier et le deuxième étage respectivement. Pendant les événements de temps de pluie, nous avons observé une plus grande variabilité des performances selon la charge appliquée, allant jusqu'à 3.17 fois la charge nominale en NK. La Figure 9 montre que malgré cette grande variabilité, les performances ont été globalement de 70 % pour le 1er étage (supérieurs à celles relevées dans littérature), et de 66 % pour le deuxième étage. Généralement, les performances sont supérieures en temps sec. Les concentrations en NK à la sortie du premier étage sont toujours inférieures à 18.4 mg/L, ce qui respecte déjà les objectifs globaux de traitement de 20 mg/L. Le deuxième étage a permis de réduire encore les concentrations à des valeurs toujours inférieures à 7.4 mg/L à la sortie de la STEP.

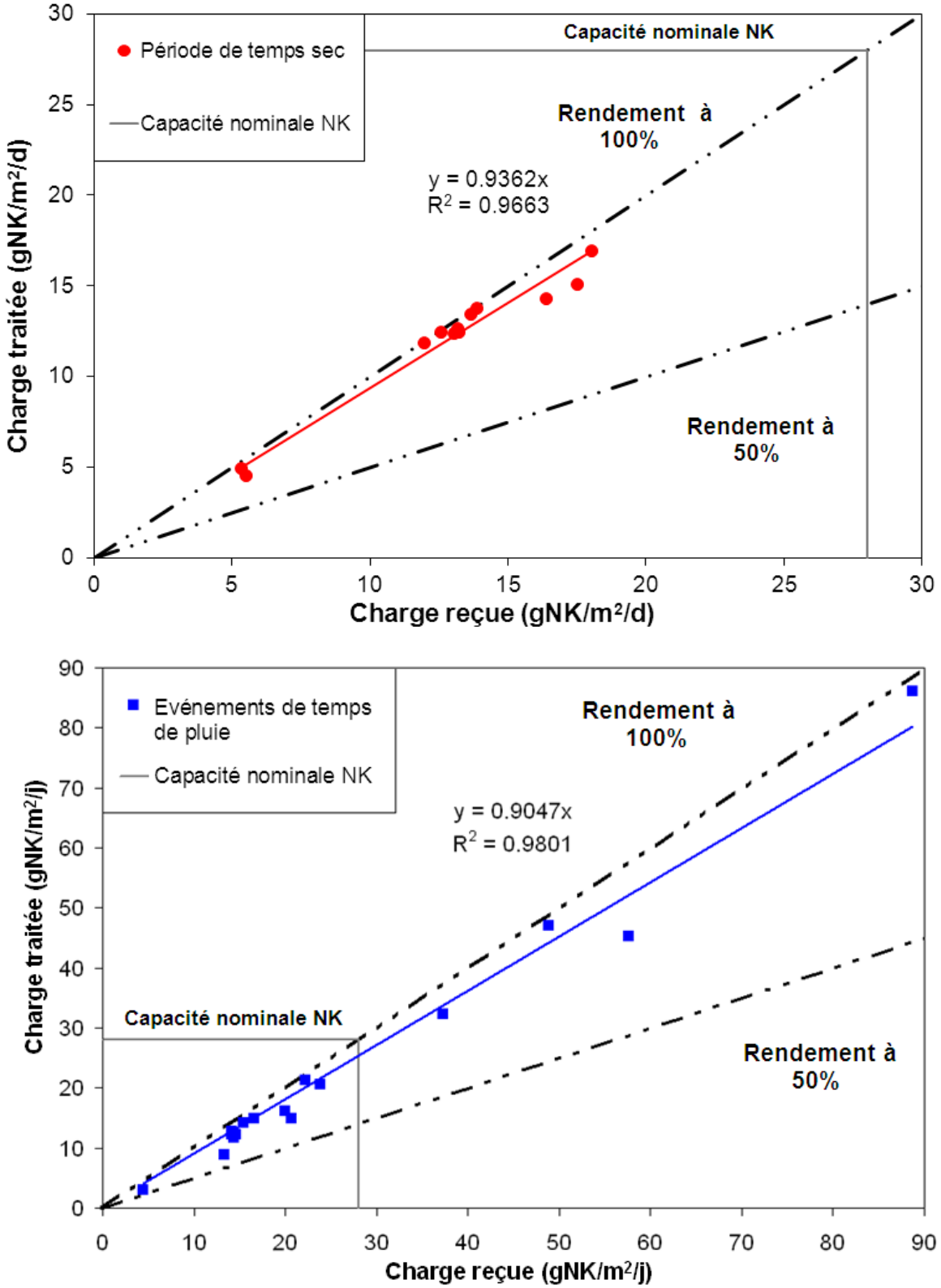

Figure 9: Performances épuratoires globales en NK par temps sec (*en haut*) et par temps de pluie (*en bas*)

L'analyse des campagnes peut donner une idée générale des performances épuratoires en fonction du temps entre bâchées, mais une analyse des mesures en continu (au pas de temps d'une minute) est indispensable. Afin d'offrir une meilleure compréhension de la dynamique de l'azote et de la nitrification, une sonde s::can a été utilisée à cet effet.

Campagne intensive

Pendant la campagne intensive, un évènement pluvieux a eu lieu au milieu des onze jours consécutifs d'alimentation d'un filtre. La charge hydraulique de l'évènement pluvieux, bien que faible (CH de 0,65 $m.j^{-1}$,1,86 fois la CHN), a permis de voir le comportement du filtre face à ce type de variation. Globalement, il n'y a eu aucune diminution notable des performances épuratoires avec les jours d'alimentation comme le montre la Figure 10.

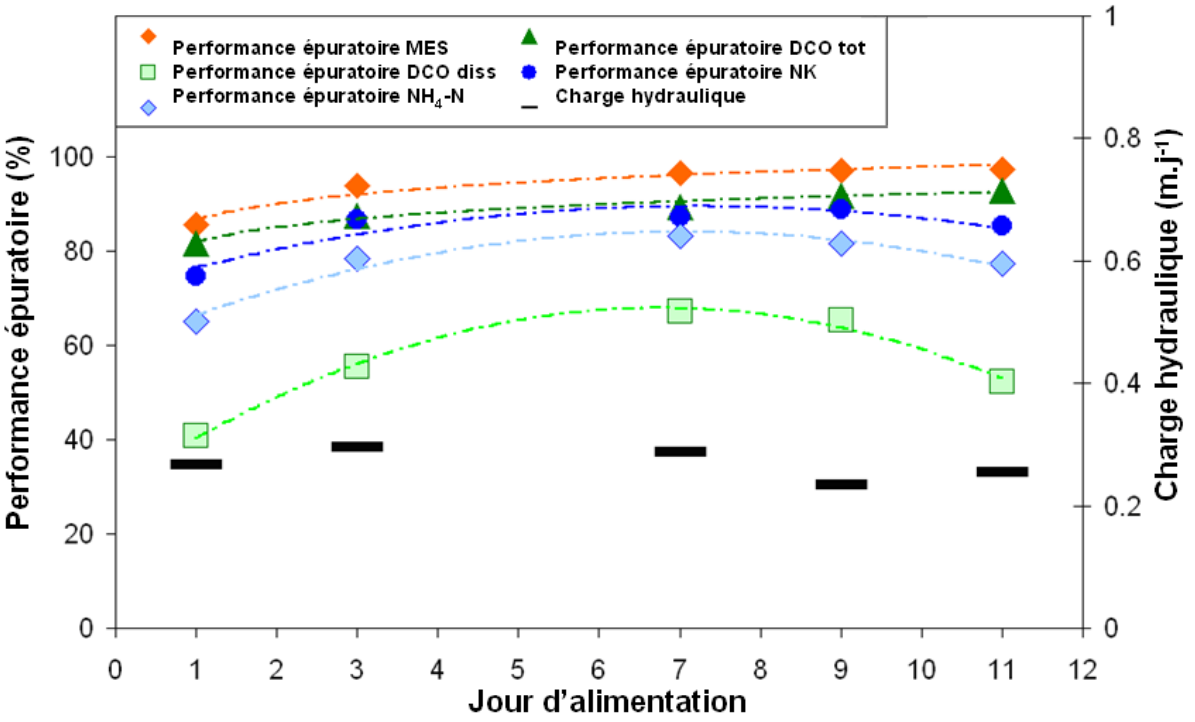

Figure 10: Performances épuratoires en fonction du jour d'alimentation pendant la campagne intensive

La Figure 10 montre une augmentation des performances épuratoires avec les jours d'alimentation pour les MES et la DCO totale, en raison de l'état d'avancement du colmatage de la surface du filtre qui favorise la filtration de l'eau. Si au début de la période d'alimentation la teneur en oxygène dans le milieu poreux est plus élevée, les performances épuratoires pour la DCO dissoute et NH_4-N augmentent au fil des jours d'alimentation. Par exemple pour NH_4-N les performances passent de 65 % à plus de 80 %. Le développement des bactéries nitrifiantes après une période de repos et une meilleure distribution de la charge hydraulique au cours des jours peuvent expliquer ce phénomène.

Suivi en continu de NO_xN par sonde s::can

Afin d'analyser la dynamique du filtre pour différentes surcharges hydrauliques, les concentrations en continu de NO_x-N à la sortie du 1er étage, fournies par la sonde s::can, ont été analysées pour plusieurs épisodes pluvieux (spécialement les CH les plus élevées). En raison de l'absence de mesures en continu de NH_4-N pendant une partie de l'étude, une relation concentration-entrée-NK/CH-entrée a été validée grâces aux campagnes d'échantillonnage. Cela a permis avec une précision acceptable de pouvoir compléter les jeux de données en NK d'entrée station.

L'étude montre que les forts débits à l'entrée de la STEP génèrent une dilution considérable de NK arrivant aux filtres, ensuite le NO_x-N à la sortie du premier étage est également dilué, suivant la même tendance que celle des concentrations d'entrée en NK. Si la concentration en nitrates à la sortie du 1er étage est faible pendant les événements pluvieux, la concentration revient à la normale une fois le temps de pluie passé. Cet effet montre que la nitrification n'est pas nécessairement affectée par les fortes CH (jusqu'à 3 m.j^{-1}). Différents événements pluvieux sont représentés (Figure 11) pour différentes surcharges hydrauliques et différents jours d'alimentation.

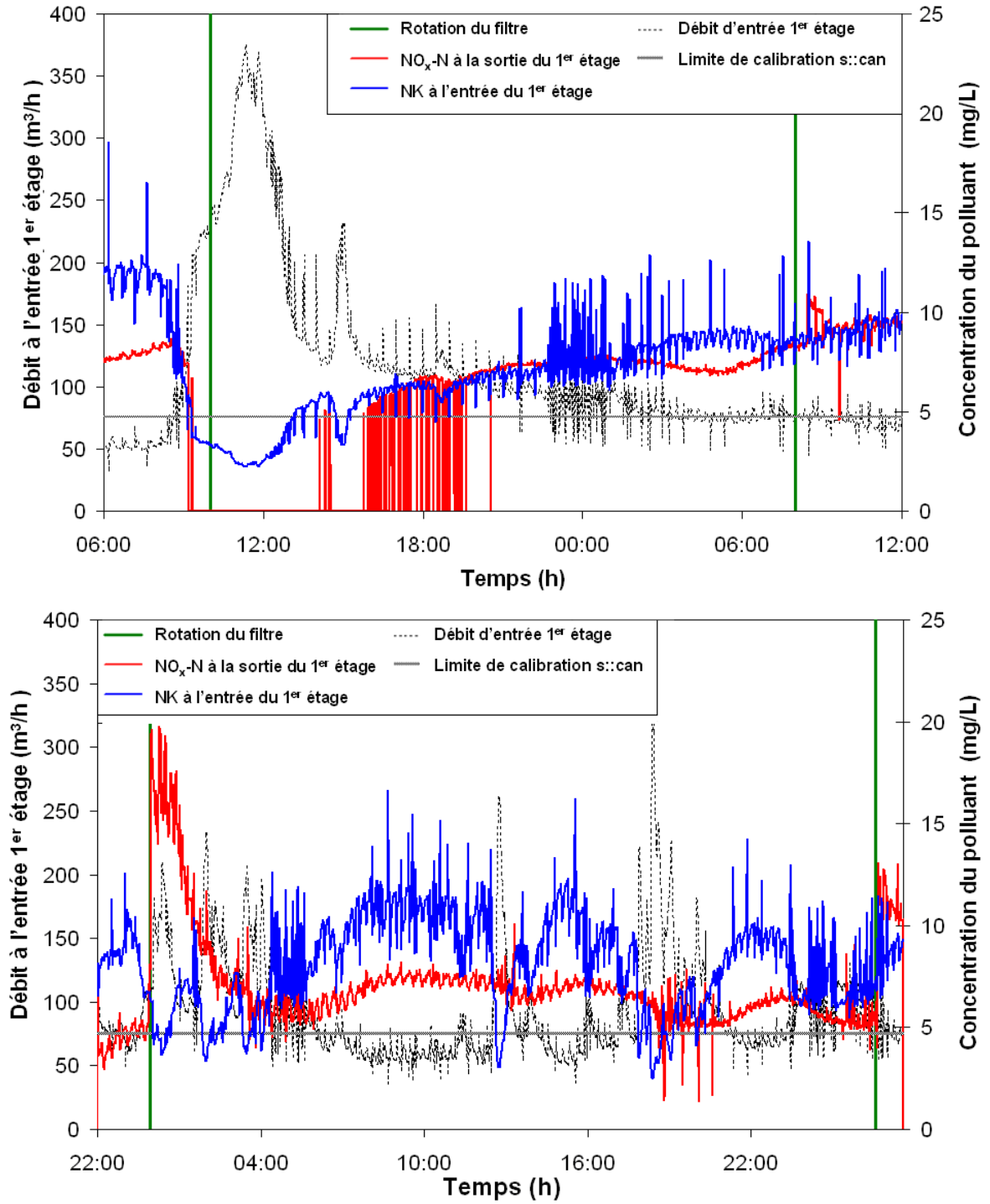

Figure 11: Concentrations en NO_x-N à la sortie du premier étage en fonction de la concentration en NK en entrée, pour le 3 janvier 2012 (*en haut*) et le 21 janvier 2012 (*en bas*)

Les résultats montrent que le filtre peut accepter de fortes charges hydrauliques (jusqu'à 3 $m.j^{-1}$) en hiver, période la plus limitante hydrauliquement, sans mettre en péril le traitement épuratoire. On voit que l'intensité de la CH a plus d'impact sur les concentrations de NO_x-N (comme le montre le 3 janvier 2012) que sa durée (comme le montre le 21 janvier 2012). L'analyse du temps de noyage de la surface du filtre lors des gros événements a servi de base pour établir les alertes de dysfonctionnement utilisées dans le cadre de la modélisation.

Critères d'alertes / Limites biologiques

Afin de relier l'hydraulique du filtre (le temps de noyage) et ses performances biologiques (le manque d'oxygène), des alertes de dysfonctionnement ont été établies. On suppose que la nitrification est le premier processus à être affecté par le noyage de la surface du filtre, en cas de manque d'oxygène dans le milieu poreux. Deux critères hydrauliques, basés sur l'intensité et la durée/fréquence des pluies, ont été établis pour définir des seuils d'alerte :

- Le temps maximal cumulé de noyage sur une journée (durée/fréquence)
- Le temps maximal de noyage continu (intensité)

Quand ces valeurs maximales sont dépassées, on peut considérer qu'un dysfonctionnement biologique peut se produire. Le suivi en continu des événements les plus chargés hydrauliquement nous a servi pour déterminer les alertes de dysfonctionnement. L'objectif était de déterminer le temps de noyage de chaque événement (consécutif et cumulé) et de le relier à un dysfonctionnement de la nitrification. La détermination du temps de noyage a été faite à partir de la simulation des événements par le modèle simplifié, en raison du manque de représentativité des mesures de hauteur d'eau fournies par les sondes ultrasons. Cependant, comme indiqué antérieurement, nous n'avons pas observé de dysfonctionnement de la nitrification. Par conséquent, les limites biologiques déterminées avec nos données seront des limites sécurisées. Les alertes de dysfonctionnement ont été définies comme suit : (i) un temps cumulé de noyage sur une journée de 15.5 heures et (ii) un temps de noyage continu de 7 heures.

Modélisation à long terme (chroniques de temps de pluie)

Après le calage du paramètre *ICP*, les comparaisons avec Hydrus-1D et l'établissement des alertes de dysfonctionnement, le modèle simplifié a été utilisé pour la simulation hydraulique du filtre à long terme (4 ans de chronique de pluies). Les principaux objectifs de cette modélisation à long terme étaient :

(i) Analyser l'impact du contexte local sur les surcharges hydrauliques des filtres :
- coefficient d'imperméabilisation (10, 17, 23 et 30 %)
- pente du bassin versant (1, 4, 7 et 10 %)
- type de climat (Bretagne et Rhône-Alpes)

(ii) Analyser la conception du filtre sur l'acceptation des surcharges hydrauliques des filtres :
- surface du filtre (0.9, 1, 1.2 et 1.5 m^2/EH)
- hauteur de revanche du 1^{er} étage (0.1, 0.3, 0.5, 0.7 mètres)

(iii) Analyser l'âge du filtre sur l'acceptation des surcharges hydrauliques des filtres :
filtre jeune (2 premières années de fonctionnement)
filtre âgé (8 ans de fonctionnement)

(iv) Pour finalement recommander un dimensionnement des filtres selon les différents contextes, afin d'accepter des surcharges hydrauliques de temps de pluie sans compromettre les performances épuratoires.

On a pu observer que l'influence du climat sur la charge hydraulique est vraiment importante. Le climat de Bretagne produit plus de CH supérieures à la CHN que le climat du Rhône-Alpes. Toutefois, le climat de Rhône-Alpes montre les débits les plus élevés à la sortie du réseau d'assainissement.

Le coefficient d'imperméabilisation (CoI) a un rôle aussi important dans la CH arrivant à la STEP. Les CH augmentent considérablement avec les CoI. Conséquence de quoi, le facteur climatique et le coefficient d'imperméabilisation apparaissent comme les plus influents sur le temps de noyage de la surface du filtre. Comme attendu, la pente du bassin versant a un impact plutôt dans la distribution de la CH arrivant à la STEP, qui peut aussi affecter le temps de noyage, par contre cet impact reste secondaire en comparaison du climat et du CoI (Figure 12).

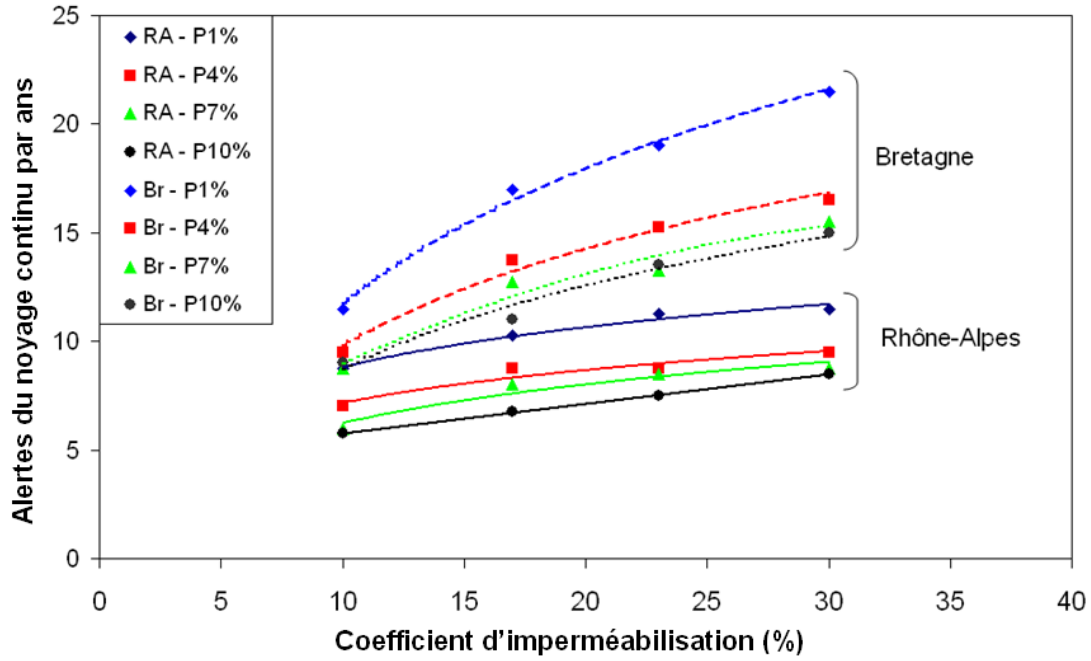

Figure 12 : Nombre d'alertes du noyage en continu par an selon le coefficient d'imperméabilisation et de la pente (P) de bassin versant pour les climats de Bretagne (Br) et Rhône-Alpes (RA) sur une surface de filtre de 1,2 m^2/EH

Un arrêté ministériel actuellement en discussion prévoit de limiter les rejets au milieu récepteur des eaux pluviales non traitées. En conséquence, une gestion optimale des déversoirs d'orage (DO) est requise. Il faut limiter les rejets des déversoirs d'orage sans mettre en danger les performances du filtre. Pour respecter la limite de déversement visée de 20 jours par an, il faudra configurer le DO au minimum à 40 fois le débit nominal de temps sec (DN-TS), selon les modélisations réalisées. Ce seuil de DO permettra quand même de traiter des charges hydrauliques importantes, 8,1 mj^{-1} et 12 mj^{-1} pour le climat Bretagne et Rhône-Alpes respectivement, dans le cas d'un grand CoI de 30% et pentes de 1%, qui est le

scenario le plus problématique. On a pu observer que même si le DO respecte la limite de 20 jours de rejet par an, le filtre peut accumuler de grands volumes d'eau à la surface qui peuvent générer des rejets au niveau du by-pass du 1er étage. Ces rejets au niveau du by-pass peuvent dépasser la limite des rejets imposée. En conséquence, il apparaît plus pertinent d'augmenter le seuil du DO pour permettre de réduire les rejets non traités. En effet, le premier étage du filtre peut fonctionner comme un bassin de rétention, en diminuant ainsi les rejets sans aucun traitement vers le milieu naturel et sans mettre en péril le bon fonctionnement biologique du filtre selon les modélisations.

En conséquence, pour tester les différentes conceptions (surface et hauteur de by-pass) et l'âge du filtre, la configuration sans limitation du DO a été prise, ainsi que le scenario le plus problématique. La Figure 13 permet de comparer, pour le climat de Bretagne, le nombre de jours avec des rejets de by-pass et les alertes de noyages cumulés par an, selon la surface du filtre, la hauteur de by-pass et son évolution lorsque les filtres vieillissent.

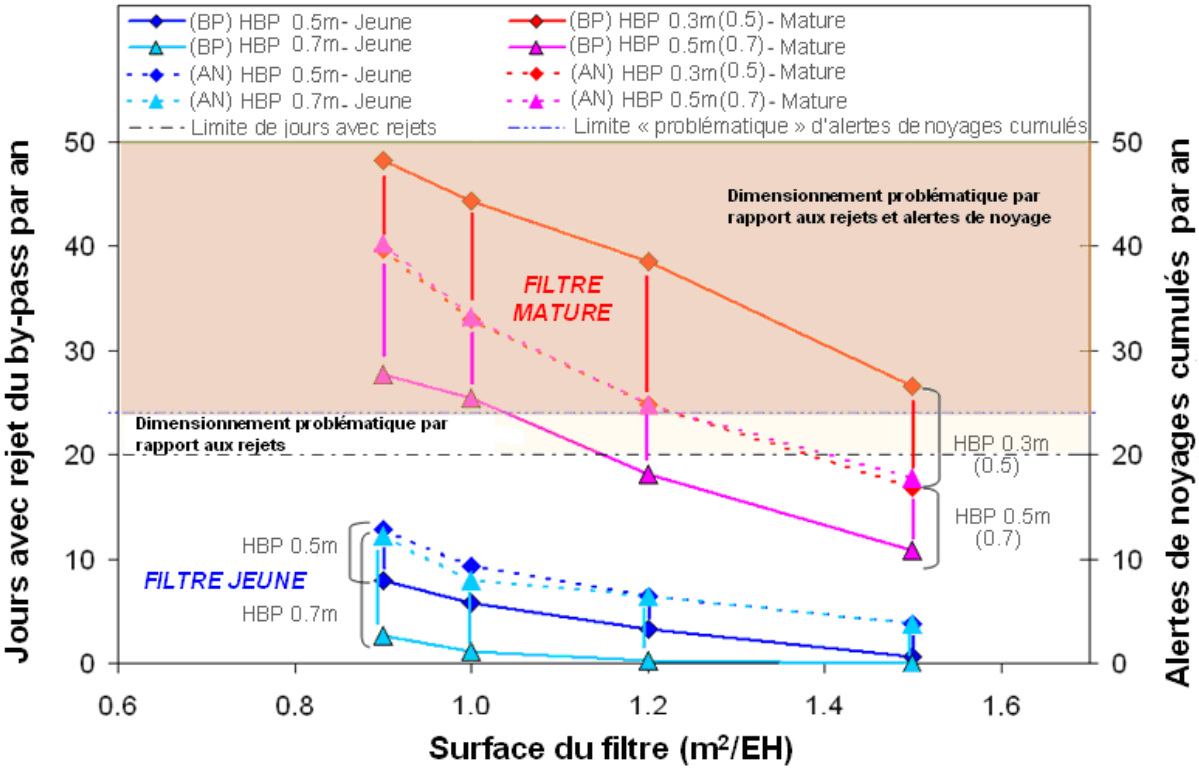

Figure 13: Alertes de noyages cumulés et des jours avec rejet de by-pass selon la surface du 1er étage et la hauteur de by-pass, pour filtres jeunes et matures avec le climat de Bretagne * avec (BP) = rejet de by-pass, (AN) = alerte de noyage cumulé et HBP = hauteur de by-pass

On peut constater que les petites surfaces de filtre (0.9 et 1 m^2/EH) ne sont pas adaptées lorsque le filtre est mature. Cela induit un nombre de jours de surverse au-delà de la limite ainsi qu'un nombre excessif d'alertes qui pourrait être problématique pour une bonne performance du filtre. Ainsi, la surface classique de 1,2 m^2/EH même avec une hauteur de by-pass de 0,7 m tend à avoir des alertes de noyages proche de la limite. La meilleure solution de filtre planté de roseaux, pour le climat Bretagne, peut être la configuration d'une surface de 1,5 m^2/EH avec une hauteur de by-pass de 0,7 m.

Pour le climat de Rhône-Alpes la Figure 14 permet de comparer le nombre de jours de surverse et les alertes de noyages cumulés par an, selon la surface du filtre, la hauteur de by-pass et son évolution lorsque les filtres vieillissent.

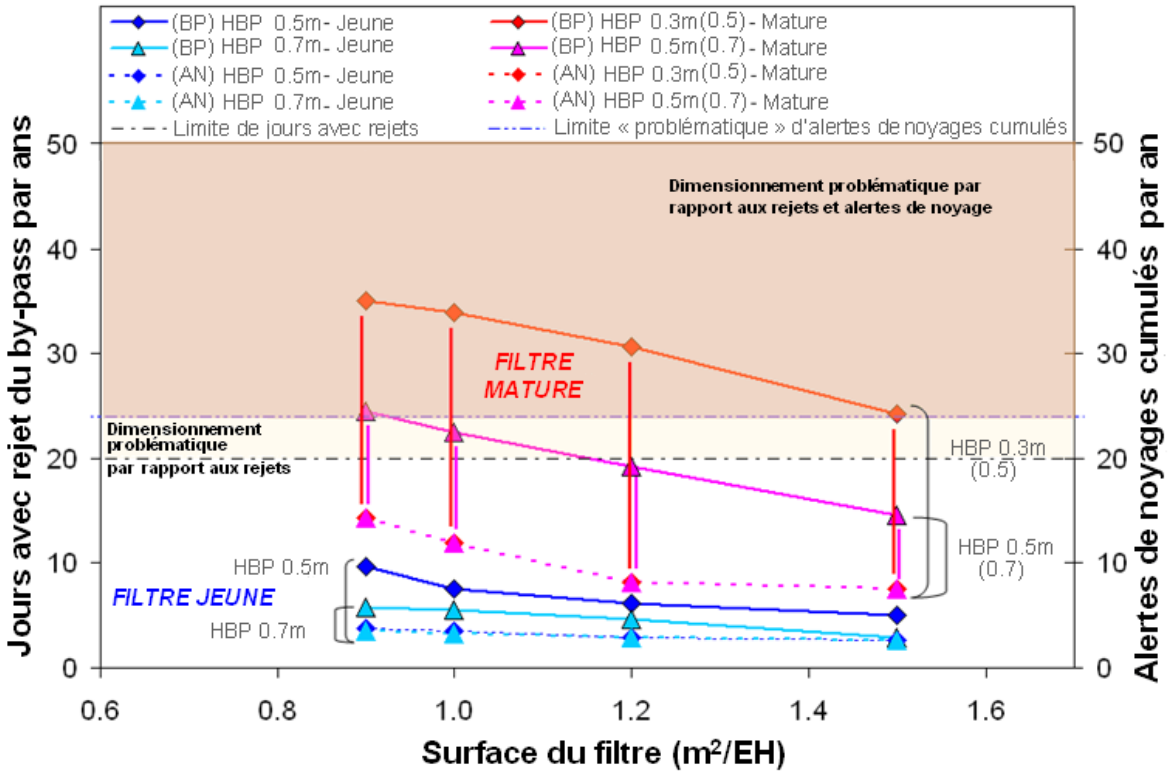

Figure 14: Alertes de noyages cumulés et des jours avec rejet de by-pass selon la surface du 1er étage et la hauteur de by-pass, pour filtres jeunes et matures avec le climat de Rhône-Alpes * avec (BP) = rejet de by-pass, (AN) = alerte du noyage cumulé et HBP = hauteur de by-pass

Pour le climat de Rhône-Alpes, nous pouvons voir que les alertes de noyage sont inférieures à celles du climat de la Bretagne, sans excéder les limites, même sur un filtre mature. Comme dans le climat de Bretagne, les petite surfaces de filtre (0.9 et 1 m^2/EH) ne sont pas adaptées lorsque le filtre est mature, en raison d'un nombre de jours de rejets dépassant la limite. Sur ce type de climat, les surfaces classiques (1.2 et 1.5 m^2/EH) permettent de respecter la limite de rejet, mais seulement lorsque la hauteur du by-pass est de 0,7 m. Par conséquent, une configuration du filtre avec une surface de 1.2 m^2/EH et une hauteur de by-pass de 0.7 m peuvent être appliquées dans des cas défavorables de coefficient d'imperméabilisation du bassin versant et de pente faible de réseau.

Conclusions

Ce travail a permis de développer un modèle hydraulique simplifié, permettant de guider le concepteur pour adapter les FPR-V afin de traiter les eaux usées domestiques de temps sec et temps de pluie. Nous avons développé une méthodologie spécifique pour atteindre ces objectifs. Tout d'abord, nous avons travaillé sur un FPR-V de grande taille (2.000 EH) spécifiquement conçu pour traiter les surcharges hydrauliques et équipé pour un suivi métrologique (hydraulique et performances épuratoires) ponctuel et en continu (2 ans). Les données obtenues ont servi au calage hydraulique du modèle et à établir les alertes de dysfonctionnement utilisées pour la modélisation à long terme. Deux campagnes métrologiques obtenues d'un FPR-V plus âgé ont aidé à l'enrichissement du calage du modèle. Ce modèle a été comparé avec succès à un modèle mécaniste (Hydrus-1D), ce qui permet de renforcer la fiabilité des résultats.

Le modèle simule le temps de noyage d'un 1er étage à différentes périodes de l'année. Le paramètre d'infiltration (ICP) évolue selon les saisons, en raison du développement des roseaux et de la dégradation de la matière organique. Il reste encore à confirmer l'évolution les valeurs ICP du modèle sur des stations différentes et plus âgées, mais dans l'ensemble, la méthodologie développée nous permet d'enrichir la base de données des valeurs ICP aisément par des mesures de débit entrée/sortie et vitesses d'infiltration .

Ce travail de simulation dynamique permet de fusionner la simulation du réseau d'assainissement avec la simulation de l'hydraulique du FPR-V, ce qui nous a permis d'apporter des éléments sur l'incidence du noyage prolongé sur les performances du filtre et de préciser comment les FPR-V peuvent être adaptés pour traiter les surcharges hydrauliques selon les différents contextes locaux.

Au terme de cette étude, les conclusions opérationnelles principales relatives à la gestion des surcharges hydrauliques de temps de pluie sur les filtres plantés de roseaux sont les suivantes :

Pour protéger le filtre contre de longues périodes de noyage sans altérer ses performances épuratoires, il est possible de configurer l'alternance des périodes d'alimentation du filtre de deux manières : (i) une alternance tous les 3,5 jours en condition de temps sec, ou (ii) une charge hydraulique maximale par temps de pluie (100 bâchées) entrant à la STEP. Ainsi, le filtre fonctionnerait sur une règle classique en temps sec et présenterait des alternances plus rapides en temps de pluie pour limiter les flaquages prolongés sur le filtre.

Selon les résultats de la modélisation, gérer les déversements de temps de pluie par le by-pass du premier étage du filtre avec décantation partielle des effluents apparaît plus pertinent que de limiter les volumes d'eau à l'entrée de la STEP par un déversoir d'orage. En effet, le premier étage du filtre fonctionne comme un bassin de rétention, en diminuant ainsi les rejets sans aucun traitement vers le milieu naturel et sans mettre en péril le bon fonctionnement biologique du filtre.

En simulation, les contextes locaux les plus défavorables ont été choisis pour établir des recommandations de dimensionnement (coefficient d'imperméabilisation de 30 %, pente du bassin versant de 1 % et aucune limite au niveau du déversoir d'orage). Nous recommandons, selon le type de climat, les caractéristiques de filtre suivantes :

1. Pour les climats avec des précipitations peu fréquentes mais relativement intenses, comme par exemple le climat de la région Rhône-Alpes :
   - une surface minimale de filtre de 1,2 à 1,5 m² /EH pour des coefficients d'imperméabilisation élevés.
   - une hauteur de by-pass du premier étage fixée à 0,7 m.

   Pour ce type de climat, les alertes de dysfonctionnement restent peu nombreuses mais les rejets du by-pass du premier étage sont le principal problème à résoudre. Une augmentation de la hauteur de by-pass à 0.7 m réduira donc les rejets sans compromettre les performances du filtre.

2. Pour les climats avec des précipitations moins intenses mais assez fréquentes et longues, comme par exemple le climat de la région Bretagne :
   - une surface minimale du filtre de 1,5 m^2/EH.

- une hauteur de by-pass du premier étage fixée à 0,7 m.

Cette augmentation de la surface du filtre permet de diminuer la charge hydraulique et par conséquent le temps de noyage qui est ici l'indicateur le plus critique.

Ces propositions de dimensionnement de filtres plantés de roseaux à écoulement vertical permettront aux petites collectivités d'optimiser leur traitement des eaux de temps de pluie et de temps sec issues d'un réseau unitaire, et de diminuer les rejets au déversoir d'orage en tête de station sans compromettre les performances épuratoires des filtres.

Mots-clés : Filtre planté de roseaux à écoulement vertical, surcharges hydrauliques, performances épuratoires, modélisation simplifié, dimensionnement

Abstract

French vertical-flow constructed wetlands (VFCW) directly treating raw wastewater are known to perform well on for SS, COD and nitrification. They are also known to robustly cope with hydraulic overloads during rainfall events. Although numerous systems have been installed in areas equipped with a combined sewer, the limits of stormwater acceptance remain ill-defined and need to be improved. Looking at the various VFCW designs and usages reported in the literature, it is difficult to draw any consensus on their hydraulic limits.

Consequently, designing VFCW to accept hydraulic overloads is a complex task, as local context strongly impacts inlet flows produced during rainfall events. Dynamic models appear a requisite for filter design in such cases. Numerical CW models have essentially focused on horizontal flow, with few attempting to study VFCW dynamics which are more commonly tackled via mechanistic models. Although mechanistic models are powerful tools for describing processes within the VFCW, they are generally too complicated to be readily used by designers. The choice between detailed description and easy handling will depend on the modelling aims. If the aim is a global design tool, simplified models offer a good alternative.

However, the simplified models geared to studying VFCW dynamics are extremely reduced. They are easy-handling for design and well-adapted to specific purposes (combined sewer overflow -CSO- treatment) but not necessarily to VFCW treating combined sewer wastewater, where long-term infiltration rates vary significantly. Consequently, this PhD thesis work focused on developing a simplified hydraulic model of VFCW to guide designers through the process of adapting VFCW systems to treat domestic wastewater in both dry and rain events.

In order to reliably characterize long-term filter hydraulics, the simplified model has been fitted (i) on a 2-year monitoring period dataset of a young full-scale 2,000-p.e. VFCW specifically equipped for research monitoring and designed to accept rain events, and (ii) on spot measurement campaigns on a mature VFCW filter presenting similar characteristics. The simplified model has been compared to a mechanistic model (Hydrus-1D) to assess its reliability. This simplified model makes it possible to link (i) hydraulics, by simulation of ponding time variations, (ii) biological performances, by establishing “dysfunction alerts” based on treatment performance assessment and variations in online N forms effluent from the young VFCW. These “dysfunction alerts” plot the maximal hydraulic load that a filter can accept without compromising its biological activity.

The simplified model was used to model long-term hydraulics in the VFCW (i) to analyse the impact of local context and filter design on hydraulic overload acceptance (using “dysfunction alerts” and bypass discharges) and (ii) to propose VFCW designs for accepting hydraulic overload in different contexts. The modelling demonstrates that VFCW can limit days with bypass discharges to less than 20 times per year without jeopardizing filter performances. Moreover, the most problematic scenario on stormwater treatment remains a watershed with high imperviousness coefficient and low slope under a Bretagne-type climate, demonstrating that the filter is more sensitive to periodicity and duration than to intensity of rainfall events. The simplified hydraulic model developed in this research requires few input data to be fitted and can use the most basic local context information. This level of simplicity makes it an easy model–tool for designers to use.

Keywords: Vertical-Flow Constructed Wetland, hydraulic overload, treatment performances, simplified model, filter design.

Table of contents

List of figures

List of tables

List of abbreviations

BOD_5 : Biochemical Oxygen Demand after 5 days
BP : By-Pass
BPH : By-Pass Height
Br : Bretagne
CA : Cumulative ponding time Alert
COD : Chemical Oxygen Demand
CSO : Combined Sewer Overflow
CW : Constructed Wetland
DW NF : Dry Weather Nominal Flow
HFCW : Horizontal-Flow Constructed Wetland
HL : Hydraulic Load
HO : Hydraulic Overloads
ICP : Infiltration Capacity Parameter
ImC : Imperviousness Coefficient
IR : Infiltration Rate
Irstea : Institut national de Recherche en Sciences et Technologies pour l'Environnement et l'Agriculture
K : hydraulic conductivity
K_a : apparent dielectric constant
KN : Kjeldahl Nitrogen
K_s : saturated hydraulic conductivity
OM : Organic Matter
OMC : Organic Matter Content
PE : Person Equivalent
PLS: Partial Least Square (regression)
PRESS : Prediction Error Sum of Squares
RA : Rhône-Alpes
RMSEP : Root Mean Square Error of Prediction
S : Slope
SAGE : Schéma d'Aménagement et de Gestion des Eaux
SD: Standard Deviation
SDAGE : Schéma Directeur d'Aménagement et de Gestion des Eaux
SF : Surface-Flow
SS : Suspended Solids
SSF : SubSurface-Flow
Sur : Surface
TDR : Time Domain Reflectometry
VF : Vertical Flow
VFCW : Vertical Flow Constructed Wetland
WFD : Water Framework Directive
θ_r : residual water content
θ_s : saturation water content

1. Introduction

The EU Water Framework Directive (WFD) 2000/60/CE created an agenda for community water management policy searching to improve the chemical and ecological state of natural water bodies. Under WFD, the receiving water body has to reach a "good chemical and ecological state" by 2015, i.e. show "low levels of distortion resulting from human activity, but deviate only slightly from those normally associated with the surface water body type under undisturbed conditions". However, given the different cases and configurations, the framework has had to postpone the deadline to 2021 or even 2027 for certain water bodies. The WFD has been implemented in each Member State according to the characteristics of each particular watershed. In France, the *Schéma Directeur d'Aménagement et de Gestion des Eaux* (SDAGE) is the outline management plan adapting the WFD into national legislation. At local level, it is the *Schéma d'Aménagement et de Gestion des Eaux* — the management plan itself — that requires local water authorities governing small communities to limit the pollutant loads diverted to the natural receiving water bodies.

Consequently, to hit their local treatment objectives, communities have to go further than treat dry-weather wastewater to also treat stormwater if they hope to attain a 'good chemical and ecological state' of receiving water bodies. As stormwater is water runoff from urban surfaces following rainfall over urban catchments (Marsalek J. & Chocat 2002), urban stormwater discharges pose numerous threats to receiving water bodies, including flooding, erosion, sedimentation, temperature rise and species succession, dissolved oxygen depletion, nutrient enrichment, eutrophication, toxicity, reduced biodiversity, and more (Marsalek 1998). Furthermore, particles that accumulate inside the sewer system during dry-weather periods can become eroded throughout the rainfall event (Gromaire *et al.* 2001), adding to the pollutant load arriving at the receiving water body. Stormwater can carry metals, suspended solids (SS) and chemical oxygen demand (COD) in pollutants loads that can equal or even surpass the pollutant loads coming from wastewater treatment plants.

According to the French Directorate for Sustainable Development (2011) figures, in 2008, 56% of French communities have a separate sewer over their entire sewer system, but only a third is dedicated exclusively to stormwater collection, with the rest simultaneously draining dry-weather wastewater and stormwater. Thus, when communities are equipped with a combined sewer system, stormwater treatment remains the key issue. The local water authorities have to decide to what extent it is preferable to adapt the wastewater treatment plant to also treat stormwater rather than engage expensive investment to build a separate sewer systems, at the risk of failing to meet WFD deadlines. Consequently, treatment plant improvement is an adapted solution. In small communities of up to 2000 population equivalents (p.e.), a vertical-flow constructed wetland (VFCW) is a popular solution as it requires no energy and little maintenance. This low exploitation needs and costs, make VFCWs attractive to small communities, where only the investment costs are subsidized.

Furthermore, French version of VFCWs is adapted to treat raw wastewater and perform well on SS removal, COD degradation and nitrification at nominal loads (Molle *et al.* 2005a). More important still, they are also known to robustly cope with hydraulic overloads during rainfall events (Molle *et al.* 2006). Although numerous systems have been installed in areas equipped with a combined sewer, but the limits of stormwater acceptance remain ill-defined and need to be improved. It is necessary to identify the maximal hydraulic loads that can be handled without hampering filter treatment performances (carbon degradation and nitrification) while still respecting the treatment objectives. Over these hydraulic loads,

excessive surface ponding can affect oxygen renewal. Correctly balancing organic and hydraulic load against oxygen renewal in the media is therefore a crucial performance factor in such systems (Platzer & Mauch 1997; Kayser & Kunst 2005). Indeed, the key process securing durable filter operation is to guarantee minimum aerobic conditions to control the growth of the attached biomass and mineralize the organic deposits resulting from SS retention on the top of the filters. Looking at the various VFCW designs and usages reported in the literature, it is difficult to draw any consensus on their hydraulic limits (Cooper 2003; Prochaska *et al.* 2007; Torrens *et al.* 2009).

A first set of rules on hydraulic overload acceptance in French VFCWs showed certain limits that are dependent on rainfall event frequency and intensity (Molle *et al.* 2006). Rainfall event frequency had simply been described in terms of weeks or months, while rain intensity limit had been described by a daily and hourly hydraulic limit. The stormwater acceptance limits have not been sharply defined, and the limitations depend on a host of factors including age of the system, season, sewer characteristics and, of course, climate conditions (the dynamics and duration of storm events). Filter design not only has to accept hydraulic overload but must also minimize surface ponding to ensure the baseline oxygen renewal needed for treatment. Maximal cumulative daytime surface ponding and consecutive surface ponding need to be defined to ensure this baseline oxygen renewal and thus biological activity.

Consequently, designing VFCW to accept hydraulic overloads is a complex task, where local context strongly impacts the inlet flow produced during rainfall events. Dynamic models appear a requisite for filter design in such cases. Most numerical models of constructed wetlands are geared to horizontal flow (Pastor *et al.* 2003; García *et al.* 2004; Małoszewski *et al.* 2006; Tomenko *et al.* 2007), with few attempting to study VFCW dynamics which are more frequently tackled via mechanistic models (Wanko *et al.* 2006; Forquet *et al.* 2009; Freire *et al.* 2009) focused on describing oxygen transport, biomass decay, pollutant kinetics, etc. Some teams, such as Giraldi *et al.*(2010), have developed more complex codes for VFCW, but the most popular code in constructed wetlands (CW) remains Hydrus–CW2D (Langergraber & Šimůnek 2005) which calculates transport and reactions of the main pollutants of municipal wastewater and describes the biochemical elimination and transformation processes involved. Although these mechanistic models are powerful tools for describing processes within the VFCW, they are generally too complicated to be readily used by designers. The choice between detailed description and easy handling will depend on the modelling aims. If the aim is a global design, simplified models offer a good alternative.

However, the simplified models geared to studying VFCW dynamics are extremely reduced (Meyer *et al.* 2008; Ross *et al.* 2011) and are focused solely on CSO treatment. They are easy-handling for design and well-adapted to specific purposes but not necessarily to VFCW treating wastewater from combined sewer systems, where long-term infiltration rates vary significantly. Indeed, there is a pressing need for a simplified hydraulic model of VFCW based on large-scale VFCW permeability data in order to reliably characterize long-term filter hydraulics. Such a model would prove valuable for global design purposes.

To recap, the key questions on VFCW hydraulic overload (HO) acceptance are :

1. What is the maximal ponding time that a filter can accept without jeopardizing treatment performances?
2. Which are the most influential local contexts governing HO acceptance by VFCWs?

3. Which type of climate is most problematic for HO acceptance by VFCWs?
4. Which are the VFCW designs best adapted to HO acceptance?

Consequently, to address these questions, this research work aimed to :

1. **Develop a simplified one-dimensional hydraulic model** simulating the hydraulic behaviour of the first stage of a VFCW, which is the hydraulically limiting step (Molle *et al.* 2006). The model focused on ponding time to link it to treatment performances and analyse the impact of seasons, feeding day and hydraulic load on infiltration rates.

2. **Link VFCW hydraulics to treatment performances** by establishing ponding-time/nitrification-dynamics relationships and, from there, set safe and secure threshold limits ("dysfunction alerts").

3. **Establish the impact of local context** (rainfall conditions, seasons, sewer and watershed characteristics) on VFCW performances.

4. Provide insights and guidance on how to **adapt VFCWs** to optimally treat hydraulic overflows according to local context.

A core objective of the project is to learn more about how to increase HO acceptance without jeopardizing treatment performances in a French VFCW. In addition, the project expects to support designers by providing an easy-to-use model as a decision-aid tool for dimensioning and scaling new French VFCWs according to the specific local-context scenario.

2. Constructed wetlands

Wetlands are areas whose location in the landscape makes them either permanently or seasonally saturated with water. They stay wet long enough to exclude plants species that cannot grow in saturated soils and to alter soil properties via the series of chemical, physical, and biological changes that occur during flooding (Kadlec & Wallace 2009).

Constructed wetlands are engineered systems designed and constructed to utilize the natural processes that take place in wetland vegetation, soils and their associated microbial assemblages to assist in treating wastewater (Vymazal 2007). They are designed to exploit many of the processes that occur in natural wetlands but to do so within a more controlled environment (Hammer 1989). Although originally used to treat domestic and municipal wastewater, constructed wetlands are now employed to treat a large variety of wastewaters including stormwater runoff, industrial wastewater, agricultural sewage, leachate, and more.

According to Fonder & Headley (2013), CW can be categorized under various design parameters (Figure 15), but the two most important criteria are hydrology (flow direction, media saturation and influent loading) and vegetation (type of macrophyte growth).

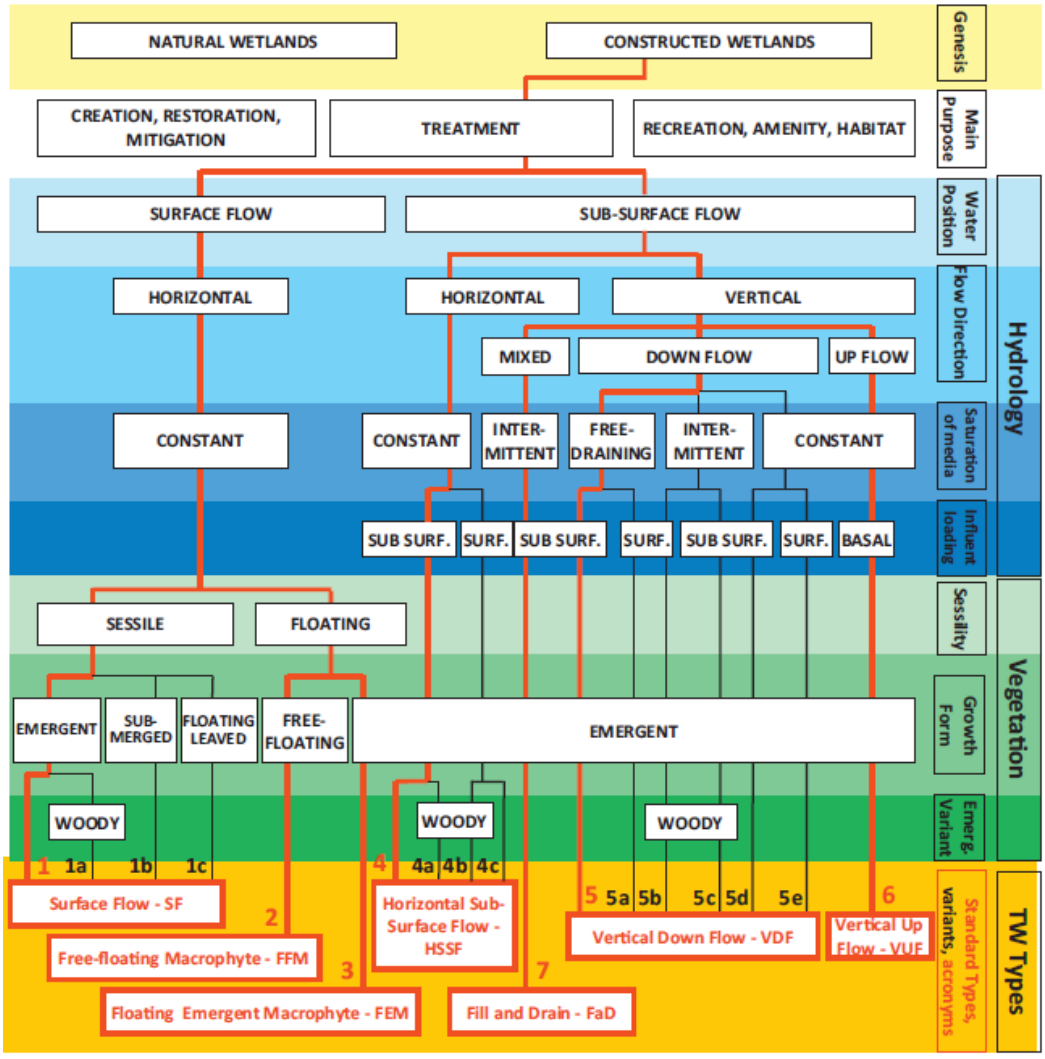

Figure 15: Classification of CW for wastewater treatment according to Fonder & Headley (2013).

Average removal efficiencies are lowest for surface-flow (SF) CW, mainly due to the limited contact with the soil or filter medium, whereas the best all-round performances (total nitrogen removal is poor) are recorded in subsurface-flow (SSF) CW, especially vertical flow systems (Rousseau *et al.* 2004).

This study is focused on SSF-CW. In agreement with hydrology-based criteria, SSF-CW are classified as :

- Horizontal-Flow Constructed Wetland (HFCW) — this CW commonly uses a gravel filter with planted vegetation, with flows passing through the bed horizontally in a saturated medium.

- Vertical-Flow Constructed Wetland (VFCW) — composed of a gravel or sand filter, with planted vegetation. The water is distributed homogenously onto the surface, and flows vertically in an unsaturated medium.

In France, the Cemagref [French environmental and agricultural land management research institute] developed the first filters built at Saint Bohaire (Lienard 1987). The system then expanded rapidly across the country during the 1990s, and SSF-CW have since gained a good reputation as a solution for small communities in France (Molle *et al.* 2005a), made popular due to its low running costs and requirements ideally geared to smaller communities where only investment costs are subsidized.

2.1. Subsurface CW

2.1.1. Vertical-flow

VFCW consist of a filter of porous medium through which water flows down vertically (inlets are located vertically above outlets). Most VFCW systems are set up free-draining (numbers 5 and 5a on Figure 15) and spend most of the time unsaturated (Fonder & Headley 2013). This subsurface flow system harnesses a biological aerobic treatment using the bacteria that grow onto the porous medium of the filter. The filter is generally a watertight excavation filled with different material layers (gravel or sand) at a grain-size that increases along the depth of the bed. The deepest layer of medium features a network of perforated drainage pipes ventilated to the atmosphere to promote passive aeration of the substrate (Cooper *et al.* 1996). In Europe they are mostly planted with reeds (*phragmites australis*). The system is developed to provide high levels of oxygen transfer by convection (batch feeding) and diffusion to enable full nitrification. Intermittent feedings (batches) are assured via a network of pipes with multiple outlets, either placed within the filter or distributing the flow across its upper surface.

The system is usually fed with pre-treated water -the ‘settling’- phase (Brix & Arias 2005) – with a first infiltration layer of the filter composed of sand (Brix 1994a), but in France the system has been adapted to treat raw sewage (Lienard 1987, 1990) and demonstrates good performances. The vertical filter needs a second stage to obtain good nitrification and organic matter removal rates (Molle *et al.* 2005a). As our study was carried out on a French system, we provide a more detailed description of this system below.

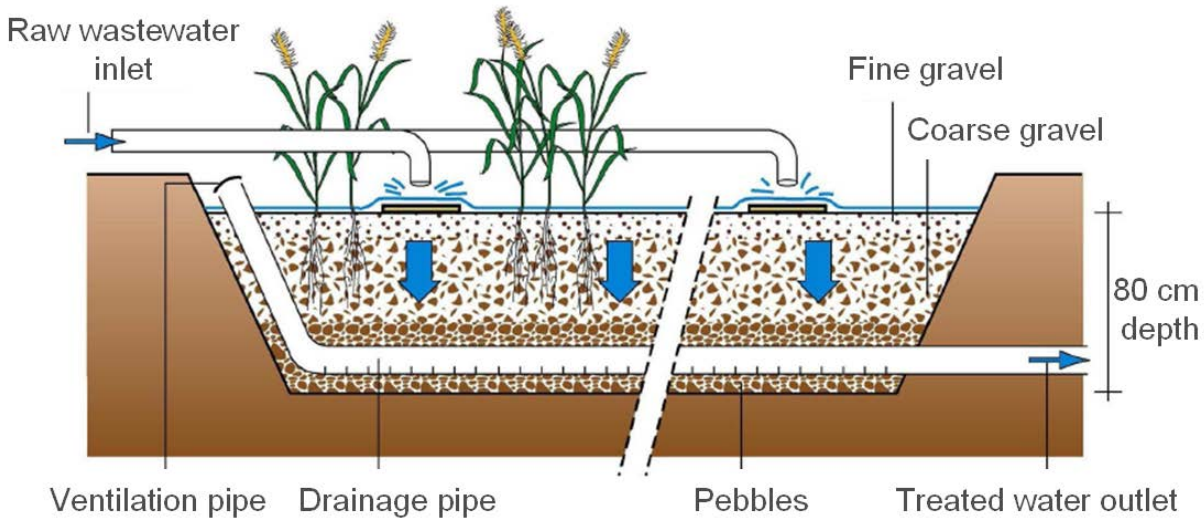

Figure 16: Transverse-view schematic illustration of a French VFCW, adapted from Iwema *et al.* (2005)

The French system is composed of two VF stages, the first stage built of three stacked cells and the second stage built of two parallel cells, as recommended by French guidelines (Molle *et al.* 2005a). Each cell in the first stage is fed for 3.5 days with a 7-day rest period, while the second stage is fed for 3.5 days with a 3.5-day rest period. The alternating feeding and rest periods are essential to (i) control the growth of the attached biomass on porous filter medium, (ii) minimize clogging due to mineralization of the organic deposits by suspended solids (SS) contained in the raw sewage which are retained on the surface of the primary-stage filters (Lienard 1990), and to (iii) maintain aerobic conditions within the filter.

Most filters are composed of three or four material layers. The first layer of the first stage is built of fine gravel while the first layer of the second stage is built of sand (Figure 17). These layers play a crucial physical and hydraulic role in the system, conferring the permeability needed to control both solid filtration and infiltration rate. The other layers play a transition and drainage role.

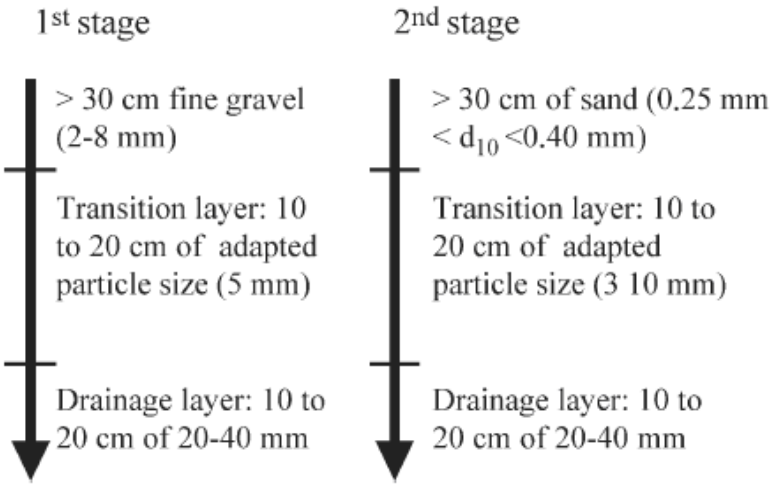

Figure 17: Grain size and depth of material layers on French VFCW's (Molle *et al.* 2005a)

Each treatment stage has specific characteristics and plays a different role in treatment. Flow infiltrated through the porous medium of the first stage undergoes a first treatment step via SS retention at the surface and superficial infiltration layer. SS retention promotes the formation of a sludge layer at the surface that increases by about 1.5 cm per year (Molle *et al.* 2005a). Sludge is highly mineralized thus not fermentable. This deposit layer tends to decrease the infiltration rate of filter, allowing a long contact time between the wastewater and the aerobic biomass fixed in the non-saturated medium but at the same time diminishing oxygen transfers. In this stage, treatment mainly concerns SS and COD removal due to the rich oxygen supply of VFCW. This promotes higher carbon degradation than nitrification, however it does enable measurable total Kjeldahl nitrogen (TKN) removal (≈ 50–60%).

The second stage polishes off the carbon degradation and SS retention processes, but its primary role is to complete nitrification. Low COD concentrations mean there is more oxygen available in the medium and consequently less competition for oxygen between nitrification bacteria and carbon-degrading bacteria. The low SS content in the second stage means no sludge layer develops at the surface, so an infiltration layer with a finer grain-size is required to control infiltration. In French systems, the d_{10} of the sand has to be between 0.25 mm and 0.40 mm.

Batch feeding promotes extra in-filter oxygenation due to convection phenomena occurring during water displacement into the filter and gaseous diffusion from the atmosphere via the surface when dewatering occurs. VFCW thus provide greater oxygen transfer into the bed, consequently producing a nitrified (high NO_3) effluent (Cooper & Green 1995). Nitration and nitrification can only proceed if the medium contains enough available oxygen. Oxygen consumption during these two steps is less than 4.3 gO_2 per gram of NH_3-N (Metcalf & Eddy 1998). On the other hand, VFCW do not provide suitable conditions for denitrification, which can only occur under anoxic conditions, and the complete conversion of NO_3 to gaseous nitrogen forms able to escape to the atmosphere cannot be completed (Vymazal 2011).

The French system visibly requires a feed flow of at least 0.6 $m^3.m^{-2}.h^{-1}$ to ensure satisfactory distribution for the first feeding after a rest period, when infiltration rates can be greater than 1.4 $10^{-4} m.s^{-1}$ (Molle 2003). This feeding flow level ensures good sludge and water distribution on the filter. Iwema *et al.* (2005) recommend a maximum of 50 m² of surface for one feeding point to ensure good water distribution at the first stage and avoid short-circuits in porous media. Furthermore, the height of surface water produced at each batch has to be between 2 and 5 cm. Below 2 cm, equal distribution becomes difficult, while above 5 cm, infiltration rate increases and preferential flows get stronger, which decreases treatment performances. Molle *et al.*(2005a) studied more than 80 VFCW in France and found that an overall surface for both stages of 2 m².PE is a prerequisite in order to attain sufficient nitrification. Surface sizes greater than 2.5m².PE do not appear to improve removal rates.

Although the VFCW system achieves high organic treatment and nitrification performances, it only gives low phosphorous removal due to the need to mineralize organic matter and the fact that the media/phragmites cannot significantly adsorb phosphorus given the loads applied (Brix 1997). A study found high phosphorous removal performances on domestic wastewater by a VFCW just put into operation, but P removal fell to 20% once the mineral adsorption sites were saturated and even cases of P release produced by hydraulic overload. However, research teams are seeking out alternative materials for phosphorous sorption (Prochaska & Zouboulis 2006; Prochaska *et al.* 2007; Harouiya *et al.* 2011; Vohla *et al.* 2011). According to Arias & Brix (2005), under the usual design parameters for VF systems (approx. 2.5 m² P.E.

and a 1 m bed depth), using sands with high Ca content could remove P for approximately 5 years, which represents high material volumes, but removal efficiency would then decrease over time until effluent concentration eventually exceeds discharge demands. Other materials, like apatite, shows good potential in terms of kinetics and saturation capacity, making it possible to use relatively small volumes of material for long-term P removal (Molle *et al.* 2005b). France already has a set of guidelines on P removal by apatite (Molle *et al.* 2011).

2.1.2. Horizontal flow

HFCW is the most widely used CW concept in Europe (Vymazal 2005). HFCW features biological anaerobic treatment. The design typically consists of a rectangular filter planted with common reed and lined with an impermeable membrane. The filter is completely saturated, and a water level control structure at the outlet adjusts in-bed water height to maintain saturated conditions in the filter during feedings without any surface flooding.

The system uses gabions (pea gravel) at the filter inlet and outlet to improve water distribution and recovery. Feeding can be continuous, although the distribution system needs to properly spread water across the full filter width. As this kind of filter is more sensitive to clogging, a pre-treatment is necessary to remove solids.

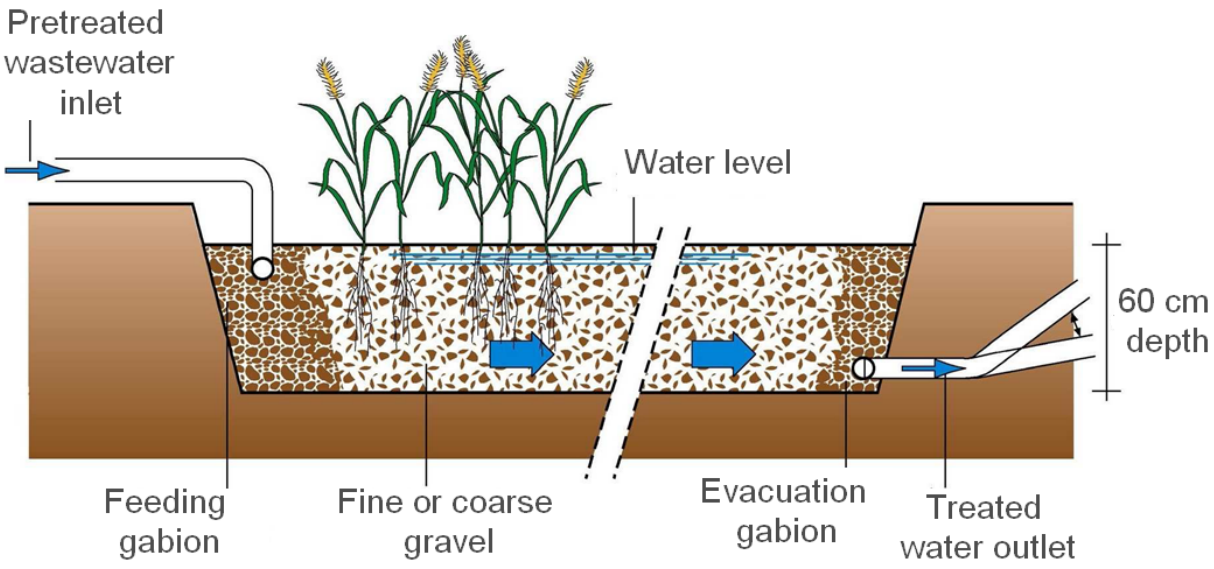

Figure 18: Transverse-view schematic illustration of a HFCW, adapted from Iwema *et al* (2005)

2.2. Filter components and their roles

Efficiently running a CW hinges on finding a balance between the different mechanisms at work in the filter (hydrodynamics, gas transfers, biological activity, reed activity, etc.) that interact with physical, biological and chemical mechanisms to maintain a balance in the system. Each component plays an important role in filter dynamics, where the most important processes CW are based on physical and microbial processes. The active reaction zone of CW is the root zone (or rhizosphere) which plays host to physicochemical and biological processes

induced by the interaction of plants, microorganisms, soil and pollutants (Stottmeister *et al.* 2003). As shows Figure 19, system performances and reliability are dependent on a number of parameters, some of which are controlled (design, operation) and others uncontrolled (climate) or "predictable" (Molle 2012).

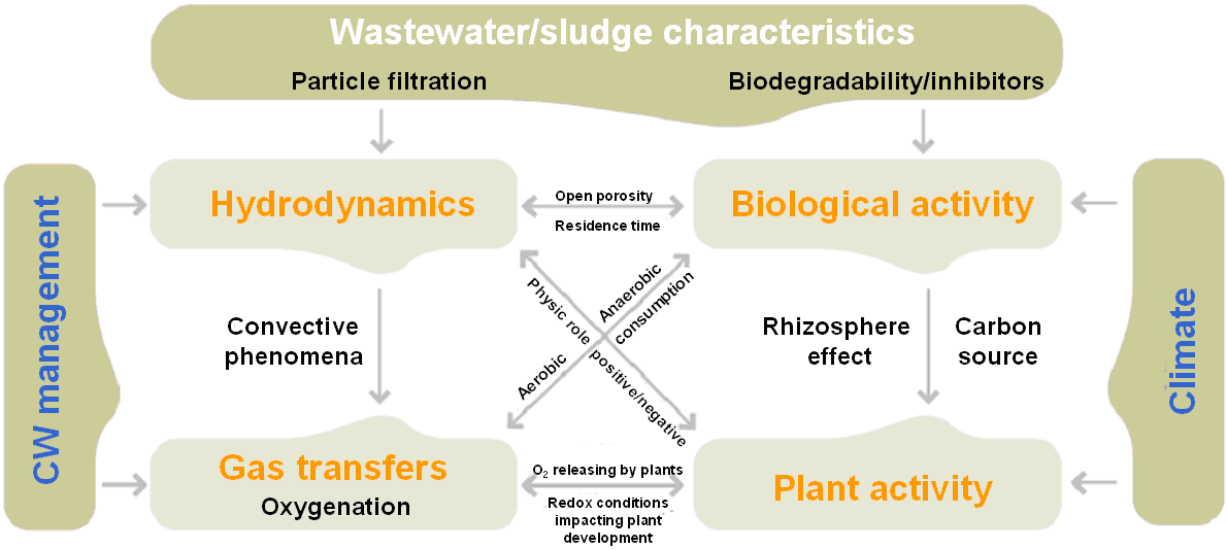

Figure 19: Interactivity between internal and external CW components, adapted from Molle (2012)

Hydrodynamics and gas transfers will be discussed in detail in chapter 2.4, but it is important here to briefly discuss the role of other components.

2.2.1. The role of plants

In the first stage of a French VFCW, the main impact of plants is mechanical, due to the dense development of stems that pierce the superficial deposit layer to create pathways from the outside air to the gravel layer below. Stems allow water to infiltrate through the hydraulically-limited deposit layer and, if there is no ponding, they allow air to transfer to the gravel layers. In winter, when reeds are harvested, the stems lose their mechanical role and the deposit layer becomes the limiting step for water and gas transfers. At this point, water flow is governed by the hydraulic conductivity of the deposit layer, water pressure shaped by ponding depth, and suction into the filter (see chapter 2.4.1). These parameters combine to ensure a stable infiltration rate. The mechanical role of plants is visible in the increasing infiltration rates with reed growth (Molle *et al.* 2006). Reeds also permit the filter to dewater during rest periods.

This mechanical effect of plants keeps the filter surface open to water and gas transfers and prevents clogging via organic matter mineralization. Nevertheless, as filters are fed by raw wastewater in the French system, an alternation between filters is necessary to mineralize the high organic matter loads applied on the filters.

The CW plants play other important roles :

- They add the bacterial density and diversity that give robustness to the system. The biofilm attached to the root system, dead reed material and porous media is largely responsible for the microbial processing occurring in system (Brix 1997).

- Their insulation impact, as the dead still-standing reed material shields the surface from winter frost (Brix 1994b). In summer, foliage coverage stops the filter drying out by providing shadow that helps bacteria develop and organic matter to mineralize.

- They assimilate nutrients. Also termed "phytopurification". Note that this kind of system as developed in France, cannot attribute plants a real nutrient removal role and nutrient assimilation stays too insignificant given the loads applied.

- Their oxygenation role. Although the roots do release oxygen into the rhizosphere that can influence the bacterial community (Barko *et al.* 1991; Sorrell & Boon 1992), the oxygen transfers involved are too insignificant given the treatment needs of the high load applied. According to Brix (1997), the non-homogeneity of oxygen release by roots makes it difficult to calculate oxygen flux. Various authors have given flux assumptions ranging from 0.002 $g.m^{-2}.d^{-1}$ (Brix 1990) to 5-12 $g.m^{-2}.d^{-1}$ (Armstrong *et al.* 1990). This large range of differences could be explained by the diversity in measurement techniques used and sampling seasons studied. However, these oxygenation rates should be compared to the 300 g of COD and about 150 g of oxygen necessary to nitrify KN per day and per m² on the first stage of the French system.

2.2.2. Microorganisms

The medium is the main substrate for bacterial growth in CW. The particle size of the media defines pore space and thus surface area for biofilm growth. Microorganisms are the main drivers of nutrient and organic matter transformation and mineralization (Stottmeister *et al.* 2003). Bacterial development is tends to be carried out in the top 10% of filter layers (Tietz *et al.* 2007). The zone where the endorhizosphere (the root interior) and the ectorhizosphere (the root surroundings) meet is known as the rhizoplane. It is in this area that the most intensive interaction between the plant and microorganisms is to be expected. Morvannou *et al.* defines the first 20 cm in the French system as a very biologically-active zone. This does not mean the under-layers are not important. Headley *et al*. highlighted that deeper filters yield better performances, especially for nitrification.

Microorganisms present in the root system can be under numerous forms, as biofilm, bacterial colonies or without specific geometric form. They contribute to organic matter degradation and excrete other more biodegradable lower-molecular-weight matter. The microbial transportation processes are typically strongly dependent on water temperature, thus creating seasonal patterns of microbial transformation (Kadlec 1999).

Nitrification is the main process of nitrogen treatment in VFCW and is typically associated with the chemoautotrophic bacteria (*Nitrosospira, Nitrosovibrio, Nitrosolobus, Nitrosococcus and Nitrosomonas*), that derives energy from the oxidation of ammonia (and or nitrite) using carbon dioxide as carbon source to synthesize new cells. As the nitrification process is highly sensitive to physical-chemical conditions (temperature, oxygen content, carbonate content, inhibitors), it is common practice to monitor limitation conditions in aerobic processes as a

process parameter. Nitrification involves two steps: one oxidizes ammonium-N to nitrite-N, in a step executed by chemolithotrophic bacteria (strictly aerobic) and nitrite-N, and the other step oxidizes nitrite-N to nitrate-N. This second step is also performed by chemolithotrophic bacteria that can use organic compounds. Thus one species of nitrite-oxidizing bacteria – *Nitrobacter winogradskyi* (Grant & Long 1981), cited by Vymazal (2007) – is found in both soil and freshwater.

Among classical limitations that can hinder nitrification, it seems necessary to precise the one concerning temperature, oxygen content and carbonates content.

- *Temperature* : The optimum temperature for nitrification ranges from 25 to 35°C in pure cultures and from 30 to 40 °C in soils. Cooper *et al.* (1996) put the minimum temperatures for *Nitrosomonas* and *Nitrobacter* growth at 5 and 4°C, respectively.
- *Oxygen content* : The process needs approximately 4.3 mg O_2 per mg of ammoniacal nitrogen oxidized to nitrate-N (Metcalf & Eddy 1998).
- *Carbonate content* : A large amount of alkalinity is consumed, approximately 8.64 mg HCO_3^- per mg of ammoniacal nitrogen oxidized (Cooper *et al.* 1996).

2.3. Dry period/stormwater runoff treatment by VFCW

2.3.1. Dry periods

In dry periods, the French system demonstrates good all-round treatment performances on SS removal and COD degradation at nominal loads, with removal efficiencies of 95% and 91%, respectively, and > 85% for TKN according to Molle *et al* (2005a). Classical removal performances of the French system are presented in the Figures 20, 21 and 22, in relation to organic load for the first stage (100% removal represented by the dotted line).

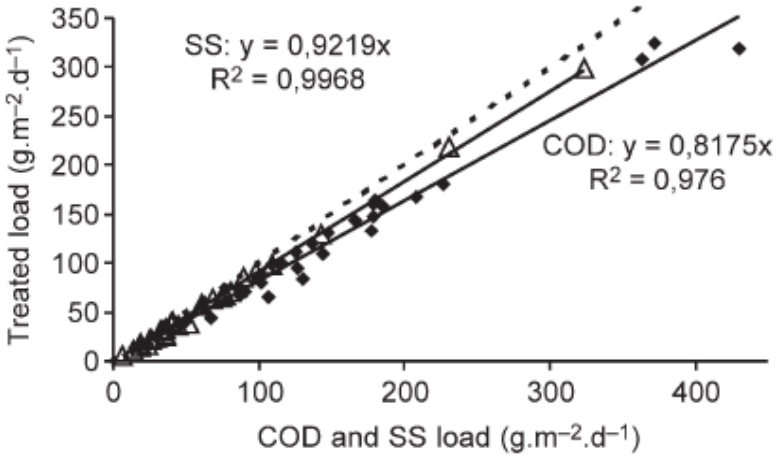

Figure 20: COD and SS treated on the first stage: at COD concentrations between 520–1400 mg.L-1, 0.15 < HL< 0.6m.d-1 (Molle et al. 2005a)

Note that even at higher-than-nominal organic loads, COD and SS removal performances stay stable (Figure 20 and 21). For nitrification, at nominal loads, about 50%–60% of removal

rates are measured on the first stage, and load level appears to impact nitrification efficiency (Figure 22).

The second stage improves SS and COD treatment performances. For COD removal, high hydraulic loads seem to decrease treatment efficiency (Figure 21). The reasons put forward to explain this negative relationship include (i) lower water retention time and (ii) low pollutant concentrations at the inlet of the second stage during rain events.

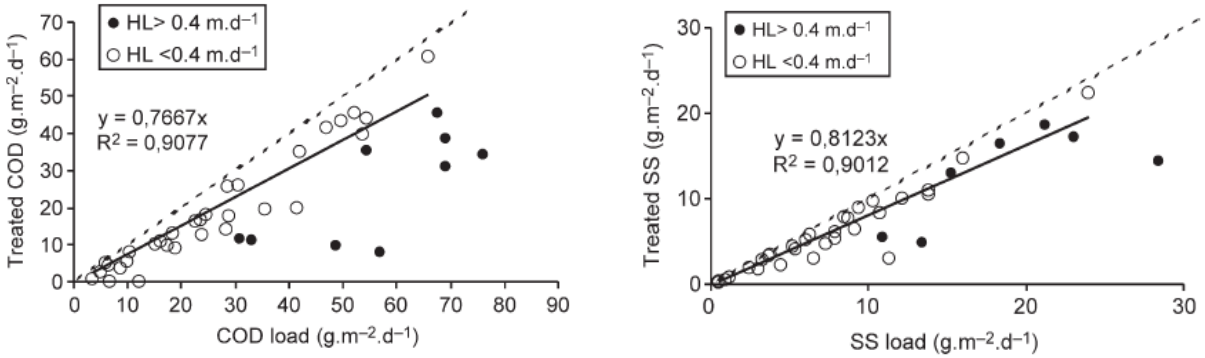

Figure 21: COD and SS treated on the second stage at different hydraulic loads (Molle et al. 2005a)

While performances appear to stay stable with organic load for COD and SS under dry weather flows, the decreasing nitrification performances with increasing nitrogen load translates a different pattern of nitrogen dynamics and transformation in the filter.

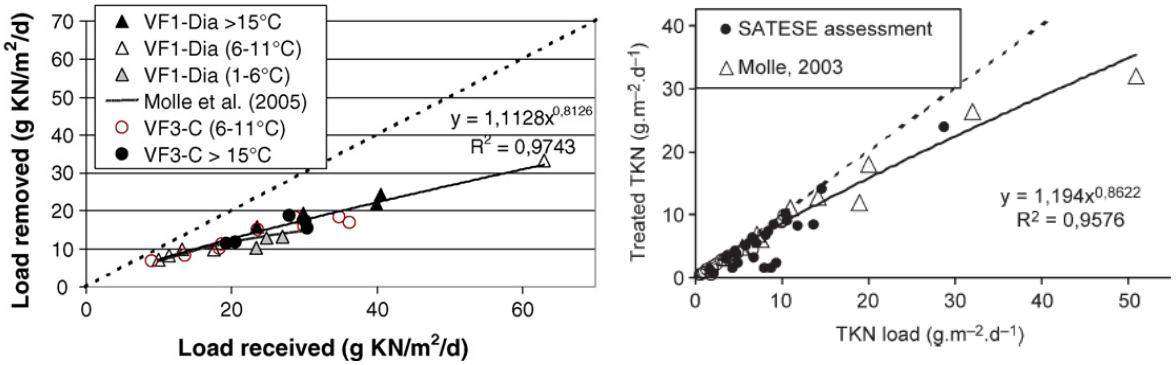

Figure 22: Treated KN on the first stage (filters with aeration drains at the bottom + intermediate aeration pipes –Dia- and classic filter –C- at different temperatures with HL 0.39 m.d-1) at left (from Molle *et al.* (2008) and on the second stage (0.05 <HL < 2.2m.d-1) at right (adapted from Molle *et al.* 2005a).

As KN formed at the inlet is mainly dissolved (about 70% under NH_4-N), the filtration efficiency of the filter has less impact. Consequently, nitrification performances depend on processes that mainly impact the dissolved fraction. Molle *et al.*(2008) and Morvannou (2012) showed that if a share of ammonium is directly nitrified, adsorption onto organic matter is a key factor. The increasing N load diminishes the share of ammonium adsorbed onto media due to saturation of adsorption sites. In addition, the increase in oxygen consumption with increasing organic load preferentially affects nitrification over COD removal. Oxygen renewal can also be reduced by a higher number of batches and greater ponding time and depth during storm events, which reduces oxygen renewal and thus nitrification. Ammonium adsorption during feeding periods is assumed to be a major factor. Loads of 10 (first stage) and 15 TKN $g.m^{-2}.d^{-1}$ (second stage) seem to be thresholds from which nitrification decreases

drastically. Nitrification is also affected by batch volume (Molle *et al.* 2006): higher batch volumes mean greater preferential flows, thus decreasing the proportion of adsorbed ammonium.

2.3.2. Stormwater

Stormwater is water running off urban surfaces after rainfall over urban catchments (Marsalek J. & Chocat 2002). Urban stormwater discharges have numerous adverse effects on both urban areas (flooding) and on receiving waters (flooding, erosion, sedimentation, temperature rise and species succession, dissolved oxygen depletion, nutrient enrichment, eutrophication, toxicity, reduced biodiversity) (Marsalek, 1998). Also, particles that accumulate in the sewer system during dry weather periods get eroded throughout the rain event proportionally to the energy of the flow (Gromaire *et al.* 2001), thereby increasing pollutant load. Stormwater treatment is therefore vitally important, particularly as the pollutant load of metals, SS and COD carried by stormwater runoff can sometimes prove heavier than the pollutant loads coming from wastewater treatment plants.

Stormwater characteristics vary strongly according to geographic area, local features, length of dry period before a rain event, intensity and duration of the rain event, local atmospheric pollution sources, topography, soil pollutant deposits, and other factors, as shown in Table 5. The net result is that urban runoff is more difficult to characterize than wastewater (Lee & Bang 2000), making the treatment of stormwater a truly complex task.

Table 5: Range of event mean SS, VSS, COD and BOD5 concentrations in different types of rain-event runoff from a French urban catchment (Le Marais, Paris) with a combined sewer system, and comparison against average rain-event concentrations quoted in the literature (Gromaire *et al.* (2001)

		SS (mg l^{-1})			VSS (mg l^{-1})			COD (mg l^{-1})			BOD5 (mg l^{-1})		
		10%	median	90%	10%	median	90%	10%	median	90%	10%	median	90%
Roof runoff	Marais	6	17	74	3	7	26	12	27	73	2	4	13
	Literature (1)		(5)–(30)			—			(3)–(40)				
Yard runoff	Marais	13	40	152	8	23	64	31	63	213	6	14	29
Street runoff	Marais	53	97	276	29	51	152	74	135	391	15	31	71
	Literature (2)		(45)–(937)			—			(77)–(146)				
Sewer outlet	Marais	121	221	519	87	140	331	190	331	639	81	139	262
	Literature (3)		(152)–(670)			—			(114)–(570)			(48)–(270)	

Note: (1) Sakakibara (1996), Shinoda (1990), Artières (1987), Boller (1997) and Xanthopoulos and Hahn (1993). (2) Constant (1995), Ranchet *et al.* (1993), Balades *et al.* (1994), Gautier (1998), Xanthopoulos and Hahn (1993), Herrmann *et al.* (1992). (3) Hoghland *et al.* (1984), Geiger (1986), Saget (1994).

2.3.3. Impact of rain events on filter behaviour

Wastewater characteristics and the resulting increased flow during rain events can impact the performances and durability of the filter. Storm events will :

- increase the number of batches on the filter, thus decreasing the between-batch oxygenation period,
- influx the filter with a higher amount of solids, with a risk of clogging,
- reduce the water retention time of the constituent pollutants.

The higher number of batches produced by a storm event increases filter ponding height and ponding time. It also alters retention time due to the pressure exerted by hydraulic head variations, which plays a key role in infiltration processes (Beach et al. 2005). Consequently, the proportion of water that passes directly from filter inlet to filter outlet by preferential flows increases with hydraulic load and with batch volume, limiting ammonium adsorption efficiency. Nitrification efficiency appears to be a good parameter to evaluate the impact of rain events due the sensitivity of nitrification with adsorption rate and oxygen content that are both affected by hydraulic loads. The upshot is that good stormwater treatment performance in VFCWs is a trade-off between oxygen renewal and hydraulic load acceptance.

Studies show good treatment performances of VF with low hydraulic overloads of pre-treated water (up to a 2.6-fold dry weather load; (Avila *et al.* 2013). In experiments on French VF systems, Paing & Voisin (2005) observed no significant differences in effluent quality (first and second stage) for hydraulic loads varying between 0.2 and 3.2-fold the nominal capacity and for organic loads between 0.2 and 0.96-fold the nominal load. One likely explanation is that hydraulic loads lightly higher than the nominal load can improve flow distribution in the system, increasing the filter surface in contact with the pollutant without penalizing oxygen renewal and retention time, resulting in a net improvement of treatment efficiencies. According to Molle *et al.* (2006), no infiltration problems are observed after hydraulic overloads of 4 $m.day^{-1}$ (>10-fold the dry weather hydraulic load). Rain events can be handled while staying within the quality objectives set for the respective receiving water body (COD: 125mgL^{-1}, BOD5: 25 mgL^{-1}, KN < 10 mgL^{-1}).

However, while hydraulic overloads may be physically acceptable on filters, constant ponding can be unfavourable for biological activity due to a lack of oxygen renewal. The issue here is HO acceptance limits to maintain good treatment performances through to satisfactory oxygen renewal rates. The minimum in-filter oxygen transfer rate would be 28 gO_2/m^2 day according to Platzer (1999), since it takes 4.3 gO_2 to oxidize 1 g TKN. Forquet *et al.* (2009) affirmed that oxygen renewal in VFCW is mostly dependent on HL and number of batches per day, and showed that the threshold value (up to 170 gO_2/m^2 day) above which a linear relationship between HL and oxygen income by convection breaks down depends on the number of batches per day, and that over this value, oxygen renewal by convection becomes limited. Consequently, oxygen renewal by convection might be a limiting factor at high HL.

This capacity to support variations in organic and hydraulic loads is a strong advantage of the VFCW, but hydraulic load acceptance limits still have to be defined

2.4. VFCW dynamics

As presented earlier, hydrodynamics greatly affects the biological processes of the system as well as in-system oxygen transfers. Here we look at filter hydrodynamics and the parameters that influence it.

2.4.1. Hydrodynamics on VFCWs

2.4.1.1. Water flow through porous media

A porous medium is a polyphasic environment containing air, water, medium, and biomass that involves complex nonlinear fluxes at a variety of velocities. Filter water movement is shaped by different mechanisms involving energy and water potentials where water moves from high-energy-potential points to low-energy-potential points. The intermittent feeding of VFCW complexifies the filter hydraulics, creating variably saturated conditions. For saturated conditions, gravity is the main force controlling flow, whereas in unsaturated conditions matric forces (capillarity and hydration) in addition to gravity are the principal forces controlling in-filter flow (Figure 23).

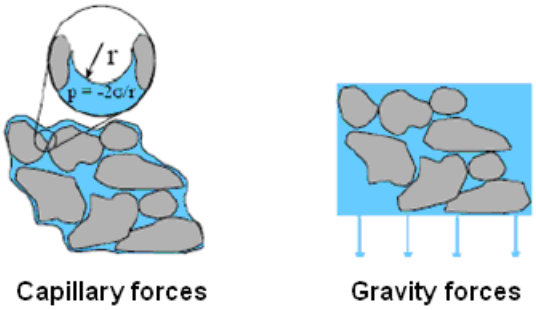

Figure 23: Schematic illustration of the main forces controlling water flow in porous media, adapted from Vincent (2011)

The interface separating two immiscible fluids is the site of energy or tension that stems from the fact that the molecules of each phase are attracted to each other via the contact surface. This tension creates superficial forces at the water/air interface, and the curvature of this interface produces a differential pressure between the liquid and gaseous phases. Differential pressure can be calculated by Laplace's law :

$$\Delta p = \sigma\left(\frac{1}{R}+\frac{1}{r}\right) \qquad \textbf{Equation 2}$$

where R and r are the radii of curvature surface, σ is the constant of superficial tension, and Δp is the pressure differential created by the curvature of the surface.

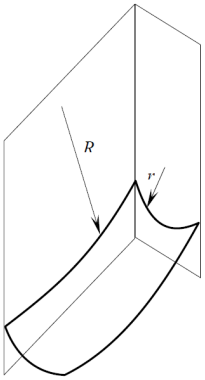

Figure 24: Radii of surface curvature

The interface is convex in the water phase, which is thus in depression in relation to the air phase. Thus, taking atmospheric pressure (g) as reference, capillarity pressure (ψ) in water is given by :

$$\psi = -\frac{\Delta p}{\rho g}$$ **Equation 3**

When soil water content decreases, water is first stripped from the largest pores and remains connected to smaller-diameter pores. The radius of curvature of the interface decreases, and thus the differential pressure increases as the soil dries.

As flow velocities in soil are pretty low, the energy state of the liquid phase is mainly potential. Consequently, the concept of total potential energy can be used to quantify the energetic state of water and describe its movement in soil. The sum of capillarity forces, gravity forces plus osmotic and geostatic forces (the last two are negligible) is defined as total water potential, currently expressed as the pressure exerted by a vertical height column (H).

$$H = h + z$$ **Equation 4**

where

h = matrix pressure
z = depth

In an unsaturated soil, water infiltration and evapotranspiration mean that water content is lower in the shallower layers of the filter, with a non-constant load. The intensity of retention forces and the resulting matrix potential are dependent on the water content, thus promoting space-time variation of motion forces. Figure 25 presents the relationship between volumetric water content and pressure potential, called the water-retention curve, which is a key curve in the study of hydraulics in unsaturated soils

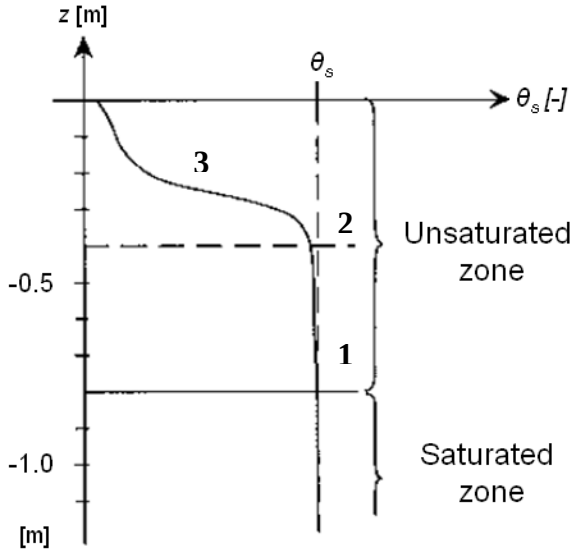

Figure 25: Hydraulic profile, adapted from Musy & Soutter (1991)

A soil water-retention curve can be divided into three parts :

1. The part near the saturation water content (θ_s), where the curve is practically vertical, corresponding to the capillary fringe.
2. The point where the slope of the curve is relatively low (entrance of air).
3. The part where slope becomes higher as we approach the residual water content (θ_r). The gradual drying of the soil produces a weaker radius of curvature of interfaces.

Water under the influence of capillary and gravity forces shows two opposing drainage behaviours that are nevertheless complementary to filter hydraulics. When porous media has a high water content, the gravity forces control water infiltration and hydraulic conductivity (K) progresses according to water content (Figure 26).

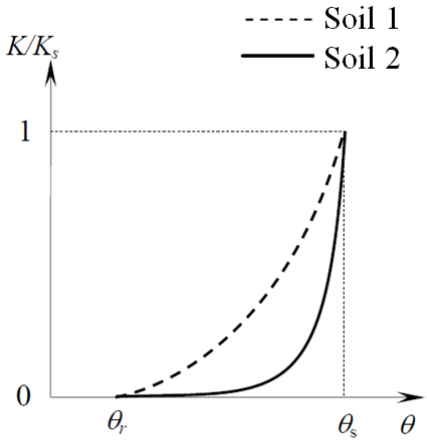

Figure 26: **Hydraulic conductivity (*K*)/water content (θ) curves: sandy soil (soil 1) *vs* clayey soil (soil 2)**

In coarse materials, this infiltration could be increased by the presence of preferential paths. On the other hand, at low water content the capillary forces govern water infiltration, and high pressure gradients are exerted over longer distances, promoting higher infiltration on the media. However, below a certain water content (residual water content), the pores are not connected, capillary forces are no longer exerted, and the water stays trapped. Hydraulic conductivity thus becomes zero.

Pressure forces and adsorption depend on porous media organization and specific particle surface defining soil capacity retention and permeability, respectively. The shape of the soil water–retention curve is related to the soil texture, as shown in Figure 27.

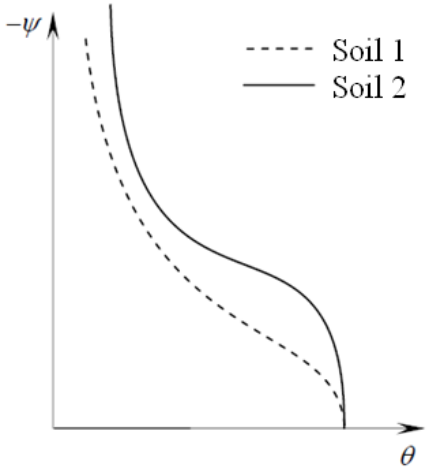

Figure 27: Soil water-retention curve for a coarse texture soil (soil 1) *vs* a fine-textured soil (soil 2)

The magnitude of the attractive force that soil exerts on water is governed by the size of the porous space, the smaller the porous space, the harder it is to remove the water from the void. The hydraulic conductivity of a filter is very sensitive to media size (Knowles *et al.* 2011), and influences both infiltration rates and water retention. On VFCWs, the particle-size material is designed to play a hydraulic role in the system, and the choice of material is made to reach an equilibrium between water and gas transfers and sufficient water retention to govern retention time. This depends on the characteristics of the influent to be treated (clogging risk) and the treatment objectives set. Hydraulic residence time is one of the main operational parameters affected by water content distribution (Giraldi *et al.* 2009). A higher water retention means a higher contact time between pollutants and microorganisms, and a better pollutant removal rate as long as oxygen can pass through the different layers.

In saturated and homogeneous soils, saturated hydraulic conductivity (K_s) represents the infiltration rate limit on the filter. Molle *et al.*(2006) stated that the inside of the filter always stayed in unsaturated conditions even when batches were passing through the filter only the surface deposits on the first stage were saturated, being hydraulically limiting.

On a VFCW, the observed infiltration dynamics are dependent on various factors. Infiltration rate (*IR*) determines hydraulic load able to pass through the surface layer, the ponding depth and ponding time that can occur on the filter, and thus the oxygen content in porous media.

2.4.1.2. Infiltration rate

According to Beach *et al.*(2005), infiltration rate is controlled by the following main factors :

1. **Hydraulic conductivity of the infiltration surface (including the biomat)**

   Hydraulic conductivity is influenced by different parameters, mainly water content in the filter (initial water content and the surface water content), soil type (structure, texture, porosity), and the capillary and adsorption forces.

   Observations on VFCWs find that when feeding begins, infiltration velocity decreases quickly to reach stable post-batch values (Figure 28). The increase in soil moisture means suction forces decrease and, with the partial clogging of the surface by fresh deposit, infiltration rate also decreases.

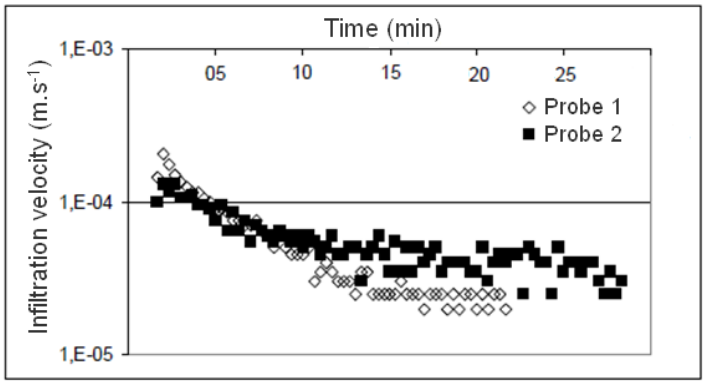

Figure 28: Infiltration velocity according to time after batch feed, adapted from Molle (2003)

IR decreases during operation according to feeding period. In the first stage, the IR is controlled by the superficial layer deposit where the infiltration rate decrease is sharper (Figure 29). In this stage, IRs are higher at the beginning of the feeding period as the deposit layer presents dried fissures produced during the rest period, through which water can drain easily. However, when the sludge layer gets wet, it start to swell and, as new added organic matter is carried out, infiltration is then limited. Consequently, the first stage appears to be the hydraulic limiting step. In the second stage, the absence of deposit layer means that infiltration is controlled by the grain-size characteristics mentioned earlier. The decrease in IR tends to stabilize itself once the moisture content of the media reaches stable values. According to Molle (2003), in the first stage the infiltration velocity curve stabilizes stable after the third day of feeding.

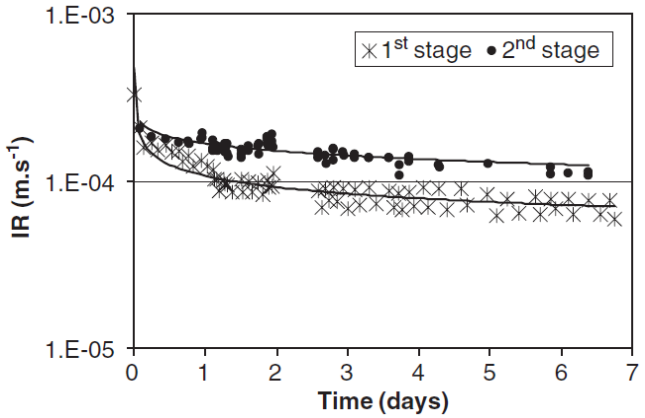

Figure 29: IRs for each stage during a feeding period for the Colomieu plant in October (Molle *et al.* 2006)

In agreement to season, in low temperatures (winter) when reeds are not developed, the sludge layer present on the filter is less mineralized, so infiltration is governed by its hydraulic conductivity, decreasing infiltration rates. In contrast, when seasonal high temperatures (summer) have enabled the reeds to grow to roughly 1 m in height (in June), they promote the flow of water down around the stems via the tubular cavities formed at the reed-sludge interface as the reeds sway in the wind, in which case the reeds reduce the role of the deposit layer.

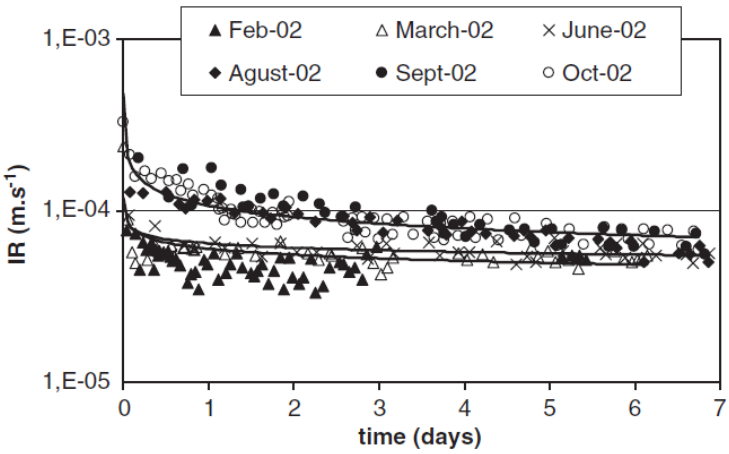

Figure 30: IR changes in a first-stage filter in different seasons and feeding days at the Colomieu plant (Molle *et al.* 2006)

2. Level of ponding above the infiltration surface

The pressure due to surface ponding increases with ponding depth. During hydraulic overloads, ponding depth is greater than during dry-period feeds, thus causing higher infiltration velocities and a decrease in retention time.

The influence of ponding depth on infiltration velocity can be observed in Figure 31 for a first-stage filter. On a second stage, infiltration velocity is less dependent on ponding. Note that under a certain ponding depth, the IRs are dispersed, thus reflecting local phenomena.

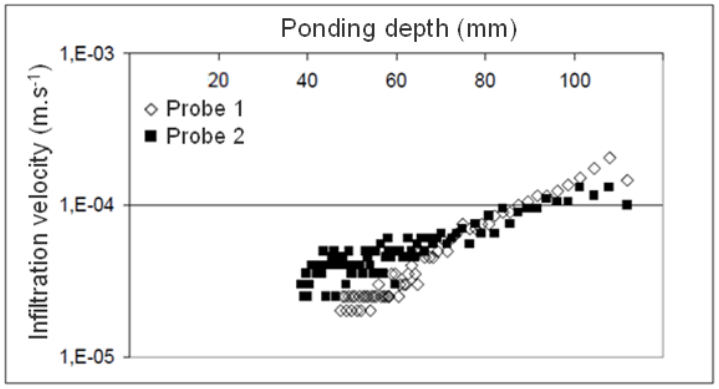

Figure 31: Infiltration velocity according to ponding depth, modified from (Molle 2003)

3. Thickness of the biomat

As the filter ages, the biomat develops and creates an increased resistance to flow, which consequently strongly influences the unsaturated flow regime in porous media and the subsequent pollutant removal performances.

Molle *et al.*(2006) observed an age-related variation in infiltration rates in different treatment plants in France, with different deposit layer levels :

- Evieu (1 cm of deposit level, IR > 3.6 x 10-^{4}ms^{-1})
- Colomieu (7 cm of deposit level, IR > 0.5 x 10-^{4}ms^{-1})
- Gensac la Pallue (22.5 cm of deposit level, IR > 0.3 x 10-^{4}ms^{-1})

These results show how infiltration capacities decrease with deposit height. However, the authors remark that the new (poorly mineralized) deposit layer is the most hydraulically limiting and not directly the total deposit height.

2.4.1.3. Operating regime of a VFCW

The operating regime has an important influence on filter hydraulics, as it dictates infiltration and retention time, ponding time, oxygen renewal, and consequently treatment performances.

Feeding/rest period

The feeding/rest periods are fundamental in controlling the growth of the attached biomass on the filter media to maintain aerobic conditions within the filter bed and thus mineralize the organic deposits resulting from the SS, contained in the raw sewage (Lienard 1990). According to French guidelines, a first stage needs 3.5 feeding days/7 days of rest in order for the VFCW to run as intended. Molle *et al.* (2006) found that after each feeding period on a plant running for one year, three or four days of rest (without any water infiltration) were necessary to return to the IRs observed at the beginning of the feeding period. Consequently, under hydraulic overloads, we can assume that the rested filters could be rotated more frequently, without penalizing their hydraulics, and thus minimize ponding times to avoid long periods of oxygen privation.

Batch feeding regime

Longer intervals between batches allow better drainage of the media and thus lower residual water content and high infiltration rates due to greater pressure gradients (greater submersion and drying of the media for longer periods between successive batches). However, these longer intervals with large water volumes can place limitations on pollutant removal, as an important fraction of water volume drains through the preferential paths, leading to a shorter contact time for biomass treatment. In contrast, high HL generates a shorter interval between batches, which gradually increases the filter water content (as the porous medium is not given enough time to dewater). This more frequent feeding with lower water volume can increase retention times and consequently treatment performances, as long as enough oxygen stays available on the filter. Better treatment performance is thus a trade-off between retention time and oxygen renewal on porous media. Once the filter has reached saturation, infiltration is dictated by the permeability of the media and the pressure forces exerted by ponding depth.

2.4.1.4. Towards an excess of water: ponding

In a VFCW system, feeding is programmed to be greater than infiltration capacity so as to establish a good water distribution onto the filter surface. This ponding scenario is the case of mature French filters where the low hydraulic conductivity of the organic deposit layer is vital for limiting infiltration rate and improving surface distribution (Morvannou 2012). It also means that the hydraulic flow able to pass through the filter is also limited. However, this is not necessarily the case on a newly-commissioned treatment plant where the infiltration material is still clean (Molle 2003).

In saturated conditions, infiltration is mainly governed by gravity forces, where hydraulic head variations play an important role in the infiltration processes. During batch feeding, the change of water amount on the filter surface induces a positive pressure profile conducive to water infiltration. These pressure head profiles are also affected by media moistening during feeding (Molle *et al.* 2006). On the other hand, during ponding, air cannot escape at the top surface and the subsequent compression of the air phase in the porous media can ultimately constrain the infiltration velocity (Forquet *et al.* 2009).

During storm events, the filter is liable to pond, thus increasing infiltration velocity. Longer and more intense storm events will produce longer and heavier ponding, meaning oxygen

supply can be restricted for a longer time. Long periods of oxygen restriction can severely affect filter performances due to nitrification and organic matter degradation limitations.

2.4.2. Oxygen transfer

Since oxygen fluxes into the filter are strongly influenced by the dynamics of the water content into the top media section (Schwager & Boller 1997), studying filter hydraulics gives us a picture of oxygen content on porous media and consequently the possible treatment process dysfunctions. Oxygen transfer into the media can occur in different ways :

- Diluted oxygen present in wastewater (maximum about 10 mgL^{-1})
- Convection (due to batch loading and its displacement into the filter)
- Diffusion (from aeration pathways and filter surface to pore space)

If dissolved oxygen present in wastewater can be neglected given the oxygen needed for organic matter oxidation and nitrification, contrary for oxygen supplied by convection and diffusion processes where both mechanisms are dependent on the feeding operation in vertical filters. Convection, which involves mass movement of the gaseous phase, mainly takes place during batch feeding. Diffusion is dependent on oxygen gradient between the porous media and the atmosphere as well as the available airspace within the porous media (i.e. the water content of the media). It is easy to see how system hydrodynamics affect air renewal. Batch flow feeding will impact convection phenomena while drainage rate will impact diffusion phenomena as it requires open pores to be effective (no water at the surface).

In normal conditions (dry weather flow), oxygen status in the first stage of a French CW during feeding and rest periods evolves as shown in Figure 32.

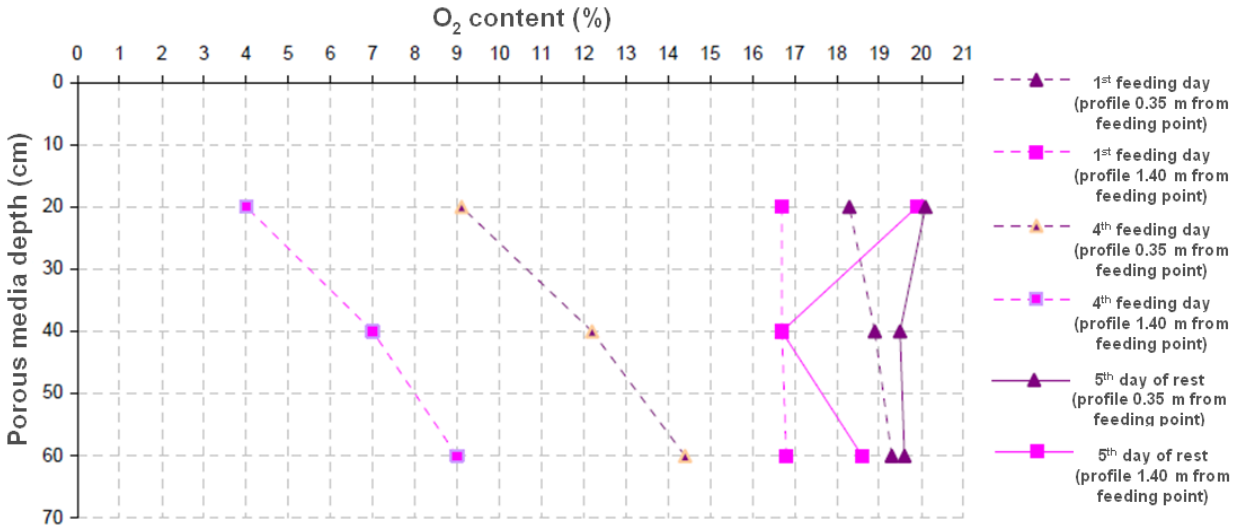

Figure 32: Time-course of first-stage VFCW oxygen content at different depths and distance from feeding point for 1st feeding day, 4th feeding day and 5th day of rest, adapted from Bolomey (2006)

Figure 32 illustrates how oxygen tends to decrease from saturation to values around 5% in the air phase (at 20 cm depth) after 4 days of feeding. The rest period allow oxygen status to get

back to saturation, which usually takes about 4-5 days. Filter oxygen content varies according to hydraulic and organic loads applied and water distribution over the filter surface.

Schwager & Boller (1997) discussed the importance of convection and diffusion rates. The oxygen content in the filter's pores reaches high values similar to the oxygen content (under optimal conditions) of air before each feeding. The oxygen transportation mechanisms only function as long as the upper layers of the bed have a high drainage capacity and the filter surface is able to dry between batches. Batches only account for a short fraction of the process duration, but most of the flow occurs during these periods and the next few minutes (Forquet 2009). After a batch feed, pores on top are open for fresh air entering through the surface at moderate rates. Underneath there is a constantly increasing layer of upward drift caused by air pressured to release. At the end, the air is still pushed downward but at low rates (Schwager & Boller 1997), as shown in Figure 33. However, in large-scale VFCW systems, water is rarely homogenously distributed on the surface, so oxygen can also move horizontally.

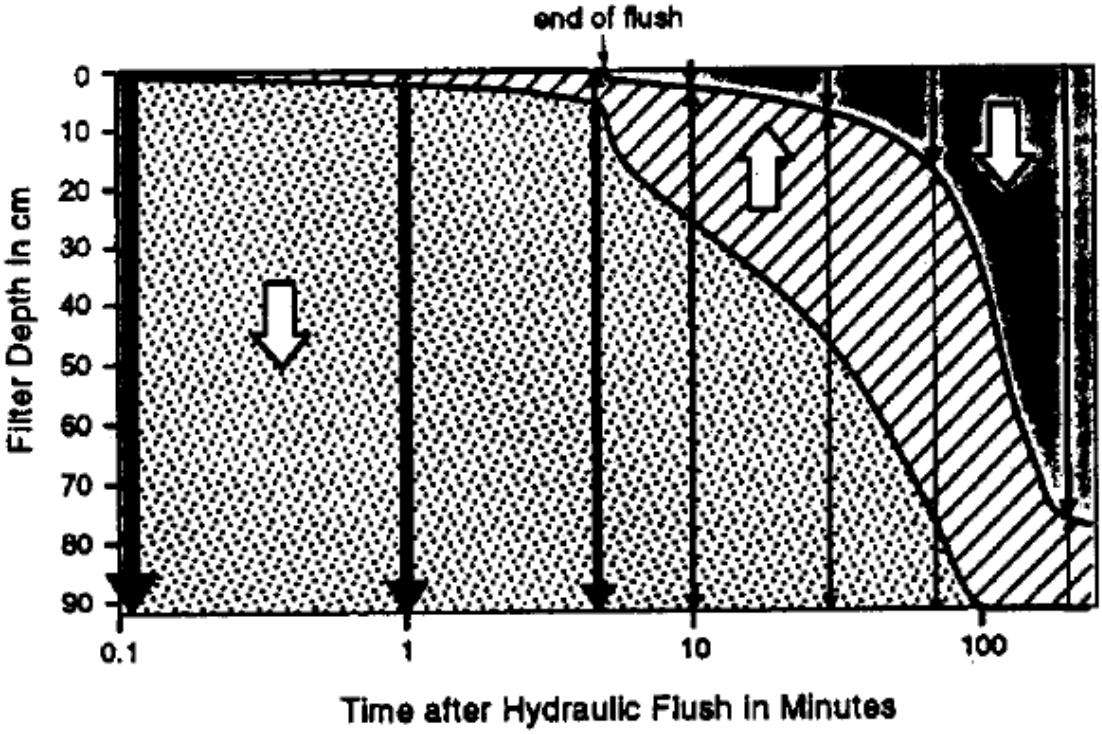

Figure 33: In-filter airflow in the course of a flush (batch). Direction and flow rates are indicated by different-sized arrows (Schwager & Boller 1997)

Research by Forquet (2009) showed that a sufficient batch loading rate is necessary to allow good distribution of water over the filter surface and avoid the formation of preferential paths within the bed. However, batch loading rate does not affect the quantity of oxygen entering by convection. Daily hydraulic load has more impact on oxygen transfers, as convective oxygen intake increases linearly with daily HL until an asymptotic value that corresponds to the moment when seepage starts at the bottom before ponding ends at the surface. Multiplying the number of batches per day can bypass this issue. As batches get more frequent, the filter has less and less time to drain out the water. A wet filter lets less oxygen enter by convection than a dry one, which is why oxygen decreases as number of batches increases. However, as Figure 34 shows, this decrease is less than the benefit brought by more regular batches (Forquet 2009).

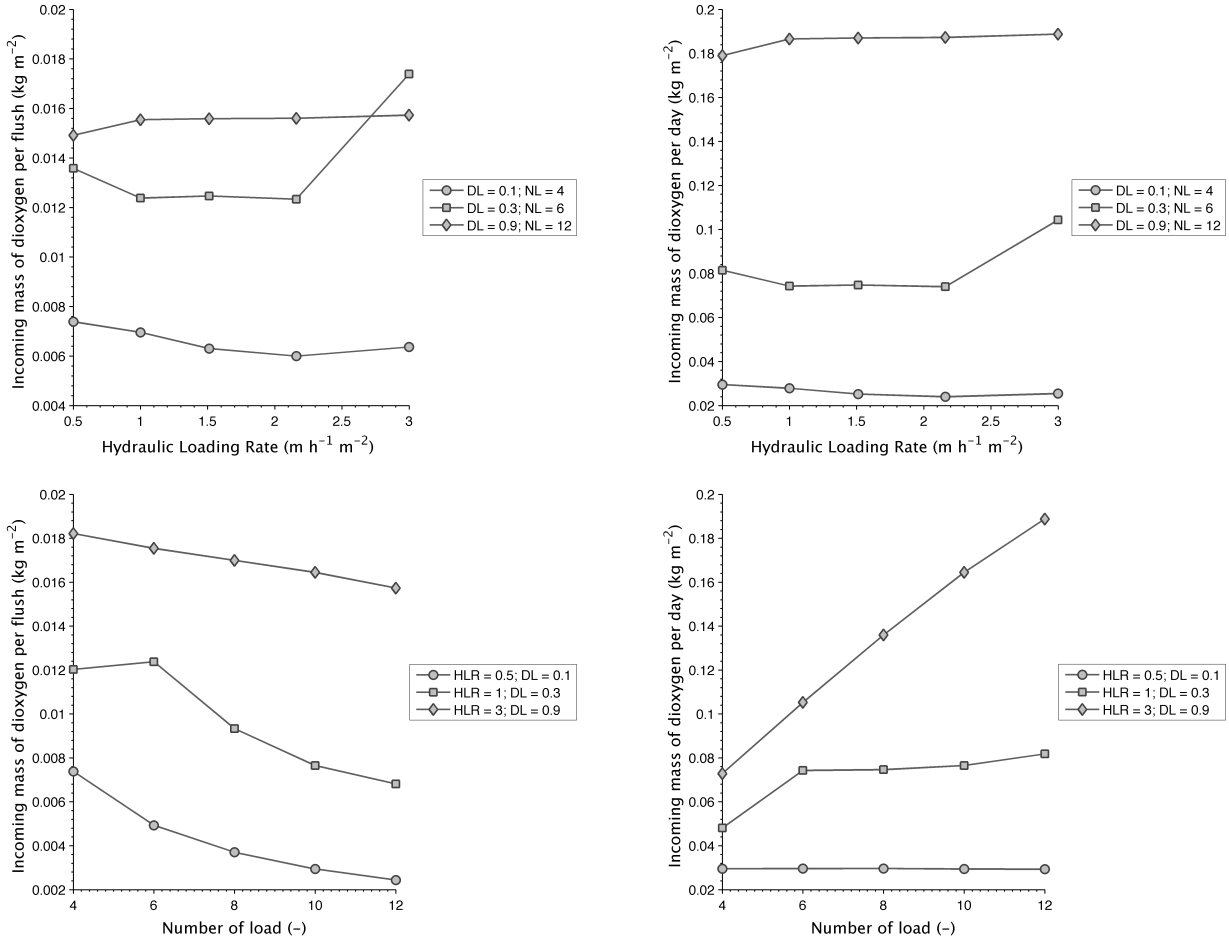

Figure 34: Incoming mass of oxygen per day (right) and per flush -batch (left) *versus* hydraulic load rate (top) and *versus* number of batches (bottom). DL = hydraulic daily load (m); NL = number of flushes (-); HLR = hydraulic loading rate ($m^3m^{-2}h^{-1}$) (Forquet 2009)

Fast dewatering is an important driver of efficient oxygen transport into the filter, both by diffusion and convection. If time between beginning of batch feed and complete infiltration is short, the applied water volume equals the volume of air entering the soil by convection (Platzer 1999). As diffusion is highly dependent on the pore space characteristics of the soil, a quantity of the oxygen contained in the pores can be supplied by the air fraction moving upwards after the batch feed, when compressed air is released.

Hydraulic loading rate does not significantly affect the quantity of oxygen entering by convection (Forquet *et al.* 2009). However, low-frequency batch feeding with a HL of 2–5 cm/m² per batch enables high filter oxygenation thanks to convection phenomena. With low hydraulic loads, the oxygen input by diffusion plays an important role for the oxygen balance in soil (Platzer 1999). According to Kayser & Kunst (2005), the rates of oxygen transfer by diffusion into the first centimetres of a filter can achieve values near the oxygen transfer rates in air. This is especially interesting given that most of the aerobic conversion and degradation processes are already completed after the first cm in the filter. However, hydraulic loads that produce constant ponding can trigger a substantial drop in treatment performances (Platzer & Mauch 1997) due to starvation of fresh oxygen. The nitrification process can be seen as a very sensitive indicator of the state of the VFCW since it is rapidly affected by oxygen deprivation, as well as to competition for oxygen consumption for carbon degradation in the first stage.

As ponding phenomena and drainage efficiency are dependent on the permeability and OM content of the medium, it is easy to see how the deposit layer (age of the system) affects the oxygen transfers. In addition, hydraulic overloads can bring high pollutant loads that in parallel to this lack of oxygen can clog the porous space in the filter if the organic load cannot be degraded. Filter clogging counteracts efforts to ensure good aerobic conditions.

Several studies propose oxygen transfer relations for VF filters. Schwager & Boller (1997) estimated overall oxygen intake as 39 $mgO_2/m^2/min$. Platzer (1999) assumes that the rates of oxygen entering by convection are equal to water rates infiltrating the system, and so as air contains about 300 mg O_2/L, oxygen input by convection is easily calculated using inlet water volume. Platzer (1999) also estimated oxygen transfer by diffusion as 1 gO_2m^2/h. Forquet (2009) reported that maximum incoming mass of oxygen was 18 gO_2/m^2 per batch and 192 gO_2/m^2 per day. These studies paint a picture of the role of diffusion/convection in oxygen transfers; however, all the above studies were carried out in sand-based filters, where oxygen transfers are lower than in filters built with coarser-grained materials like gravel, which is the infiltration material used in French first-stage VFCW systems. According to inlet nominal loads for French VFCW treating domestic wastewater, daily global oxygen demand (GOD) requirement is 404 $gO_2/m^2/d$. This high oxygen requirement highlights the importance of diffusion in oxygen transfers to not penalize nitrification and organic material degradation.

2.4.3. Clogging

Clogging of porous media can have different causes, all characterized by a considerable drop in infiltration capacity. Clogging limits infiltration rate and creates ponding at the surface. Lower infiltration rates cause a reduced oxygen supply and lead to a rapid failure of treatment performance (Langergraber *et al.* 2003b).

In VFCW, the cumulative biological, chemical, and physical treatment processes may cause gradual clogging of the porous media (Knowles *et al.* 2011). Platzer & Mauch (1997) report that clogging occurs mostly in the upper 15 cm of the infiltration layer, citing its causes as :

1. **Organic and inorganic deposit** of solids at the surface, developing a deposit layer and leading to outer blockage of soil pores (‘surface filtration’). Deposition at the grain surface into the pore volume and leading to inner blockage is called ‘volume filtration’ (De Vries 1972).

2. **Biomass** production and excretions in the soil pores due to a constant nutrient supply in wastewater, which is why the rest period is so important for biomass mineralization.

3. **Chemical** adsorption and precipitation in the pores.

4. **Rhizome and root** development into the pore volume of the media

The firsts two are the most important causes of clogging in CW. Filtration of large particles is the major mechanism of solids removal in VFCW, and predominantly takes place in the first few cm of the filter. As particles accumulate within this part of the medium, the efficiency of subsequent removal is often enhanced due to the reduced pore space (Knowles *et al.* 2011). The load of suspended solids (SS), especially the non-biodegradables, is a mean factor

influencing reduction in pore space (Platzer & Mauch 1997; Caselles-Osorio *et al.* 2007), but some studies (Tanner *et al.* 1998; Nguyen 2000) show that organic matter can also cause clogging. If organic solids can be mineralized by the micro-organisms, this process requires oxygen, thus if clogging occurs and inhibits oxygen supply from the surface, the inner blockage increases exponentially (Langergraber *et al.* 2003b). Langergraber *et al.* (2003b) state that substrate clogging is mainly caused by SS load and not by biomass growth.

In CW, biomass is mainly attached to the medium; the suspended fraction in the water can be neglected (Khatiwada & Polprasert 1999). A majority of biofilms secrete a gel-like extracellular polymeric slime that decreases pore diameter, making the pores relatively impermeable and proficient at forming associations with other inorganic and organic materials (Knowles *et al.* 2011). This biofilm can develop webs across pore spaces that can trap particles more proficiently than uniform biofilm coatings (Mays & Hunt 2005), thus reducing the hydraulic conductivity of porous media.

At a minor scale, chemical precipitation of different metals and other components can form film-like coatings on media surfaces and ultimately clog the porous spaces in the filter. Concerning clogging by rhizomes and roots, IWA (2000) states that a dense macrophyte population will have 500–5000 g of dry weight per m² of subsurface roots and rhizomes, providing additional surface area for accumulation and occluding an important pore volume in the root zone. Furthermore, root material contributes to subsurface clogging and leaf litter-fall contributes to surface clogging (Knowles *et al.* 2011).

French systems are engineered to accumulate a deposit layer at the surface, which is beneficial to treatment performance (Chazarenc & Merlin 2005) as long as system hydraulics do not hinder oxygen renewal. Nevertheless, as the deposit layer is a limiting step regarding water and gas transfers, rest periods are essential in the French system to mineralize the organic matter build-up and recover acceptable infiltration rates.

As VFCW systems are used in different ways (primary treatment, secondary treatment, continuous or batch feeding, with or without rest periods) and with different filter media (gravel, sand, etc.), it is difficult to estimate ‘blanket’ clogging limits. In French systems, batch feeding naturally and normally creates ponding, but daily ponding does not necessarily mean that the filter is clogged (Morvannou 2012).

Routine problems associated with clogging are hydraulic malfunctions, such as undesirable wastewater ponding on the filter surface continuing until ponding no longer completely drains down between batches. This constant ponding affects oxygen transfers within the filter, with knock-on effects on nitrification and organic matter degradation. According to Kayser & Kunst (2005), the oxygen content of air in a clogged filter is below 5% and is relatively unaffected by dosing cycles (convection phenomena diminish under long ponding). All the above mentioned problems can be aggravated during rainfall events. Rain events can bring high SS and organic matter loads that accelerate the clogging process. Introducing an overflow structure above the filter surface can limit excessive ponding and input loads, but the limiting load and/or ponding duration has not yet been defined in the French system.

2.5. Hydraulic load and performance limits

As seen earlier, heavy hydraulic overloads can produce ponding on the filter surface, which minimizes oxygen exchanges and hampers performances (see chapter 2.4.1.4). According to Cooper (2005), the key target factors when designing a VFCW are :

- Produce a bed matrix that allows wastewater to pass through the bed before the next dose arrives whilst at the same time holding the liquid back long enough to allow contact with the bacteria growing on the media and achieve the required treatment.
- Provide sufficient surface area to allow oxygen transfer to take place and sufficient bacteria to grow.

Due to the different designs and uses of VFCW, it is complex to find any consensus about hydraulic limits of VFCW in the literature. Avila *et al.*(2013) studied treatment performances for combined-sewer wastewater and stormwater on a hybrid system (VF-HF-FWSCW) and found that a VFCW can accept hydraulic overloads 2.6-fold higher than dry weather flow (0.12 $m.day^{-1}$) without jeopardizing treatment. Platzer (1999) stated that HL was not limiting up to 0.25 $m.day^{-1}$ in VFCW design. Kadlec & Wallace (2009) indicate that HL up to 1 $m.day^{-1}$ have been employed in VFCW and still yield good BOD/COD and ammonia reduction. Cooper (2009) reports that compact VF systems (systems with only one bed, no dosing and resting period) can accept HL up to 0.47 $m.day^{-1}$ with good treatment results. The maximal HL applied in the literature are lower than the HL on French systems.

In experiments led by Molle *et al.*(2006) on French systems, the Colomieu treatment plant (9 years in operation) shows no infiltration problems after episodic hydraulic overloads up to 4 $m.day^{-1}$ (>10-fold dry weather HL). After 3 or 4 days of resting, the IR had recovered to the IR observed at the beginning of the feeding period. Over a 5-month period, the system can handle continuous overloads of 1.8 $m.day^{-1}$ (5-fold dry weather HL) and still meet the quality objectives (COD: 125mgL^{-1}, BOD5: 25mgL^{-1}) with TKN always under 3.5 $mgNL^{-1}$.

Molle (2003) studied observed infiltration rates and their evolution according to the amplitude of the dynamics of hydraulic overloading, the overload itself and its duration, and proposed the following hydraulic limits for French VFCW :

Table 6: Hydraulic limits proposed by Molle (2003) according to sludge layer depth, overload recurrence and intensity.

Sludge layer (cm)	*0-10*		*10-25*	
Hydraulic overload	**Weekly**	**Monthly**	**Weekly**	**Monthly**
$m.day^{-1}$	1.80	3.50	0.90	1.80
$m.hour^{-1}$	0.25	0.25	0.11	0.11

The rule set for the French system (Table 6) for hydraulic overload acceptance showed certain limits that are dependent on rain event frequency and rain intensity. However, rain event frequency had simply been described in terms of weeks or months, whereas rain intensity limit was described by a daily and hourly hydraulic limit. Moreover, the biological response was not precisely defined for this first rule set of hydraulic overload acceptances. Even though many VFCW are installed in areas equipped with a combined sewer, stormwater acceptance limits have not been sharply defined, as the limitations depend on a host of factors including

age of the system, season, sewer characteristics and, of course, climate conditions (dynamics and duration of storm events). Many communities are implemented with a combined sewer overflow (CSO), which can protect VFCW from hydraulic overloads. However, due to the lack of treatment, the water discharged by CSO can cause serious problems to the receiving water body. Although, to limit the untreated stormwater discharge to the receiving water body (Water Framework Directive 91/271/EEC), the General Local Authorities Code - Article R2224-17 (Code général des collectivités territoriales) requires that water entering a sewer system must undergo treatment before being discharged into the natural environment, except on unusual situations. To attaint this objective a new regulation is under construction to limit the CSO discharges (see section 6.2.2).

Subsequently, filter design not only has to accept hydraulic overload but must also minimize surface ponding to ensure sufficient oxygen renewal needed for treatment. Maximal cumulative day-time surface ponding and consecutive surface ponding need to be defined to ensure oxygen renewal and thus biological activity.

It is therefore imperative to establish hydraulic overload acceptance limits without jeopardizing the biological component of system. For this purpose, as the first stage is the most hydraulically limiting step on French VFCW, sound filter functioning visibly hinges on: (i) studying first-stage treatment performance dynamics in response to hydraulic overloads received at the system. However, as local contexts dictate the hydraulic loads flowing into the VFCW, it is essential to (ii) study local rainfall dynamics (duration and intensity) and watershed and sewer characteristics (CSO, slope and imperviousness area). In addition, (iii) the treatment plant design (surface, firs-stage by-pass) and operational conditions (rotation) will also impact the hydraulic overload acceptance. The sum of these three factors is the key to establishing hydraulic overload acceptance limits, and consequently the key to filter design.

This all makes engineering VFCW to accept storm events a complex task. Therefore, dynamic models can prove extremely helpful tools for describing system hydraulic in response to this high number of influencing characteristics. Applying such models thus emerges as a requisite for better understanding VFCW hydraulics and designing the appropriate filters.

2.6. Hydrodynamic modelling of VFCW

The main objective of the modelling effort is to gain deeper insight into the dynamics and functioning of complex CW systems by using modelling tools capable of describing hydrodynamic, transformation and/or degradation processes. The principal hydraulic modelling approaches for CW are recapped below :

- *Mechanistic models*

  In this type of model, the basic elements of the model are directly linked to the underlying mechanisms being modelled. Mechanistic models are powerful tools for describing in-filter hydraulics and processes. However, as they integrate high numbers of input variables, they are very difficult to fit and to apply to other sites since the requisite data is not always available for every single VFCW. They also prove complex to handle for filter design purposes due to the fact that they are originally designed and used for research purposes.

- *Simplified models*

  These models use simple concepts to represent the functioning of the system. They consider the system as a "black box" without intending to represent real internal phenomena. However, they integrate low numbers of input variables, which makes them far easier to use in practice. They are popular for their robustness and their ability to represent the behaviour of complex systems.

2.6.1. Hydraulic approach

Due to the nature of the processes involved, flows in VFCWs are based on the hydrodynamics of porous media. Darcy's law is the base of hydraulics in saturated porous media. Obtained from movement equations and supposing a laminar flow, the equation is :

$$V = K\frac{\partial H}{\partial x}$$ **Equation 5**

where:
V: velocity (M T^{-1})
H: hydraulic load (M)
K: hydraulic conductivity (M T^{-1})
x: length (M)

Hydraulic conductivity is given by :

$$K = k\frac{\rho}{\mu} = \frac{k}{\nu}$$ **Equation 6**

where:
k: intrinsic permeability
μ: water dynamic viscosity (M $L^{-1}T^{-1}$)
ν : water kinematic viscosity (M L^{-1} T^{-1})
ρ: water density (M L^{-3})

Intrinsic permeability is linked to the geometry of the porous media (pore size distribution, connectivity, etc.). Consequently, hydraulic conductivity fits the geometric characteristics of the media as well as the characteristics of water.

This equation is not used in VFCW due to the unsaturated conditions involved. As hydraulic conductivity is dependent on water content of the media, Darcy's law has been adapted to represent water movement in unsaturated soils. The Richards equation is a combination of the continuity equation and Darcy's law. The continuity equation is determined directly by a mass balance of a volume element $dV = dx.dy.dz$, giving :

$$\frac{\partial(\theta.\rho)}{\partial t} + \vec{\nabla}\cdot\left(\rho\cdot\vec{V}\right) = \rho\cdot q$$ **Equation 7**

where:
θ: volumetric water content (L^3L^{-3})
t: time (T)
ρ: soil bulk density (M L^{-3})
q: flow velocity (M T)
$\vec{V}$: velocity vector of point (M T)

This continuity equation for unsaturated soil is broadly similar to the one for saturated soils, but the difference lies in the water content parameter *(θ*) which is non-constant.

The one-dimensional approach for the resulting Richards equation is :

$$C(h)\cdot\frac{\partial h}{\partial t}=\frac{\partial}{\partial z}\left[K(h)\left(\frac{\partial h}{\partial z}-1\right)\right]+q \qquad \textbf{Equation 8}$$

where:
C(*h*): capillary capacity (M^{-1})
K: hydraulic conductivity (M T)
t: time (T)
h: hydraulic head (M)
q: flow velocity (M T)

Capillarity is represented by :

$$C(h)=\frac{d\theta}{dh} \qquad \textbf{Equation 9}$$

2.6.2. Mechanistic models

Most numerical models of CW are geared to horizontal flow (Pastor *et al.* 2003; García *et al.* 2004; Małoszewski *et al.* 2006; Tomenko *et al.* 2007), with only a few tackling VFCW dynamics where mechanistic models are more common. Straddling the two, McGechan *et al.* (2005) modelled dairy wastewater treatment by developing a reactive transport model for variably-saturated flow, where hydraulics is explained as water flows through different layers, vertically, to the CW bottom. (i) One of the models focused on nitrogen kinetics in a hybrid system (HF-VF), and also illustrates how organic matter decomposition produces ammonium (McGechan *et al.* 2005b), while another (ii) was geared towards oxygen transport through the water by diffusion and convection, and via the macrophyte plants to the microorganisms that reside in their roots (McGechan *et al.* 2005a).

Also worthy of mention is Freire *et al.*(2009) whose hydraulic model is based on the assumption of an infinite number of “micro” zones of diminished mixing all along the main channel. This channel can be conceptualized as a number of narrow channels exchanging limited flows with neighbouring zones. Thus, a set of infinite continuous stirred-tank reactors (CSTRs) operating in series and simulating a plug-flow reactor component was used to establish a non-ideal flow model. The model outputs measurements of outlet flow and outlet

concentration obtained while treating a synthetic wastewater containing the azo-dye Acid Orange. This model takes into account ponding and season variations.

Forquet *et al.* (2009) re-adapted a dysphasic (water-air) numerical model (Binning 1994) to the specificity of VFCWs and focused on describing the in-filter movement of air and water during a feeding. The study was carried out on lab-scale sand columns under clear water simulations to test various hydraulic loading parameters.

Between the mechanistic models employing the Richards equation to calculate water flow through porous media and the Van Genuchten (1980) equation for soil properties, we find Wanko *et al.* (2006) who developed a model that considers organic matter removal from wastewater and focuses on oxygen transport in VFCW. This model uses Monod-type kinetic equations (active biomass growth) and first-order kinetic biomass decay. Giraldi *et al.*(2010) used the FITOVERT code for VFCW to combine evapotranspiration, degradation of organic matter and nitrogen, and transport of dissolved and particulate components, and their model can also estimate the reduction in porosity due to bacterial growth and the accumulation of particulate components, which consequently doubles up as a simulation of the clogging process as an effect of pore size reduction. Moreover, Maier *et al.* (2009) used the MIN3P code to implement a flow and transport model describing CW processes for contaminated groundwater remediation.

HYDRUS

The most popular code in CW, especially VFCW, is Hydrus, which numerically solves the Richards equation for variably-saturated water flow and advection-dispersion type equations for heat and solute transport (Šimůnek *et al.* 2009). For common applications to CW, the model implements two additional boundary conditions: (i) surface ponding produced during wastewater loading is considered as an extension of the atmospheric boundary condition, and (ii) a limit outflow boundary condition at the bottom of the filter is established to make it possible to model the reduction of peak flow when feeding with a combined-sewer outflow. The reduction of these peaks is used to increase treatment performance and curb impacts on receiving water bodies.

Uniform Water Flow

For a 2-3D isothermal uniform Darcian flow in a rigid porous medium, the modified form of the Richards equation use by the model is :

$$\frac{\partial \theta}{\partial t} = \frac{\partial}{\partial x_i}\left[K\left(K_{ij}^{A} \frac{\partial h}{\partial x_j} + K_{iZ}^{A} \right) \right] - S \qquad \textbf{Equation 10}$$

where:
θ: volumetric water content (L^3L^{-3})
h: pressure head (L)
S: sink term (T^{-1})
xi (i=1,2): spatial coordinates (L)
t: time (T)

Kij A: components of a dimensionless anisotropy tensor **K***A*,
K: unsaturated hydraulic conductivity (LT^{-1})

At same time, *K* is given by :

$$K(h, x, y, z) = K_s(x, y, z)\, K_r(h, x, y, z) \qquad \textbf{Equation 11}$$

where:
Kr: relative hydraulic conductivity (LT^{-1})
Ks: saturated hydraulic conductivity (LT^{-1})

If the modified Richard's equation is assigned to planar flow in a vertical cross-section, $x_1=x$ is the horizontal coordinate and $x_2=z$ is the vertical coordinate.

Unsaturated Soil Hydraulic Properties

In the Richards equation, the unsaturated soil hydraulic properties θ(*h*) and *K*(*h*) are in general highly nonlinear functions of the pressure head (Šimůnek *et al.* 2006). Hydrus includes various models for soil hydraulic properties, the most popular being the Van Genuchten model (1980) which uses the statistical pore-size distribution model of Mualem (1976) to obtain a predictive equation for the unsaturated hydraulic conductivity function in terms of soil water retention parameters. The Van Genuchten-Mualem closed-form expressions are :

If $h < 0$

$$\theta(h) = \theta_r + \frac{\theta_s - \theta_r}{\left[1 + |\alpha h|^n\right]^m} \qquad \textbf{Equation 12}$$

If $h \geq 0$

$$\theta(h) = \theta_s \qquad \textbf{Equation 13}$$

Where
θ_r: residual water content (L^3L^{-3})
θ_s: saturated water content (L^3L^{-3})
h: the actual pressure head (L)
α and *n*: dimensionless Van Genuchten shape parameters
m = 1-1/*n*, and

$$K(\theta) = K_s S_e^{\lambda}\left[1 - \left(1 - S_e^{1/m}\right)^m\right]^2 \qquad \textbf{Equation 14}$$

with,
K_s: saturated hydraulic conductivity (LT^{-1})
γ: pore size distribution factor(-)
and the effective fluid saturation :

$$S_e(-) = \frac{\left(\theta - \theta_r\right)}{\left(\theta_s - \theta_r\right)} \qquad \textbf{Equation 15}$$

Counting among the most important works on VFCW using Hydrus, Langergraber & Šimůnek (2005) developed a multicomponent reactive transport model called CW2D (Constructed Wetlands 2D) as an extension of HYDRUS-2D. This submodel calculates the biochemical transformation and degradation processes in VFCW for domestic wastewater treatment while taking into account the influence of temperature on the processes involved. This code is currently the most complete in terms of VFCW modelling.

As seen in the literature, the variably-saturated water flow of VFCW is often modelled by the Richards equation, which assumes that water content and pressure head are at equilibrium at a given node. However, VFCW systems have a porosity that creates preferential flow paths through which water can irregularly bypass most of the porous soil matrix. On French VFCW, these preferential flow paths are mainly due to the sludge layer that has developed on the filter surface (swelling/shrinking during the feeding/rest periods) and the roots and rhizomes present in the filter. Consequently, non-equilibrium conditions in pressure heads are created between preferential flow paths and the soil matrix pore region (Morvannou *et al.* 2012).

Preferential flows limit the applicability of standard models for water flow that are commonly based on the Richards equation. Even if it remains possible to simulate water content variations within a VFCW, the solution cannot correctly model outflow with the standard Van Genuchten-Mualem function (Morvannou *et al.*, submitted). Therefore, a model representing a non-equilibrium water flow and solute transport would be a more appropriate dual-porosity model. This type of model assumes that flow only takes place within the macropores (the mobile region) and neglects the flow in the rest of the matrix (water in the rest of the matrix constitutes the immobile region).

Only Morvannou *et al.* (2012) has applied preferential flow models to flow and transport in VFCW. Studying and simulating hydrodynamic behaviour and solute transport through a simplified representation of a French VFCW using both models – a classical equilibrium model (Richards) and a non-equilibrium model (dual-porosity model: mobile-immobile water model, with water content mass transfer) included in the HYDRUS-1D software package – the obtained modelling results were compared to a solute breakthrough curve obtained from a tracer experiment carried out on a VFCW, which determined that the non-equilibrium approach is the most appropriate.

To summarize, while mechanistic models are powerful tools for describing biochemical degradation, transformation processes, oxygen transfers, evapotranspiration, and even clogging, they are generally too complicated to fit, due to: (i) the numerous variables present on the biochemical side, and (ii) the fact that the hydraulic components, even if they include less variables to be fitted, still remain problematic, as the in-filter soil hydraulic properties still have to be obtained. As these models are originally designed and used for research purposes, they are not viably workable for non-expert users (such as local land planning authorities). The trade-off between detailed description and easy handling will depend on the modelling aims – when the aim is a global design, using simplified models appears to be a good alternative.

2.6.3. Simplified models

While mechanistic hydraulic models oriented to study VFCW dynamics are already reduced in number, the simplified models are even more so. Looking at the relevant literature, Meyer *et al.* (2008) developed a simplified mass balance hydraulic model coupled with first-order equations to study the dynamics of pollutant such as ammonium. In this simplified model, water flow is described one-dimensionally as a sequence of retention volumes with variable water contents (retention space, filtration layer and drainage space). The model is used to simulate flows and pollutants from a combined-sewer overflow treatment working with vertical filters over long periods. The main objective of this work was to offer a simplified tool for designing VFCW for CSO treatment. This model was fitted against lab-scale VF test rings of Ø 190 mm. with hydraulic loads of about 0.5–2 m/d, controlled outflow conditions, and short time step modelling. Although the model showed good fitting, CSO treatment filters are quite different from French VFCW systems treating domestic wastewater since the CSO treatment uses a throttle to regulate drainage.

Along the same lines, Ross *et al.* (2011) proposes five simplified hydraulic models with multiple compartments based on water-balance and Darcy and Richards equations for VFCW with CSO treatment. The models take into account reed evapotranspiration and capillary forces. The aim of the study is to identify optimal design parameters, considering the consequences of climate change (impact of storm events and variability in CSO discharge) and the sewer system characteristics. The models consider the filter as a multiple storage component and have different configurations, such as number of storages, evapotranspiration and capillary forces assumed, and equations used (Darcy and simplified Richards equation). The models have been tested with data from different VFCWs in Australia and France, with no long-term perspectives. Two of the five models are based on the concept of barrier filters and simplified Richards equations, and visibly perform well with good experimental agreement. However, outflow peaks (consequently ponding) are not well represented, and they fail to consider the effects of the seasonality factor on infiltration.

The simplified models developed to date for VFCW are particularly limited, and focused solely on CSO treatment. Although easy-to-handle for design purposes, they are well adapted for their individual purposes but not necessarily for VFCW treating domestic wastewater. Indeed, there is a pressing need for large-scale VFCW permeability data in order to reliably characterize long-term filter hydraulics so as to acquire a simplified hydraulic tool that, once coupled to treatment performances, could be a valuable aid for general-purpose design.

2.7. A simplified model as a decision-support tool

The modelling approach is indispensable to designing VFCW for load acceptance following storm events, since local context strongly impacts the inlet flow produced during rainfall episodes. Research such as Kadlec (2000) points out that simplified models are generally ill-suited to modelling reactive and degradation processes in CW, but then the aim is not to understand the inside processes, they can often prove useful for evaluating water flow and transport of inert solutes. Simple model approaches essentially assume that flow can be simplified to one-dimensional behaviour (Langergraber *et al.* 2009).

Consequently, this research to produce an easy-handling model for design purposes aims to :

1. Develop a simplified one-dimensional hydraulic model, based on Darcy's law, simulating the hydraulic behaviour of the first stage of a VFCW, which is the hydraulically limiting step (Molle et al. 2006).

    - Focus on ponding time (tied to treatment performances due to lack of oxygen).
    - Relate ponding depth to infiltration velocity.
    - A short time-step model to analyse the impacts of storm event duration and intensity on ponding.
    - Few input parameters to fit the model.
    - Compare the simplified model to specialized software (HYDRUS-1D).
    - Analyse the impacts of seasons, feeding day and HL on infiltration.

    To fit the simplified model, we employed one-minute time-step experimental data from a full-scale first-stage VFCW. The data include inlet/outlet flow, hydraulic head variations and water content within the first-stage filter. To fit the HYDRUS-1D model, a hydrodynamic characterization of the material was also carried out using lab procedures to obtain the Van Genuchten (1980) equation parameters.

2. Establish relations connecting ponding time to loss of nitrification performance so as to set threshold limits (which we have named "alerts"), cumulative ponding time per day or consecutive ponding time for use in long-term modelling scenarios.

    For this purpose, we used treatment performance data from a large-scale VFCW, including classical sampling campaigns, continuous pollutant concentration monitoring, and intensive sampling campaigns.

3. Long-term hydraulic modelling of VFCW to analyse the impact of rain and CSO characteristics on filter design :

    - Sewer characteristics (slope, impermeability surface, etc.).
    - Climate conditions (number and characteristics of rainfall events).
    - Seasonality

    Four-year rainfall time-series data from two different and contrasting regions in France was used for this point.

The long-term modelling will focus on reducing the number of dysfunction problems (alerts) per year, scaling filter dimensions, and filter management to improve the system. With the ultimate goal of providing designers with an easy-to-use model for decision-support on scaling new VFCW according to locally-specific climate conditions, the main objective of this research project is to gain insight into how to increase hydraulic overload acceptance in VFCWs without decreasing treatment performances.

3. Material and methods

3.1. Experimental site

3.1.1. Challex catchment

The study was carried out on a French VFCW treatment plant specially designed for research purposes, located in the village of Challex, in the Rhône-Alpes region of France. The VFCW is sited alongside the Rhône river (receiving water body). The physico-chemical water quality of this receiving water body is fairly high. The village of Challex is at 508 m altitude, in an area of dual Mediterranean–continental weather influence where temperatures average 3°C in winter and 19°C in summer (Figure 35). Annual average rainfall is about 820 mm.

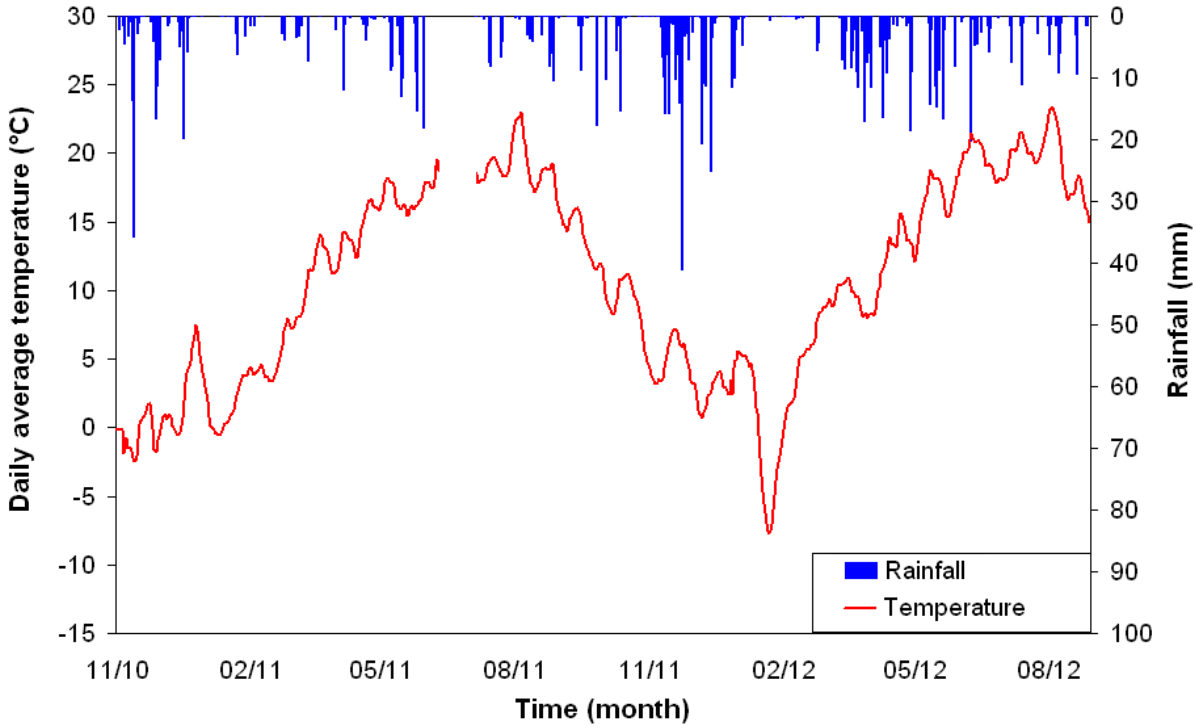

Figure 35: Daily average air temperature and rainfall measured at the Challex treatment plant.

Challex counts about 1400 inhabitants, annual population growth is 2.2% and connexion rate to the sewer of 88%.

The village has some agricultural activity and a very local-scale wine industry, which can send heavily-loaded effluent to the treatment plant when the wine tanks are washed, although this is a rare event and was not taken into account for treatment plant design. The VFCW treats mainly domestic wastewater. The predominantly combined-type sewer system has a total length of 14 km. Valley topography presents a high slope (up to 9%) leading to a quick wastewater transfer to the VFCW. As we will see section 5.1, inflow pollution is mostly particulate.

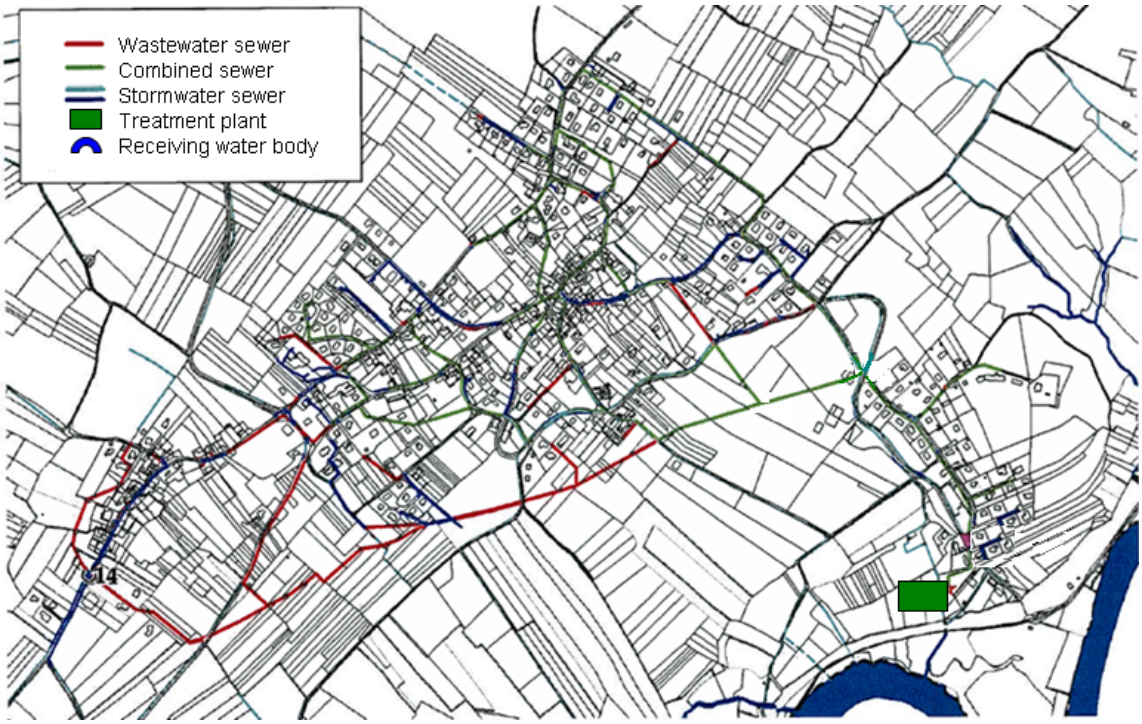

Figure 36: Schematic illustration of the Challex wastewater sewer, adapted from SAFEGE (2008).

The urban watershed has a total surface of 60 ha , including an impervious area covering 1.4 ha (2.3%) in accordance with the Challex Urban Homesteading Plan (SAFEGE 2008). The stormwater collected by the impervious areas is drained by the combined sewer system, and peak flows arriving at the treatment plant can reach different intensities according to rainfall, as shown in Table 7.

Figure 37: Challex treatment plant — location in the watershed

Table 7: Hypothetical treatment plant in-flows produced by different rainfall events (SCIRPE 2010)

	Rain period		
	1 month	**1 year**	**10 years**
Flow	0.58 m³/s	2.43 m³/s	4.80 m³/s
X times dry-weather peak flow	56	233	461

Dry-weather flow, defined as the time period where precipitations do not disturb sewer system functioning (Chocat 1997), is not always simple to define, as the watershed response after a rain event can last hours to days. In winter, this response is clearly affected by the presence of freshwater intrusion into the sewer (snowmelt, high groundwater table). In winter, at the Challex plant, the watershed can take up to 8 days to completely dry, as shown in Figure 38.

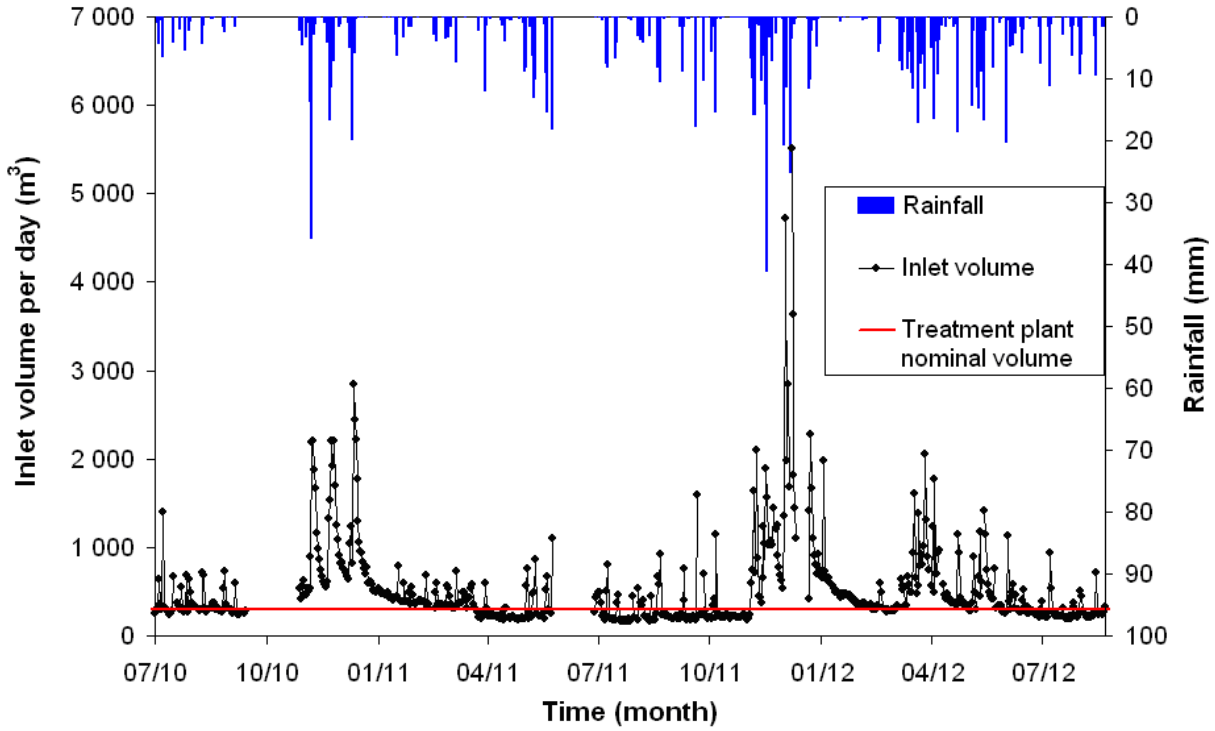

Figure 38: Hydraulic loads arriving at the treatment plant per day

Winter is the most hydraulically charged period of the year (Figure 38), with frequent heavy precipitations (up to 40 mm/d) reaching inlet volumes of 5500 m³ per day in the treatment plant (18-fold the nominal treatment-plant dry weather flow). From December to March, inlet volumes are continuously higher than nominal flow, mainly due to freshwater intrusion into the sewer. Summer precipitations are lower, and watershed response lasts just a few hours. In addition, the inlet volumes observed in dry weather are often less than nominal flow (82% of dry weather nominal flow).

3.1.2. Full-scale monitoring

The Challex VFCW has been running since April 2010. The plant (2,000 p.e.) was designed to treat wastewater from a combined sewer covering a 60-ha domestic catchment area. No precise daily rain volume is assigned for the treatment. The experimental project was to treat the maximum of rain event to limit overflows to the water body.

Designed for a total surface area of 2 m² p.e., the plant is composed of two VFCW stages. The first stage is built of 3 parallel cells and the second stage is built of two parallel cells, as recommended by French guidelines (Molle *et al.* 2005a). Each cell measures 861 m² in the first stage (41 m long x 21 m wide) and 712.5 m² in the second stage (37.5 m long x 19 m wide).

3.1.2.1. Treatment plant operation

Inlet separation systems (dry weather flow/stormwater)

Water from the combined system enters the treatment plant via a flow splitter. For flow rates less than 8–fold the nominal dry weather flow rate (100 m³/h), the wastewater passes through the usual distribution system (dry weather distribution system) over a grit chamber and then through an automatic screener (20 mm).

For flow rates higher than nominal dry weather flow and up to 3600 m³/h, excess wastewater is channelled into the rainwater distribution system over a grit chamber. After passing through a 50 mm screener, the wastewater goes through a channel on one side of the first stage and overflows onto the filter running without homogeneous distribution. For flows higher than 3600 m³/h, the plant is protected from these extreme storm events by a CSO at the gate to the treatment plant (Figure 39).

Figure 39: CSO of Challex plant in a storm event

Each filter is fed by batch-feeding systems that deliver about 18.1 mm (15.6 m³; first stage) and 13.9 mm (9.9 m³; second stage) of water onto the in-operation filter. Batches are delivered at a flow rate of about 0.38 m³/h and 0.29 m³/h per m² to the first and second stage,

respectively. Flow rate and batch volume are lower than the French guidelines (Molle *et al.* 2005a) which do not ensure good water distribution onto the filter surface (the system requires 20 to 50 mm of water at a minimal flow rate of 0.5 m³/h per m²). As shows Figure 40, on the first stage, water is spread by H-type diffusers, at an inlet point density of one per 27 m² of filter (32 inlet points per cell), while in the second stage batch distribution features pipes placed along the length of filter, at an inlet feeding point density of one per 2.47 m² of filter.

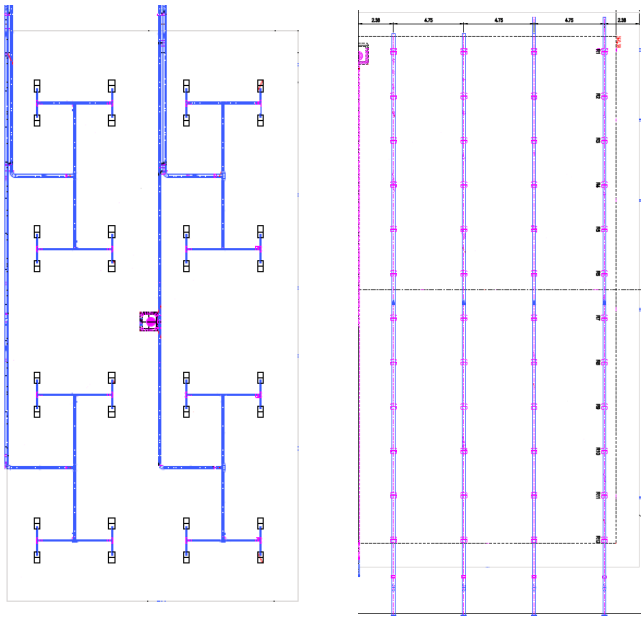

Figure 40: Feeding distribution in the first (*left*) and second (*right*) stages

The first-stage filters have a by-pass at 50 cm above the surface to protect them from extreme ponding and excessively high oxygen depletion. Water filtered on first stage is collected and drained to subsequently feed the second batch feeding system. The treated water then diverts to the receiving water body.

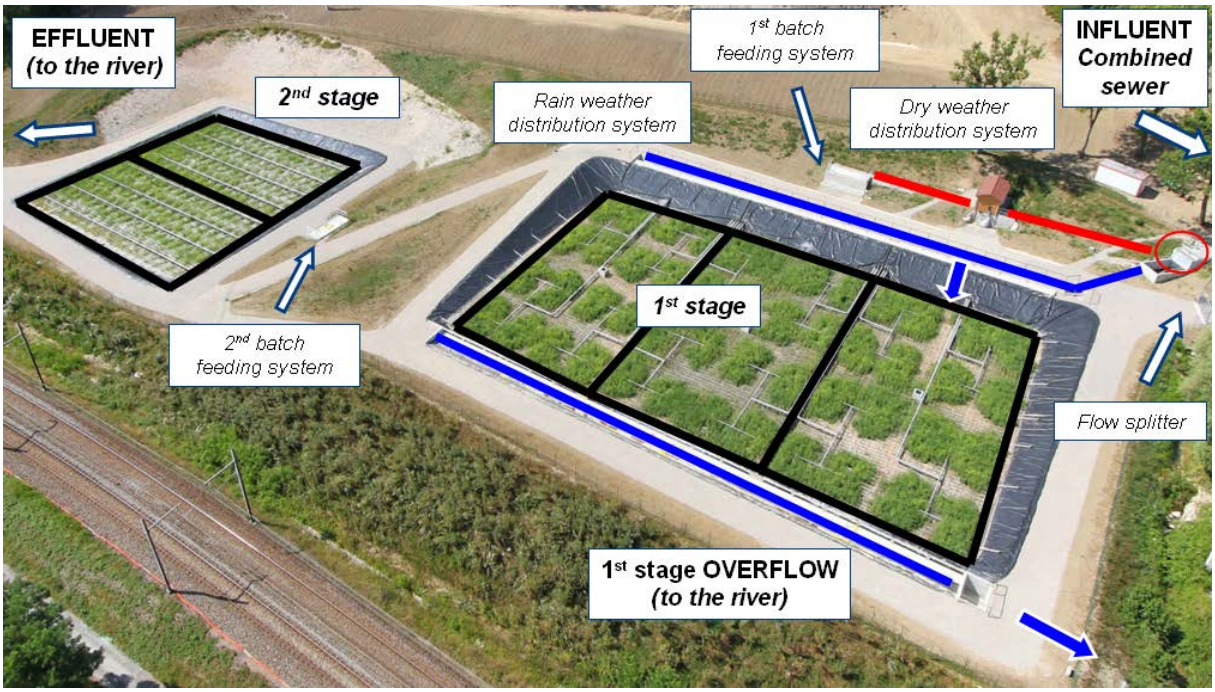

Figure 41: Schematic illustration of the Challex plant

For dry weather flow, each cell of the first stage is fed for 3.5 days with 7-day rest periods while the second stage is fed for 3.5 days with 3.5-day rest periods. For rain events, the system can handle a maximum of 100 batches (1.81 m of water) before rotating the cells.

3.1.2.2. Filter composition

Both (the first and second stage) filters are 0.8 m deep. They are composed of different layers of sand or gravel material with grain-size increasing from top to bottom as shows Figure 42. The filters are lined with an impermeable membrane (geomembrane). Twelve drainage/aeration pipes are implemented at a density of 0.21 m/m² to promote aeration from the bottom of the filter.

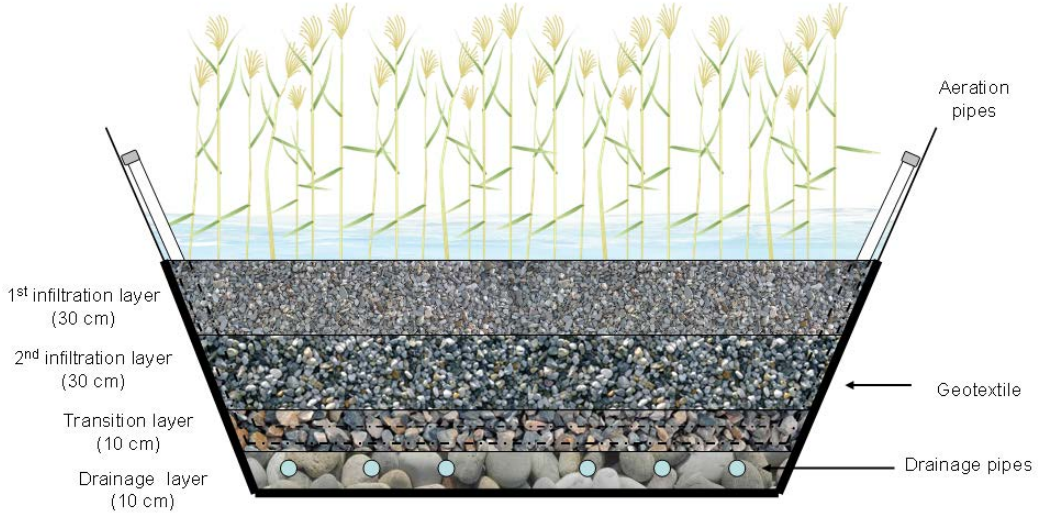

Figure 42: Material composition of the Challex filter beds

Each layer plays a specific role in the filter. The first is the hydraulically-limiting layer, where due to its small grain-size composition, the most of the biological treatment is handled. The first infiltration layer is composed of fine gravel in the first stage and sand in the second stage. The next layer down promotes flow transition and the last layer collects and drains the treated water to the next step of process. Table 8 reports the media used at each stage. Detailed analysis particle size is presented in section 4.2.2.1.

Table 8: Characteristics of the filter media.

Material		Function	Thickness (m)	Grain size (mm)
First stage	Gravel	First infiltration layer	0.3	2–5
		Second infiltration layer	0.3	4–10
		Transition layer	0.1	10–20
	Pea gravel	Drainage layer	0.1	20–60
Second stage	Sand	First infiltration layer	0.3	0–4
	Gravel	Second infiltration layer	0.2	2–5
		Transition layer	0.1	4–10
	Pea gravel	Transition layer	0.1	10–20
		Drainage layer	0.1	20–60

3.1.2.3. Treatment objectives and influent hydraulic load

The treatment objectives have been established for dry weather periods (Table 9), the aim being to not exceed the following discharge concentrations at the plant outlet.

Table 9: Treatment objectives in dry weather periods

Pollutant	Maximal 24 h mean concentration
BOD_5	25 mg/L
COD	90 mg/L
SS	35 mg/L
TKN	20 mg/L

The ratio of average dry weather flow rejected by the VFCW-to-Rhône river low tide is about 0.003% according to the Zoning Plan (Schwartzmann 2007), which means the receiving body has a significant power of dilution.

3.1.3. Hydraulic monitoring

The study focused on the impact of hydraulic overloads on VFCW treatment performances over a two-year monitoring period. Hence, a purpose-engineered apparatus was implemented in the experimental treatment plant to track system hydrodynamics at each stage. All hydraulic measurements were monitored and recorded on a datalogger (Gartner®) at 1-minute time-steps.

Dry weather distribution system inflow and treatment plant outlet flow were measured via an ultrasonic probe (ISMA) on a Venturi flume (Figure 43). Inlet wastewater flowing through the rain weather distribution system and at the first stage by-pass were measured by ultrasonic probes (SIGMA 980) placed on the overflow structures.

Figure 43: Flowmeters on the rainfall event system (*left*) and dry weather system (*right*)

Batch feeding volume and flows were monitored by measuring water height on pressure probes (Endress+Hauser) in each feed system (first and second stage). Infiltration rates and ponding were measured by 6 ultrasonic probes (Baumer) on 2 of the 3 first-stage cells (3 probes/cell). First-stage water contents were measured by a set of 15 homemade time-domain reflectometers (TDR) covering 5 filter profiles and different filter depths (10 cm, 25 cm and 40 cm).

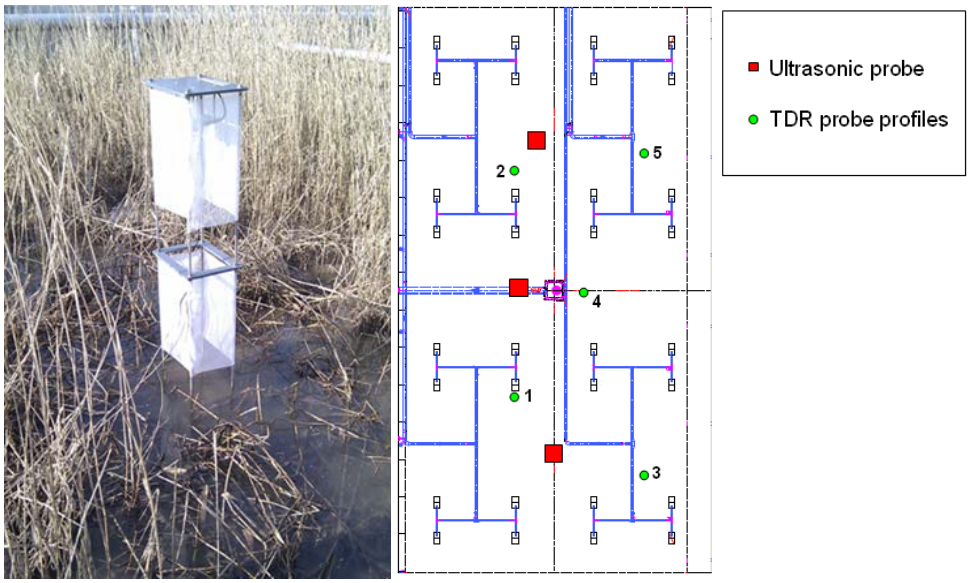

Figure 44: Ultrasonic probe (left), and map of ultrasonic probes and TDR profiles in a first-stage cell

The TDR profiles were installed in different filter locations and different distances to a feeding point (Table 10), with the objective of studying water content distribution as well as time-course evolution of water content in porous media during feeding and rest periods.

Table 10: TDR probe profiles and distances from a feeding point

Profile	Distance from a feeding point
1	0.23
2	1.17
3	1.94
4	3.22
5	3.23

The ultrasonic and TDR probes were not installed on the second stage due to its extremely uneven surface planarity. Climate conditions (temperature, rain, humidity) were also measured on-site and recorded on the datalogger at one-minute time-steps.

3.1.3.1. Calibration of the TDR probes

Time-domain reflectometry is a popular method for measuring the apparent dielectric constant (K_a) of soil, which is highly sensitive to the volumetric water content (θ_v) of the porous media (Topp *et al.* 1980). The homemade TDR probes are composed of three 30-cm steel rods and a 10-m coaxial cable. The apparent dielectric constant is obtained by the time-course (t) of an

electromagnetic wave along the probe rods inside the test medium. Several studies have been carried out to resolve calibration issues and estimate the sampling water volumes associated with specific materials (Topp *et al.* 1980; Jacobsen & Schjonning 1993; Malicki *et al.* 1996; Schaap *et al.* 1997). An inappropriate calibration is detrimental to accuracy, especially at low water contents. Jacobsen & Schjonning (1993) studied and ranked the different available methods but concluded that despite including more parameters, general calibration laws will remain less accurate than soil-specific calibration.

At the "Institut national de Recherche en Sciences et Technologies pour l'Environnement et l'Agriculture" (Irstea) , we performed a site-specific calibration of the relationship between water content and material dielectric constant. The dielectric constant is obtained from travel time along the waveguide in the studied media :

$$\Delta t = \frac{2L\sqrt{K_a}}{c} \qquad \textbf{Equation 16}$$

where:
Δt: time-course (s)
L: waveguide length (m)
K_a: dielectric constant (-)
c: light speed ($m.s^{-1}$)

Equation 16 can be simplified to express dielectric constant as a ratio of apparent probe length :

$$K_a = \left(\frac{L_a}{L}\right)^2 \qquad \textbf{Equation 17}$$

Where L_a is apparent probe length (m) defined as: $L_a = c \bullet \Delta t/2$. Experimentally-measured apparent probe length differs from L_a because it also includes an offset value (L_{aO}) related to the length and material of the probe head. We thus first measured the offset value for each probe as per the protocol given by Heimovaara (1993) and then removed it from the measurements.

In-lab probe calibration using the first-stage first infiltration layer material (gravel) appeared a requisite for more accurate results. Measures of K_a were carried out by the probe in different known water contents (from dryness to saturation) obtained by a direct method. The objective was to establish a mathematical relationship for θ-K_a. Clean material samples were packed into PVC cylinders (diameter = 0.4 m, height = 0.15 m) whose volumes were reduced by two PVC plates to obtain a 5 L working volume. The wave generator/analyser software (Campbell Scientific™ TDR100) acquired 50 continuous in-material measurements with specific water content. This process was done for all water contents measured, and triplicate tests were performed for each water content.

The experiment started with 12 different water content values, ranging from dryness to saturation. However, the θ-K_a curve contained large empty spaces for θ from 0.20 m^3/m^3 to saturation. In order to improve the accuracy of the curve, more water content values were added to the experiment (Figure 45).

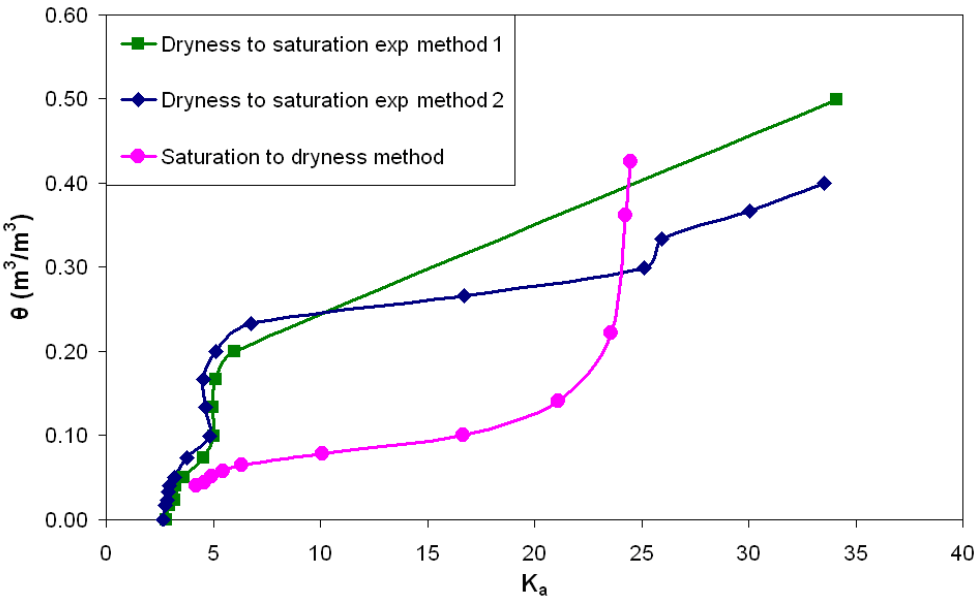

Figure 45: θ-K_a curves with different water content values and methods

Nevertheless, the high hydraulic conductivity of the coarse grain-size and the low organic matter content (OMC) of the media still made it difficult to measure a homogenous water content in the container, as water quickly moved to the bottom of the container, thus distorting the measure. We consequently used another method, moving from saturation to dryness via a drop-by-drop drain and linking the water content obtained by the Van Genuchten (1980) equation to the dielectric constant (Figure 46).

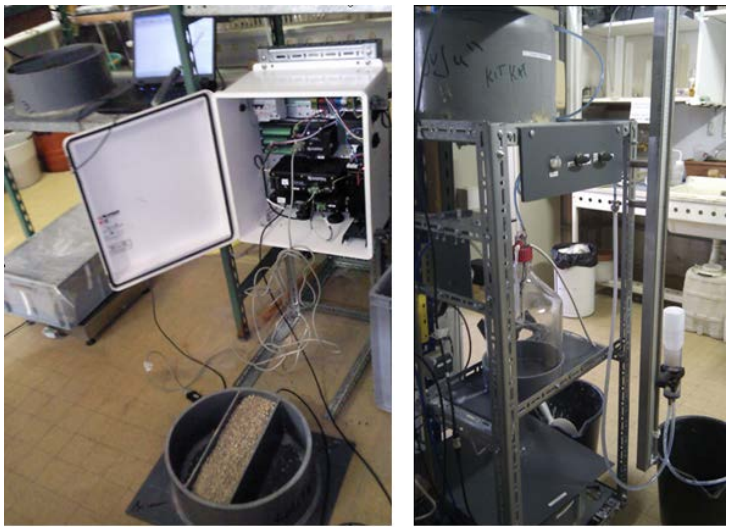

Figure 46: Increasing (left) and decreasing (right) water content TRD probe calibration methods

However, this decreasing water content method took a long time to drain the water out and was unable to did avoid water accumulation at the bottom of the container.

Figure 47 shows the uncertainties of K_a for different water contents, and confirms the difficulty and instability of measurements on high water contents. Despite several experiments, we opted to use the most popular empirical calibration for TDR, developed by Topp *et al.* (1980), which is based on various soil types ranging from sandy loam to heavy clay. Topp *et al.* suggest to use a second-order polynomial relationship (equation 18) between

dielectric constant and volumetric water content. Drungil *et al.* (1989), like others, have found that the empirical relationship derived by Topp *et al.* (1980) is valid for coarse textures.

$$\theta_v = -0.053 + (0.029 \cdot K_a) - (5.5E-4 \cdot K_a^{\,2}) + (1.3E-6 \cdot K_a^{\,3}) \qquad \textbf{Equation 18}$$

Figure 47 compares the *θ-Ka* curve obtained by the dryness-to-saturation method and the Topp formula. The Topp formula presents a more harmonious increase in θ_v according to *Ka* than the dryness-to-saturation method, which enables a better study of the time-course evolution in on-filter volumetric water content.

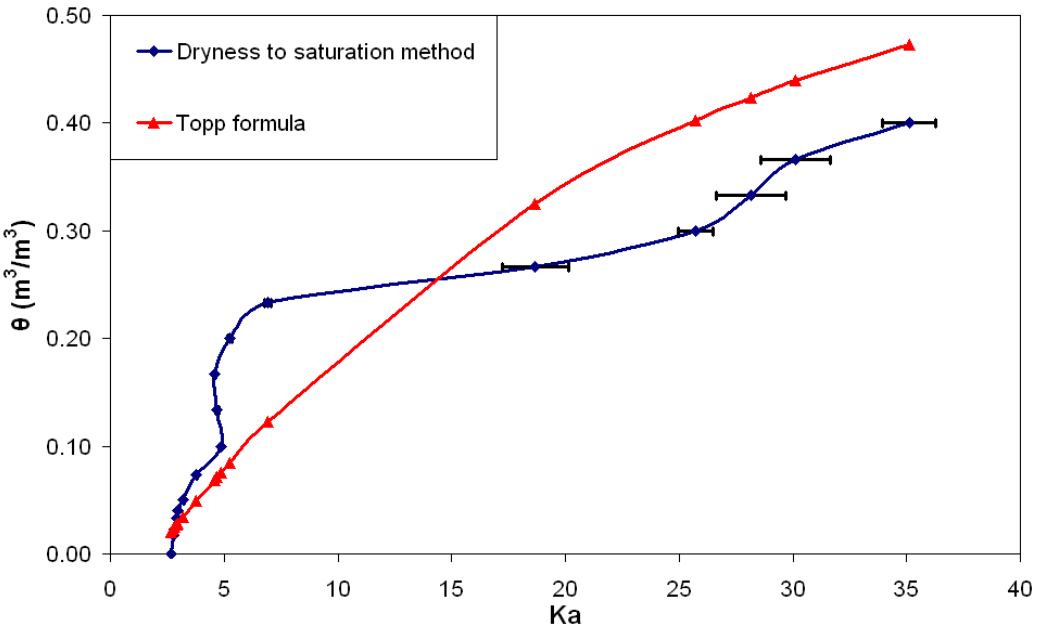

Figure 47: θ-K_a curve with different water content values for the Topp Formula and the dryness-to-saturation method with K_a uncertainties

The water content analysis campaigns are reported in section 4.1.1.

3.1.4. Treatment performances monitoring

The filter's treatment performances were evaluated using different approaches :

- Classical sampling campaigns were regularly led to evaluate performances under different seasons and loads.
- Some specific parameters at the outlet of the first stage were continuously monitored to observe the dynamic behaviour of the filter in response to rain events.
- An intensive campaign was led to study decline in treatment performances over long feeding periods.

3.1.4.1. Classical campaigns

Twelve classical monitoring campaigns were carried out for different hydraulic loads on different feeding days and seasons over the 2-year monitoring period. Each campaign consisted of 24-h composite samples divided into 3 periods per day to separately analyse (i) night, morning and afternoon in dry-weather periods and (ii) beginning, middle and the end of the rain event for rain-event periods.

The campaigns used three automatic refrigerated samplers (ISCO 4700) located at :

- The inlet to the dry weather distribution system (treatment plant inlet)
- The inlet to the second-stage batch distribution system (first-stage outlet)
- The outlet of treatment plant

Composite samples were used to analyse treatment efficiency at each stage of the plant. The parameters analysed by the Irstea lab were SS, total and dissolved COD, BOD_5, TKN, NH_4-N, NO_3-N, NO_2-N and PO_4-P in accordance with international standard methods (APHA 2005).

Dry-weather campaigns

Seven dry-weather campaigns were completed for different feeding days and seasons. Samples were taken from 0h00 to 23h59. The samplers pumped 80 mL every 6 minutes and contained 24 litre bottles, each corresponding to one hour of the day. The composite samples were built proportionally to measured flow at each sampling point.

Table 11: Dry-weather campaigns to gauge treatment performance

Campaign	Date	Feeding day	Average air temperature (°C)	Hydraulic load (m^3/m^2)
1	29/03/2011	0.5	10	0.42
2	25/05/2011	1.42	19	0.27
3	27/08/2012	0.01	16	0.27
4	29/08/2012	3	18	0.30
5	02/09/2012	7	16	0.29
6	04/09/2012	9	19	0.23
7	06/09/2012	11	19	0.26

Campaigns 3 to 7 formed part of the intensive campaign; see section 3.1.4.2.

Rain-event campaigns

In rainy weather periods, composite sample duration varied according to rainfall event, and was again divided into 3 periods to analyse the beginning, middle and end of the rain event. The samplers pumped 80 mL every 3 minutes, corresponding to 0.5 h of the day for each bottle. A total of 12 h of sampling for the inlet to the treatment plant and the second-stage batch feeding system was implemented to gain a finer analysis of the rainfall event. Given the residence time in the filters, i.e. about 3 h for water to transit the entire treatment plant during big rain events, samples at the treatment plant outlet were taken every 6 minutes over a 24-h

period, so all the water fractions sampled at the inlet to the system could be recovered at the outlet. A decrease in electrical conductivity at each stage of the system confirmed the passage of stormwater (Figure 48, *bottom*) and provided the lag-time needed to reconstruct the mean samples.

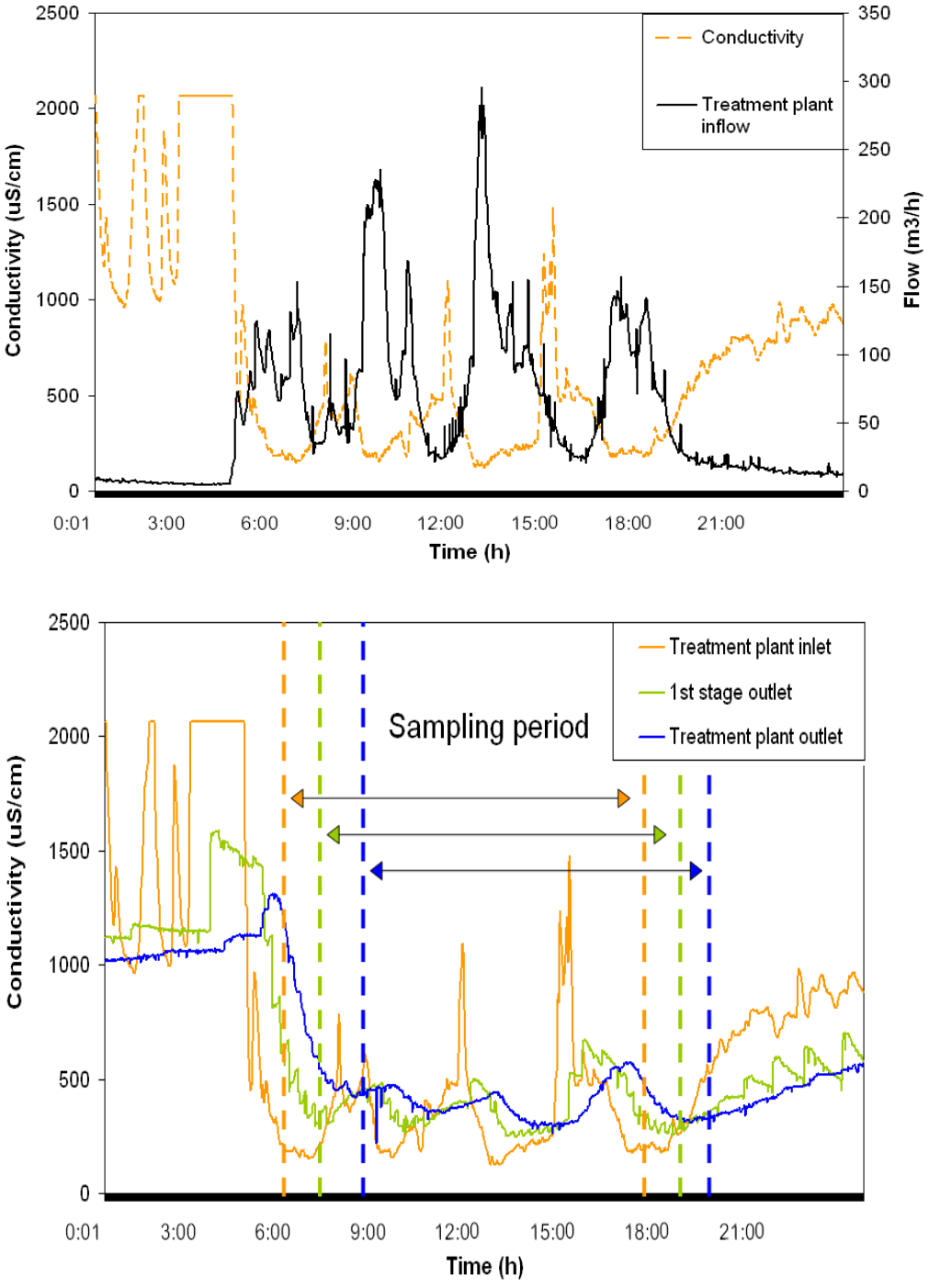

Figure 48: Treatment plant inflow and inlet conductivity during a rain event (*top*), treatment plant conductivity at different stages of treatment during a rain event (*bottom*)

To be sure to start the sampling during rain events, an inflow threshold of 80 m³/h was used to automatically trigger sampling. The distance between the lab and the treatment plant (130 km) made it difficult to carry out the rain-event campaigns. On many occasions, inlet peak-flow

was a short burst that did not induce a long high rain event. The high rain event could arrive a few hours after starting the samplers, making it impossible to catch the longest rain events.

In order to obtain rain event data for different seasons, hydraulic loads and feeding days, a total of 5 rain event campaigns were successfully carried out, as shown in Table 12.

Table 12: Rain-event campaigns to gauge treatment performances

Campaign	Date	Feeding day	Average air temperature (°C)	Hydraulic load (m^3/m^2)
1	04/11/2011	1.75	10	1.49
2	13/12/2011	3.13	3.5	0.77
3	20/12/2011	0.19	0	1.17
4	04/04/2012	1.29	12	0.68
5	12/06/2012	0.25	14	2.26

3.1.4.1.Continuous monitoring

The objective of the online measurements was to gain a finer analysis of the influence of rain events on treatment performances, especially performances on NOx-N forms, as nitrification is sensitive to oxygen conditions as well as ammonium adsorption capacity. In addition to electrical conductivity measurements at each treatment stage (WTW LF 470 probes), we also determined SS, COD (total and filtered) and NOx-N using an on-line UV-vis probe (S::can Messtechnik, GmbH, Vienna, Austria) at every 60-second interval (Rieger et al., 2004, De Bénédittis & Bertrand-Krajewski 2006). Specific calibration based on Partial Least Square (PLS) regression (Aji et al., 2003) was carried out using grab samples taken during the experiment for rain-event and dry-weather periods. The probe was installed at the first-stage filter outlet (Figure 49).

Figure 49: s::can probe at the inlet of second batch feeding system

The probe is a 60 cm-wide 44 m-diameter aluminium cylinder that measures light attenuation across the measuring gap, i.e. 5 mm here. The wavelength from 200 to 750 nm in 2.5 nm steps covers the ultraviolet and visible domain (De Bénédittis & Bertrand-Krajewski 2006). A

xenon flash lamp emits two beams – one to measure and the other as reference analysed by a receptor – and the absorption spectra are translated into pollutant concentrations.

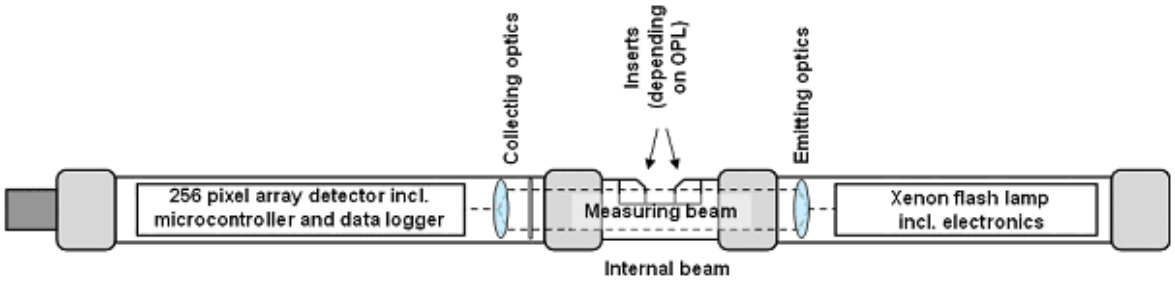

Figure 50 : Schematic illustration of the UV–vis spectrometer (Provost 2010).

S::CAN probe calibration

For each measurement, the probe provides the complete absorption spectrum as the concentration values evaluated by the system software (*ana::pro*) according to the calibration (*global calibration*) integrated by the manufacturer. This manufacturer-established calibration was based on analyses on several treatment plant outlet wastewater samples and is assumed to be adapted to standard domestic wastewater. However, global calibration does not provide reliable and accurate values as each wastewater has its own specific characteristics. A *local calibration* needs to be established for each pollutant with the local wastewater studied in order to take into account its variability and specificity. This local calibration establishes a linear or polynomial mathematical relationship between the values provided by the probe in *global calibration* mode and the reference values obtained. This calibration calculates a new value for the equivalent concentration :

$$C'_{eq} = a + bC_{eq} \quad \text{or} \quad C'_{eq} = a + bC_{eq} + cC_{eq}^{2} \qquad \textbf{Equation 19}$$

where:

C'_{eq}: concentration estimate from local calibration (mg/L)

C_{eq}: concentration estimate from global calibration (mg/L)

a, *b*, *c*: numeric coefficients obtained from regression

The specific calibration based on PLS regression (Aji *et al.* 2003) proved the most robust, especially for concentration-spectra relationships. Consequently, we chose to proceed with this method. Calibration was carried out using grab samples taken during the experiment (97 for SS, 99 for NOx-N, 97 for total COD and 75 for dissolved COD) in rain and dry periods, collected to gain a large panel of concentrations and achieve better calibration. It compares the values for pollutant concentration (*C*) given by standard laboratory methods and the values of absorbance $A(\lambda\ i)$ in *n* wavelengths (λi) measured by the probe. This approach establishes, for each pollutant parameter, a relation that gives an estimate (*Ceq*) of the pollutant concentration *C* based on absorbencies (De Bénédittis & Bertrand-Krajewski 2006) and thus yields more accurate values than *local calibration* :

$$C \approx C_{eq} = \sum_{i=1}^{n} \left(A(\lambda_i) a_i \right) + K$$ **Equation 20**

where:

a_i: numerical coefficients obtained by regression (m.mg/L)

$A(\lambda i)$: absorbance for wavelength λi (m^{-1})

C: sample concentration (mg/L)

C_{eq}: concentration estimate from the spectrum (mg/L)

K: numerical constant obtained by regression (mg/L)

n: wavelength number used to calculate C_{eq}.

Calibration includes all wavelengths to determine the concentrations of the different parameters taking into account the variability of dry weather and rain-event periods.

PLS regression is a multivariate method for predicting the outputs of a given system from input independent variables. In UV–vis spectrometry, the independent variables are the absorbencies at different wavelengths, represented by the matrix X, and the output variables are the pollutant concentrations, represented by the matrix Y. Regression consists in decomposing the matrices X and Y into principal components, called latent vectors, in order to explain the covariance between X and Y. The choice of the number of latent vectors is essential to obtain the optimal PLS regression parameters and allow a good fit to the calibration data and good concentration predictions. It is important to take into account only the information relevant to the calibration data and not the intrinsic sample variance (noise). If more latent vectors are taken than needed, it enhances the description of the calibration data but will decrease the quality of new sample predictions. Number of latent vectors is chosen based on two considerations (Aji *et al.* 2003): (i) the quality of the fit to the data, which is taken into account by the percentage of variance explained by matrix X and the absorption spectra of vector Y concentrations; (ii) the quality prediction (Prediction Error Sum of Squares; PRESS) by jackknife or leave-one-out cross validation that consists in separating *n* calibration data into two datasets: first *n-1* samples to build the PLS model, and second a set containing the last sample to test quality of prediction. The square of the difference between the sample value and the value predicted by the model of the validation sample is then calculated. This is then repeated *n* times so that all samples are used for validation. We can then obtain the root mean square error of prediction (RMSEP), which is calculated using the following formulae.

$$RMSEP = \sqrt{\frac{PRESS}{M}}$$ **Equation 21**

and

$$PRESS = \sum_{m=1}^{M} \left(C_m - C_{eqm} \right)^2$$ **Equation 22**

where:

m: validation data

C_m: reference concentration value for validation data *m*

C_{eqm}: concentration value predicted by PLS for validation data *m*

M: total number of validation data

The number of latent vectors retained is the number that gives the minimum RMSEP while explaining the best covariance of matrices X and Y. Many multivariate regression algorithms using PLS regression have been developed to date, and authors recommend selecting 5 to 7 latent vectors to determine SS, COD and NOx concentrations (Langergraber *et al.* 2003a). However, in our calibration procedure, equilibrium was achieved using just 3 latent vectors (Figure 51). Here, we used the *pls package* (2007) developed by (Mevik & Wehrens 2007) in conjunction with the "pls library" bundled with *R* statistical software.

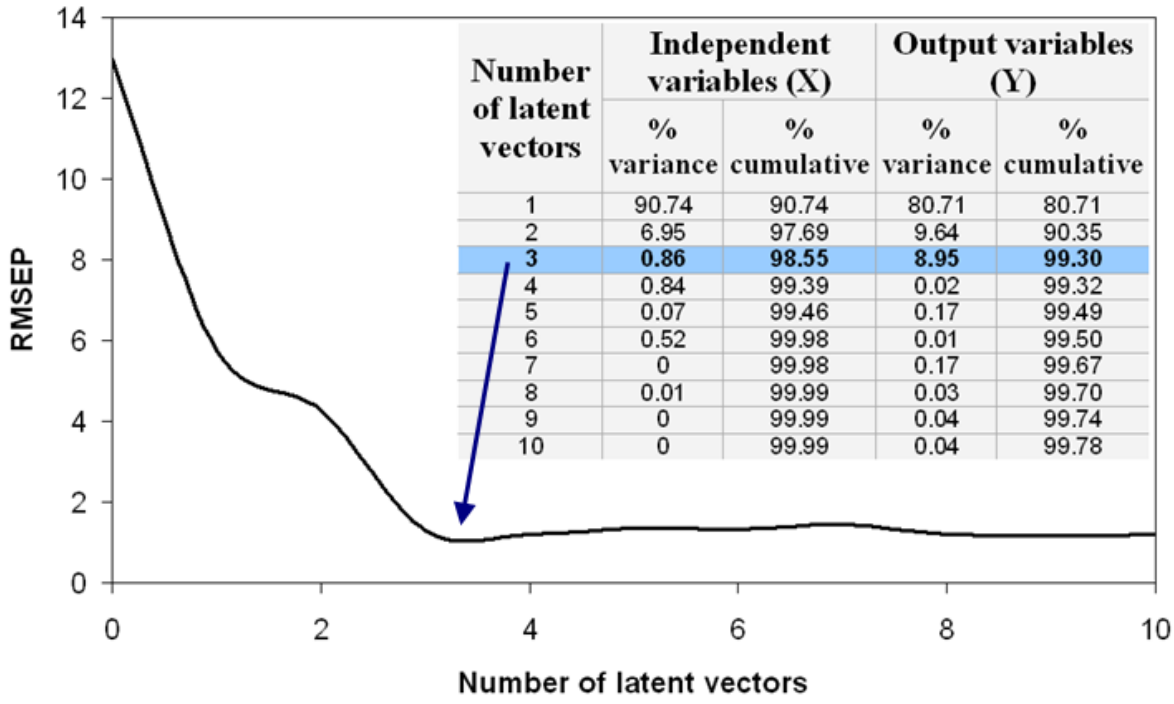

Number of latent vectors	Independent variables (X)		Output variables (Y)	
	% variance	% cumulative	% variance	% cumulative
1	90.74	90.74	80.71	80.71
2	6.95	97.69	9.64	90.35
3	**0.86**	**98.55**	**8.95**	**99.30**
4	0.84	99.39	0.02	99.32
5	0.07	99.46	0.17	99.49
6	0.52	99.98	0.01	99.50
7	0	99.98	0.17	99.67
8	0.01	99.99	0.03	99.70
9	0	99.99	0.04	99.74
10	0	99.99	0.04	99.78

Figure 51: Selection of number of latent vectors: table shows percentage of variance explained by X and Y (PLS components), and plot shows evolution in the Prediction Error Sum of Squares (PRESS)

For the calibration, the probe is placed under a controlled flow (24 mL/s, peristaltic pump, Figure 52) to avoid sedimentation around the measurement cell. Each sample was submitted to 5 measurements, whose spectra were averaged for calibration.

Figure 52: Samples measurement by the S::CAN probe for calibration

As wastewater composition differs between rain events and dry periods, we needed to check whether theirs particularities are still differentiable at the outlet of the first-stage filters. Consequently, PLS calibrations were run separately for each dataset (Figure 53). In order to exclude the particulate component in the dissolved COD and NOx-N measurements, the spectra were turbidity-compensated (s::can) for these parameters.

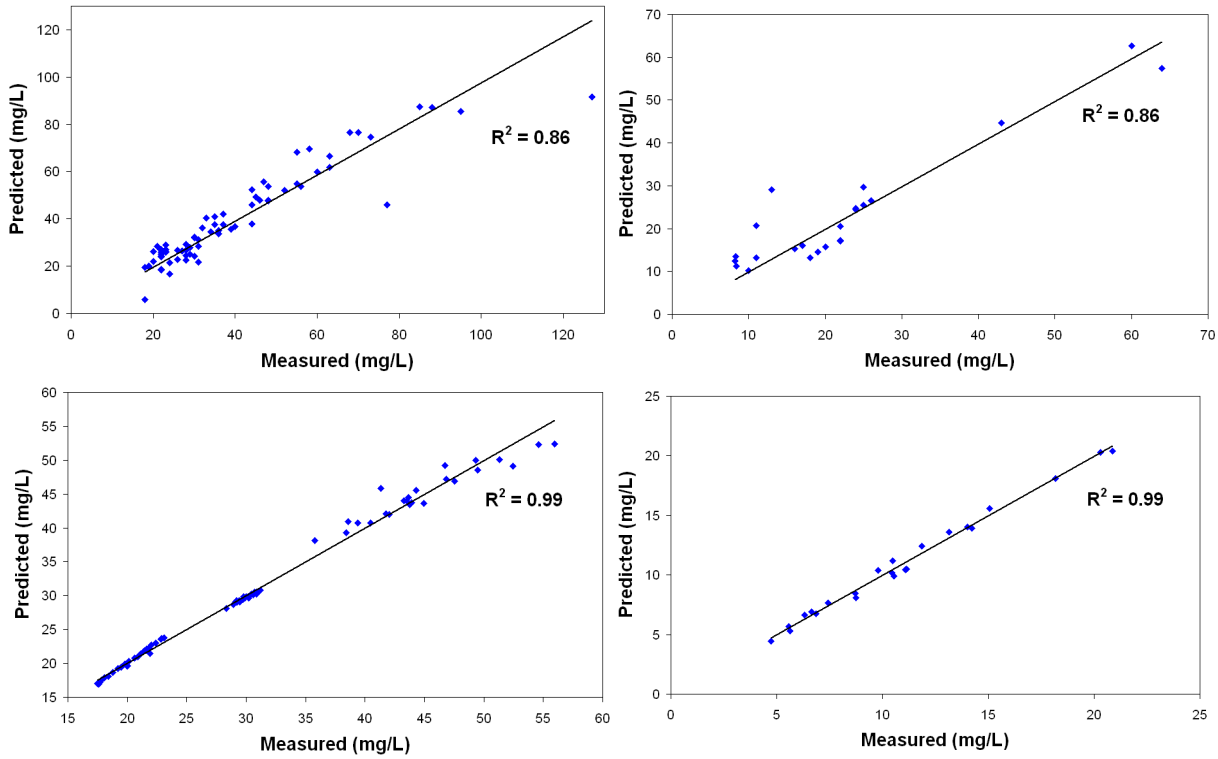

Figure 53: Predicted *vs* measured concentrations for NOx (*bottom*) and SS (*top*). PLS calibration for dry weather (*left*) and rain-event weather (*right*)

For total COD, SS and NOx-N parameters, we found no difference in PLS calibrations between dry and rain-event weather (Figure 53, for SS and NOx-N). Thus, the full data-set could be used for calibration at the same accuracy and on a wider range. PLS calibrations demonstrated very satisfactory results for the NO_x, total COD and SS parameters, with

regression coefficients of 0.99, 0.91 and 0.84, respectively (Figure 54). For dissolved COD, the measurements were too inaccurate to hold predictive value.

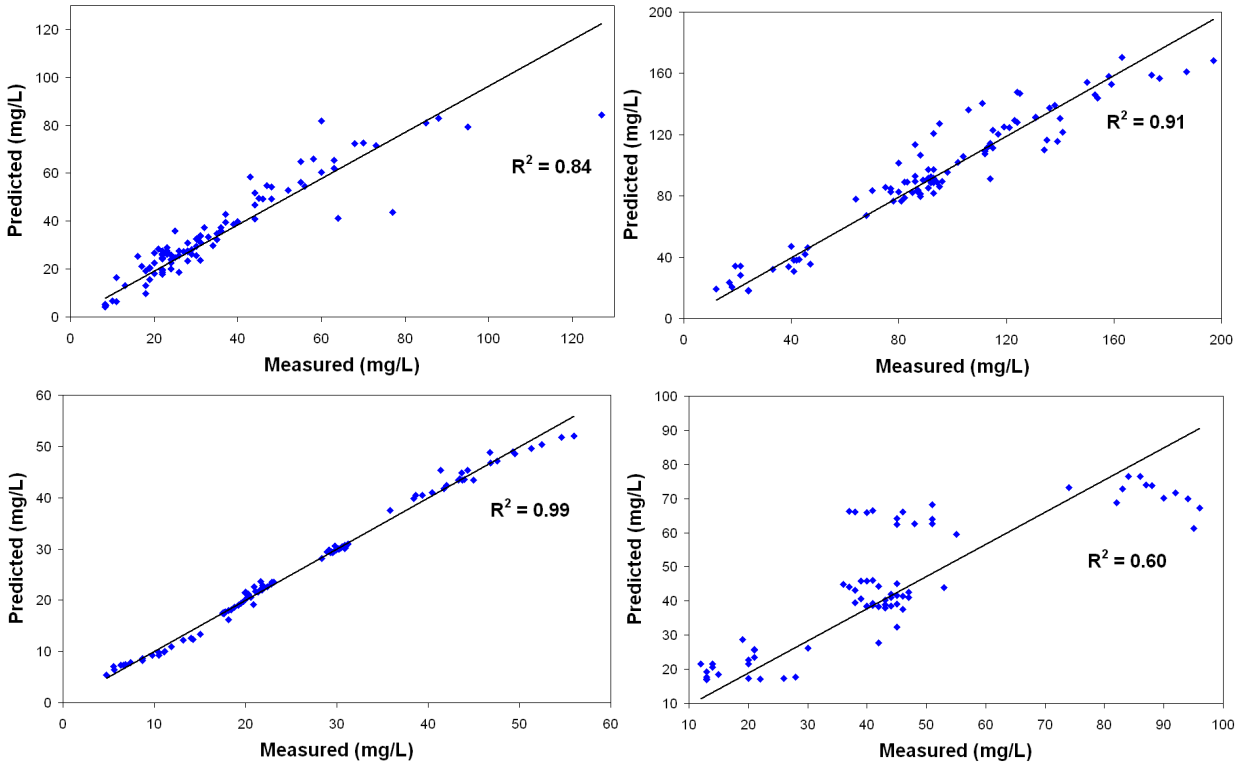

Figure 54: Total PLS predicted *versus* measured concentrations for SS (*top left*), total COD (*top right*), NOx (*bottom left*) dissolved COD (*bottom right*)

The calibration ranges extend from 8 to 127 mg/L for SS, 12 to 197 mg/L for total COD, and 5 to 56 mg/L for NOx.

3.1.4.2. Intensive treatment performance campaign

In this campaign, one first-stage cell was fed for 11.5 consecutive days from 27th September to 7th October 2012, with the main purpose of observing the relationship between oxygen depletion and decline in treatment performances. In addition to the hydraulic measurements presented above and the S::CAN probe, the intensive campaign also included :

- Continuous measurements of N-NH_4 and N-NO_3 at the inlet and outlet of the first stage (VARiON®Plus probes, WTW). Probes were calibrated with wastewater corresponding to the measurement points with a regression coefficient of 0.99 and 0.96 for the inlet and outlet of the first stage, respectively.
- Five 24-h composite samples at each treatment stage (classical sampling campaigns) were taken every two days.
- On the days in between the 24-h composite samples, batch feeding samples were taken 3 times a day (9 a.m., 1 p.m. and 5 p.m.) for SS, N-NH_4 and COD analysis (APHA 2005). These samples were used to estimate daily loads during the campaign.

- Gaseous oxygen concentration measurements (twice a day, at depths of 10, 20 and 30 cm; Dräger Sensor XS©gas analyser) on the first stage. Oxygen content is expressed as percentage of air phase (O_2 saturation in air being 20.9%). Measures were done 45 min post-feeding batch at 5 different distances (from 0.1 m to 4.8 m) from a feed point.
- Four fluorescein tracing campaigns were carried out (GGUN-FL22 fluorimeter) between the 24-h composite samplings.

Figure 55: VARiON®Plus probe (*left*) and Dräger XS©gas sensor (*right*)

3.2. Hydraulic modelling

3.2.1. Modelling objectives

Our study aimed to establish a simplified model to evaluate hydraulic overload acceptance on VFCWs. The simplified model is oriented to include the following characteristics :

- One-dimensional approach (for easy handling)
- One-minute time-step
- Focused on ponding time (to link lack of oxygen to treatment performances)
- Focused on ponding depth (which influences infiltration rate)
- Focused on seasons (due to reed growth and degree of mineralization of the deposit layer, both of which are factors that influence infiltration rate)

3.2.2. Simplified model

Under hydraulic overload conditions, the deposit layer is saturated and is the hydraulically limited step, producing surface ponding at high hydraulic loads. Consequently, in a rain-event period, water pressure caused by ponding is one of the main factors influencing infiltration rate. We chose a simple law inspired by Darcy's law. As Darcy's law has fixed parameters, it

cannot follow the changes in the hydraulic properties of the deposit layer (clogging, mineralization, physical effects of the reeds, etc.). It was important to follow infiltration rate behaviour for different seasons and ages.

The model is built by different components from which water flow is calculated by mass balance and specific laws. The first component is a storage volume above the filter surface that receives wastewater from the batch feeding system and infiltrates wastewater by an infiltration rate. Hydraulic head variations play a key role in the infiltration processes (Beach *et al.* 2005). Discharge from the storage volume was modelled by a simple infiltration law (Equation 23), where the hydraulic conductivity (*K*) of Darcy's law is replaced with a parameter representing the infiltration capacity (*ICP*) proportional to infiltration rates, and *h* is the ponding water depth (hydraulic head). When used on batch feeding, this simple equation assumes that the sludge deposit is saturated. Consequently, the hydraulic gradient of Darcy's law (*dh/H*) can be approached via ponding depth.

$$IV = ICP \cdot h$$ **Equation 23**

where:

IV = infiltration velocity, in m/s^{-1}

ICP = infiltration capacity parameter, in s^{-1}

h = hydraulic head, in m

The second component – the filter – is only represented by a time-lag that accounts for water flow within the media. Outlet flow and ponding water depth can be calculated by mass balance at one-minute time-step intervals (Figure 56). As in the experimental site, the model also uses a by-pass to protect the filter against long-sustained ponding.

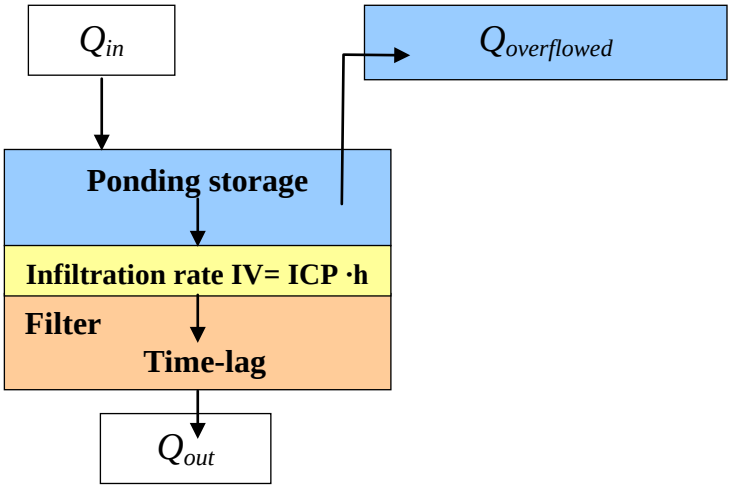

Figure 56: Schematic diagram of the simplified hydraulic model

The simplified model does not take into account evapotranspiration and water storage inside the filter pores. In VFCW's, it is safe to neglect evapotranspiration during feeding periods, but not water storage during the first day of feeding, as discussed later in section 3.2.2.1.

3.2.2.1. Calibration of the simplified model

Calibration of the simplified model has to start by defining (i) time-lag representing the filter itself, (ii) water storage on porous media to see its impact on outflow, and iii) *ICP*.

Defining the time-lag

As the filter material layers are not directly represented in the simplified model, water storage is not calculated and the filter is only represented as a time-lag to account for water flow within the porous media. To define the time-lag value, the first-stage outflow was compared to simulation data.. The time-lag is then fitted to superpose the simulated and measured outflow peaks after a batch feeding (Figure 57).

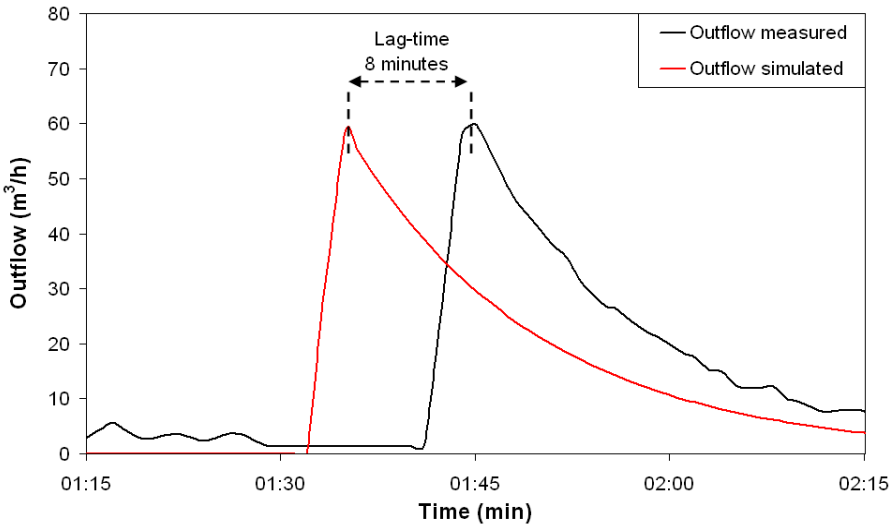

Figure 57: Time-lag between measured and simulated first-stage outflow peaks at Challex treatment plant

Based on the entire set of events (rainfall and dry-weather events), the time-lag is 8 minutes (SD: 3.5 for dry-weather flow and 1.8 in rain events) for young VFCW (Challex plant) and 11 minutes (SD 8.49) for mature VFCW (Evieu plant, see section 3.2.2.1. *ICP* fitting). These values were then introduced into the model to fit the *ICP*.

Water storage in porous media

To evaluate water storage over a feeding period, 11 TDR campaigns were carried out during the two-year monitoring period. Two inlet-flow/water-storage relations were established according to season (summer and winter) ready to be applied in the simplified model to study the impact of stored water on the *ICP*.

In-filter water storage was calculated using the water content of the first TDR profile, assuming a homogenous distribution of water content (Figure 58). The evolution of water storage volume before each batch entering the filter led to an estimate of saturation progress in the porous media. Once water storage volume has become relatively stable, water storage can be neglected.

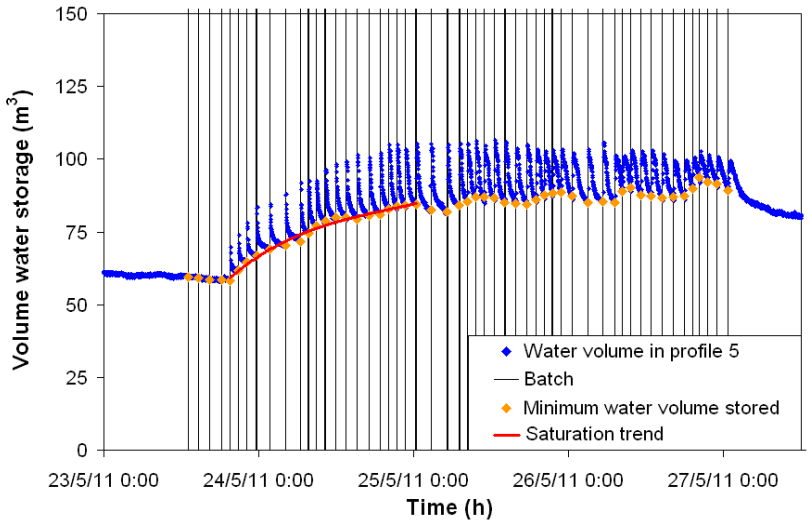

Figure 58: Time-course evolution of first-stage water storage in summer

The two "inlet-flow/water-storage" relations determined by TDR measurement are presented in Figure 59.

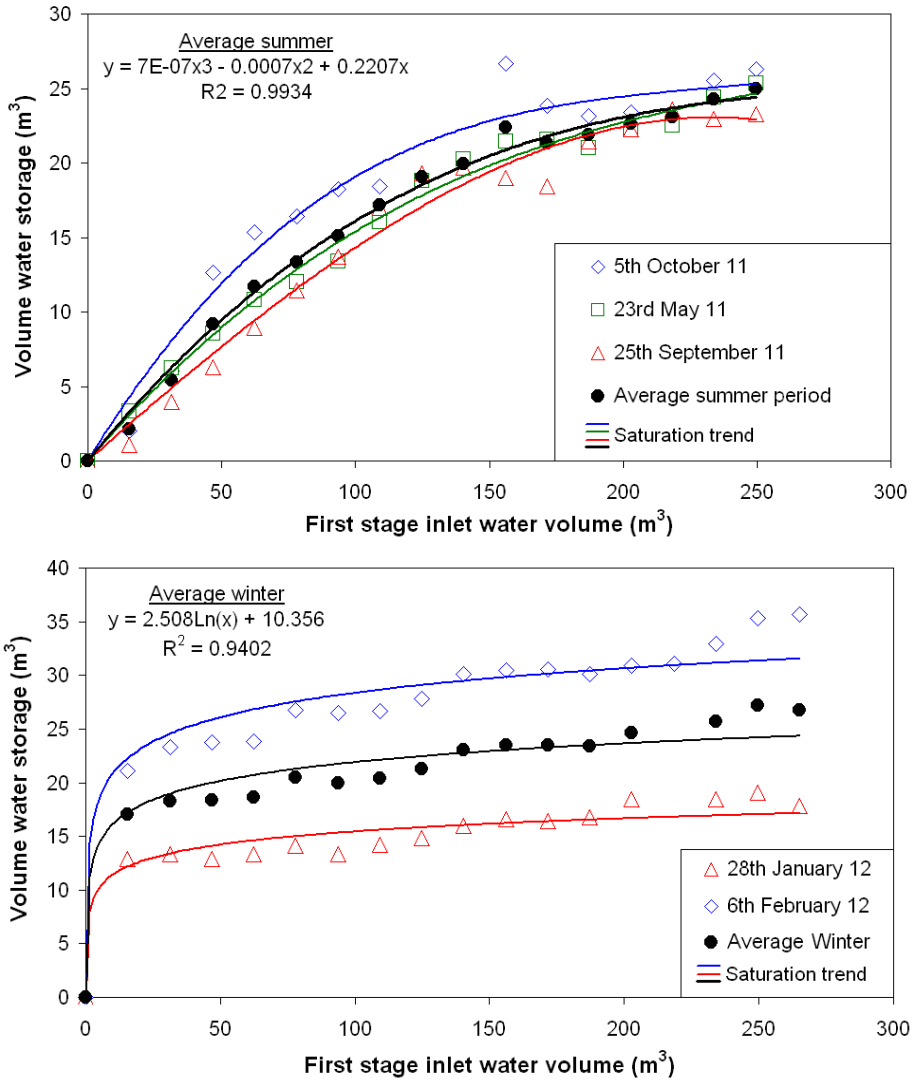

Figure 59: Inlet-flow/water storage relations for summer (*top*) and winter (*bottom*)

Based on the TDR campaigns, peak storage is about 25 m³, i.e. only 10% of inlet flow. Figure 59 shows that water is stored slower in summer than winter, possibly due to reeds promoting infiltration into the media. Equations 24 and 25 (for summer and winter respectively) were introduced in the model to include the impact of water storage on outflow and *ICP*. The maximal stored volume is extracted from simulated ponding depth values.

$$ws = 7E\text{-}07(Iv)^3 - 0.0007(Iv)^2 + 0.2207(Iv) \quad \textbf{Equation 24}$$

$$ws = 2.508\mathrm{Ln}(Iv) + 10.356 \quad \textbf{Equation 25}$$

where:

ws: water stored, in m³

Iv: first-stage inlet-water volume, in m³

ICP fitting

To study the sensitivity of the *ICP* and its evolution over time, the model was fitted on outflow according to :

- *Hydraulic load (dry-weather and rainfall event)*

  Figure 60 presents the hydraulic loads dataset distribution used for the fitting. Hydraulic loads ranged from 0.20 to 2.53 m.day⁻¹, distributed in 33 rainfall events and 59 dry-weather events (including snowmelt and/or freshwater).

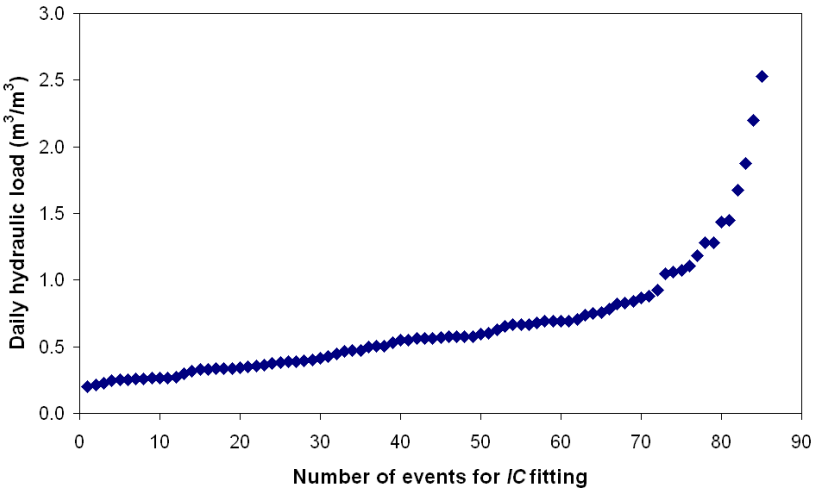

Figure 60: Distribution of hydraulic loads from events used for IC fitting

- *Feeding day (saturation progress)*

  The feeding days were homogenously distributed in :

  24 first feeding day events

34 second feeding day events

28 third feeding day events

- *Season (reed growth patterns)*

In order to obtain good representatively, the events were distributed over seasons with presence of fully-grown reeds (April to October) and with few or no fully-grown reeds (November to March), giving 44 and 42 events, respectively. The events were less numerous from May to November due to the scarcely workable rainfall events and the homogeneity of dry-weather events.

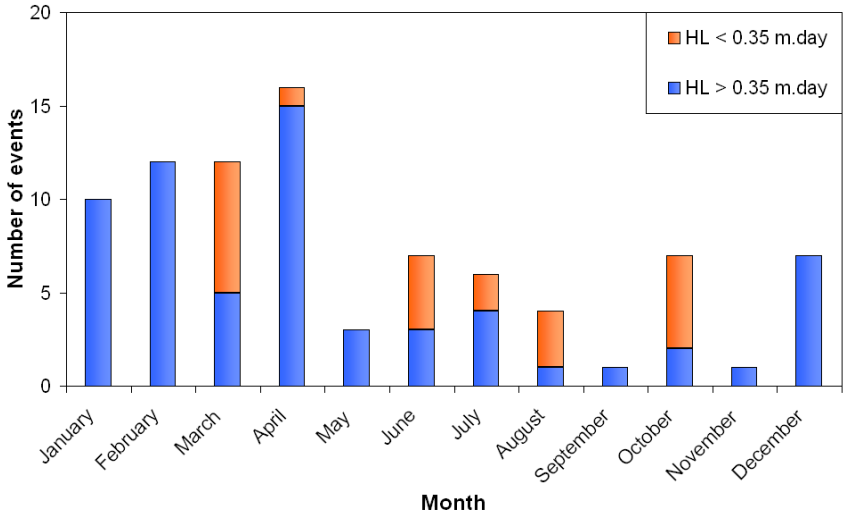

Figure 61: Number of events distributed by month

- *Age of the system (sludge layer and organic content of the porous media)*

The *ICP* values obtained from the Challex VFCW with 2 years in operation and approximately 2 cm of sludge layer were compared to the ICP values obtained from the Evieu VFCW studied in previous Irstea work (Morvannou, 2012) and which has treated domestic raw wastewater at nominal load in 8 years of operation and 20 cm of sludge layer. The Evieu plant has an infiltration layer grain-size of d_{10} = 2.46 mm and batch feeds of 5 cm at a rate of 1.23 $m^3.h^{-1}.m^{-2}$ on average, and a 3.5/7-day feed/rest regime. The two VFCW are designed and operated according to French guidelines. They are situated in the same region and exposed to similar climate conditions.

Only two campaigns on the Evieu treatment plant could be studied. These campaigns took into account seasonal variability. One campaign was performed at the end of winter (April 2010) and another at the end of summer (October 2010). These campaigns were led from the first to third feeding day, in dry weather, with an average hydraulic load of 0.48 $m.d^{-1}$ and a standard deviation of 0.08.

For the full set of scenarios, the *ICP* was fitted in three steps :

a. As ponding water depth was not homogeneous over the entire filter surface (due to uneven sludge deposits and uneven surface planarity), the *ICP* was fitted on first-stage outlet flow by the least squares method.
b. Simulated surface ponding was then compared to measured surface ponding to verify the coherence of the model.
c. Finally, the simplified model was compared to a mechanistic model, Hydrus 1D (for the Challex filter only).

a. Fitting of the IC parameter from first-stage outlet flow

Fitting was carried out over 24-h measurements for dry weather flows and over variable times for rainfall events. Water volumes entering the filter by dry weather and rainfall distribution systems were introduced into the model. Batches were simulated and infiltration was calculated via the *ICP* (lag-time already included). First-stage outflow measured on experimental sites was used to fit the *ICP* by the least squares method. Simulated outflow showed high harmony with measured values using the Nash-Sutcliffe efficiency coefficient (Equation 26), a normalized statistic that determines relative magnitude of residual variance ("noise") compared to measured data variance ("information"), where 1 represents perfect accuracy. Results showed a better agreement with measured data in summer than winter, with efficiency coefficients of 0.83 and 0.74 for dry weather events and rainfall events for summer against 0.56 and 0.74 for winter, respectively.

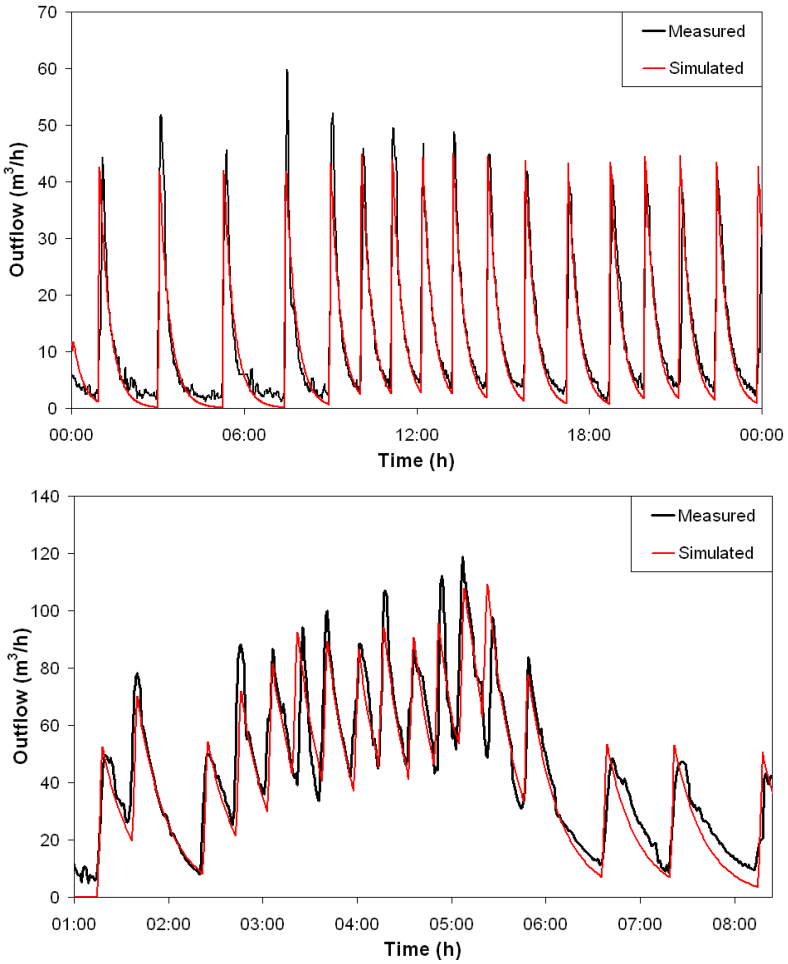

Figure 62: First-stage outflow measured and simulated for dry weather event -22nd July 2012- (*top*) and rainfall event -6th June 2011- (*bottom*) in summer

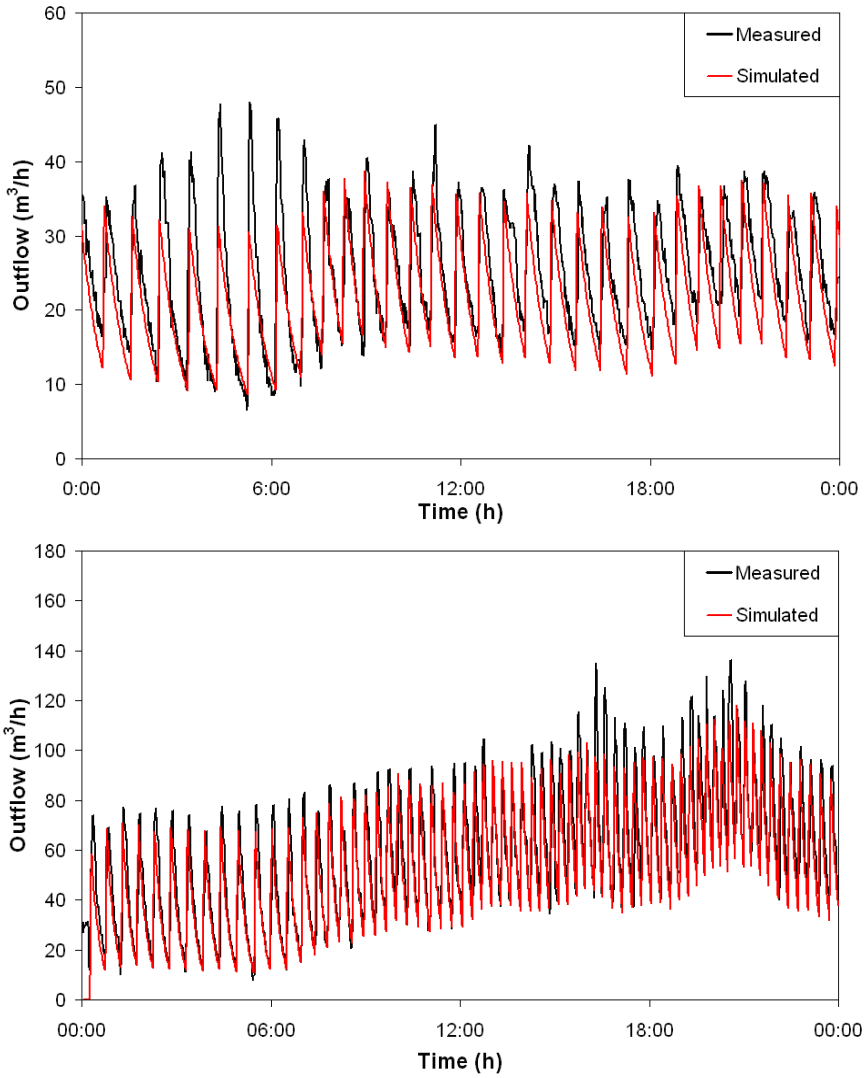

Figure 63: First-stage outflow measured and simulated for dry weather event -30th January 2012- (*top*) and rainfall event -21st December 2011- (*bottom*) in winter

$$E = 1 - \frac{\sum_{t=1}^{T}\left(V_o^t - V_m^t\right)^2}{\sum_{t=1}^{T}\left(V_o^t - \overline{V}_o\right)^2}$$ **Equation 26**

where:
V_o = observed value at instant t
V_m = modelled value at instant t
$\overline{V}_o$ = average observed value
T = total number of values

b. Simulated and measured ponding

Ponding depth measures from ultrasonic probes at the first-stage were used to validate the data from the simplified model. Despite the probes just provide the local ponding depth, ponding depths measured in the winter period demonstrated that the simulated data fitted between the three different measured levels. High infiltration rates in summer sometimes made it difficult to measure ponding with all the probes (surface heterogeneity), but simulated

ponding depths remained reasonable. Figures 64 and 65 demonstrate that results provided by the simplified model are in a correct order of magnitude compared to measured results.

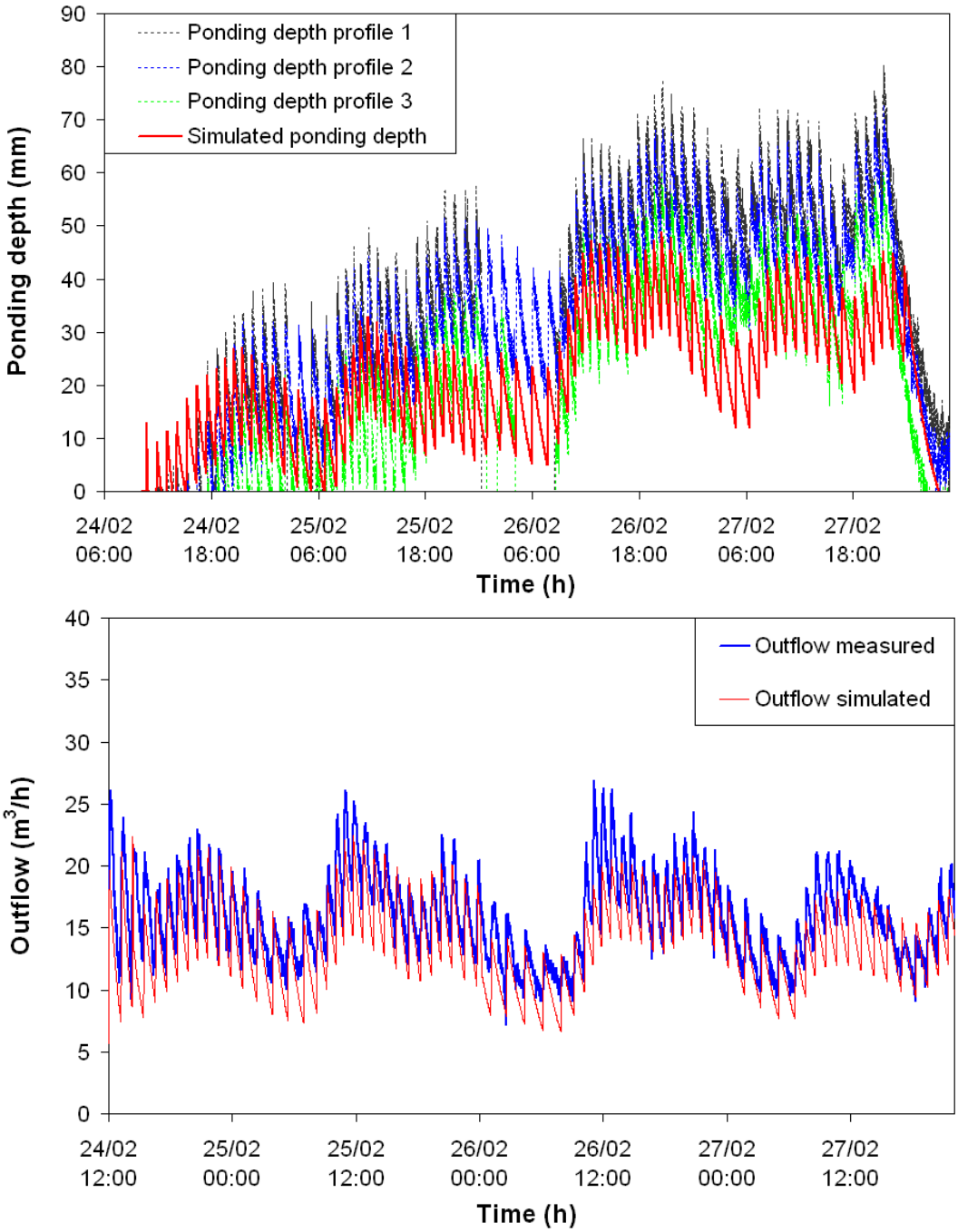

Figure 64: Ponding depth (*top*) and first-stage outflow (*bottom*) measured and simulated for winter feeding period

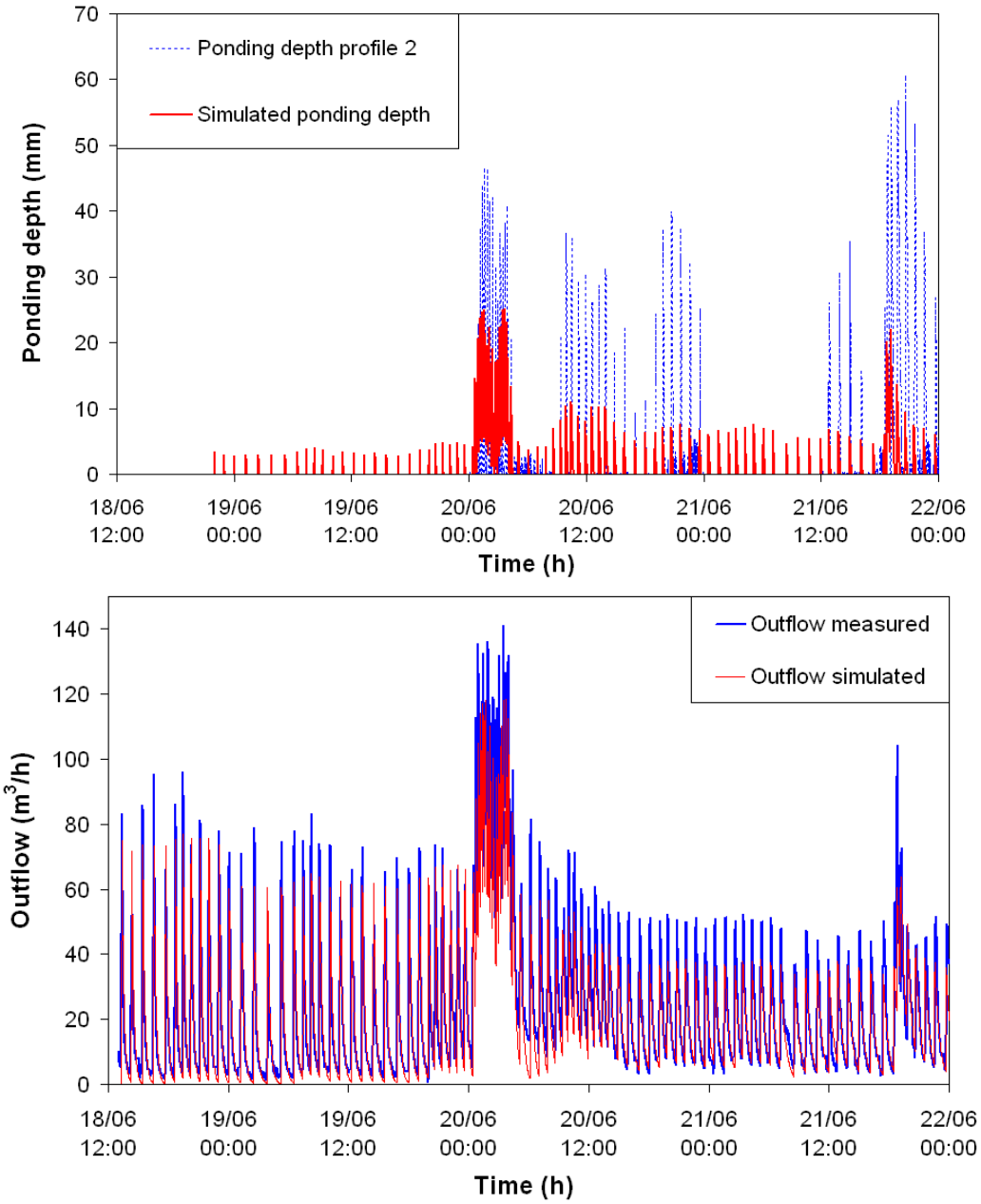

Figure 65: Ponding depth (*top*) and first-stage outflow (*bottom*) measured and simulated for summer feeding period

Ponding depth simulated comes visible before the experimental site ponding depth measurements. This consequently increases ponding time and makes the simplified model more secure according to the oxygen depletion on filter. Rational simulated ponding depths and ponding times make it possible to accurately identify problems tied to lack of oxygenation in the filter.

c. Comparison with Hydrus

The simplified model was compared to the mechanistic Hydrus model, which is the most popular code in CW. The comparison was made in terms of outflow, ponding time and depth. The advantage of comparison with Hydrus is that the model is fitted not only with an external parameter (first-stage outflow) but also with water content as internal parameter. This helps

confirm the capacity of the simplified model to reproduce the hydraulics of a VFCW. Hydrus-1D was chosen due to the one-dimensional approach of the simplified model.

3.2.3. Hydrus modelling

The filter was reproduced in Hydrus-1D with a single porosity model. The Van Grenuchten-Mualem and no hysteresis approach was used. The Hydrus model was 0.8 m in height with a mesh of 101 nodes separated into 4 different material layers mirroring our filter configuration. The Hydrus modelling step was focused on the first part of the infiltration layer, as Challex has accumulated very little sludge. Three observation points were inserted in the model at the same locations as the first TDR probes.

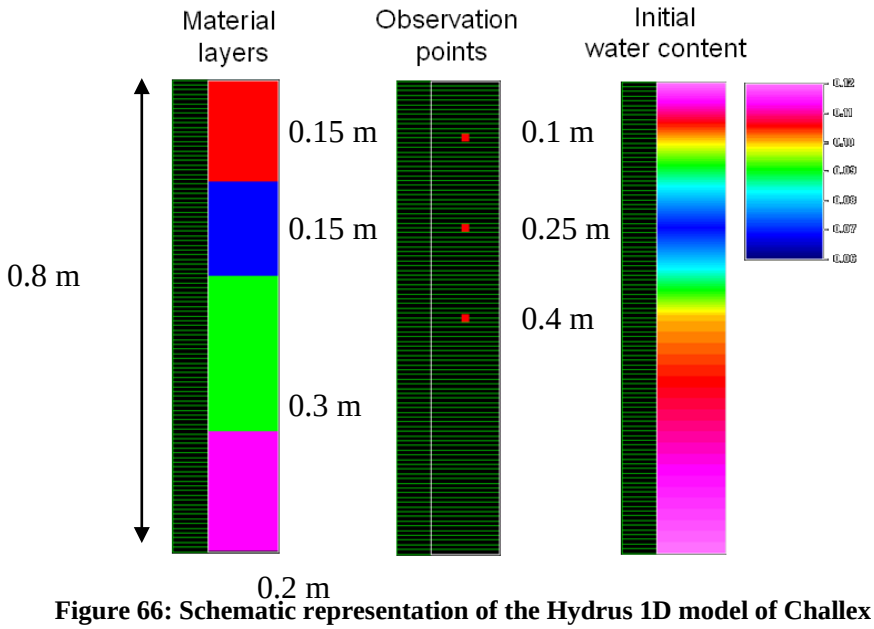

Figure 66: Schematic representation of the Hydrus 1D model of Challex VFCW

To calibrate the Hydrus-1D model, infiltration material was hydrodynamically characterized as described in section 3.2.3.1. This produced a set of parameters (initial values) that were used on the inverse optimization module included in Hydrus 1D. Starting calibration with these initial values limits the risk of non-convergence as they are likely to be close to optimal values.

3.2.3.1. Hydrodynamic characterization of the infiltration material

Characterizing the hydraulic properties of the filtering material of a VFCW is a prerequisite to model wastewater treatment using process-based filtering. A physical and hydrodynamic characterization of the first-infiltration-layer material was carried out by laboratory procedures to determine the parameters needed for Hydrus calibration of van Genuchten-Mualem closed-form expressions (Mualem 1976; Van Genuchten 1980) :

- Saturation hydraulic conductivity (K_s)

- Residual water content (θ_r)
- Saturation water content (θ_s)
- Alpha (α) and *n* parameters

As these parameters are used as initial parameter for inverse modelling, they are determined via simple approaches. Residual water content, alpha and *n* parameters were estimated from water retention curves (obtained by the sandbox method). Saturated hydraulic conductivity (K_s) was estimated by the Chapuis formula (Chapuis 2004) using lab-based particle-size distribution and pycnometry data. The Mualem pore connectivity parameter (λ), also necessary in Hydrus, has little influence on flow modelling (Ritter *et al.* 2003), and thus was set at 0.5 (Morvannou 2012). While some studies suggest that θ_s may be smaller than porosity due to entrapped air or the presence of flow irregularities (Wessolek *et al.* 1994; Richard *et al.* 2001), we presume that it is particularly true for finer-textured porous media or soils with high OMC, which is not the case of the clean gravel material of Challex. Consequently, saturation water content was assumed to equal porosity.

Particle-size distribution

Particle-size distribution was measured by the French standard protocol NF P 94-056 (AFNOR, 1996) for the first infiltration layer of the first stage and the second stage of Challex treatment plant. A total of 6 measurements for the first stage and 5 for the second were carried out in order to verify the repeatability of results.

Pycnometry

This method measures material density based on material masses at dryness and saturation. The protocol used was the French standard method NF P 94-054 (AFNOR 1991). Material density was combined with bulk density to calculate material porosity. We performed 25 density measurements for each of the two materials to get a good statistical distribution.

Porosity

Porosity can be calculated from mass density and bulk density via the equation :

$$n = 1 - \frac{\rho_{volume}}{\rho_{material}} \qquad \textbf{Equation 27}$$

with:
n = porosity (-)
ρ_{volume} = bulk density in g.cm^{-3}
$\rho_{material}$ = mass density in g.cm^{-3}

Bulk density takes into account the arrangement of the particles of material, linking the mass of dried sample to its volume. For the first stage, 5 samples were recovered *in situ*, taking care not to disturb the arrangement. Samples were dried at 105°C for 2 days before being weighed.

Saturation hydraulic conductivity

The saturation hydraulic conductivity of clean sand or gravel is frequently estimated with the Hazen (1911) equation where porosity, *n*, is close to its maximum value. To use this equation, soil has to meet three conditions: (i) loose compactness (*n* or *e* close to their maximum values), (ii) coefficient of uniformity *C*U less than 5, and (iii) diameter d_{10} between 0.10 and 3.0 mm. The extended Hazen equation at 20°C for routine laboratory conditions is :

$$K_s = 1.50 \bullet (d_{10})^2 \qquad \textbf{Equation 28}$$

Equation 27 gives us a K_s of 8.85 cm.s^{-1}. However, Chapuis (2004) compared the extended Hazen formula with a long number of measured K_s, and found that the formula tends to overestimate the measured K_s value for uniform gravels, which is our case. Consequently, we decided to use the Chapuis formula (Chapuis 2004) that can also be employed to predict the saturated hydraulic conductivity of clean sand and gravel. This formula is inspired by the extension of the Hazen (1911) and Kozeny-Carman (Kozeny 1927; Carman 1937, 1956) formulae and is extended to any *n* value the soil can take between its minimum and maximum values (clean soil). It uses the d_{10} values and soil void ratio (*e*) to predict a K_s, usually between 0.5 and 2 times the measured K_s value for the considered data (Chapuis 2004). The Chapuis formulae were fitted with different kinds of materials (sand and gravel) with d_{10} up to 1.98 mm and with *C*U (<1.8 to 6.0) that are close to the values of our experimental site and a void ratio (0.66–0.82) that is in our range of values.

$$K_s = 2.4622\left[\frac{d_{10}^{\,2} \cdot e^3}{1+e}\right]^{0.7825} \qquad \textbf{Equation 29}$$

and

$$e = \frac{n}{1-n}$$

with K_s in cm.s^{-1}, d_{10} in mm, and *e is* unitless.

Water retention curves

Water retention curves were obtained by the sandbox method (Stackman *et al.* 1969) measuring range underpressure related to water content from saturation to residual (up to 10 kPa suctions). RETC software computed the θr, θs, α and *n* parameters needed for Hydrus modelling.

To determine the moisture characteristic, 10 undisturbed samples of first layer were collected using 100 cm³ stainless steel rings. The sandbox contains synthetic sand with a roughly 73 µ grain size as infiltration media. Samples are saturated and subsequently balanced to increasing values of moisture tension obtained by creating a series of underpressures using a suction levelling stand. Weighing the sample after each balance adjustment yields the moisture content for each moisture tension, and helps subsequently plot water retention curve.

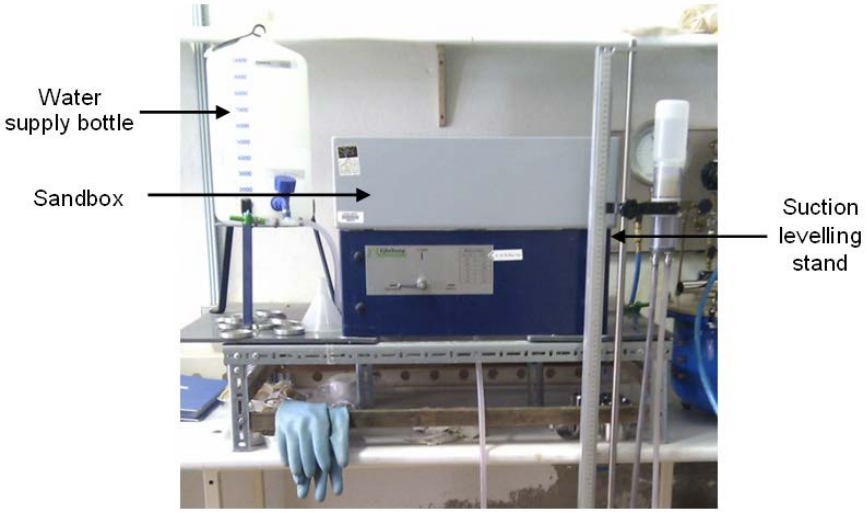

Figure 67: Laboratory sandbox method (Eijkelkamp set for pF determination)

For the first stage, several experiments were led with different OMCs for the first infiltration layer material, going from clean porous media to high OMC and strict sludge samples. First-stage hydrodynamic parameters obtained via the lab methods were used as initial values for the inverse modelling to obtain the parameter set used for the Hydrus/simplified model comparison (see section 4.2.2). However, the parameters of the second stage are given as illustrative information for future work.

3.2.3.2. Inverse modelling using *in situ* measurements

Selected experimental site data was used for the inverse modelling. In order to reduce the size of the dataset to speed up optimization, one single batch with the longest post-event drainage period (normally at night) was taken to fit the model. The selected batch had to present a large water content variation and thus permit better hydraulic parameter estimation. Hydraulic parameters obtained by the lab procedures were used as starting values for the inverse modelling of *in situ* data. The top boundary condition was a time-dependent atmospheric boundary condition, and evapotranspiration was neglected. The bottom hydraulic condition was a seepage face. Ponding of water above the surface is taken into account. In a first step, K_s was separately fitted for the first two layers using first-stage outflow for the corresponding batch. After that, α and then n parameters were fitted using water content at 10 cm and 25 cm observation nodes. As the fitting of α and n values also affects the outflow, the entire process of fitting K_s, α and n parameters was repeated in an effort to refine the results. In order to reduce the number of parameters to fit, we worked with the assumptions of fixed θ_s and θ_r for all layers and non-limiting K_s for the last two layers. The accuracy of results was analyzed using the Nash-Sutcliffe model efficiency coefficient.

Given that season is one of most important factors shaping filter hydrodynamics, the inverse modelling procedure was done for two different seasons (winter and summer) in dry weather events. The aim was to compare and validate the simplified model in terms of outflow and ponding (depth and time) on these two different hydraulic behaviours. The final set of parameters obtained from the inverse modelling is presented in section 4.2.2.2.

3.2.4. Simplified model and factors influencing hydraulic acceptance

After calibration on different scenarios (HL, feeding day, seasons) and comparison against HYDRUS-1D, the simplified model can been used for long-term hydraulic modelling of VFCW. The principal objectives of this long-term modelling are (i) to analyze the impact of local context and filter design on hydraulic overload acceptance over the year (using by-pass discharges and dysfunction alerts based on ponding time) and (ii) to establish hydraulic overload acceptance limits on the VFCW according to different contexts. Long-term modelling hinges on pairing the combined sewer system with the VFCW. The process for this part of the modelling effort is summarized below :

a. *Defining local context*
   The local characteristics of the combined sewer system have to be defined, due to their influence on flow rates arriving at the VFCW.

b. *Defining climate variables*
   Dry weather and real rainfall time-series are introduced into the "sewer system" model in order to reproduce authentic dynamics of hydraulic overloads arriving to VFCW.

c. *Calculating flow rates arriving at the treatment plant*
   Consequently, a sewer system model simulates the transformation of the rainfall events into flow entering the sewer system and transport to the treatment plant.

d. *Calculating ponding*
   These flow rates are introduced into the simplified filter model which simulates plant operation (flow splitter, rain event and dry-weather distribution systems, batch feeding system, first VFCW itself and the first-stage by-pass). Ponding will thus be calculated.

e. *Calculating number of dysfunction alerts and by-pass discharges*
   To link filter hydraulics (ponding) to biological performance (oxygen depletion), "dysfunction alerts" are established based on the treatment performance campaigns and continuous monitoring (see section 5.6.1) to plot the maximal HL that a filter can accept without affecting biological activity. In addition, a by-pass height protects the filter from long ponding periods. By-pass discharges occur when filter in-flow is greater than the volume it can drain and store at the surface. The surplus overflows directly to the receiving water body, with a minimum of treatment due to the sedimentation occurring on the filter. By-pass discharges and dysfunction alerts established in this study are described in section 5.6.1 and 6.2.2.

f. *Reducing dysfunctions and discharges*
   The main objective is to analyse the effects of local context and filter design on ponding time in order to reduce by-pass discharges and dysfunction alerts as a step towards defining scenario-by-scenario HL acceptance limits.

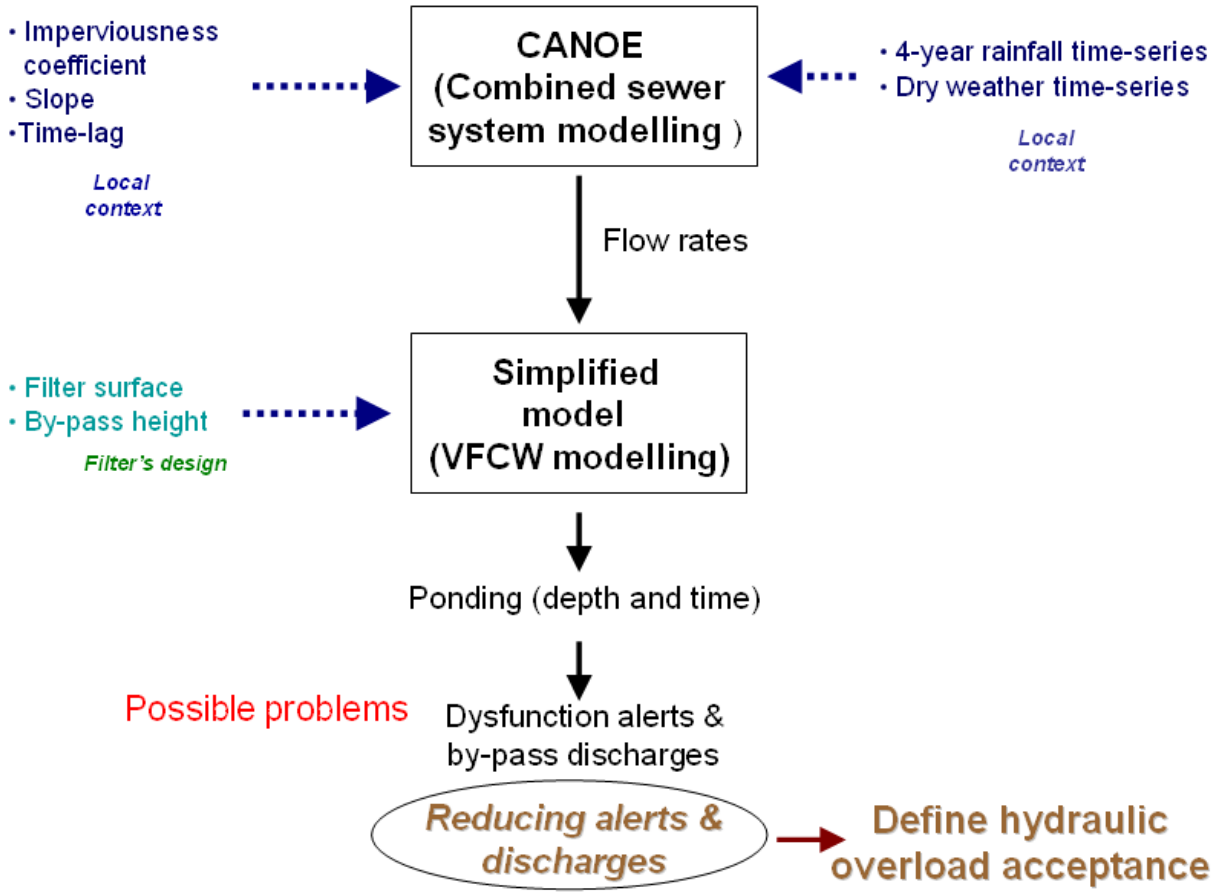

Figure 68 : Process of long-term modelling

To achieve the two long-term modelling objectives , it is necessary to :

1. Set up the control parameters of base of the "sewer system" model.
2. Establish a range of local context and filter design parameters to be tested.

3.2.5. Sewer system modelling

This part of the study was led using an urban hydraulic model software CANOE V6 designed in France by Lyon INSA "Laboratoire de Génie Civil et Ingénierie Environnemental" (LGCIE) and private-sector company SOGREAH. This software is popular in France due to its easy-handling and robustness for urban hydraulics. Modelling was carried out via the Muskingum approach whose modest data requirements make it attractive for practical use. Modelling in CANOE is split into two successive steps: (i) production and (ii) transfer.

(i) The production function is used to define the part of the rain precipitated (raw rainfall) that will effectively flow at the watershed outlet. The result of this first transformation is a hyetograph of net rainfall. Net rainfall is calculated as the difference between raw rainfall and flow losses (evaporation, retention by vegetation, storage in surface depressions and soil infiltration). Net rainfall is then expressed as a flow rate by multiplying the instantaneous intensity of the net rainfall by catchment area.

(ii) The transfer function aims to transform the flow of net rainfall to flow at the sewer system outlet. This is a conservative operation (the net rainfall hydrograph has the same volume as the hydrograph at the sewer system outlet). Its purpose is to represent the transformation of the shape of flow wave during its passage through the sewer system.

The principal parameters integrated by the model are :

1. Watershed area
2. Initial and continuous losses
3. Number of linear reservoirs (to the on-sewer transfer)
4. Imperviousness coefficient
5. Slope
6. On-sewer time-lag

For modelling, the total number of parameters was limited in order to study the main general parameters shaping most of the flow arriving at the treatment plant. Consequently, the first 3 parameters were fixed. Given the specificity of the area for each scenario, we chose to use the Challex watershed area. As the initial and continuous losses have a low impact on flow arriving to treatment plant compared to the other parameters, initial and continuous losses were fixed at 1 mm and 0 mm, respectively, assuming that water from the beginning of the rain event does not arrive at the sewer and there are no continuous losses on the watershed. Thus, almost all the rainfall drains through the impervious areas that are directly connected to the sewer system, which increases the importance of the imperviousness coefficient on flows arriving at the treatment plant.

In this “production/transfer” model, over-watershed and in-sewer system flow propagation was modelled using the linear reservoirs approach. Number of linear reservoirs has an impact on flow distribution. According to modelling carried out with Challex data (rainfall events and VFCW inflow), the best distribution of flow peaks is obtained with two linear reservoirs. Consequently, this number of reservoirs was fixed for all modelling. The other 3 parameters taken into account were imperviousness coefficient, slope (of watershed and sewer system), and consequently time-lag. Section 6.2 analyses the influence of these 3 principal parameters.

3.2.6. Local context and filter design

Since local context plays a key role in flow rate at the filter, the parameters to be tested are :

3.2.6.1. Sewer characteristics

The principal sewer system parameters analysed were :

- *Imperviousness coefficient*
  Due to its influence on production process, 4 coefficients were tested, corresponding to low-urbanized areas (10%) up to relatively high-urbanized areas of small communities (30%), with two intermediary values (17% and 23%). Each value was

coupled with imperviousness surface directly connected to the sewer system, assumed to be half of the imperviousness coefficient.

- *Slope*
  Due to its influence on transfer process, 4 watershed slope values were tested, from 1% to 10%. Watershed slope values were coupled with slope of the sewer system to simplify the modelling.

- *CSO*
  CSO limits the hydraulic load entering to treatment plant, thus influencing ponding time and by-pass discharges. The CSO configurations tested ranged from 5-fold dry-weather nominal flow to no-limit CSO.

Working from the fixed and variable parameters, the time-lag was calculated according to the modified Desbordes equation (1974) used in CANOE software for the peri-urban watersheds, as is the case for most of the small communities where VFCW are installed.

3.2.6.2. Climate conditions

To test different climate conditions, 4-year rainfall time-series were used. This 4-year period was defined since, according to Chocat (1997), it allows to define an annual rainfall water volume produced with an accuracy of about 25%. Theoretically, this period could obtain a good range of representativity of local climate. The objective of climate selection was to study the system's hydraulic performance under two different rainfall characteristics. The rainfall time-series were selected from the study by Coupe-Canu (2005). Each rainfall time-series was elaborated from Météo France data from the same rainfall station at 6-min time-steps (time-step chosen to avoid over-long simulation time and over-heavy results files). Two different French regions were selected: Bretagne and Rhône-Alpes.

As shown in Table 13, the Bretagne climate features more frequent but lower-precipitation and less-intense rainfall events per year than the Rhône-Alpes region.

Table 13: Rainfall characteristics for the Bretagne and the Rhône-Alpes region

	Average rainfall events per year	Total precipitation per year (mm)	Duration (h)	Average precipitation per rainfall (mm)	Average intensity (mm/h)	Max intensity (mm/h)
Bretagne	594	1 302	1.51	2.19	1.25	54
Rhône-Alpes	204.25	933	2.05	4.57	2.00	90

Figure 69 charts the distribution of rainfall precipitation and average rainfall intensity for both regions. Note the substantial number of low-intensity rainfalls in both, although the percentage is higher for the Bretagne region. In the Rhône-Alpes region, more that 10% of rainfall events are beyond 4.2 mm/h average intensity *versus* just 2% in Bretagne. Furthermore, extreme storm events counting 60 mm-plus precipitation can occur in the Rhône-Alpes region, which could be problematic for HL acceptance of VFCWs.

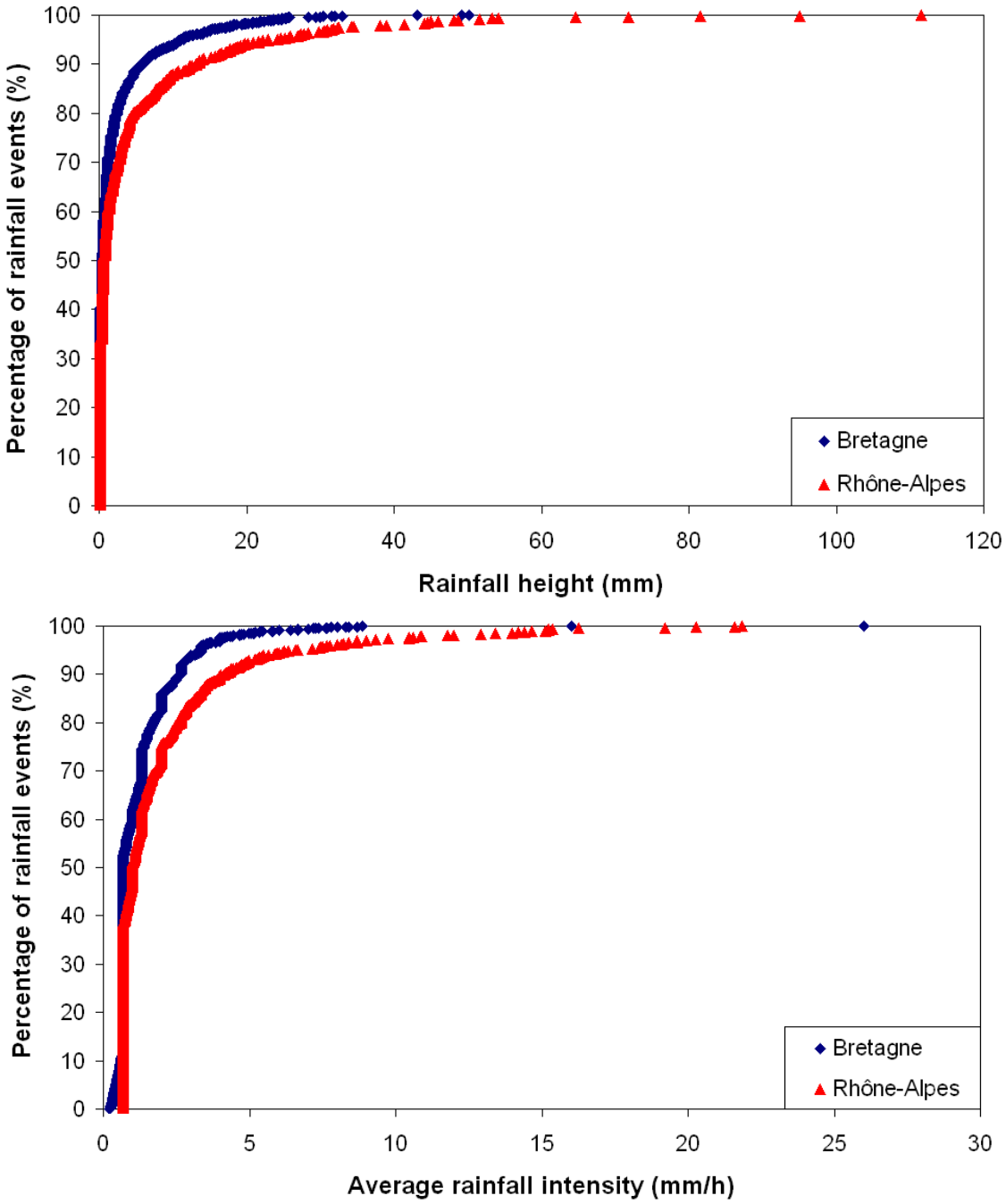

Figure 69: **Distribution of rainfall precipitation (*top*) and average intensity (*bottom*) over the 4-year time-series for the Bretagne and Rhône-Alpes regions**

Note that the rainfall time-series events from Coupe-Canu (2005) considered that any two given rainfall events are mutually independent if the effects on watershed of the first rainfall event stop before the start of the second one. In Coupe-Canu (2005), the threshold between two rainfall events was established as 1 h, which can explain the high number of events per year but does not affect the modelling.

According to the dry-weather time-series, a hydrograph based on flow rates arriving at Challex treatment plant was introduced into the CANOE model. The dry-weather hydrographs differentiate weekdays (excluding school holydays) and weekends and were calibrated to reach the nominal load of the plant in dry-weather conditions.

3.2.6.3. Filter design and age

These different local contexts and different climate characteristics converge to induce different types of flow rates arriving at the VFCW. In order to test hydraulic overload acceptance in these different scenarios, we tested different filter design configurations :

- *Filter surface*
  Surface is essential to establish hydraulic load acceptances, and forces a trade-off between performances and filter size. The surfaces tested ranged from 0.9 to 1.5 m².p.e

- *First-stage by-pass height*
  By-pass height defines the water volume that the filter surface can store, diminishing the discharges to the receiving water body. However, a higher stored volume can increase ponding time and thus affect filter performances. Consequently, by-pass height has to be a trade-off between reducing discharges without jeopardizing treatment performances. The by-pass heights tested ranged from 0.1 m to 0.7 m.

- *Filter age*
  Filter permeability decreases with age due to the increase in OMC deposits. Two VFCWs at different ages were tested: Challex at 2 year in operation and Evieu at 8 years in operation.

These different parameters govern a considerable number of scenarios to be tested, which are detailed in section 6.2. Table 14 recaps the parameters tested.

Table 14: Summary of the parameters modelled

Modelled configurations		Values
Climate	*Bretagne*	-
	Rhône-Alpes	
Sewer characteristics	*Imperviousness coefficient*	10% 17% 23% 30%
	Slope	1% 4% 7% 10%
	CSO	5 DW NF* 12 DW NF 20 DW NF 40 DW NF No Limit
Filter design	*Surface*	0.9 m^2 p.e 1 m^2 p.e 1.2 m^2 p.e 1.5 m^2 p.e
	First-stage by-pass height	0.1 m 0.3 m 0.5 m 0.7 m
Filter age	*Young filter*	1-year old
	Mature filter	8-year old

** Note: DW NF = Dry weather, nominal flow*

First, the sewer characteristic parameters were tested in order to tease out the most influential ones to be subsequently used as basis for testing the filter design parameters, then the most pertinent scenarios were tested with the two filter ages. Note that all parameters were always tested for the two climate sets. The development of this sensitivity analysis is further explained in section 6.2. From these simulations, different hydraulic parameters were computed to identify which fraction of rainwater is treated or overflowed and to gain ponding time information. The long-term modelling is focused on reducing the number of dysfunction problems (alerts) and by-pass discharges per year, modifying filter design, and identifying the most problematic scenarios.

4. Filter's dynamics

4.1. Hydraulic of the filter

During 2-year monitoring on the experimental treatment plant, rain events represented 33.8% of days monitored, of which 16.6% produced drain flow rates higher than 8 times the nominal dry-weather flow (100 m³/h, Figure 70). This exceeding flow rate passed through the rain weather distribution system allowing the treatment of this wastewater, reducing the CSO bypasses. About 5% of total inlet volume gets drained to the first stage via the rain weather distribution system.

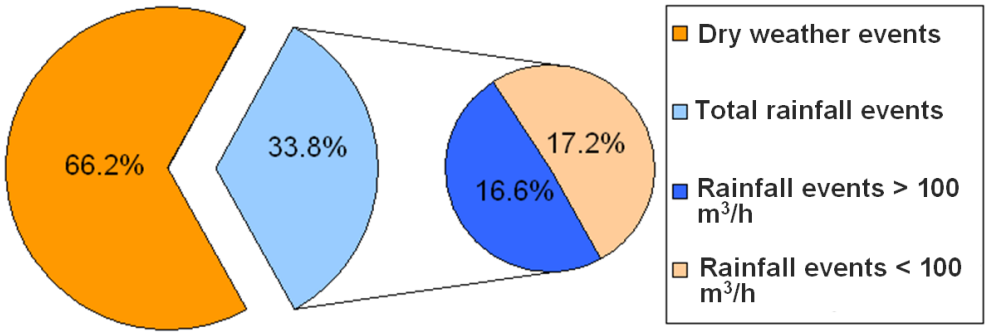

Figure 70: Distribution of dry-weather flows and rainfall events in Challex

Winter is the most hydraulically charged period. The Challex watershed was frequently exposed to heavy precipitations (up to 40 mm/day). Figure 71 presents the rain precipitation and HL of the first-stage filter in operation. During rain events, the VFCW treated a daily HL of up to 5.31 m³/m² (> 14-times the dry weather flow). Due to groundwater intrusion into the sewer from December to February, the plant often treats a HL that is higher than the NHL., whereas in the summer period, the HL treated is more often under the NHL.

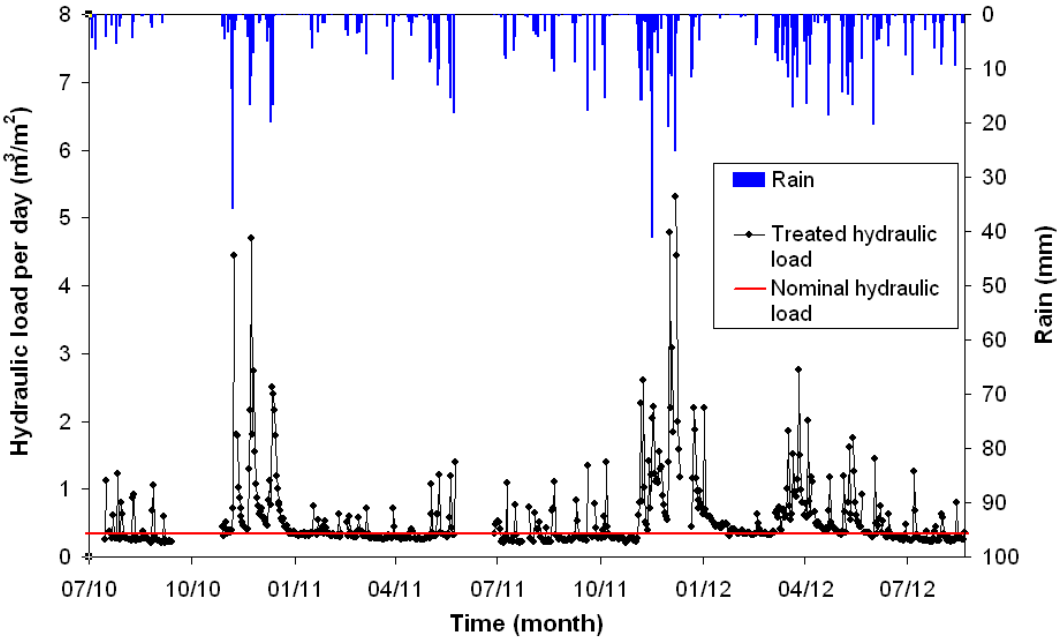

Figure 71: Total hydraulic load treated and rain events during the 2-years monitoring period

Figure 72 shows that the months with higher hydraulic loads are January and December. This period is already defined as the most hydraulically sensitive period due to poor sludge mineralization during winter (low temperatures) and poor reed development (no mechanical effect for water infiltration) that could affect treatment performances. Indeed, oxygen transfers are more limited due to higher water content in the sludge deposit and the media. These treatment impacts will be discussed in section 5.

On the other hand, as shown in Figure 72, the months from August to November present the lowest HLs. Besides the high temperatures in these months that trigger high bacterial activity and reed root development, lower HLs promote better oxygen renewal in the system, which improves treatment performances. Note that the period from April to June presented more numerous rain events during the second year than the first year.

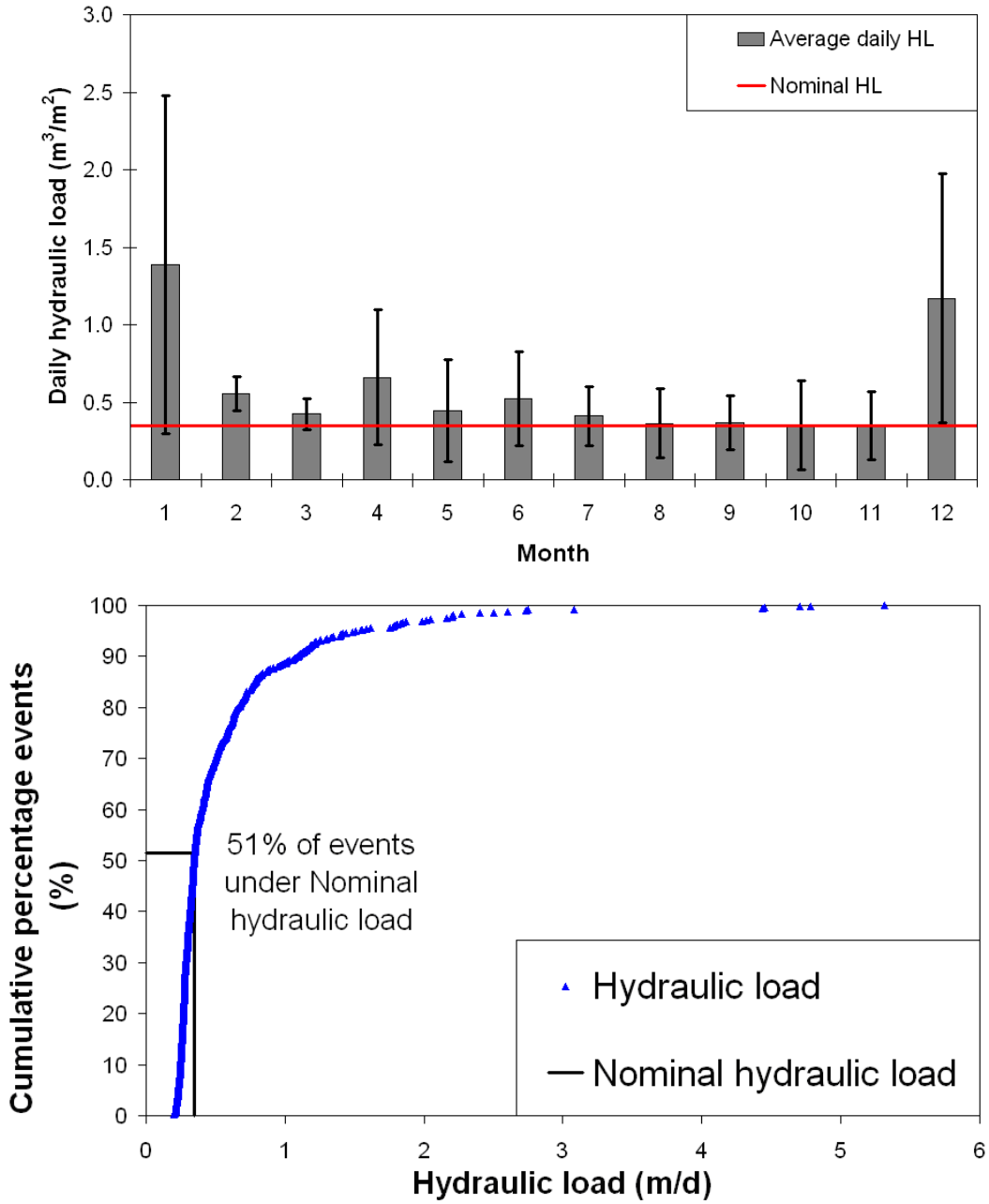

Figure 72: Average daily inlet HL over the year with standard deviation (SD) (*top*), and daily HLs treated (*bottom*)

About 51% of treated HLs are below the NHL, and less than 1% of observed events were over 10 times the NHL (peaking at 14.35-times the NHL). This demonstrates that the infiltration rates of first stage are high enough to accept high HL during the first years of operation, in accordance with results from French systems in operation for 7–8 years (Molle *et al*. 2006)

Even if the exceptional high HL events never reached the maximal flow that can be accepted by the rain event distribution system (3600 m^3/h), the CSO registered discharges on 11.74 days per year for varied inflow rates. This system malfunction is a consequence of different kinds of refuse and solid wastes flushed out with each stormwater clogging the 50 mm rain weather system screener placed at the entry of rain event distribution system (beside the CSO). This malfunction prevented the filter from operating at its maximum capacity, and highlighting that some maintenance is needed to manage heavy rain events. Nevertheless, the maximal flow rate that has been accepted on the filter is about 434 m^3/h, which equates to 35-times the dry-weather flow.

As seen in section 3.1.2.1, feeding flow rate and batch volume are lower than the design guidelines (Molle *et al.* 2005) and do not ensure good water distribution onto the first-stage filter surface. Consequently, the on-filter deposits are unevenly flat, which aggravates the water distribution issue.

To gain deeper insight into on-filter water distribution, we led a series of TDR campaigns (see below) and analysed the one-minute time-step ponding depth measurements (see section 4.1.2).

4.1.1. TDR Campaigns

Eleven TDR campaigns were carried out over the 2-year monitoring period, distributed along seasons and hydraulic loads. Five TDR profiles placed in the first stage at different distances from the nearest water feeding point made it possible to observe water content and thus water distribution in the filter.

Figure 73 presents water content evolution over a feeding period for different depths. Note that water content decreases with depth due to the organic matter content in the first infiltration layer that promotes water retention. The probe at -10 cm depth recorded the highest water content. At the end of the feeding period, water content was about 0.3 m^3/m^3 without reaching media saturation (0.42 m^3/m^3). The probe at -25 cm depth showed a lower water content that was only slightly different to the -40 cm depth probe. This can be explained by the similar organic matter contents in both layers at this filter age (1.5 years in service) and the same particle size (second infiltration layer). The aggregate results of the TDR campaigns showed an increase in water content (from 0.15 to 0.23 m^3/m^3 at the end of a feeding period) at the -25 cm depth over the 2-year monitoring period due to organic matter accumulation within this zone of porous media.

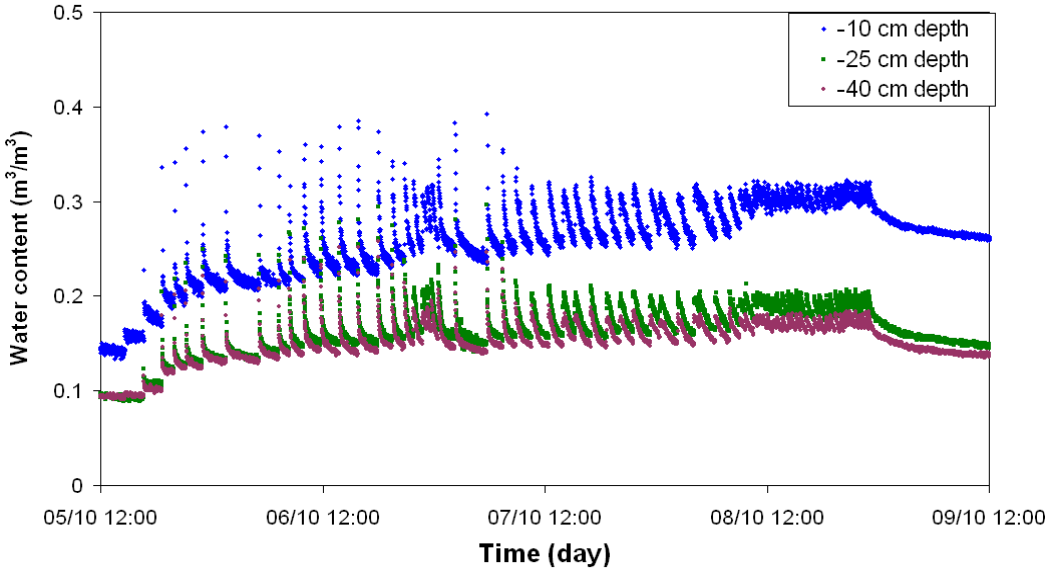

Figure 73: Water content per depth point in TDR profile No. 1 during a batch feeding period, from 5 to 8 October 2011

The TDR campaigns made it possible to chart change in water distribution over feeding periods. Due to the low batch feeding flow, the TDR profiles evolved differently according to distance from a feeding point. To illustrate, Figure 74 presents the evolution of TDR value at -10 cm from the surface of all profiles.

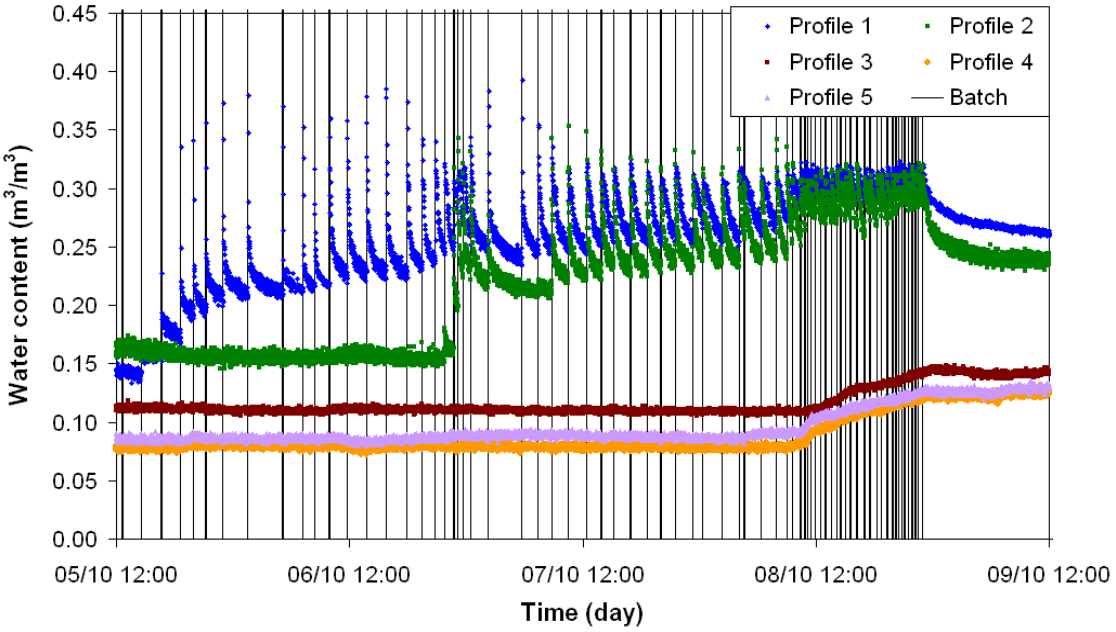

Figure 74: Evolution of water content values at -10 depth for the five TDR profiles over feeding period from 5 to 8 October 2011

During this campaign, from the start of the feeding period, two batches were needed before water reached the first TDR profile at 0.23 m from the feeding point. Water content in porous media increases gradually with batches. The initial dryness of the media when feeding begins produces shrinkage cracks in the deposit layer, after which preferential pathways move water quickly through dry porous media (and the probe rods) without being distributed in the porous space. With the progressive increase of the water content and the fresh deposit that is created at the top surface, water distribution improves.

Consequently, there is a water distribution front, during a feeding period, that is impacted by season as well as by hydraulic load (Figures 75 and 76). When a rain event arrives, the water distribution front evolves faster. This is important for establishing the effective filtration surface that is used during feeding. The diversity of surface water distribution trends during the monitoring period makes it difficult to establish a relationship for seasons and applied HL.

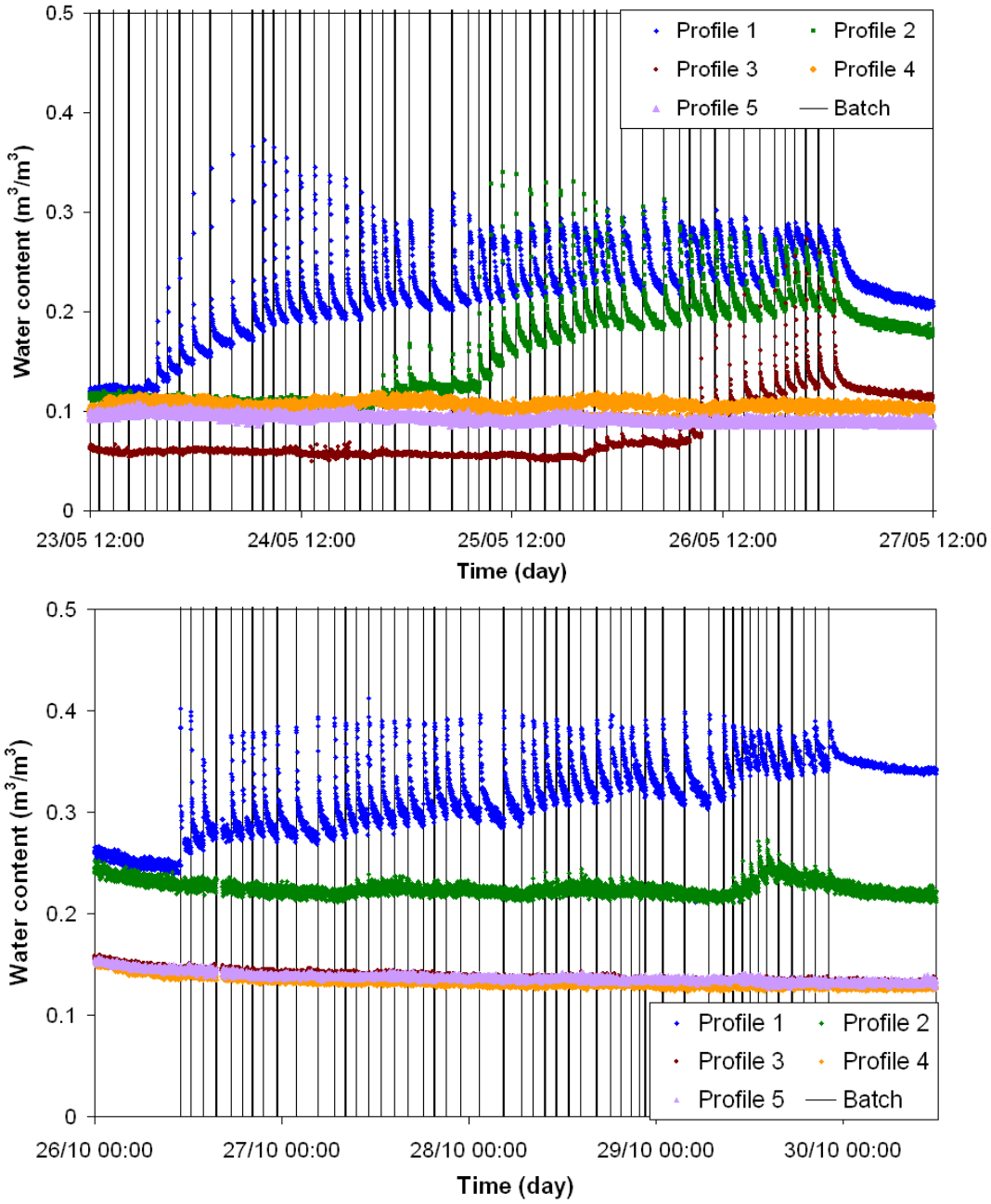

Figure 75: Water content evolution in a feeding period for different campaigns on May 2011 (*top*) and October 2011 (*bottom*)

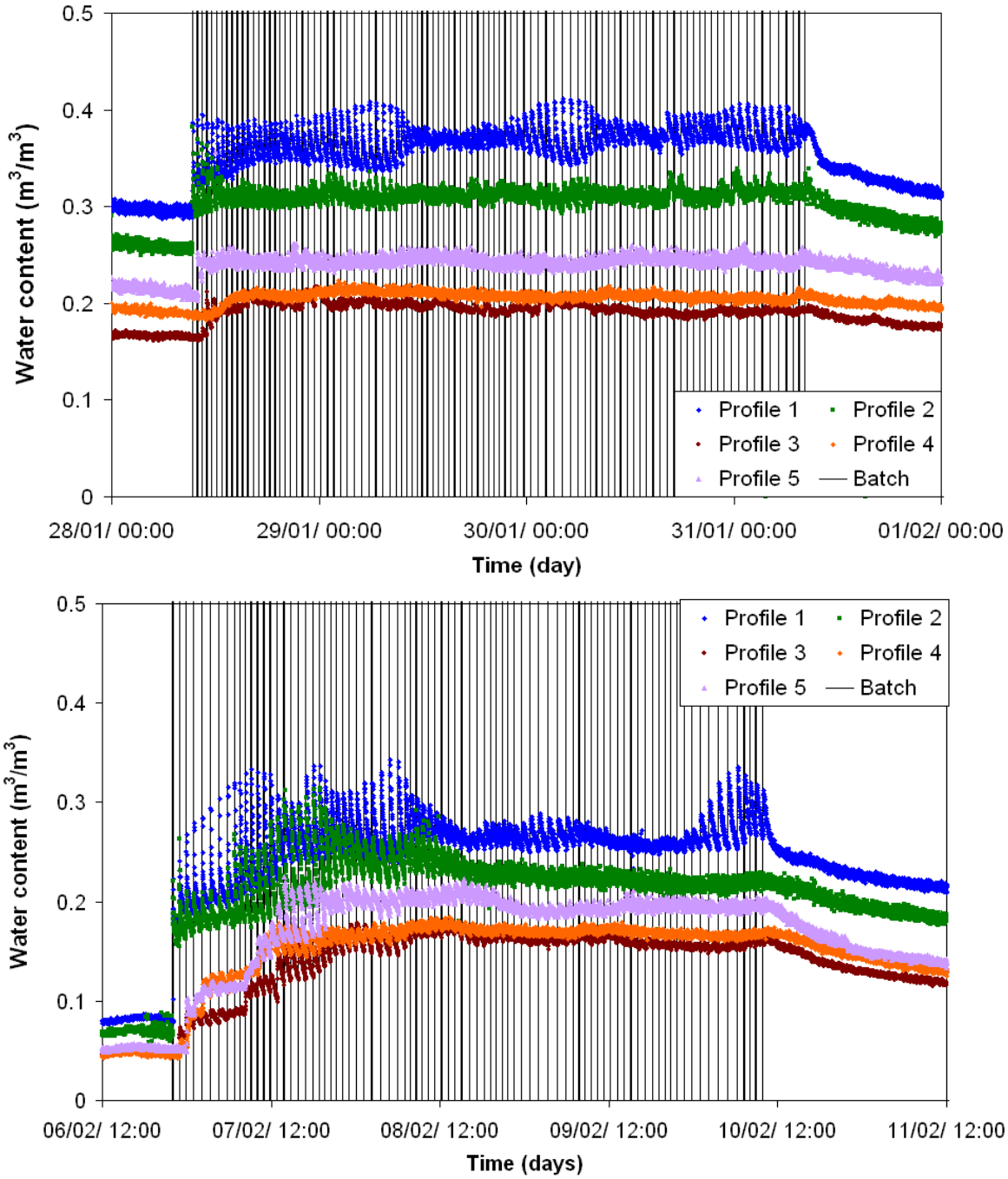

Figure 76: Water content evolution in a feeding period for different campaigns on January 2012 (*top*) and February (*bottom*)

As shown in Figures 75 and 76, the dynamics of the water distribution front varies according to season, presenting a better and rapid distribution in winter (event of 06/02/2012). Different factors could explain this pattern: the absence of mechanical reed effect, a low atmospheric temperature (average -7°C) that can create a frozen layer at the surface (Figure 77) and a higher deposit layer of un-mineralized sludge.

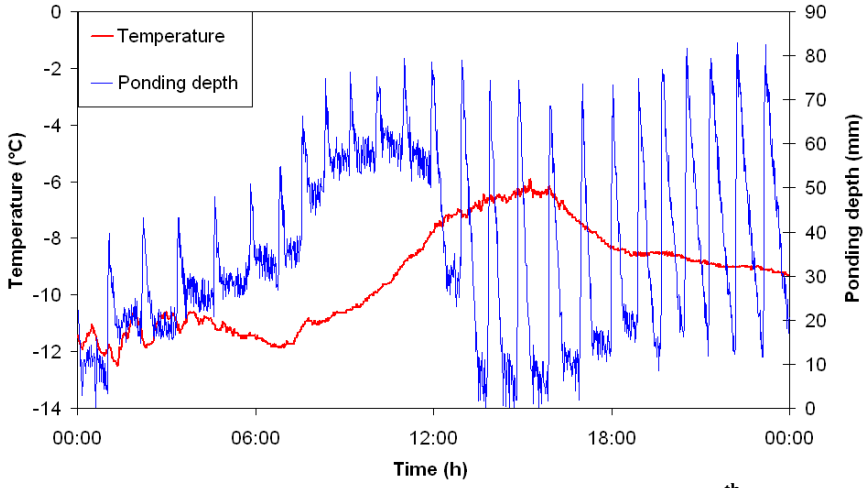

Figure 77: First-stage ponding depth and ambient temperature on 7th February 2012

The water distribution front does not appear dependant on initial water content of the media but rather on season (reeds presence, sludge mineralization...). Figure 78 charts the evolution in water distribution front according to HL. The winter season clearly stands out. TDR campaigns confirmed the inhomogeneous water distribution onto the filters.

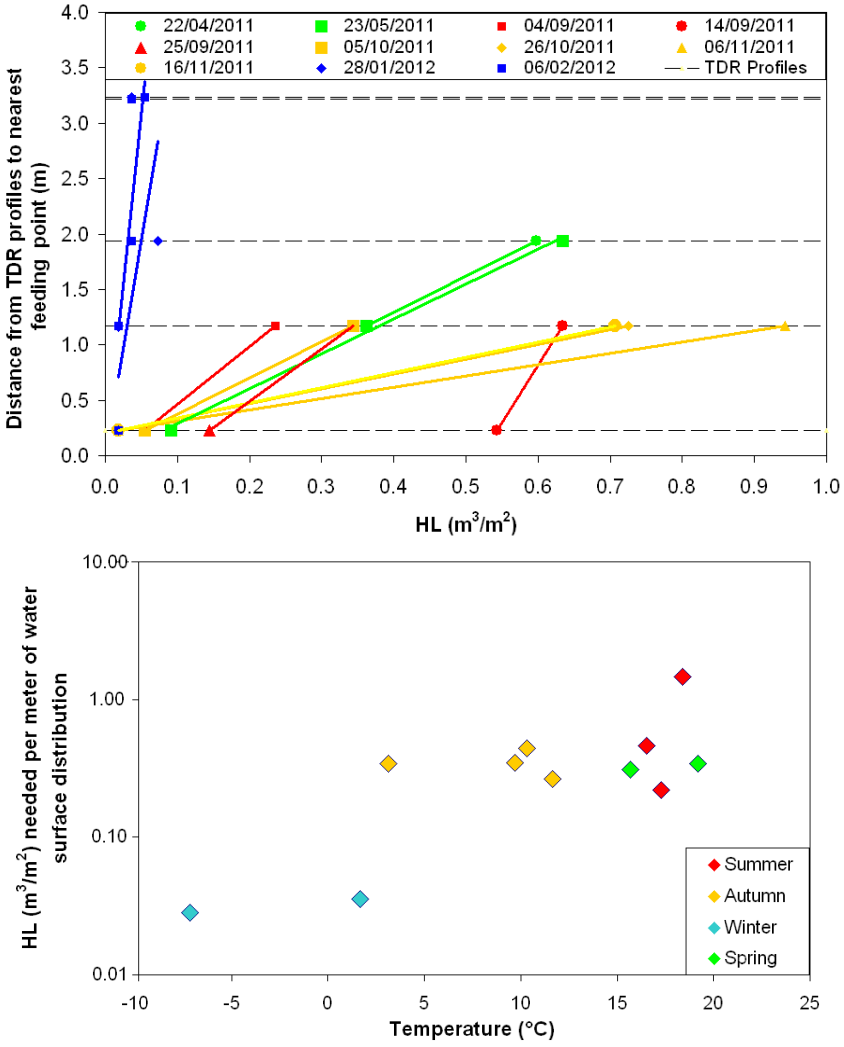

Figure 78: HL needed to reach TDR profiles per campaign, grouped by season (*top*), and HL needed per meter for water surface distribution according to ambient temperatures at (*bottom*)

Most summer and autumn campaigns just moisten the first and second profiles, after 0.94 m^3/m^2 of HL. The bad surface water distribution at this age of the system is also the result of a lack of deposit layer to better distribute the flow, which means a significant fraction of filter surface stays inactive.

Taking into account a linear distance from a feeding point, the inactive surface is approximately 51% for campaigns where water reached as far as TDR profile 2 (dry-weather flow in summer) and 20% for campaigns where water was measured at TDR profile 3 (dry-weather flow in spring). This under-operation of the filter generates pollutant overload on the effective filter surface, and could have a subsequent impact on treatment performances at the beginning of the feeding period.

These results highlight that water distribution on the Challex first stage is heterogeneous due to the young age of the system and the under-sized batch feeding flow and volume. Water distribution evolves according to HL, but at different rates according to season (reed mass, sludge mineralization).

4.1.2. Infiltration velocity

Infiltration rates were calculated through ponding depth measurements taken on ultrasonic probes (Baumer) in the first stage. Despite recording one-minute time-step data readings, only a limited number of workable events was obtained. This is due to reed interference with the ultrasound signal, the inhomogeneous water distribution, and the absence of ponding in some seasons (mainly summer) due to high filter infiltration capacities.

Infiltration velocities (*IV*) were calculated for each batch (average *IV* per batches) when ponding occurred on the entire filter surface. Due to clogging and water content change in the media, *IV* evolves with feeding day (Figure 79).

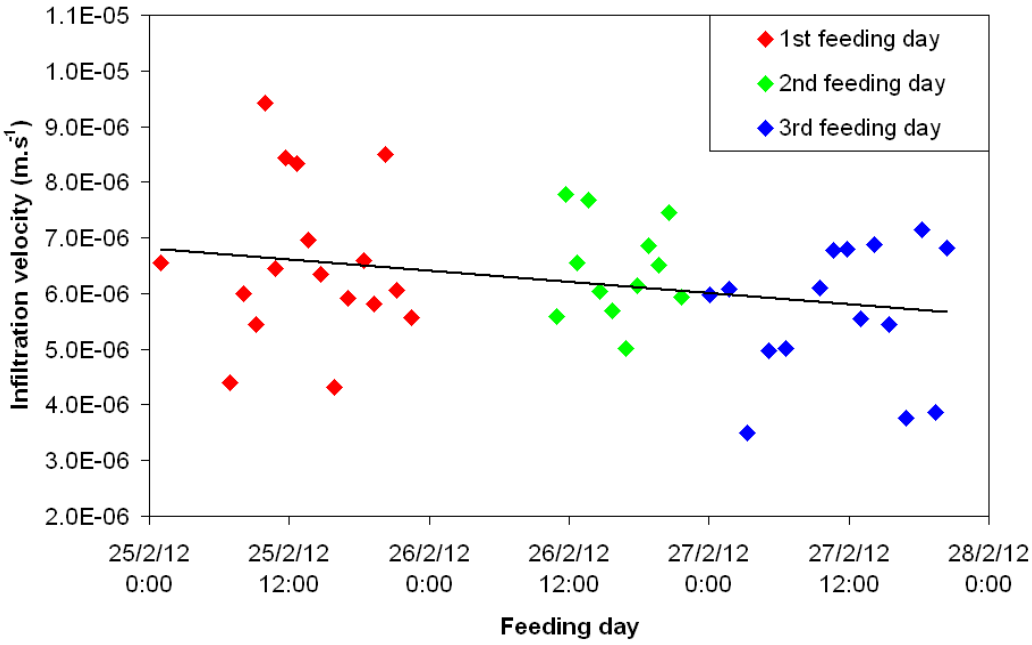

Figure 79: Evolution of batch infiltration velocities over feeding period from 25th to 28th February 2012

However, the impact of feeding period on *IV* stays low compared to other factors influencing infiltration. Maximum ponding depth per batch shows that ponding depth evolves on a day-to-day scale, as shown in Figure 80.

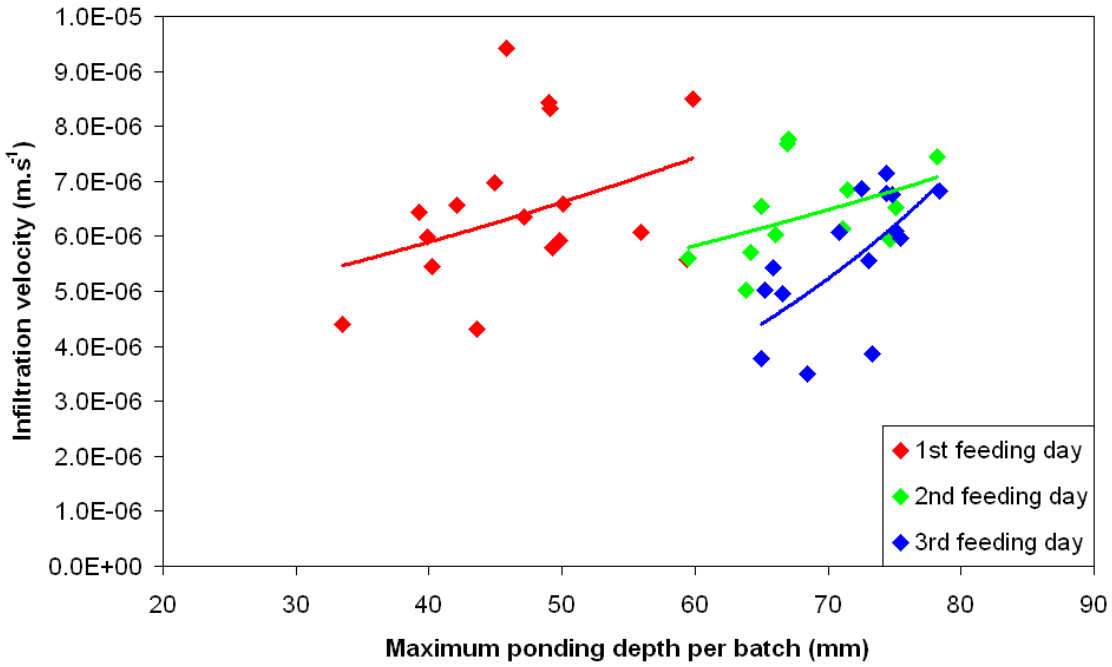

Figure 80: Infiltration velocities according to maximum ponding depth per batch per feeding day over a feeding period from 25th to 28th February 2012

The water pressure created by surface ponding increases with ponding depth, thus increasing *IV*. The relationships found between *IV* and ponding depth were not as clear as in Molle *et al.* (2006) studying an older system. The low sludge deposit and ponding depth meant that we could not calculate *IV* on the same basis (average of the entire batch here *versus* the first ten minutes in Molle *et al.* 2006). Nevertheless, we found the same trend of a decrease in *IV* with feeding days, thus necessitating more ponding depth to keep a similar *IV*. This is due to a progressive saturation of the porous media and partial clogging of the surface (fresh deposit).

Daily average infiltration velocity rates of 24 events were analysed: 8 HLs higher than two-times the NHL and 16 dry-weather events with HL lower than two-times the NHL distributed across the 2-year monitoring period. Season had a stronger impact on *IV* (Figure 81 *top*) than feeding day and ponding depth in Challex. The increase of *IV* is due to the presence of reeds that mechanically improve the permeability of the deposit layer. Likewise, the degradation of organic matter when temperatures increase during spring also improves deposit drainability (Vincent *et al.* 2012) and also explain the higher infiltration rate (Figure 81 *bottom*).

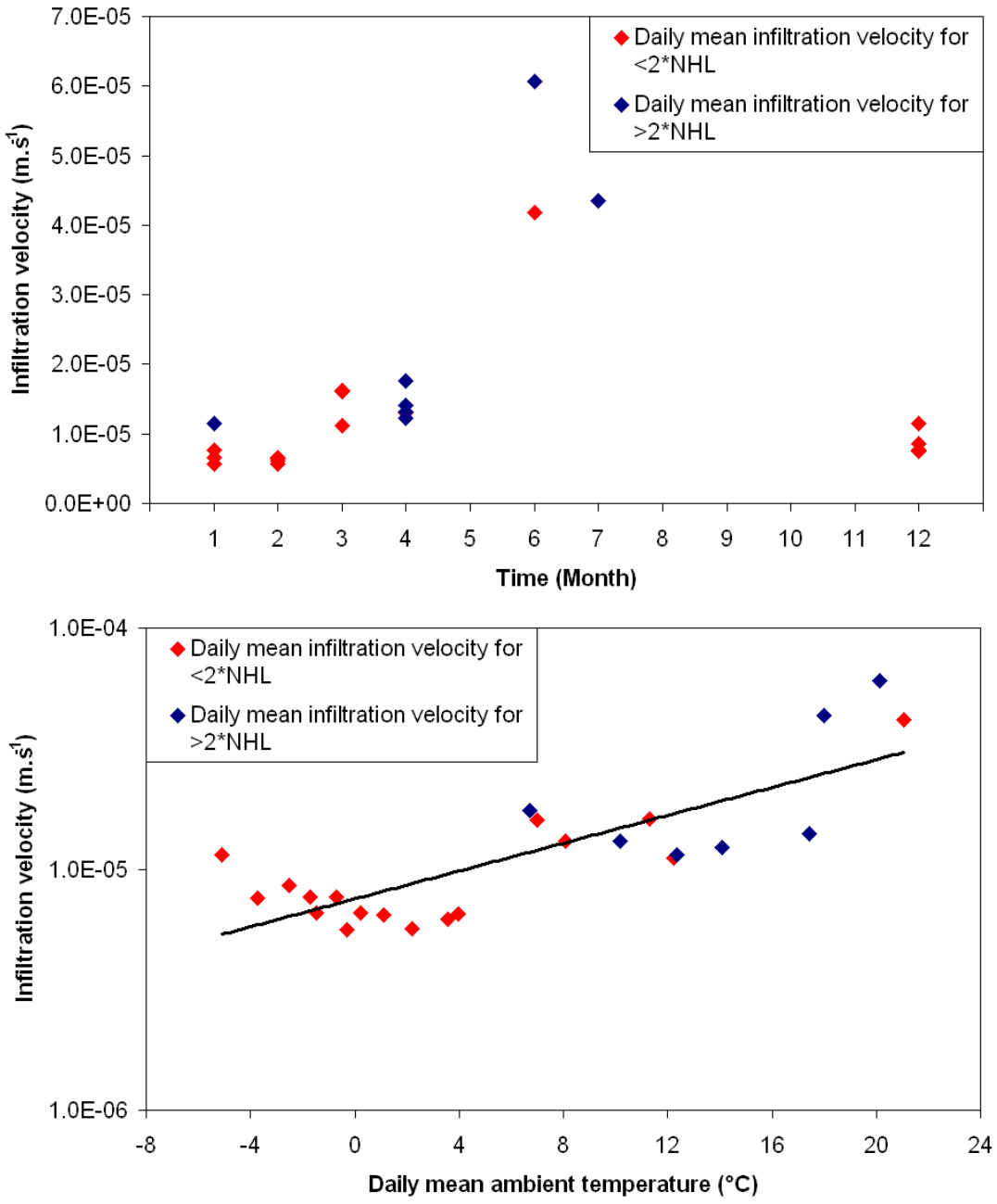

Figure 81: Daily mean infiltration velocity according to month (*top*) and temperature (*bottom*) for HL < 2xNHL and HL > 2xNHL

Note that the US probes measured different ponding depths, due to the uneven planarity of filter, however, the batch infiltration velocity rates stays similar for all the probes.

For a first-stage filter in a young VFCW with a low deposit layer on the surface, water distribution is not homogenous, resulting in localized infiltration velocities. However, the *IV* obtained give a picture of first-stage hydrodynamics. Thanks to these results, we can state that (i) *IV* are about 1E-05 $m.s^{-1}$ in winter but reach 6E-05 $m.s^{-1}$ in spring/summer, which is evidence that the winter period is susceptible to oxygenation depletion due to more extended ponding periods, (ii) feeding day and HL are not really significant for infiltration velocities given the broad variation observed over the seasons.

4.1.3. Tracer tests

To better understand the hydraulics on the first stage, 4 fluorescein tracing campaigns were led to identify water retention time and its evolution during feeding periods. To enhance the tracer analysis, the fluorimeter was calibrated specifically on Challex first-stage outlet wastewater. Tracer campaigns were achieved during the intense treatment performance campaign done on August–September 2012. Tracer tests were done between the 24 h composite samplings, approximately every two days, which meant they had to be executed during the day, under sunlight. As fluorescein is a highly photosensitive molecule, this factor may have affected the results, which would explain the low rate of fluorescein recovery at first-stage outflow. Figures 82 and 83 show the fluorescein concentrations obtained at the first-stage outlet charting the time-course evolution of feeding compared to total fluorescein recovered for the different tracer tests carried out in the intensive campaign.

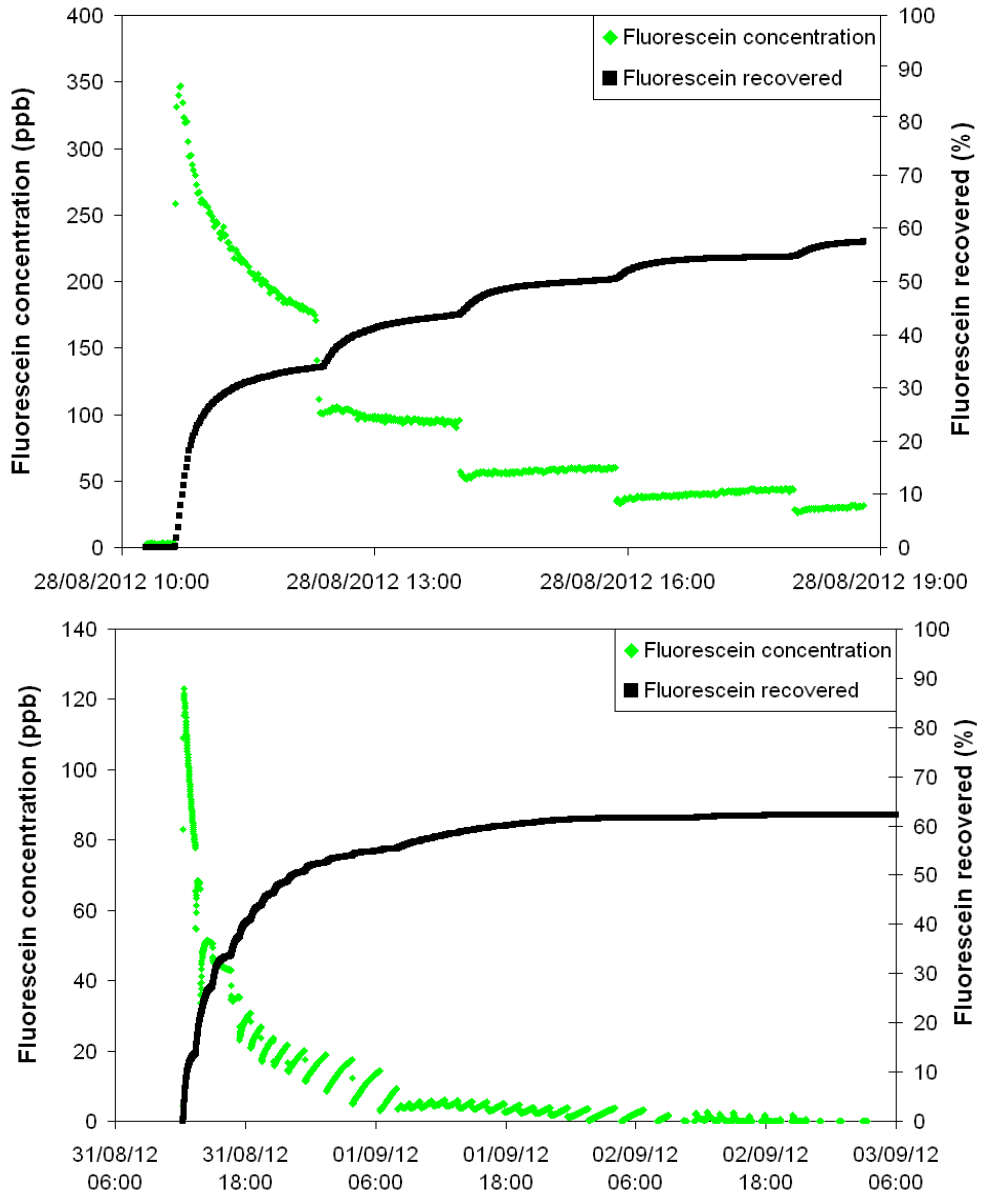

Figure 82: Fluorescein concentrations and recovered percentage at first-stage outflow in tracer campaigns for the second (*top*) and fifth (*bottom*) feeding day

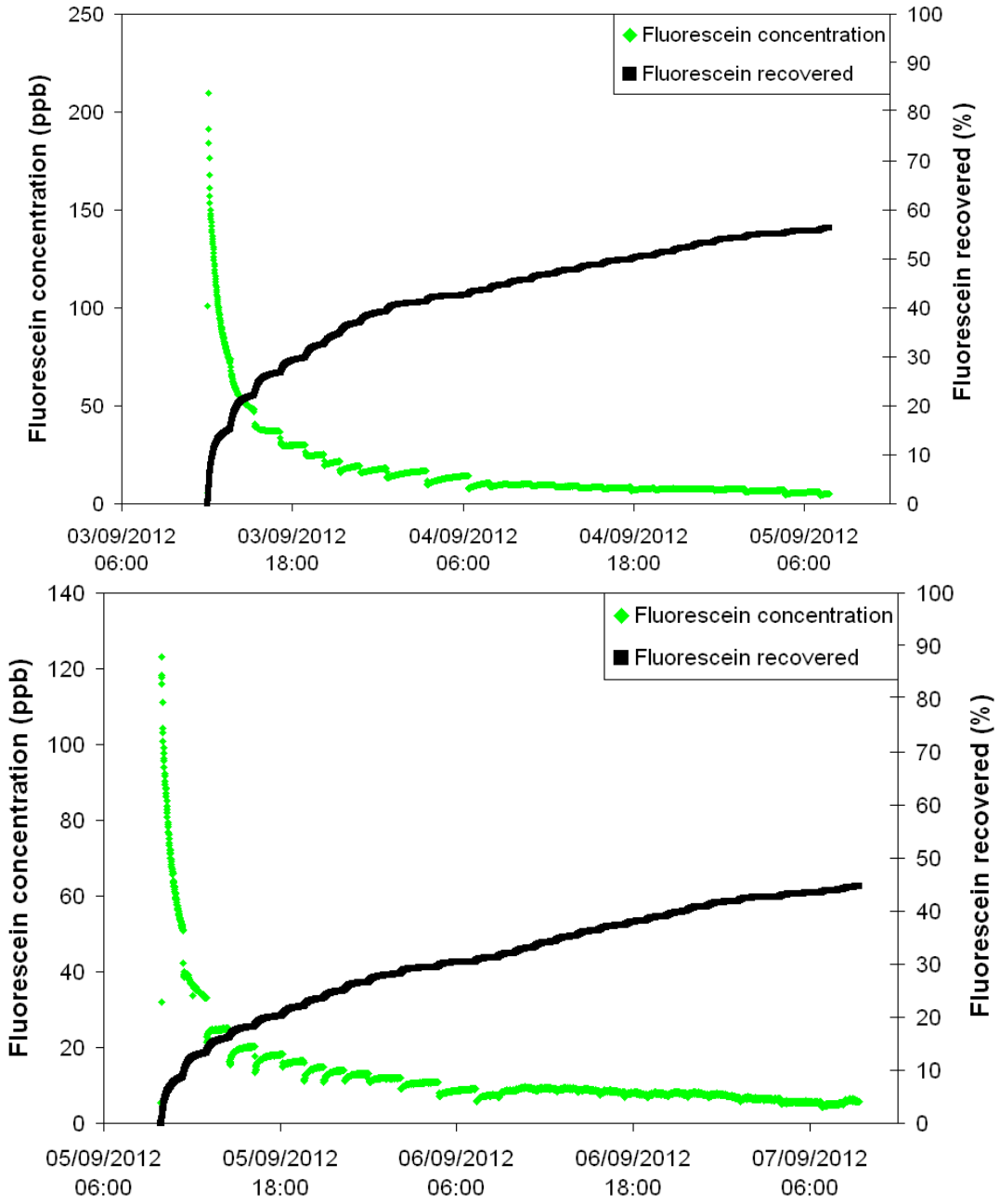

Figure 83: Fluorescein concentrations and recovered percentage at first-stage outflow in tracer campaigns for the eighth (*top*) and tenth (*bottom*) feeding day

According to Figures 82 and 83 the second feeding day shows high fluorescein concentrations in the first batches (350 ppb), with up to 34% recovery in the first batch. This highlights the short retention times and preferential pathways in the porous media liable to occur with young filters. On 8-year-old filters, Molle (2003) measured only 15–20% tracer recovery released by the first batch. The hydraulic behaviour of the Challex first stage is also affected by the bad water distribution, as discussed in section 4.1.1. On the fifth and eighth feeding days, there was better soil moisture which decreased preferential flows (lower outlet concentrations and about 15% of tracer recovery on the first batch). On the last days of the intensive campaign, 8% was recovered on the first batch, and we recorded the lowest rate of total fluorescein recovery (35%) against an average of 60% in the previous campaigns. This could reflect saturation of the porous media, producing in-filter ponding and exposing the fluorescein to more time in sunlight. Note that this result just gives an idea of on-filter water retention — the

low percent fluorescein recovery made it is unrealistic to precisely calculate water retention time. However, as an indication, Figure 84 presents the water retention time calculated assuming that final tracer recovery was the amount injected at the beginning. Figure 84 shows a linear increase in water retention time according to feeding day. Values go from 2.15 to 14.26 hours.

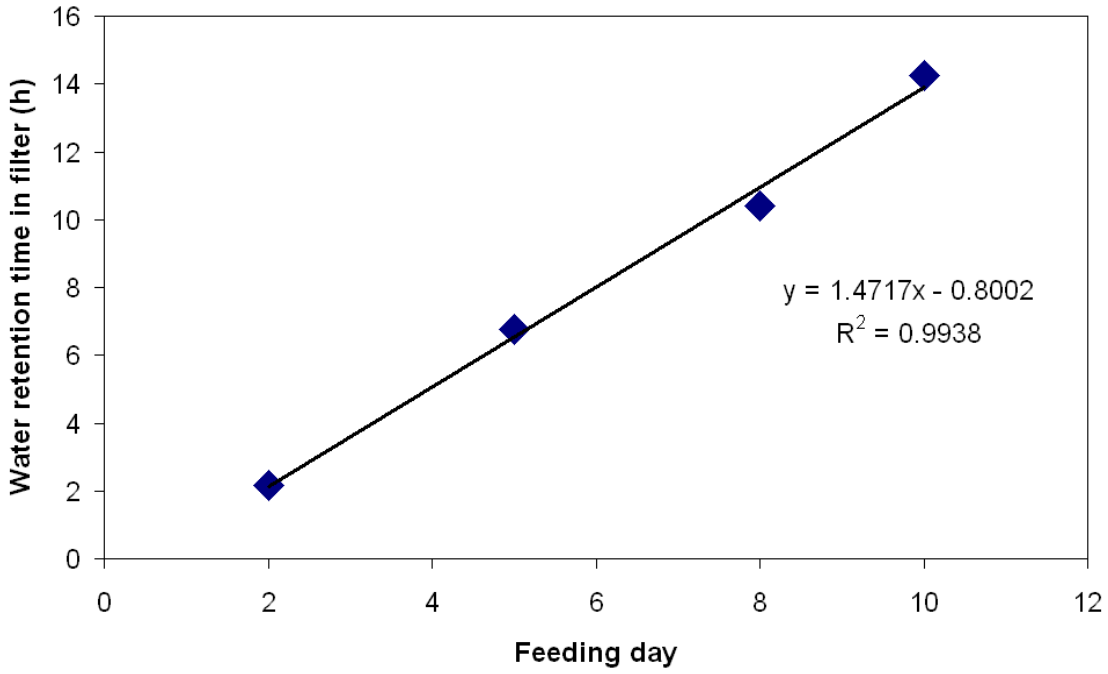

Figure 84: Water retention time in the first stage according to feeding day

The low water retention times at the beginning that then increase over time have to be linked to the low deposit layer as well as the bad water distribution. The linear increase in water retention time can be directly linked to the water distribution front. These differences will heavily impact system performances. Nevertheless, under normal filter rotation, water retention times will not vary as much as during the intense monitoring campaign. If, in dry weather conditions, water retention time on the first-stage filter is counted in a few hours, the impact of a rain event can substantially change the contact time between biomass and water. HO will accelerate the progression of the water distribution front. Consequently, if water retention time can be shorter during rain events, it can also extend subsequent water retention times when the system drops back to a dry-weather flow.

4.2. Simplified hydraulic modelling

In a first approach, the infiltration capacity parameter (*ICP)* as the main factor governing infiltration in the simplified model was fitted to first-stage outflow. As ponding depth measurements were not useful to calibrate the model (uneven water distribution), they were used to compare the order of magnitude between measured and simulated ponding depths. Then, to gain better confidence in the simplified model, it was cross-compared against the specialized hydrodynamic software Hydrus-1D. This approach aimed to assess the suitability of the simplified hydraulic model. The fitting procedure is detailed in section 3.2.2.1 and 3.2.3.

4.2.1. Infiltration capacity parameter and influencing factors

The influence of feeding day, rain event, season and age of system on *ICP* was analysed on a total of 92 events, i.e. 33 rainfall events of different duration and intensity and 59 dry-weather events, distributed across the 2-year monitoring period (on a young filter) and on different feeding days (see section 3.2.2.1).

First, the *ICP* from a young filter and dry weather events were analysed by season and feeding day independently of rainfall events, as shown in Figure 85.

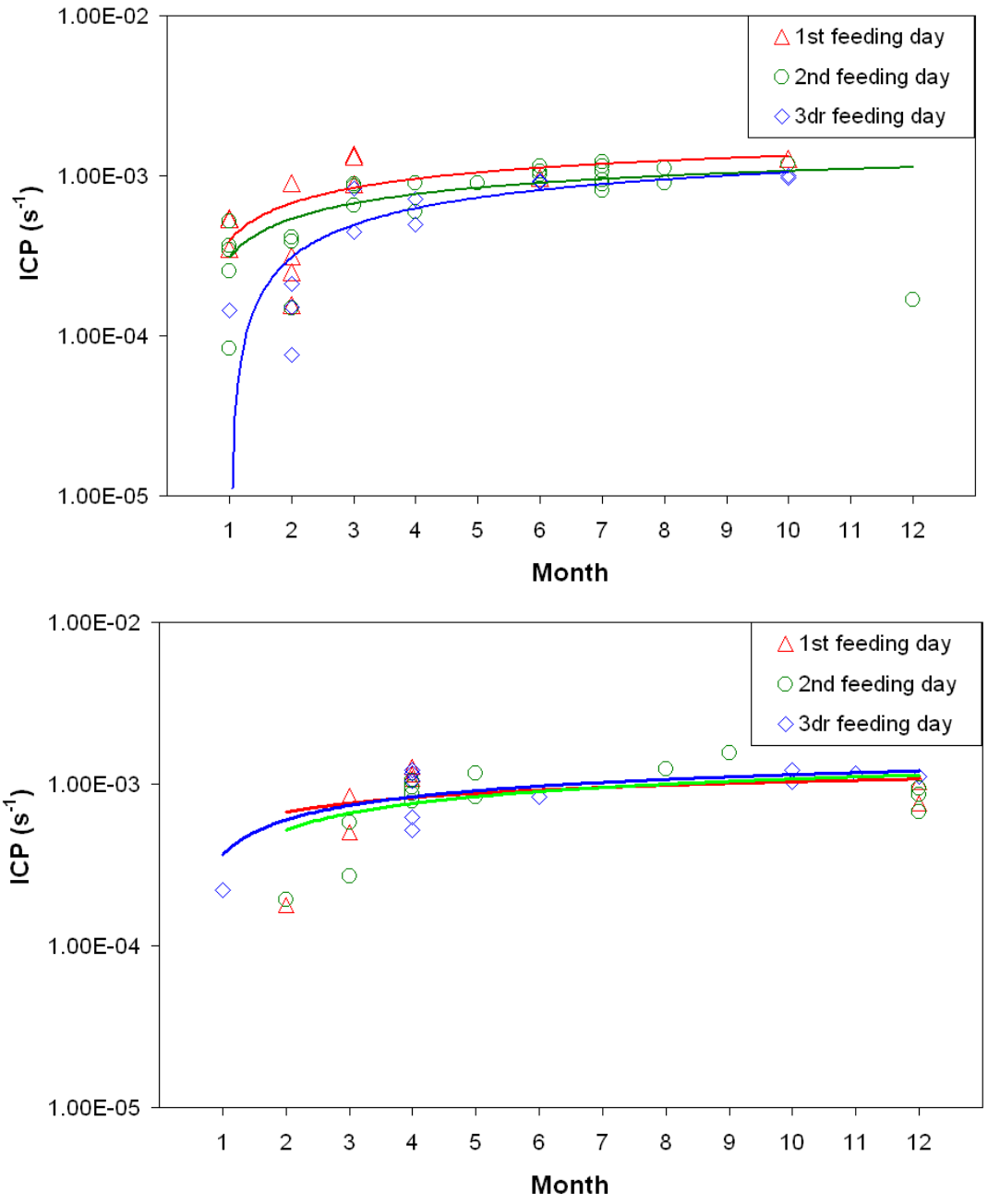

Figure 85: *ICP* according to feeding day and month, for dry-weather events (*top*) and rainfall events (*bottom*) on a young and mature filter.

ICP decreased as feeding day progressed for dry-weather events (mostly in winter season). For rainfall events, there was no significant difference between feeding day and *ICP* values in any season. However, this change in *ICP* with feeding day is not really significant compared to the broad variation observed over the seasons.

ICP values were not significantly different between rainfall events and dry-weather events (Figure 86). Since the most significant driver of differences in *ICP* values is season, no distinction by feeding day and HL is proposed for the global analysis of hydraulic behaviour.

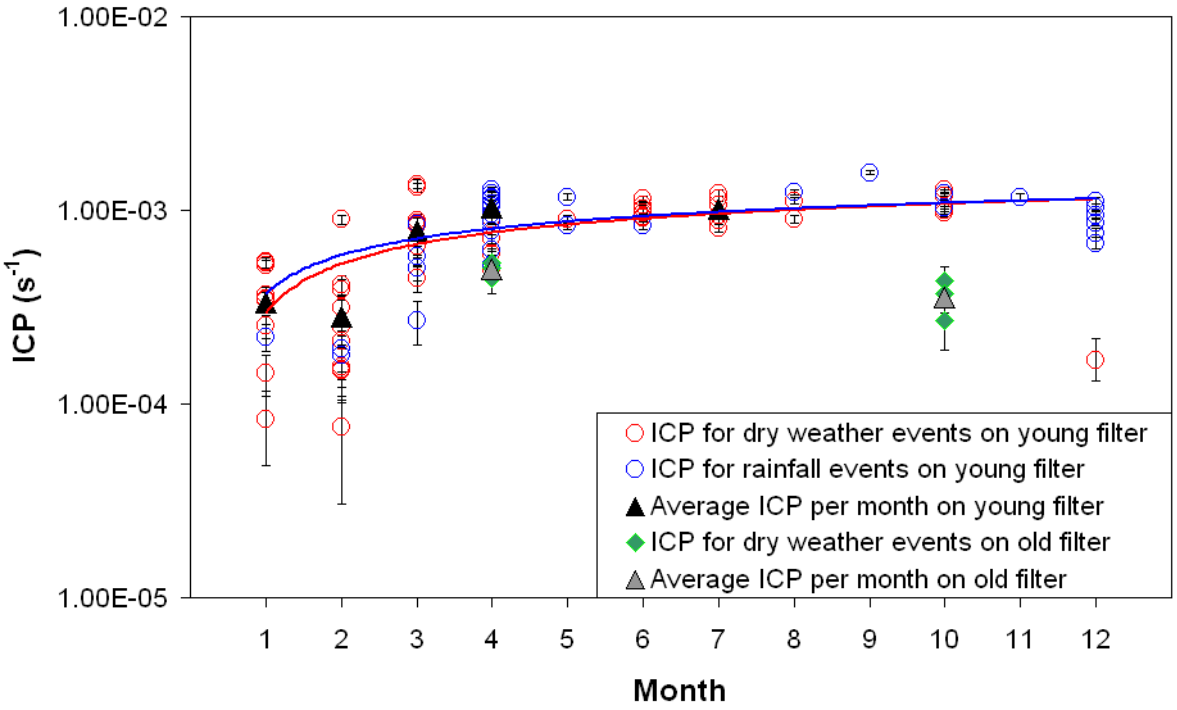

Figure 86: *ICP* evolution for dry weather events and rainfall events according to month, and 95% confidence interval

Average *ICP* varies from $2.81e^{-4}$ s^{-1} in mid-winter to $1.01e^{-3}$ s^{-1} for the May to November period on a young filter. *ICP* values for a mature filter are only available for two different months, April and October, representing the end of the winter ($3.57e^{-4}$ s^{-1}) and summer ($4.97e^{-4}$ s^{-1}) season, respectively.

Season clearly had a strong impact on *ICP*, consistently with the infiltration velocity data. This increase is due to the presence or absence, as reeds improve the permeability of the sludge deposit (Molle *et al.* 2006). The few data available showed that age of system also has an influence on *ICP* values, which are lower on a mature filter (20 cm of sludge deposit) than on a young filter in the respective seasons. This drop is due to the progressive accumulation of sludge depositing at the filter surface and organic matter in the porous media as the filter matures. The influence of season was only visible in *ICP* values over the 2-year monitoring period at Challex (young filter, Figure 87), which clearly shows the periodicity of seasonal influence. The time-course evolution of *ICP* values also suggests that in winter period, the VFCW is more sensitive to ponding.

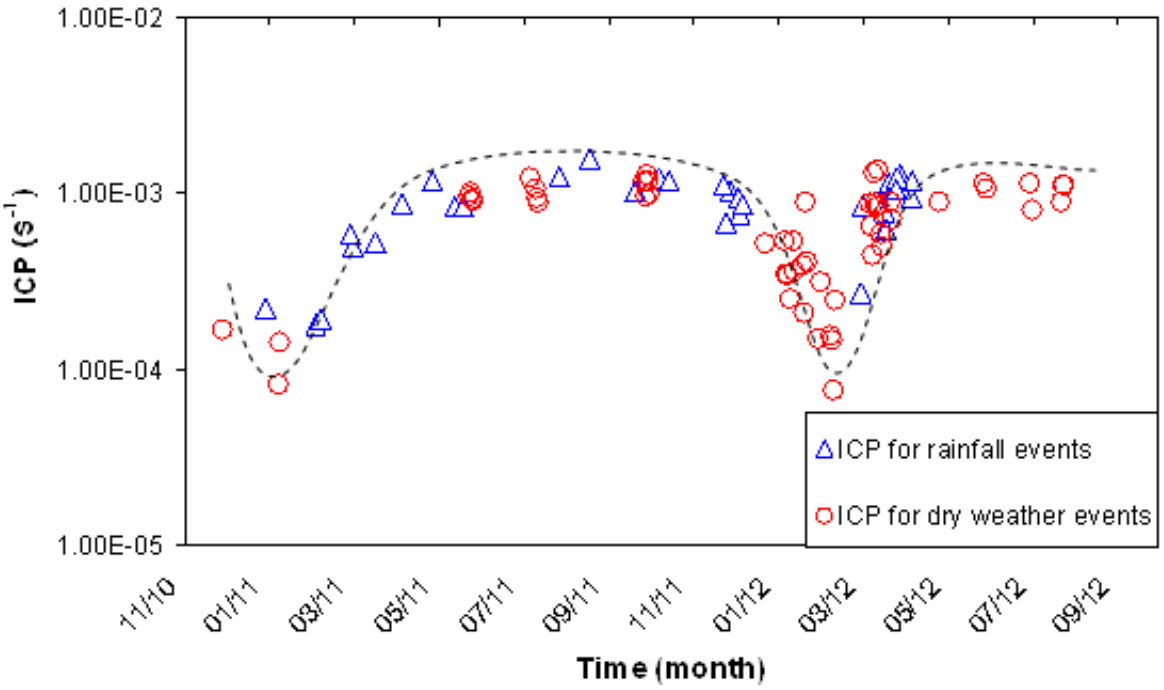

Figure 87: Time-course evolution of *ICP* over the 2-years monitoring period

Average *ICP* values per month were used for the long-term modelling. Although some uncertainties do arise from the simulation, the simplified hydraulic model allows a relatively good agreement that makes it useful for design offices to sketch first-stage filters designed to treat rain events in VFCWs treating domestic wastewater.

4.2.2. Comparison with Hydrus

The simplified model was compared to the mechanistic Hydrus model, which is the most popular code in CW. To calibrate the Hydrus-1D model, clean filter media was characterized in relation to hydrodynamic parameters. The parameter set obtained (initial values) was used on the inverse optimization module bundled with Hydrus-1D to fit the outflows as well as the water content profiles. Starting calibration with these initial values limits the risk of non-convergence, as they are likely to be close to optimal values.

4.2.2.1. Hydraulic characterization of infiltration material

A physical and hydrodynamic characterization of the first-infiltration-layer material was carried out by lab procedures to determine the parameters needed for Hydrus calibration of van Genuchten-Mualem closed-form expressions (Mualem 1976; Van Genuchten 1980). The procedure characterized is described in section 3.2.3.1.

Table 15 summarizes the hydraulic values of the infiltration material in two stages as characterized by lab procedures.

Table 15: Hydrodynamic characteristics of infiltration material layers in two stages based on lab procedures

	First stage	Second stage
Particle size (*mm*) d_{10} d_{60}	 2,43 3.87	 0.37 1.54
UC	1.59	4.16
Mass density ($g.cm^{-3}$)	2.63	2.66
Bulk density ($g.cm^{-3}$)	1.51	1.63
Porosity (-)	0.42	0.39
Void ratio (-)	0.72	0.64
K_s ($cm.s^{-1}$)	3.17	0.12
θ_r (cm^3/cm^3)	0.052	0.045
θ_s (cm^3/cm^3)	0.42 (porosity)	0.39 (porosity)
α (*1/cm*)	0.572	0.30
n (-)	2.917	2.14

As shown in Table 15, grain-size is lower on the second-stage infiltration layer than the first stage, as it is designed to 'polish' the first-stage treatment. Detailed results of the grain-size distribution of infiltration material are reported in Figure 88. We ran a total of 6 grain-size tests for the first stage and 5 for the second to check the variability of the results.

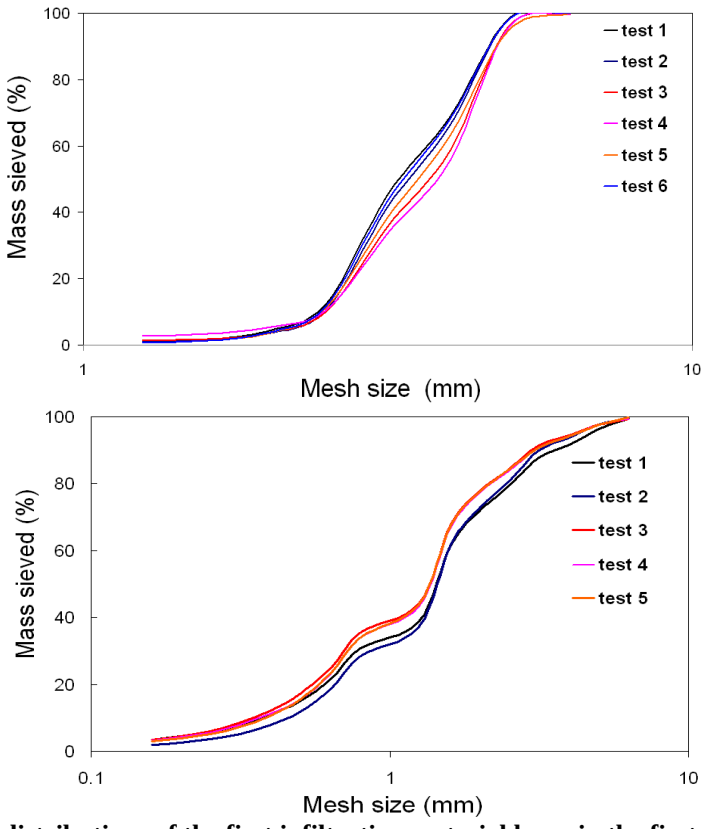

Figure 88: Grain-size distributions of the first infiltration material layer in the first stage (*top*) and second stage (*bottom*)

First-stage grain-size curves show good grain-size continuity with fairly good distribution confirmed by the uniform coefficient less than 1.59 (Table 15), contrary to the second stage.

In order to get the remaining parameters for the van Genuchten-Mualem formula, water retention curves were obtained by the sandbox method (Stackman *et al.* 1969). RETC software computed the θr, θs, α and n parameters needed for Hydrus modelling. For the first stage, several experiments were carried out with different organic matter contents (*OMC*) of the first infiltration material, going from clean porous media (no *OMC*) to high OMC. Sludge deposit was also sampled. The water retention curves obtained are shown in Figures 89 and 90.

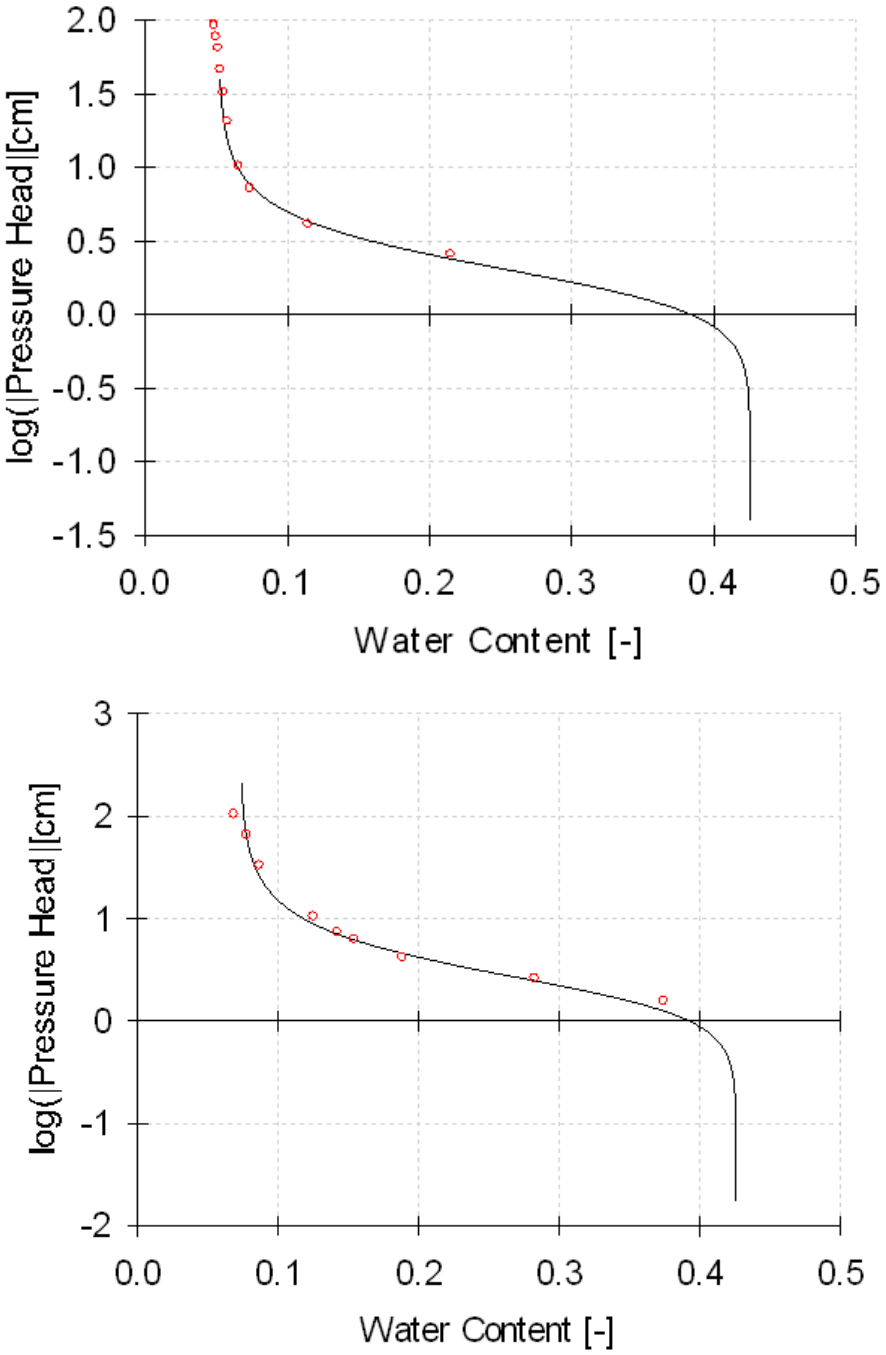

Figure 89: Water retention curves for the first infiltration layer of the first stage with no OMC (*top*), low OMC (*bottom*)

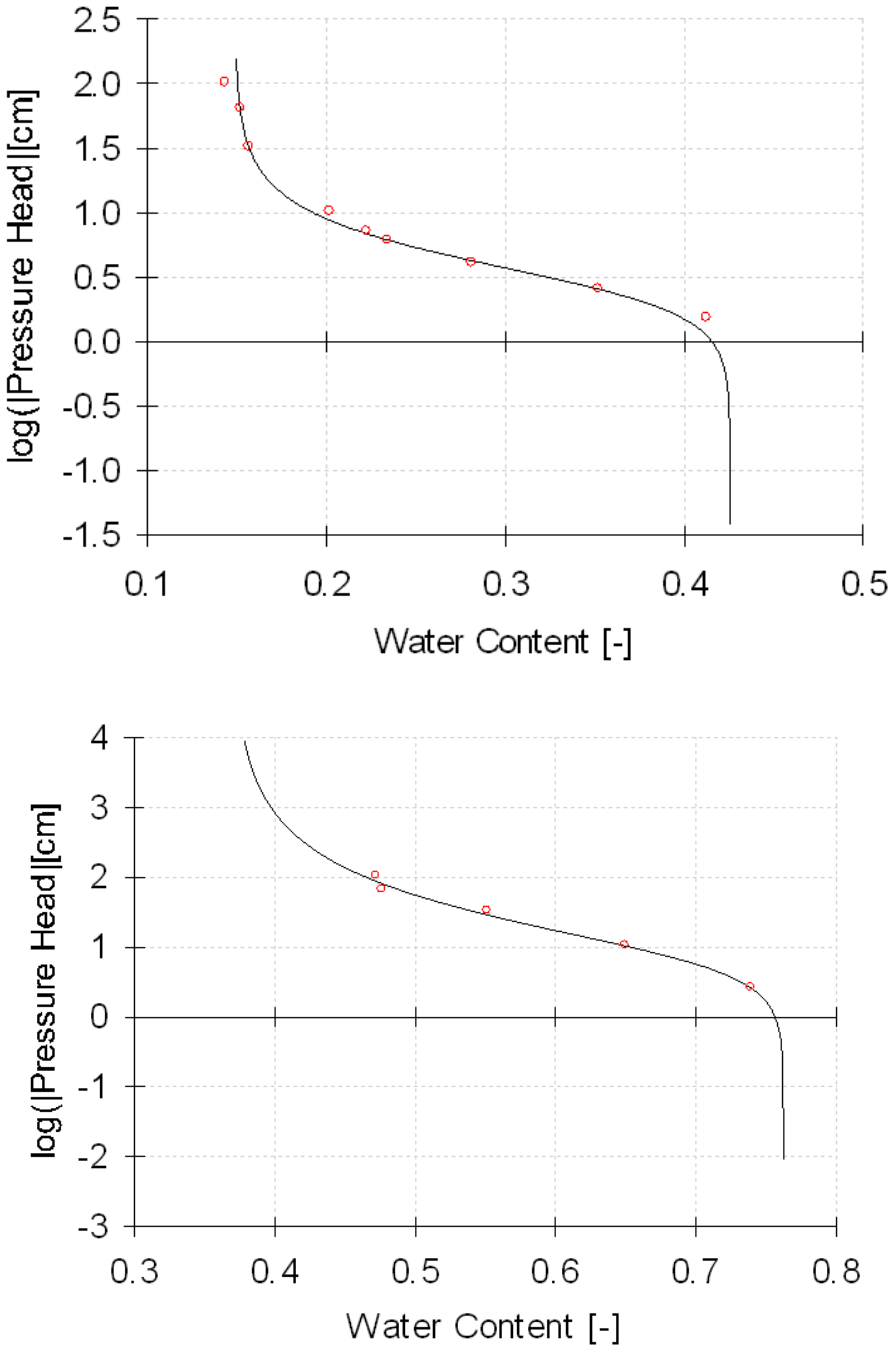

Figure 90: Water retention curves for the first infiltration layer of the first stage with moderate OMC (*top*) and sludge samples (*bottom*)

The water retention curves show that gravel with no OMC offers very low water retention (Figure 89) compared to porous sand medium (Figure 91), but that θ_r increases (and α decreases) with increasing organic matter content — a fact that reflects the impact of organic matter on the structure of the porous medium. For the second stage, only one experiment with clean first infiltration material was needed.

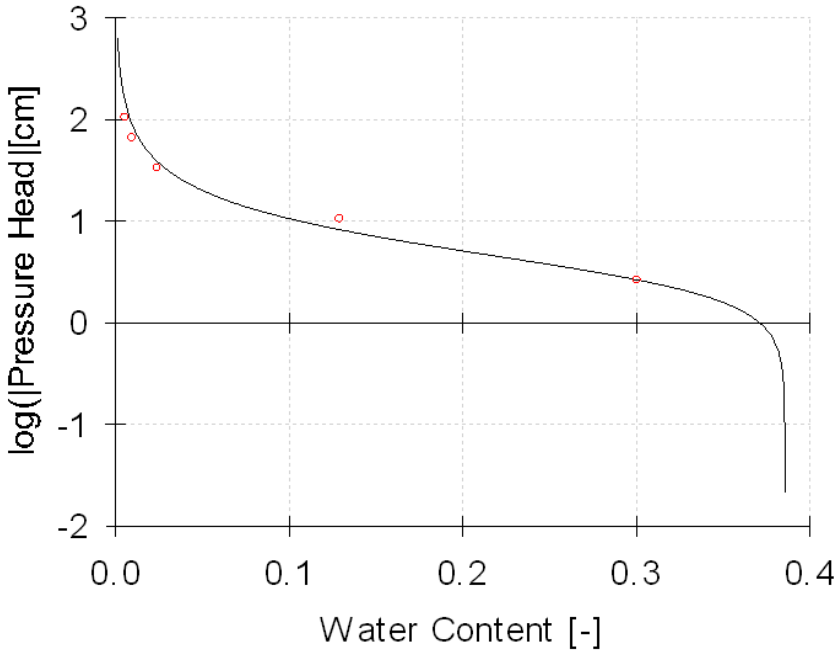

Figure 91: Water retention curve for the first infiltration layer of the second-stage

Table 16 gives the parameter outputs calculated by RETC software. For the infiltration material, the porosity value had been taken for θ_s due to the difficulty calculating it in RETC software, and for the sludge the θ_s value calculated was 0.76 cm³/cm³.

Table 16: Parameter values and 95% confidence intervals of the hydraulic properties of the first filtration layer material and sludge, for the first and second stage, as obtained by lab procedures

Samples		θr (cm³/cm³)		95% CI		α (1/cm)		95% CI		n (-)		95% CI	
		Challex	Morvannou 2012	Challex			Morvannou 2012	Challex		Challex		Challex	
First stage	Clean material (No OMC) –lowest OMC samples in Morvannou 2012	0.052	0.043	0.049	0.054	0.572	3.266	0.466	0.678	2.917	1.479	2.520	3.315
	low OMC	0.073	-	0.062	0.084	0.490	-	0.380	0.600	2.291	-	1.920	2.663
	moderate OMC	0.150	0.21	0.136	0.162	0.333	0.46	0.291	0.375	2.510	2.13	2.131	2.889
	sludge	0.370	0.37	0.349	0.392	0.130	1.2	-0.075	0.336	1.550	1.51	1.173	1.928
Second stage	Clean material	0.045	-	-	-	0.298	-	0.208	0.388	2.140	-	1.830	2.449

Note that the residual water content of second stage had to be fixed as the software struggled to fit this value. Given that the modelling aim is to describe the hydraulics of the first stage and that the second stage was not evenly planar, only first-stage hydrodynamic parameters obtained by lab methods were used as initial values for the inverse modelling in Hydrus 1D. However, the parameters of the second stage can be used for subsequent modelling.

If we compare the values obtained from Challex on a young filter against the work of Morvannou (2012) on a mature filter in terms of the respective OMC, we can see that the sludge layer characterization results converge on θr and n, but α value was substantially

higher in Morvannou's work. This difference could be related to the characteristics of porous media structure on the two types of sludge, with the mature filter presenting a more mineralized sludge. For the "moderate OMC" samples, the values of the two studies were similar, but exact OMCs are unknown for all samples, which makes it difficult to feasibly compare the results. For the clean/lowest OMC samples, in addition of the difference in OMC, the imprecise measurements of high water contents in this grain-size material (gravel) makes comparison more difficult still. However, this comparison does give us a picture of the range of values for similar OMC samples. Again, these results were only used as initial values for the inverse modelling and not for final modelling.

4.2.2.2. Hydrus fitting

Given that season is one of the most important factors affecting filter hydrodynamics, the inverse modelling procedure was done for two different seasons (winter and summer) in dry-weather events. The aim was to compare and validate the simplified model in terms of outflow and ponding (depth and time) on these two different hydraulic behaviours. The final set of parameters obtained from the inverse modelling is presented in Table 17 and compared with results of Morvannou (2012) on a similar type of VFCW (Evieu).

Table 17: Parameter set obtained by inverse modelling for winter and summer season. * λ values taken from Morvannou 2012

Layers	Depth (cm)	Parameter																	
		θ_r (cm^3/cm^3)			θ_s (cm^3/cm^3)			α (1/cm)			n (-)			K_s (cm/m)			(-) *	
		Winter	Summer	Morvannou 2012	Winter	Summer	Morvannou 2012	Winter	Summer	Morvannou 2012	Winter	Summer	Morvannou 2012	Winter	Summer	Morvannou 2012	Winter	Summer
1st infiltration surface (gravel with low biomass, Morvannou)	0 - 15	0.067		0.216	0.426		0.406	0.035	0.103	2.482	1.6	1.393	1.177	0.155	88.351	6.36	0.5	
2nd infiltration surface (clean gravel, Morvannou)	15 - 30	0.067		0.255	0.426		0.44	0.092	0.168	2.951	2.083	1.635	1.305	1	93.447	139.32	0.5	
Infiltration and transition	30 - 60	0.067			0.426			0.09			2			300			0.5	
Transition and drainage	60 - 80	0.067			0.426			0.1			2.8			300			0.5	

Inverse modelling results show that K_s rises from first to second infiltration layer, which can be explained by the higher amounts of organic matter in zones close to the surface. This organic matter has an important impact on porosity, K_s and capillary suction. In all likelihood, K_s is broadly higher in summer than in winter, and in summer, the difference in K_s between the two first layers is negligible. The α parameter followed the same trends, in contrast to n that showed higher values in winter than summer. Note that we compared the first and second infiltration layer materials of a young filter (Challex) against the deeper infiltration material of an old filter (Morvannou's experimental site) as they presented similar OM content.

Consequently, the higher values observed by Morvannou (2012) for some parameters (i.e. α) could be due to the limiting step of the two previous layers (sludge and high biomass content) that limit the robustness of the inverse modelling for the layers with low OMC.

Residual water content θ_r is visibly higher in the mature filter than the young filter due to the presence of organic matter. The n parameters of the mature filter are similar to the values obtained in summer season on the young filter. The K_s values of clean material for both filters (young and mature) are of the same order of magnitude, in contrast to K_s values on low-OMC material which were higher on the mature filter than the young filter, due probably to the difference of OMC.

As shown in Figures 92 and 93, the fitting of these different parameters with water content measurements gave Nash-Sutcliffe efficiency coefficient values of 0.77 and 0.39 for summer and winter periods, respectively. Compared to first-stage outflow, Nash-Sutcliffe efficiency coefficient values were 0.96 and 0.56 for summer and winter periods, respectively.

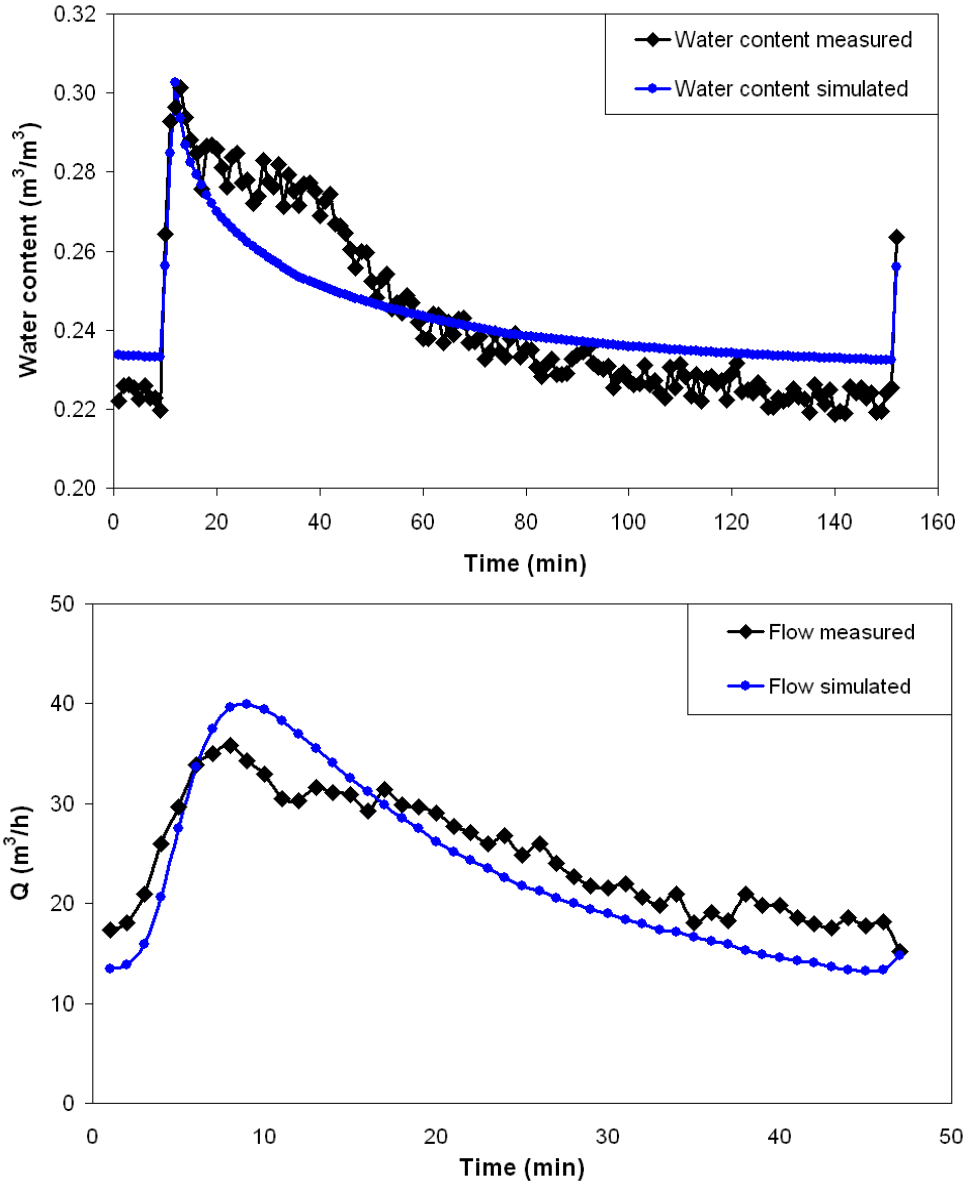

Figure 92 : Water content (*top*) and 1st stage outflow (*bottom*) measured and simulated of batch used to fitting in winter period

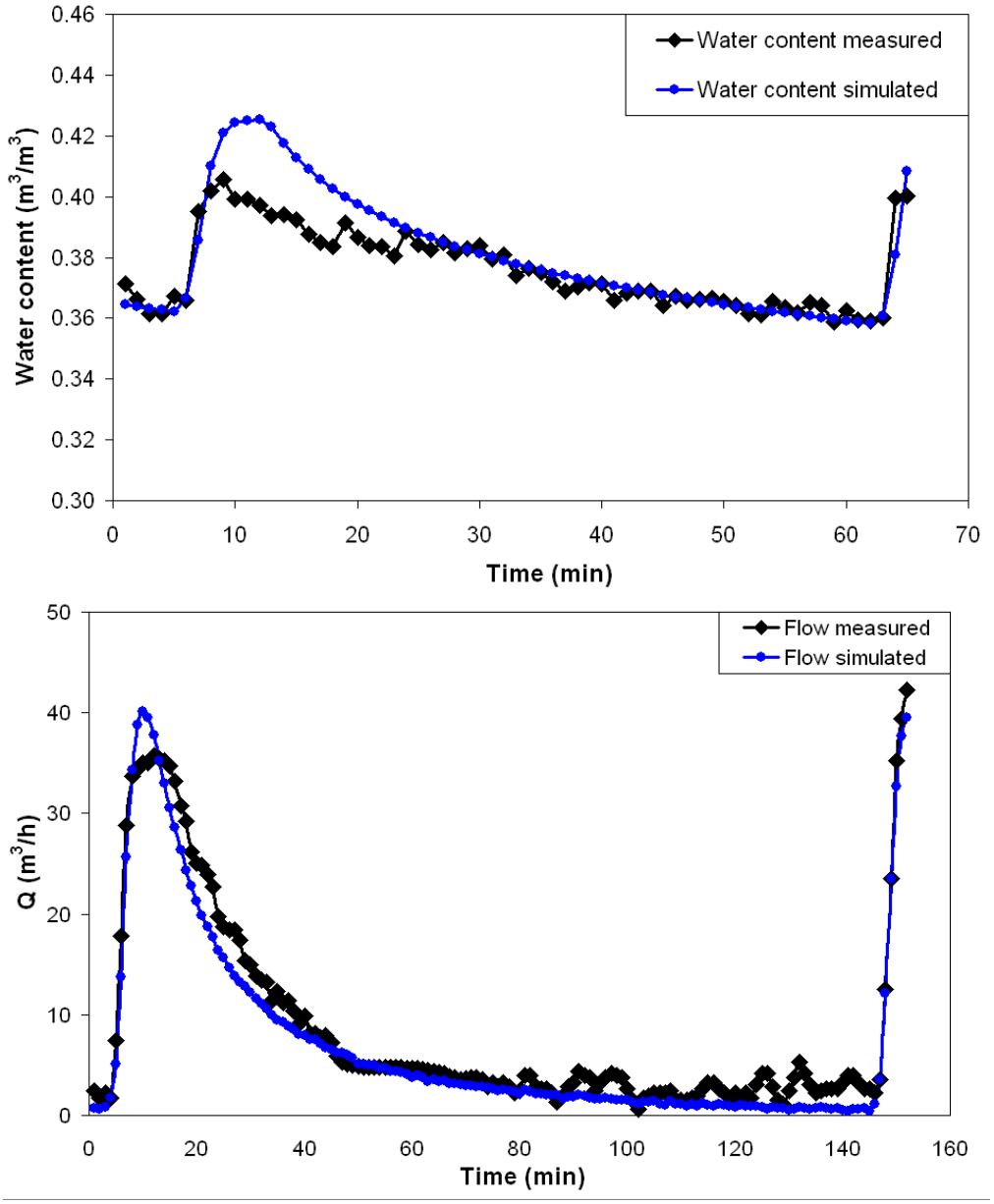

Figure 93 : Water content (*top*) and 1st stage outflow (*bottom*) measured and simulated of batch used to fitting in summer period

These curves highlight that the results are more reliable for summer events despite the irregular drainage drift (for water content curve), whereas the Hydrus model successfully reproduced water content at 10 cm depth and first-stage outflow for both scenarios.

- Comparison of results

The fitting parameters obtained on Hydrus correctly reproduced outlet flows and water content in the media. First-stage outflow measured was compared to outflow simulated by Hydrus and by the simplified model. As shown in Figure 94, the simplified model shows

good agreement with the Hydrus model results, and both models showed good agreement with measured data.

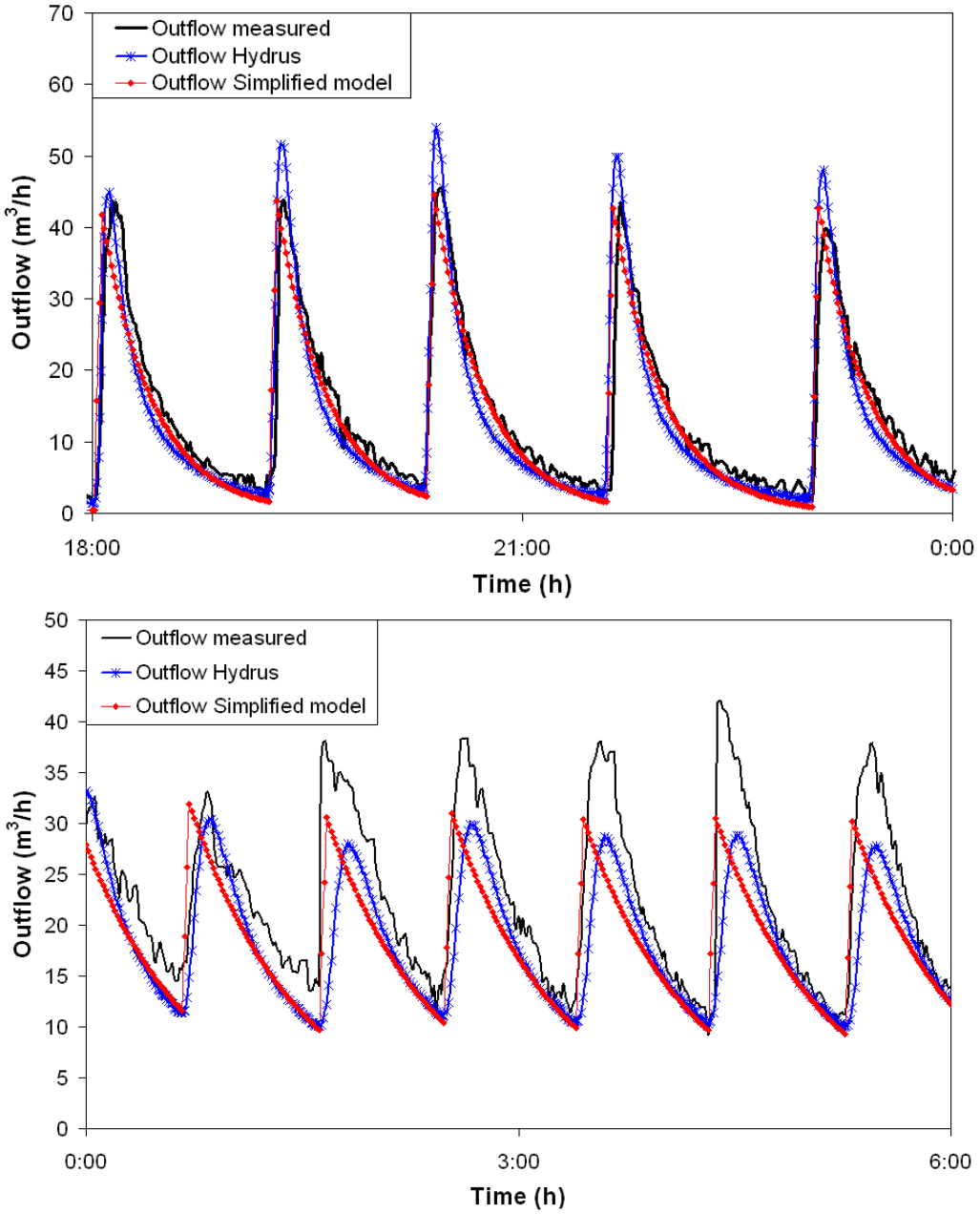

Figure 94: First-stage outflow modelled by Hydrus and the simplified model for summer (*top*) and winter (*bottom*) periods

Compared against measured data, the Nash-Sutcliffe efficiency coefficients were only negligibly different between the two models, at 0.86 and 0.9 for the simplified model and Hydrus, respectively, for summer events. For winter events, the Nash-Sutcliffe efficiency coefficients are lower but still good, reaching 0.51 for the simplified model and 0.515 for Hydrus. Globally, we reach better results in summer than winter.

These fittings, realized on each season, demonstrate the robustness of the simplified model, since the results are in accordance with both measured data and Hydrus that includes internal

parameters (water content). Figure 95 compares experimental data against the simplified model and Hydrus-1D in terms of ponding depth for a winter dry-weather event.

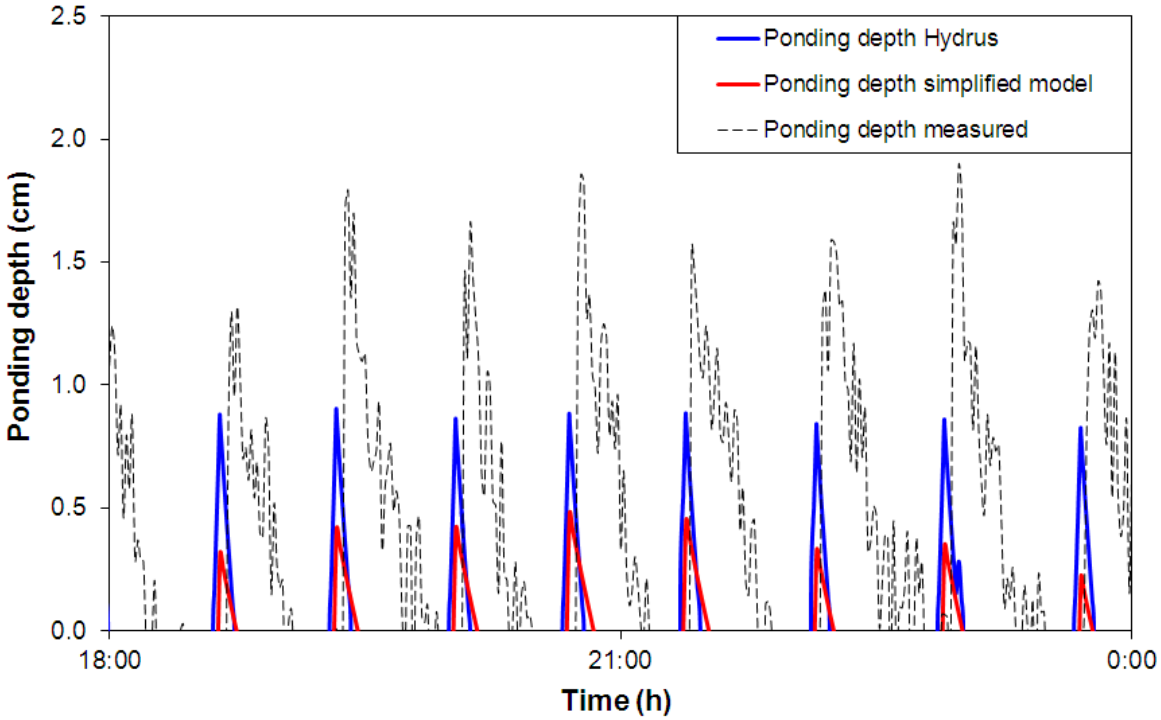

Figure 95: Ponding depth in winter as measured, modelled by Hydrus and modelled by the simplified model

Simulated ponding water depths were in good agreement with measured values, given the low ponding depths (Figure 95). There was also generally good agreement between the two models in terms of ponding time. Knowing that oxygen content in the porous media is affected by ponding duration, the simplified model proves to be secure at determining ponding limitations. The good agreement of the simplified model with Hydrus, which was fitted not only from first-stage outflow but also with internal parameters like water content, confirmed the capacity of the simplified model to robustly reproduce VFCW hydraulics.

4.3. Conclusions on the filter dynamics study

At this age of operation, the filters showed a high capacity for hydraulic acceptance, with inlet HL up to 14.3 times NHL. Only 1% of total events recorded during the 2-years monitoring period were more than 10 times NHL. TDR campaigns revealed inhomogeneous water distribution onto the filter surface due to a lack of deposit layer and to bad batch feeding flow design. The net result is that a large fraction of the filter surface stays inactive. Hydraulic load and season both have influences on water distribution, which is improved in winter due to the poor development of reeds and low infiltration rates. These infiltration rates are influenced by evolution over the feeding period, but the impacts remain low compared to the impact of season.

In the simplified hydraulic model, as ponding water depth was not homogeneous over the entire filter surface (due to uneven sludge deposits and uneven surface flatness), *ICP* was

fitted on the Challex first-stage outflow. Consistently with the infiltration velocities, *ICP* was more sensitive to season effect. The time-course evolution of *ICP* values suggested that VFCWs are more sensitive to ponding in the winter season. Age of system also showed an influence on *ICP* that suggests ponding could be higher on mature filters, but more data on mature filters is needed to confirm this hypothesis. The specialized hydraulics software Hydrus-1D was used to verify the robustness of the simplified model in two different scenarios (summer and winter season), focused on the first fraction of the infiltration surface layer which is the hydraulically limiting layer. The simplified model was in good agreement with measured outflow and ponding depth, and with the Hydrus model. This good reliability of the simplified model with Hydrus confirmed the capacity of the simplified model to reproduce the hydraulics of the first-stage of a VFCW.

5. Filters performances

5.1. Wastewater characteristics

Pollutant influent characteristics are dependent on (i) season (presence of clear water intrusion), (ii) human activity (weekends, holidays for domestic WW) and (iii) weather conditions (depending on dry weather history, rainfalls can create a dilution effect or a flush event releasing high pollutant contents) that produce variations in the hydraulic and organic loads entering the treatment plant. Table 18 reports the influent characteristics recorded in classically-led monitoring campaigns on the experimental site.

Table 18: Influent WW characteristics, organic and hydraulic loads on the first-stage filter in operation during sampling campaigns (loads during rain events have been transposed to a 24-hr basis)

	Hydraulic load (m/d)	**Pollutant load (g/m²/d)**							
		SS	***Total COD***	***Diss COD***	***TKN***	***NH_4-N***	***NO_x-N***	***PO_4-P***	***BOD_5***
Dry-weather flow (number of data)									
Average loads	0.29(7)	85(7)	136(7)	20(7)	14(7)	8.2(7)	0.25(7)	0.79(7)	56(4)
Max.	0.42	128	164	27	18	8.9	0.47	0.89	76
Min.	0.23	52	115	17	12	7	0.11	0.67	40
Standard deviation	0.06	24	19	3.7	1.8	0.64	0.17	0.08	18
Average concentrations (mg/L)		289	477	71	48	29	0.85	2.8	175
Rainfall events (number of data)									
Average loads	1.27(5)	236(5)	319(5)	63(5)	25(4)	12(5)	4.01(5)	1.58(5)	169(2)
Max.	2.26	624	890	76	49	19	7.41	2.65	288
Min.	0.68	79	49	49	13	7	0.75	0.92	49
Standard deviation	0.64	226	336	13	17	4.7	2.62	0.78	169
Average concentrations (mg/L)		179	257	40	18	8	2.4	1.11	148
Nominal loads	**0.35**	**139**	**279**		**28**	**21**		**5**	**111**
Percentage loaded									
According to average load in dry-weather flow	83 %	61%	49%		50%	39%		16%	50%
According to *average* and *maximal* loads in rainfall events	363% 646%	170% 449%	114% 319%		89% 175%	57% 90%		32% 53%	152% 259%

The plant is globally under-loaded (~49% organic load and 83% hydraulic load compared to nominal load) in dry weather but records high loads during rainfall events (~319% for organic load and 646% for hydraulic load). The concentrations measured in dry-weather conditions highlight that WW are slightly diluted — possibly due to groundwater intrusion into the sewer. Furthermore, the main carbon content is in particulate form, possibly due the high slope and the short-distance sewer system of Challex village. Figures can reach a dissolved COD/total COD ratio of 0.15 and 0.24 (SD: 0.04 and 0.14) for dry weather events and rainfall events, respectively. A first flush event can induce COD loads reaching 319% of nominal load. In addition, high SS concentrations are measured during rain events, showing the influence of sewer "cleaning" for high flows. NH_4/NK ratio was 0.6 and 0.51 (SD: 0.06 and 0.09) for dry weather and rainfall events, respectively, i.e. slightly lower than regular figures for small communities in France [about 0.75 (Molle *et al.* 2005)], consistently with the highly particulate form of pollutant measured on this treatment plant. As an important share of treatment performance relies on filtration processes, the particulate form of Challex WW will favour treatment efficiency of the system. COD/BOD_5 ratios of 2.7 and 1.7 for dry and rain events, respectively, show that the WW is perfectly biodegradable. Solids present typical domestic WW characteristics, as particulate COD/SS ratio is 1.4 and 1.2 for dry and rain events, respectively.

5.2. Treatment performances

5.2.1. SS and total COD

For the treatment performances analysis, all fractions of performances campaigns were transposed to a 24-hr basis to facilitate comparison and obtain data representing event intensity. Performances were analysed for each stage of treatment and for dry weather and rainfall events separately. Figure 96 demonstrates the high treatment efficiencies of the first stage, generally on COD and SS, of 91% and 86%, respectively, during dry weather conditions. The pollutant loads received were under the nominal loads, averaging 0.44-times and 0.55-times nominal load for COD and SS, respectively.

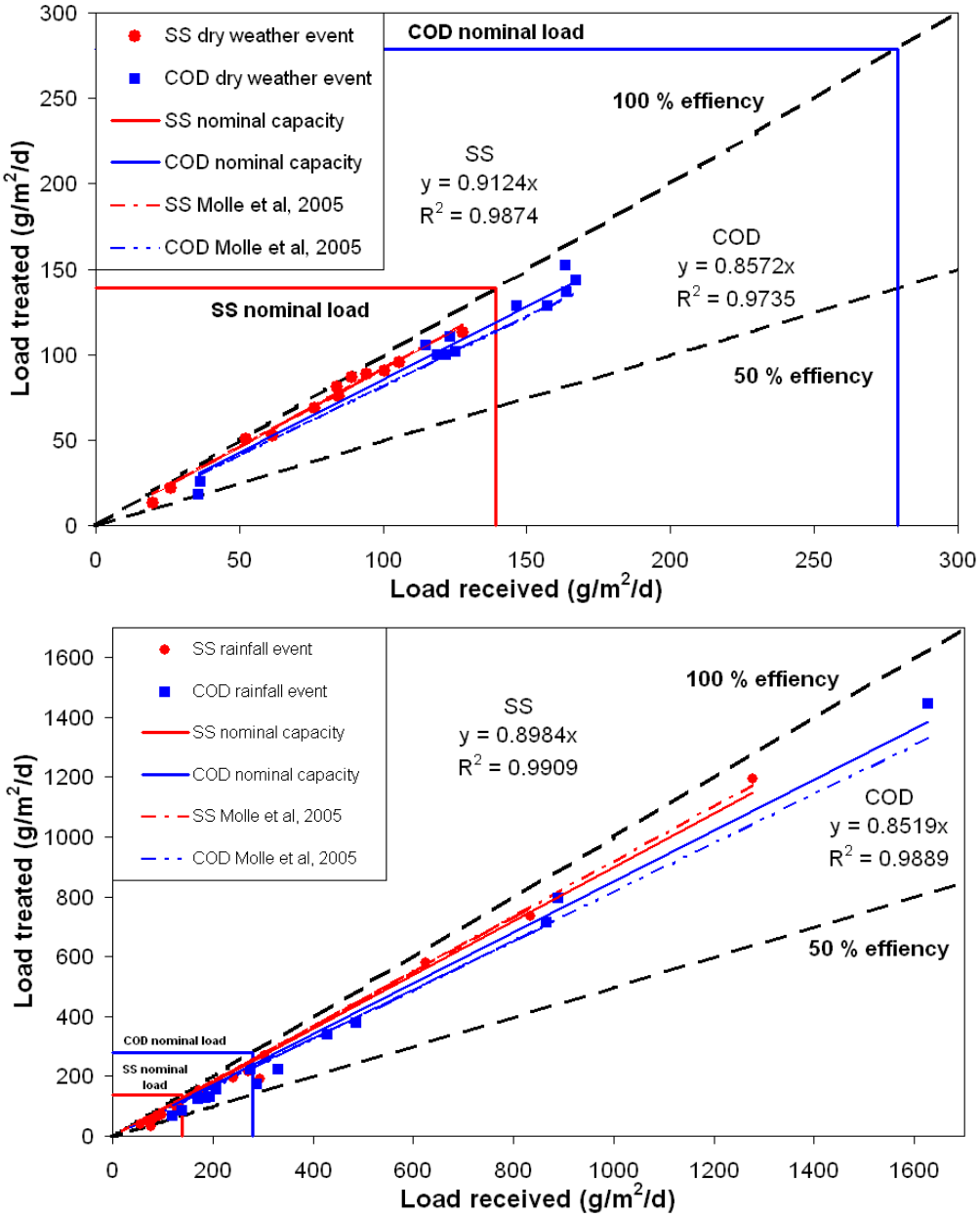

Figure 96: First-stage COD and SS removal rates in dry weather events (*top*) and rainfall events (*bottom*)

These efficiency levels are comparable to figures from over 80 different French VFCW (Molle *et al.* 2005). Globally, performances on Challex plant are similar to that observed on these systems (Molle *et al*. 2005). In response to rainfall events, the first stage showed same general removal efficiencies, at about 90% and 85% for average pollutant loads 1.96-times and 1.24-times nominal load for SS and COD, respectively.

As the COD was highly particulate, it is logical to find that COD removal rates were close to SS removal rates. First-stage outlet concentrations were generally in agreement with the total treatment objectives for the Challex plant, demonstrating the robustness of system. This efficiency led to low inlet concentrations at the second stage and consequently lower removal efficiency rates as shown in Figure 97. This fact is highlighted mostly for COD better than SS on dry weather events, with removal rates of only 49% and 75% respectively.

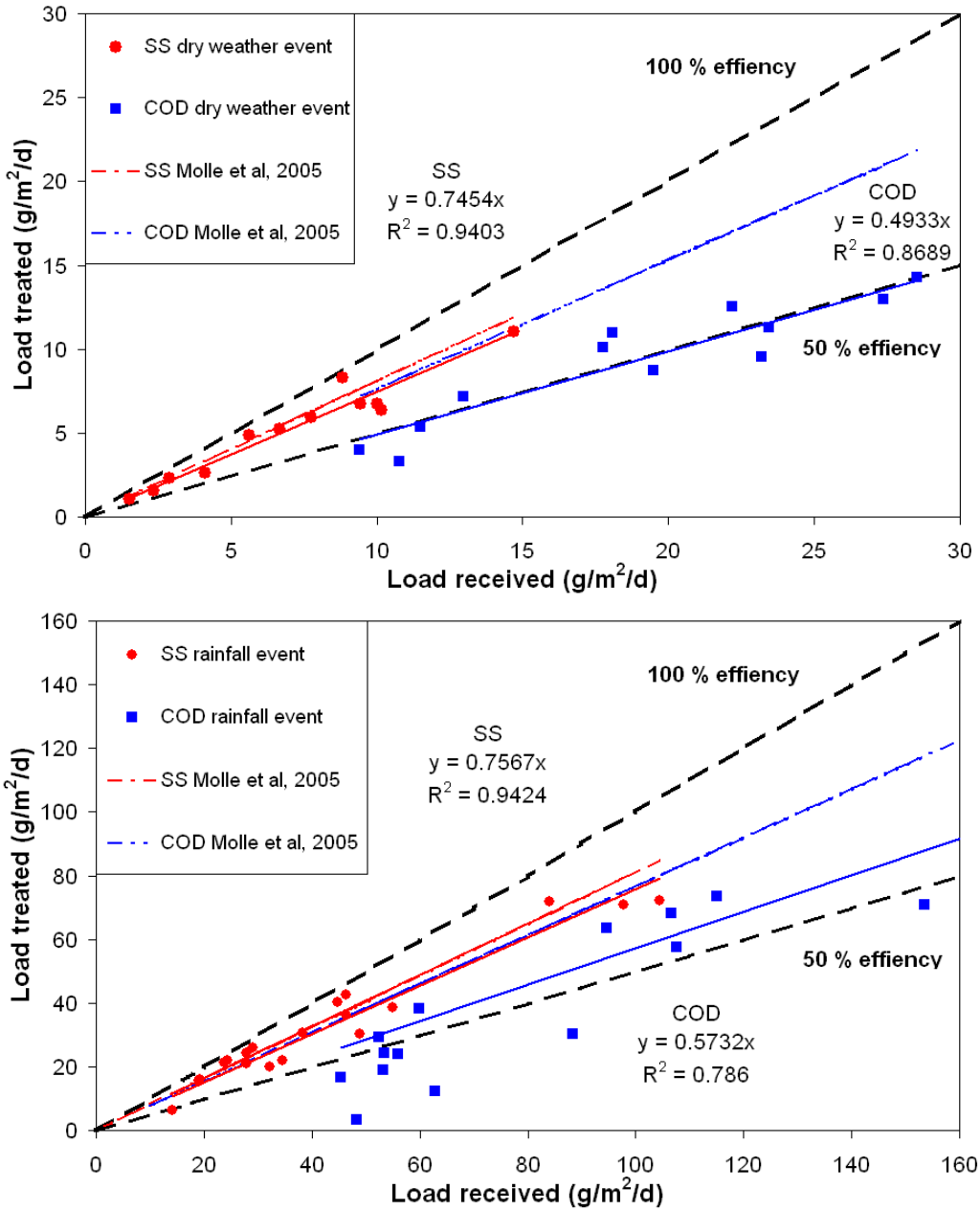

Figure 97 : Second-stage COD and SS removal rates in dry weather events (*top*) and rainfall events (*bottom*)

Figure 97 shows that second-stage SS removal rates are in agreement with observed French average performances (about 75% removal), which was not the case for COD (49%). In rainfall events, COD removal efficiencies are more scattered than other values. Since no clearly impacting factors (neither season or HL) were found, the low outlet pollutant concentrations (under the estimated lab limit of 30 CODmg/L) could have caused the value dispersion (Figure 98) leading to uncertainties of about 18% in the removal rates over the second stage of treatment.

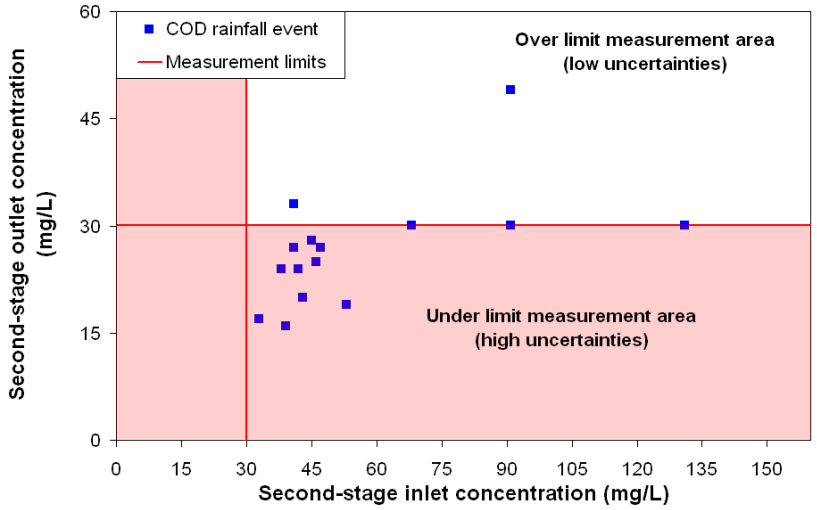

Figure 98: Second-stage inlet/outlet concentrations and measurement limits

Figure 99 shows that the treatment plant demonstrates very high SS and COD removal rates for total treatment, independently of hydraulic loads, despite the high pollutant load variations in rainfall events. Total-plant SS and COD removal rates for both conditions were 98% and 93% respectively.

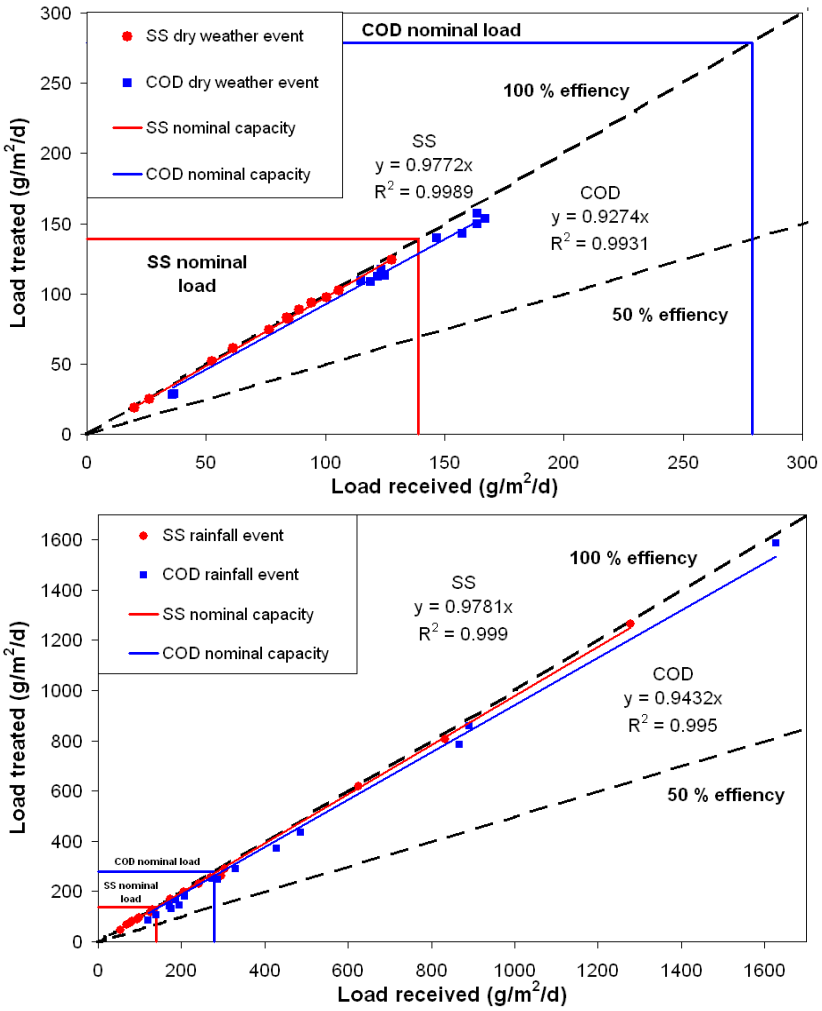

Figure 99: Total-treatment-plant COD and SS removal rates in dry weather events (*top*) and rainfall events (*bottom*)

Figures 96, 97 and 99 show how removal efficiency for dry weather and rainfall events was analysable in the same dataset, since the efficiency rates are fairly similar. Figures 100 and 101 thus summarize the removal rates of each stage of treatment independently of weather conditions.

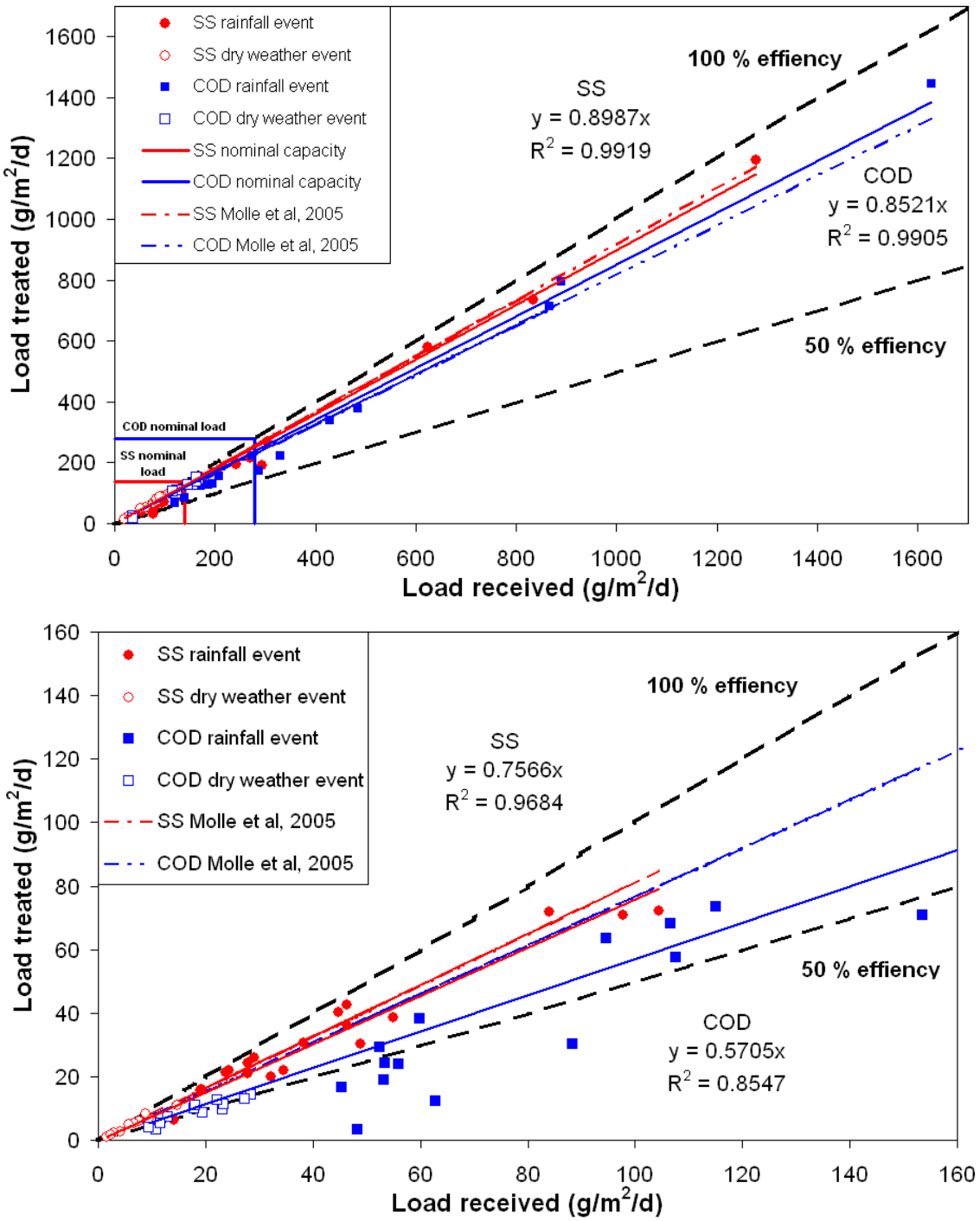

Figure 100: First-stage (*top*) and second-stage (*bottom*) COD and SS removal rates for both dry weather and rainfall events.

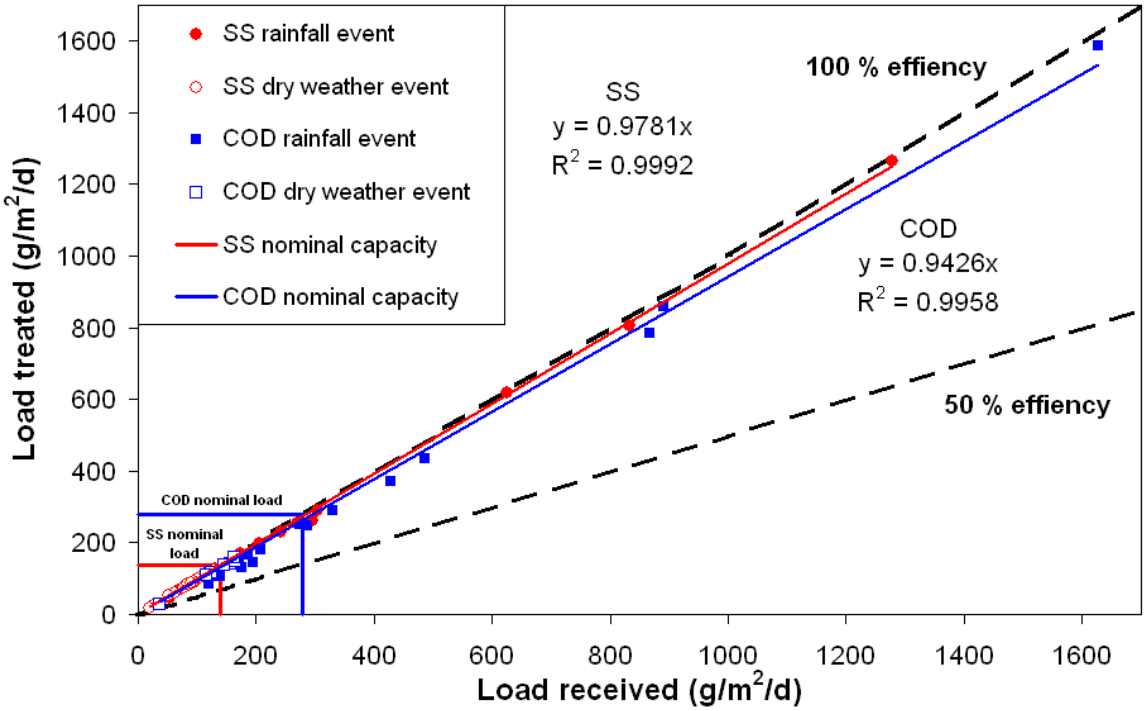

Figure 101: Total-treatment-plant COD and SS removal rates for both dry weather and rainfall events.

Outlet concentrations of COD and SS were always lower than 30 and 4.3 mg/L, respectively, which was well below the peak concentration thresholds set by the treatment objectives, i.e. COD -90 mg/L- and SS -35 mg/L-. These stable treatment performances highlight the robustness of the plant in response to overloads for each stage of treatment over the first two years of operation.

5.2.2. KN removal efficiencies

In dry weather conditions, first-stage KN removal rates mirrored the removal rates classically observed in different French VFCW systems (Molle *et al.* 2008). As relatively low loads were applied during dry weather flow (averaging 50% of nominal load), KN removal efficiencies were high, at about 76% at the first stage (Figure 102) and 70% at the second stage (Figure 103). However, at the second stage, due to low inlet concentrations and loads, removal rates appear lower than those measured by Molle *et al.* 2005.

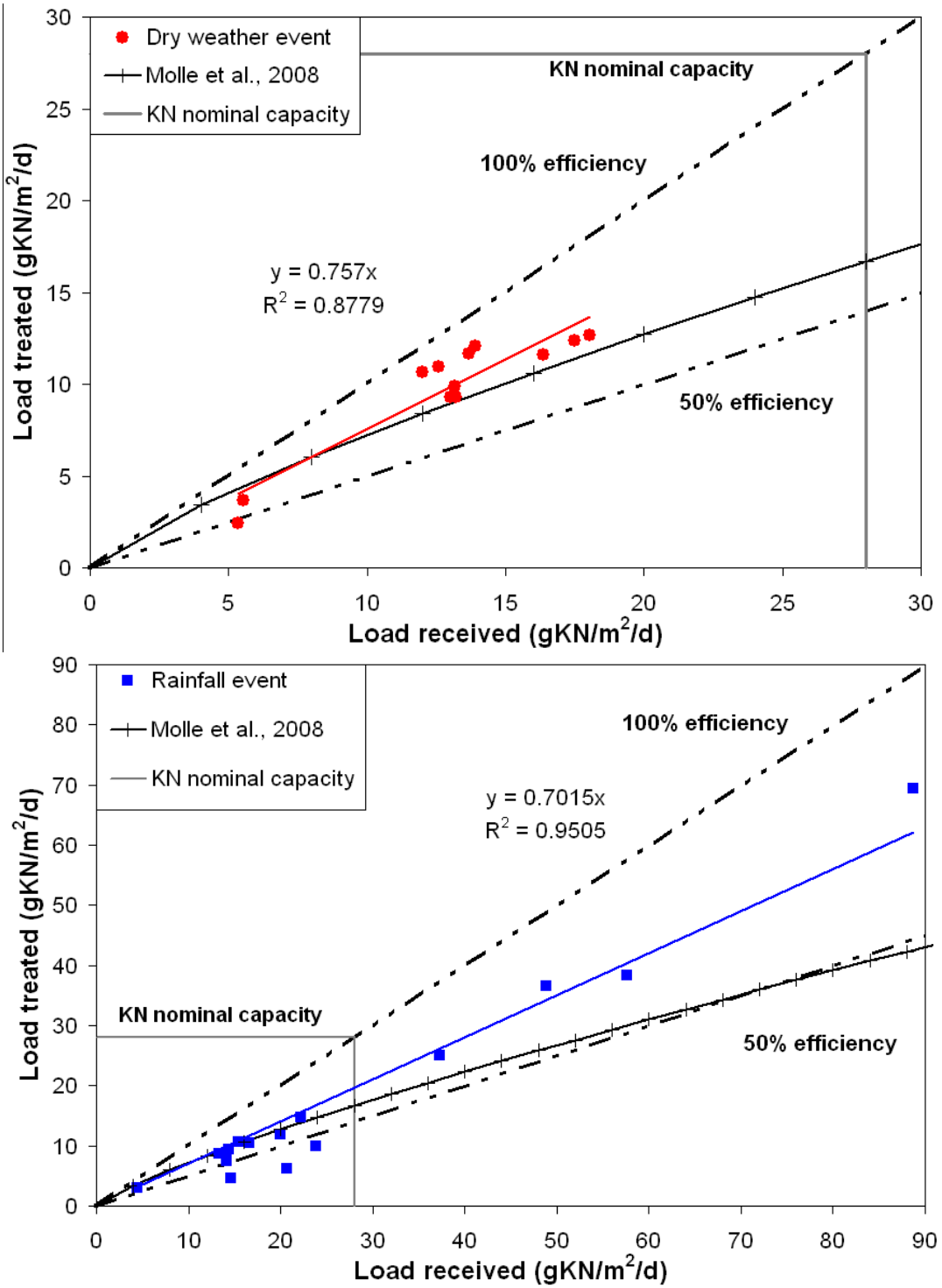

Figure 102: KN removal rates in dry weather events (*top*) and rainfall events (*bottom*) for the first stage filters

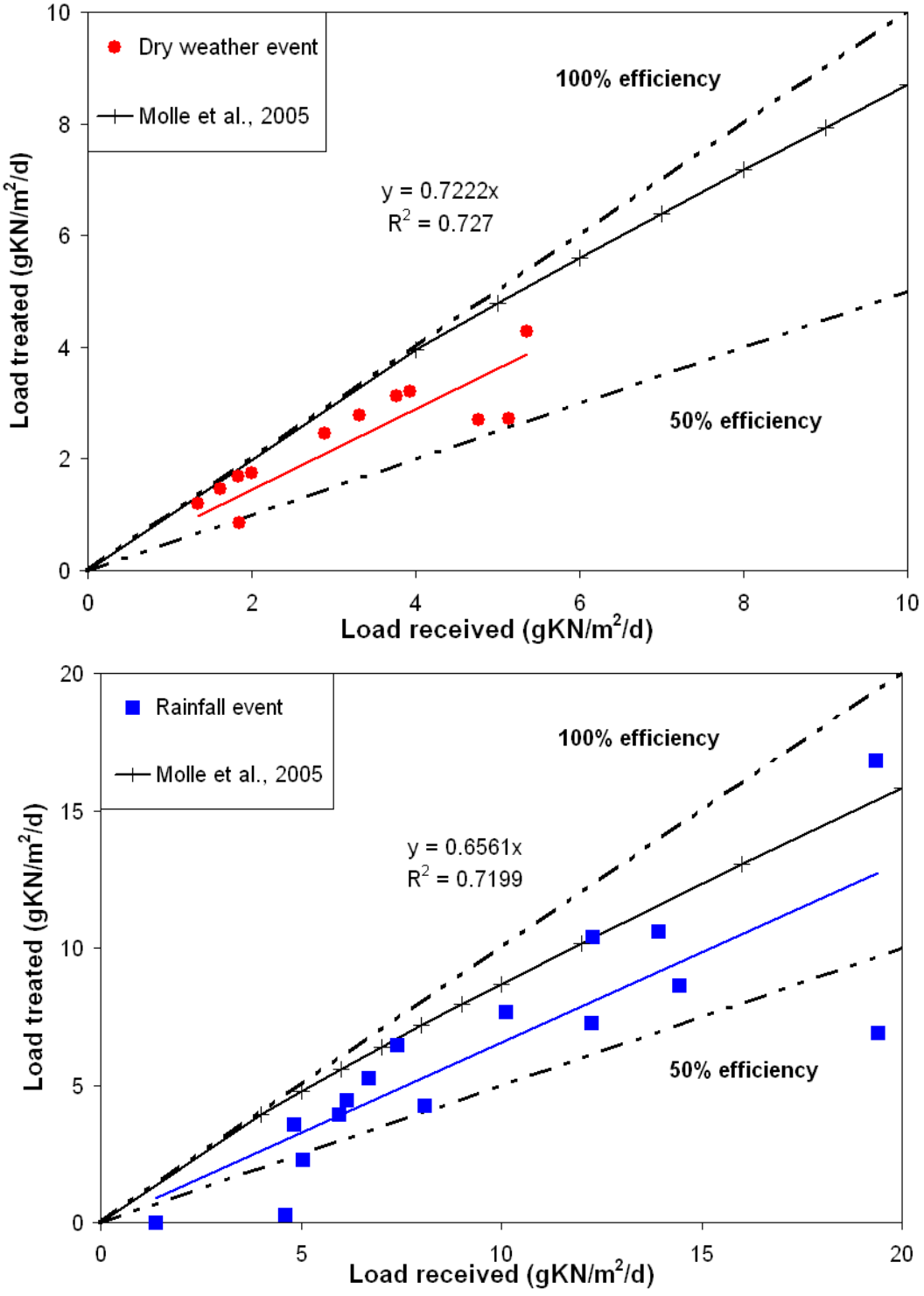

Figure 103: KN removal rates in dry weather events (*top*) and rainfall events (*bottom*) for the second stage filters

Rainfall events led to greater variability in performances according to load applied, with treated loads of up to 3.17-times the KN nominal load. Despite this higher variability, KN removal was globally 70% at the first stage (higher than literature predictions) and 66% at the second stage. At each stage of treatment, KN removal rates were slightly higher for dry weather events than rainfall events, at a total-plant removal rate of 94% and 90%, respectively (Figure 104).

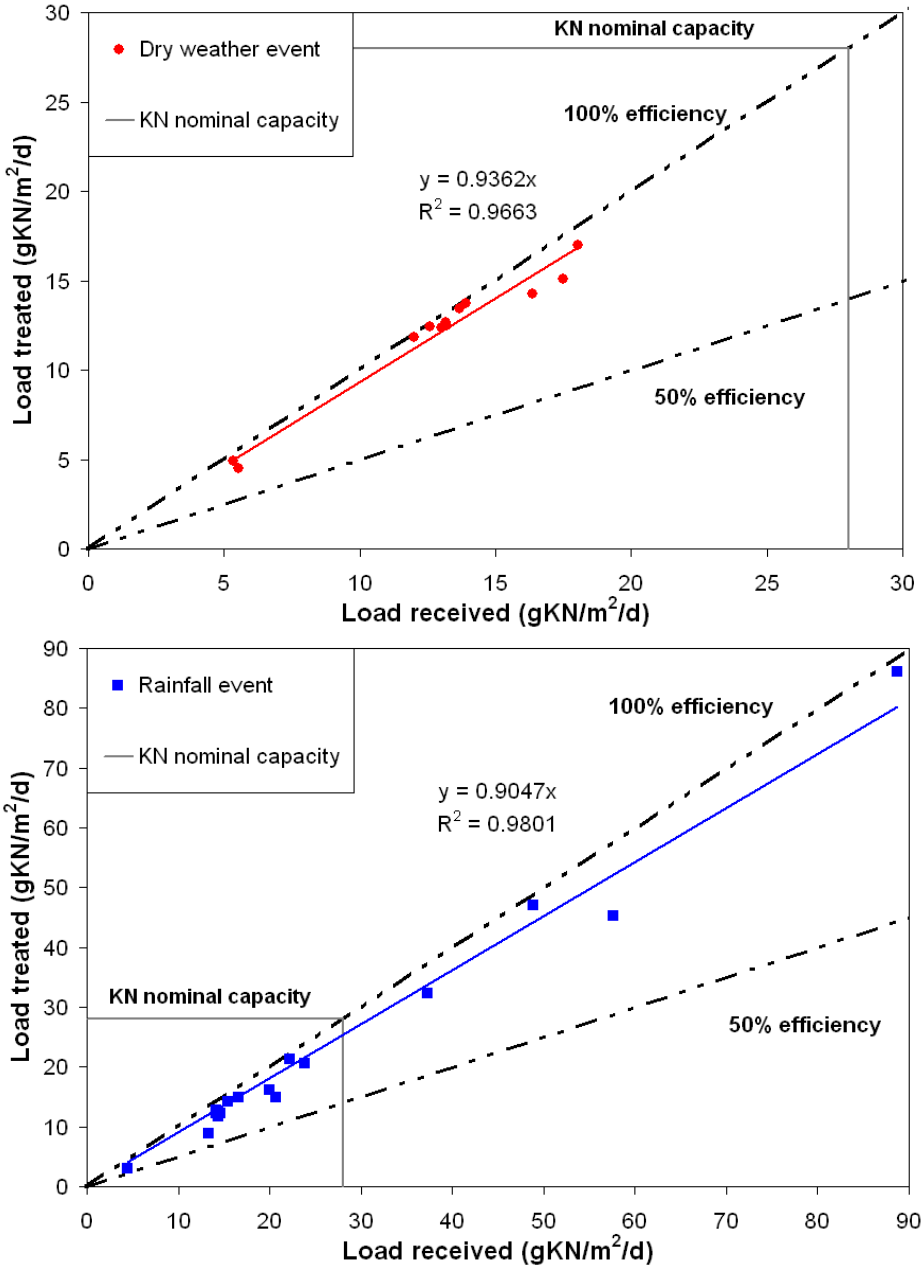

Figure 104: Total-plant KN removal rates in dry weather events (*top*) and rain events (*bottom*)

Removal rates were still good even in rain events when KN load reached more than three times nominal load. First-stage KN concentrations were always less than 18.4 mg/L, i.e. already within the total treatment threshold objective of 20 mg/L. The second stage can then reduce KN concentrations down to less than 7.4 mg/L at the treatment plant outlet. This demonstrates the robustness of treatment plant for KN removal over the first two years of operation. KN removal rates, transposed to a 24-hr basis, appeared to be independent of HL in the observed conditions.

Temperature is an influential factor in the activity of nitrifying bacteria (Vymazal 2007), and could explain a part of the observed variability in KN removal. Figure 105 presents this trend, where KN treatment performances (taken on a 24 h basis) were higher than 70% for average atmospheric air temperatures > 15°C, and generally decreasing according to temperature. These low temperatures also reflect a season effect on reed development which promotes better water infiltration and thus a better oxygenation of the porous media.

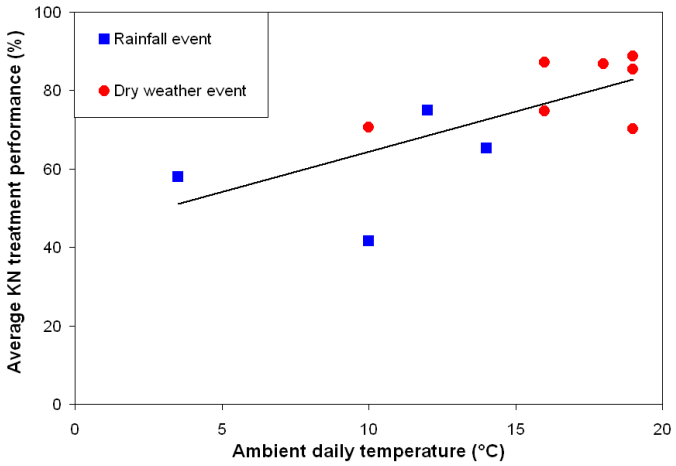

Figure 105: Influence of temperature on first-stage KN treatment performances

In addition, hydraulic loads directly impact treatment performances (Platzer & Mauch 1997) by impacting oxygen renewal capacities. High HLs produce low intervals between batches, inducing a progressive saturation of the porous media which limits oxygen renewal and disturbs nitrification (Molle *et al.* 2006). Figure 106 shows the global decrease in first-stage KN removal rates according to HL and its respective time between batches.

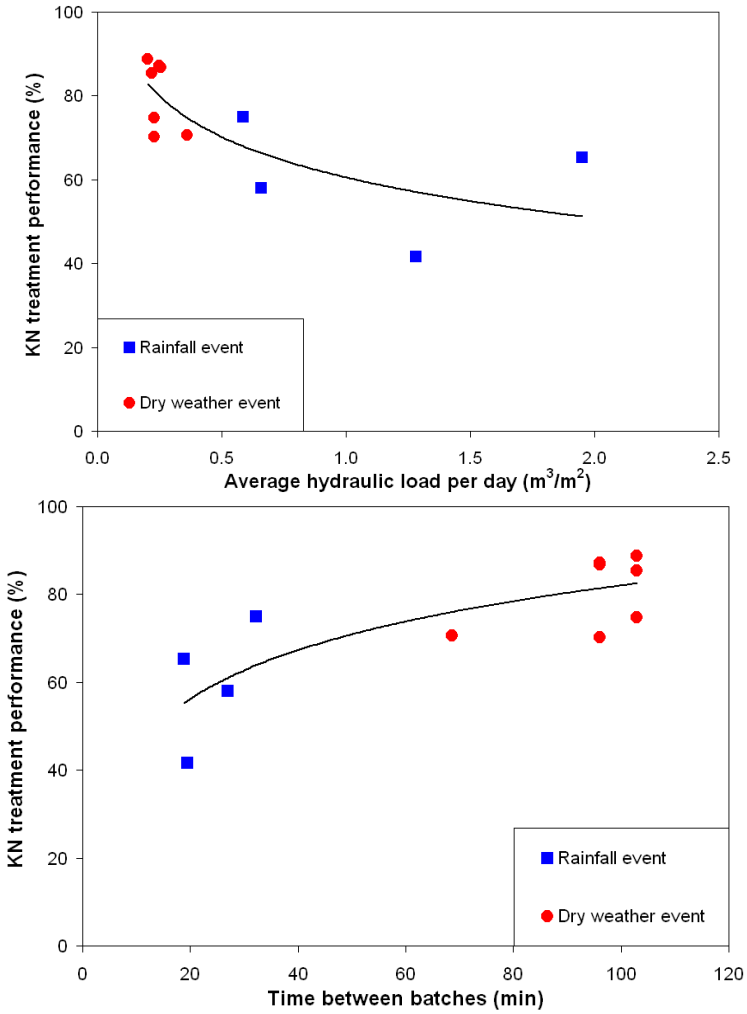

Figure 106: Influence of hydraulic load (*top*) and its consequent between-batches interval (*bottom*) on first-stage KN treatment performances

Although some variability is observable on a 24-hr basis, rain events have a clear-cut influence on nitrification. This point needs to be explored in depth to assess the biological limits of the system, as nitrification is a highly sensitive process. This discussion is presented in section 5.5.

As nitrogen dynamics in constructed wetlands are dependent on an array of processes (particulate form filtration, ammonium adsorption, ammonification, nitrification, denitrification, and more), it is difficult to pinpoint a direct relationship between KN removal and nitrate production. Figure 107 presents the relationship between first-stage KN removal and nitrate production on a 24-hr basis.

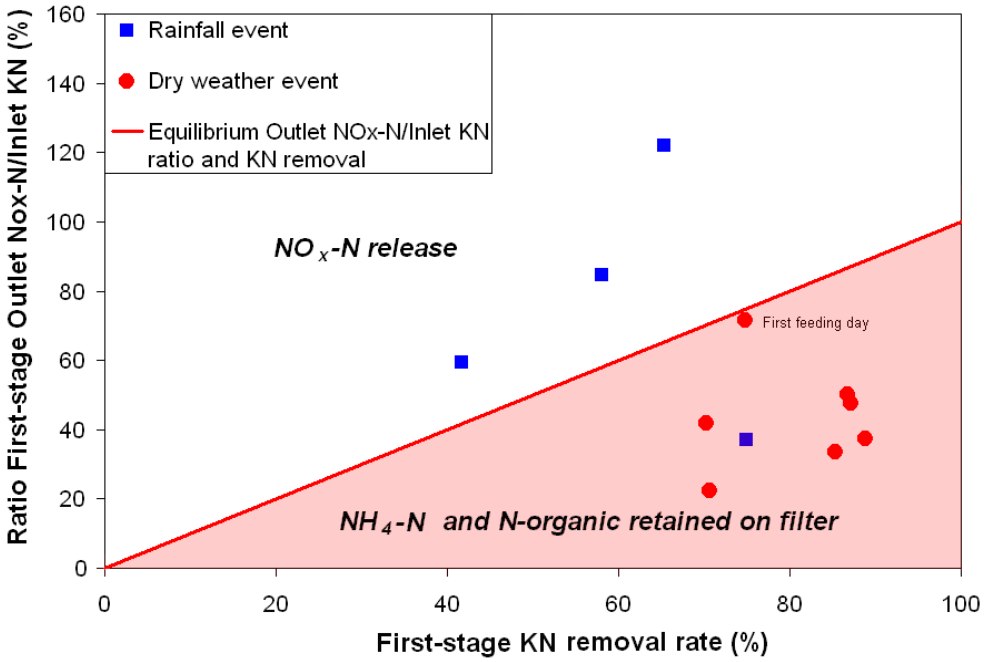

Figure 107: First-stage outlet NOx-N/inlet KN ratio according to first-stage KN removal rate for rainfall and dry weather campaigns — average event values.

Note that the data does not align to the equilibrium relationship: particulate nitrogen can be filtered and ammonified later, and the ammonium form can be adsorbed and nitrified later. This temporal effect takes part of the "spiralling" effect discussed by Kadlec *et al.*(2005) and makes it difficult to study nitrification limitation due to hydraulic overload. Indeed, Figure 107 shows that KN can be stored on the first-stage filter during dry periods whereas nitrates tend to get released during rain events. This phenomenon is tied to the hydraulics of the filter, which differ in dry and rain events: rain events induce complete water distribution over the filter surface (see section 4.1.1), allowing the release of nitrates from unused zones where full nitrification had been possible during long rest periods. The only dry weather measurement at the equilibrium corresponds to a first feeding day and thus includes nitrate release from nitrification that took place during the rest period.

The 24-hr basis analysis gives a general picture of treatment performances according to time between batches, but an analysis with continuous measurements (one-minute time-steps) is vital to bring deeper insight into KN removal rates, nitrification and filter dynamics. An S::CAN probe and VARiON®Plus probes (NH_4-N measurement) were used for this purpose (see section 5.4 and 5.5).

5.2.3. BOD_5 and dissolved COD

5.2.3.1. BOD_5

Given the scarce BOD_5 data available for rainfall events, the results are only taken as an order of magnitude of efficiency rates. During dry weather events, BOD load was about 0.44-times nominal load. As shown in Figure 108, the efficiency rates of the first stage were about 91% and 88% for dry weather and rainfall events, respectively. BOD_5 concentrations at the outlet of the first-stage filter are generally under the maximal outlet requirement for the whole plant (25 mg/L). The second stage then polishes the removal performances by a further 64% and 66% for dry weather and rainfall events, respectively, with outlet concentrations always below 11 mg/L.

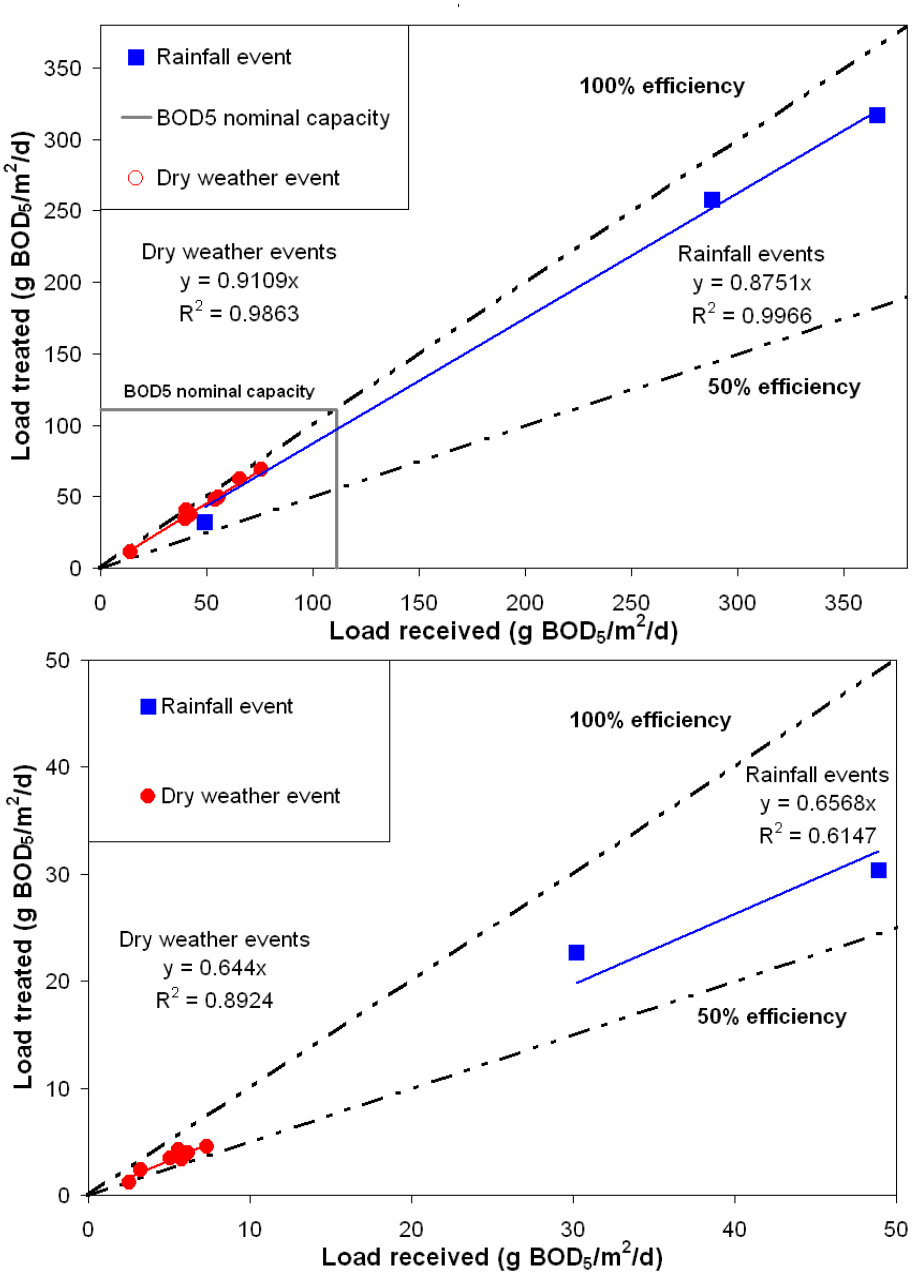

Figure 108: First-stage (*top*) and second-stage (*bottom*) BOD5 removal rates for dry weather and rainfall conditions

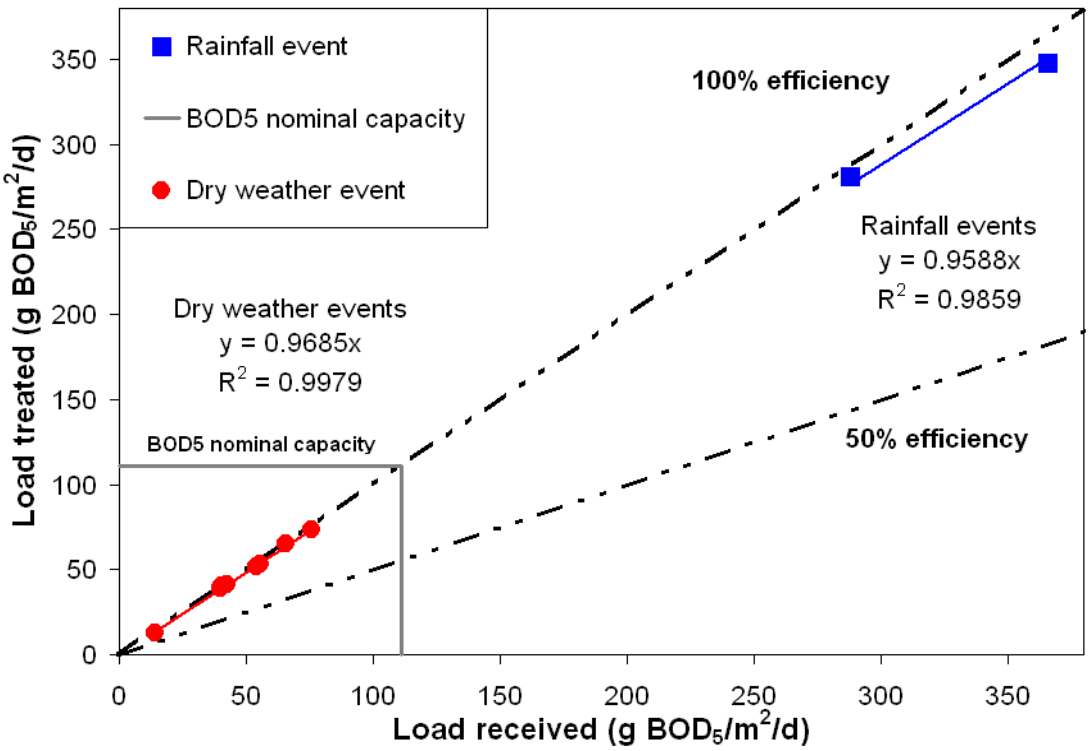

Figure 109: Total-treatment-plant BOD5 removal rates for dry weather and rainfall conditions

5.2.3.2. Dissolved COD

Dissolved COD removal performances are highly variable, especially in rainfall events, at all treatment stages. Efficiencies during rain periods vary between 11–63% and 14–76% for first- and second-stage filters, respectively (Figure 110). Degradation of the dissolved part is more sensitive to the hydraulic retention time that decreases with increasing hydraulic load. This inevitably affects removal performances as well as the low inlet concentrations of dissolved COD during rain events closer to the refractory fraction. Treatment performances are more stable in dry-weather events (about 51% and 57% for first- and second-stage filters, respectively).

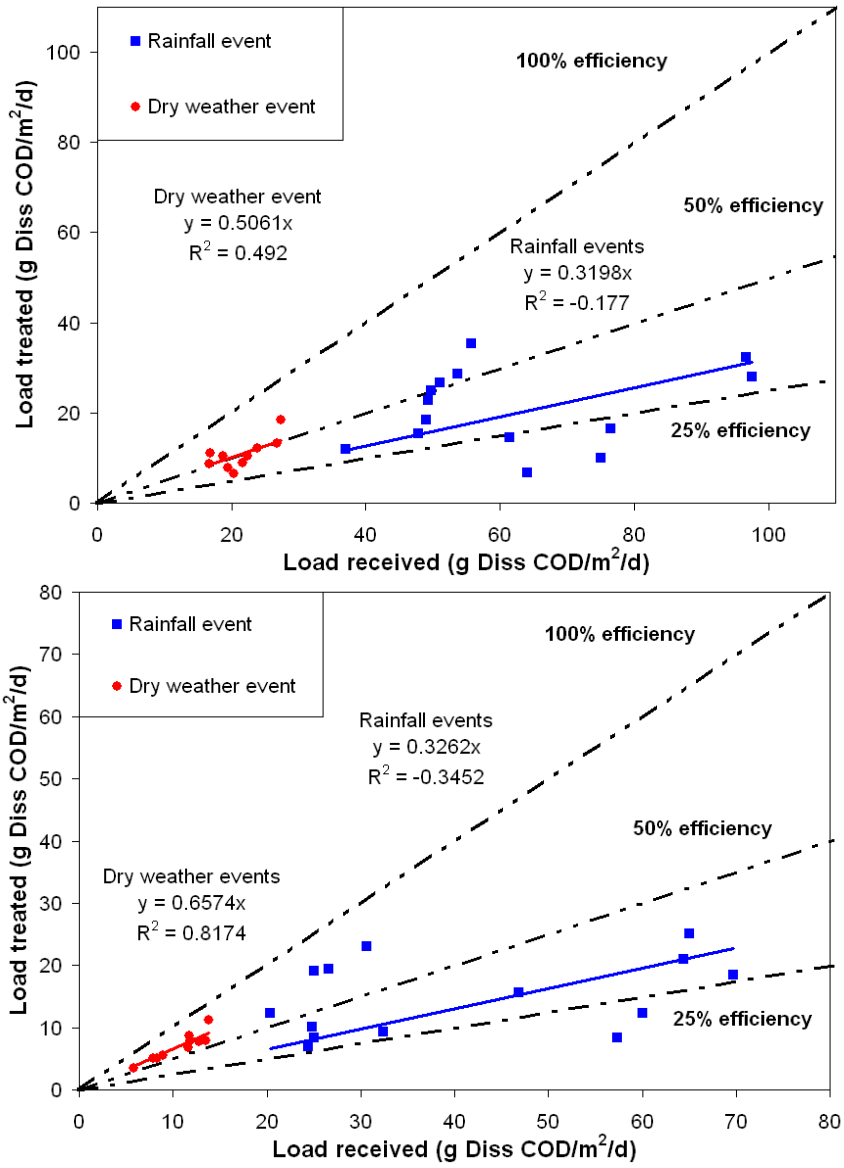

Figure 110: First-stage (*top*) and second-stage (*bottom*) Dissolved COD removal rates for dry-weather and rainfall conditions

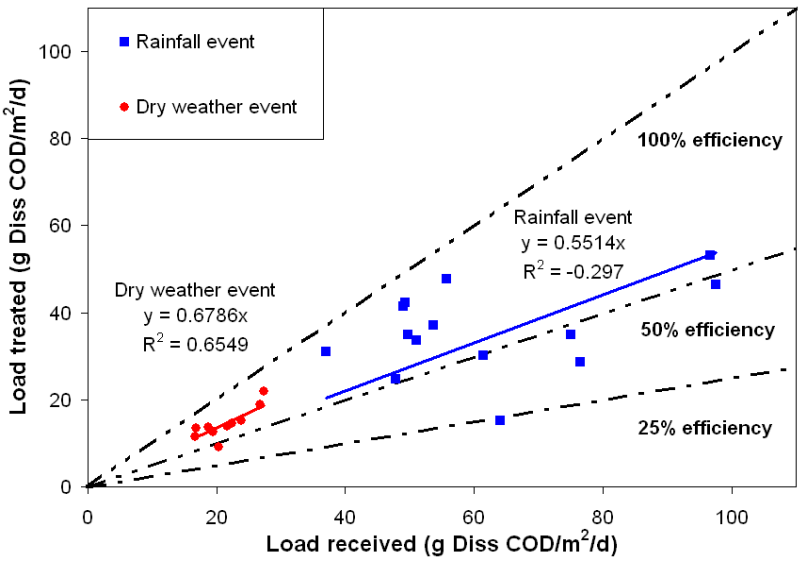

Figure 111: Total-treatment-plant Dissolved COD removal rates for dry-weather and rainfall conditions

Total dissolved COD removal performances ranged from 24% to 86% in rainfall events (Figure 111) compared to around 68% on average in dry-weather events. The data demonstrates that even at 6.5-times HNL, the plant did not show any performance problems with SS retention, COD, BOD_5 or KN removal according to the 24-hr analysis basis. Although these results give confidence as to the system's ability to cope with hydraulic overloads, they do not permit to determine the biological limit of the filter for hydraulic overload acceptance. For this, online monitoring is used to provide a more in-depth analysis of how the filter behaves in response to hydraulic overload (see section 5.5).

5.3. GOD (global oxygen demand)

As the oxygen demand induced by incoming WW generally exceeds the amount of oxygen available in the system (Kadlec & Wallace 2009), oxygen transfer can limit VFCW treatment performances. Using COD values — the biodegradable and non-biodegradable components — to estimate oxygen usage will overestimate oxygen consumption since not all the removed COD is necessarily aerobically biodegraded (Nivala *et al.*), but it does provide an idea of in-filter oxygen consumption.

Global oxygen demand (GOD) is calculated to take into account the oxygen needed for COD degradation and nitrification of ammonia. Equation 30, from Liénard *et al.* (1998), is used :

$$GOD = Total\ COD\ g/m^2/d + (4.5 \bullet TKN\ g/m^2/d) \qquad \textbf{Equation 30}$$

Figure 112 illustrates that on the first stage, pollutant oxidation efficiency decreases as HL increases due to the oxygen renewal limitations and shorter contact time that HL overloads promote. These efficiencies are of the same order of magnitude as in Molle *et al.* (2006) at the Colomieu VFCW (8 years in operation). Second-stage oxidation efficiencies tend to stay stable independently of HL.

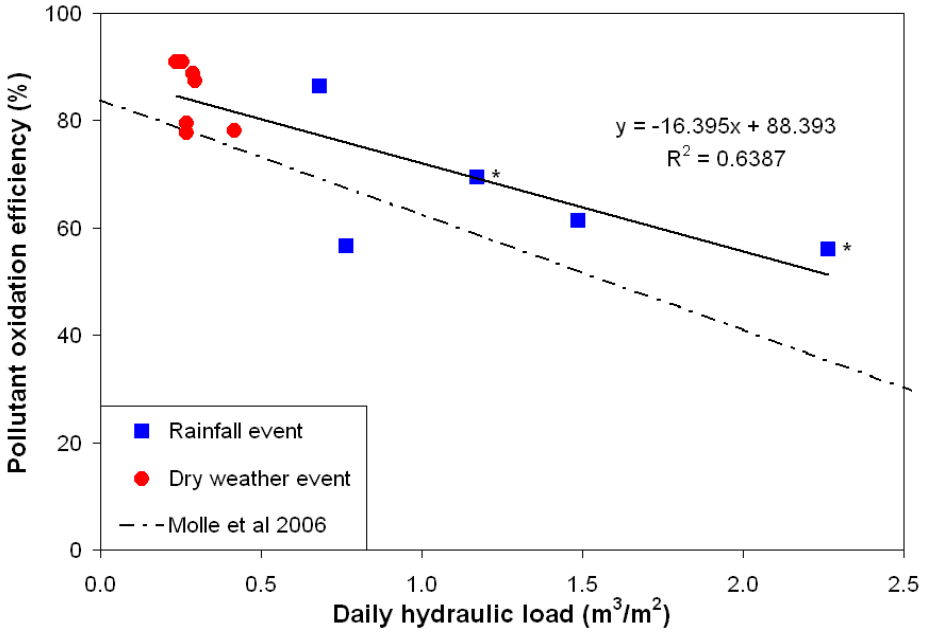

Figure 112: First-stage GOD removal according to 24-hr HL. Values marked * were calculated from rainfall average (COD/SS ratio or NK/NH_4 ratio)

The figure shows that according to load, GOD removal remains higher than 56% with no treatment performance dysfunctions recorded. Average global oxygen consumption for oxidation processes during monitoring was 167 $gO_2/m^2/d$ for dry-weather flow and 340 $gO_2/m^2/d$ for rainfall events. The dry-weather flow value remains under the nominal oxygen consumption generally achieved on a first-stage VFCW (293 $gO_2/m^2/d$). During rainfall events, global oxygen consumption is slightly higher than this nominal value. This could explain the good organic matter degradation and nitrification performances independently of HL. Data from intensive campaigns and continuous monitoring (S::CAN probe) were analysed to obtain further information on filter dynamics.

5.4. Intense treatment performance campaign

During the intensive campaign, the loads applied on the first-stage filter in operation remained lower than nominal loads for all pollutants (Figure 113). Note that data for feeding days 1, 2, 7, 9 and 11are from 24-hr composite campaigns while the other results are obtained from the average values from 3 batch samples per day at the first-stage inlet. During theses 11 feeding days, a rain event occurred producing a hydraulic load of 0.65 $m^3/m^2/d$ that was the maximal HL reached on this intensive campaign (1.86-fold NHL), but HLs were otherwise generally under the NHL.

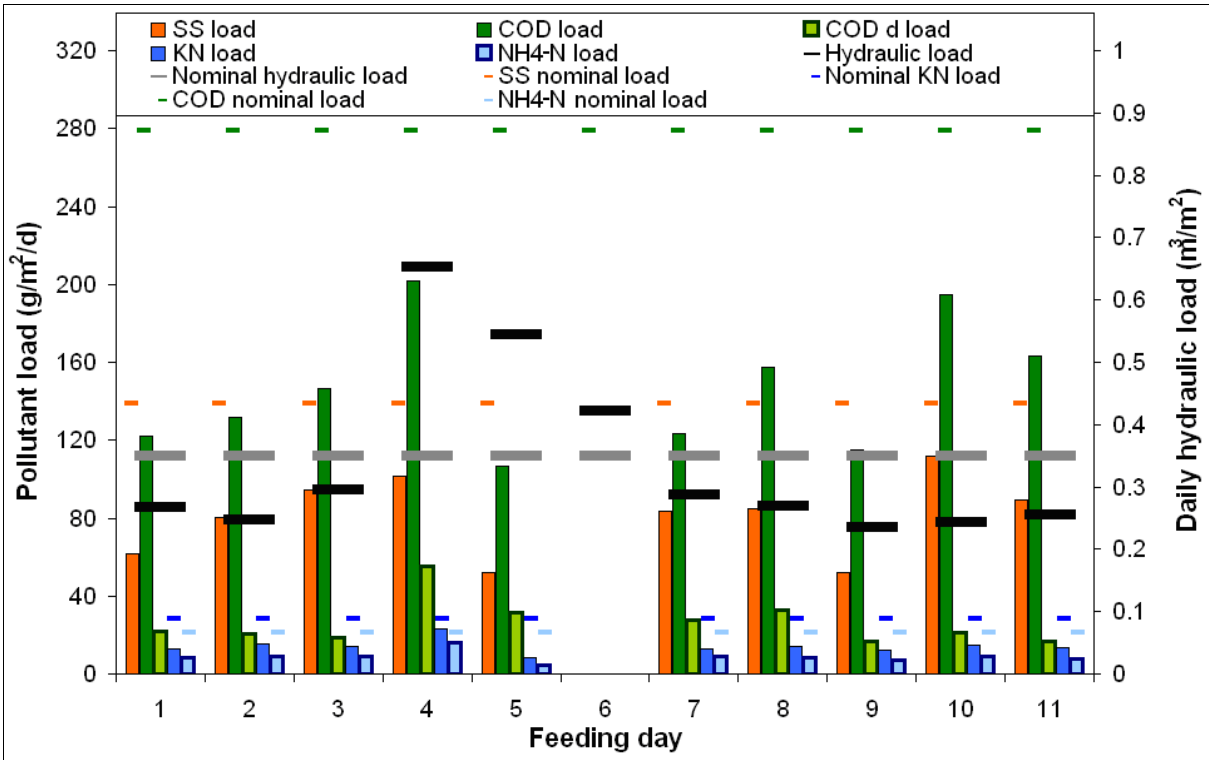

Figure 113: Pollutant load *vs* hydraulic load per day

As Figure 113 shows, inlet loads increased during the rainfall event, but the 10th feeding day also demonstrated high pollutant loads for SS and COD. This could be due to uncertainties on the grab samples taken on day 10. Globally, there was no clear-cut decline in treatment performances with feeding day, as shown in Figure 114.

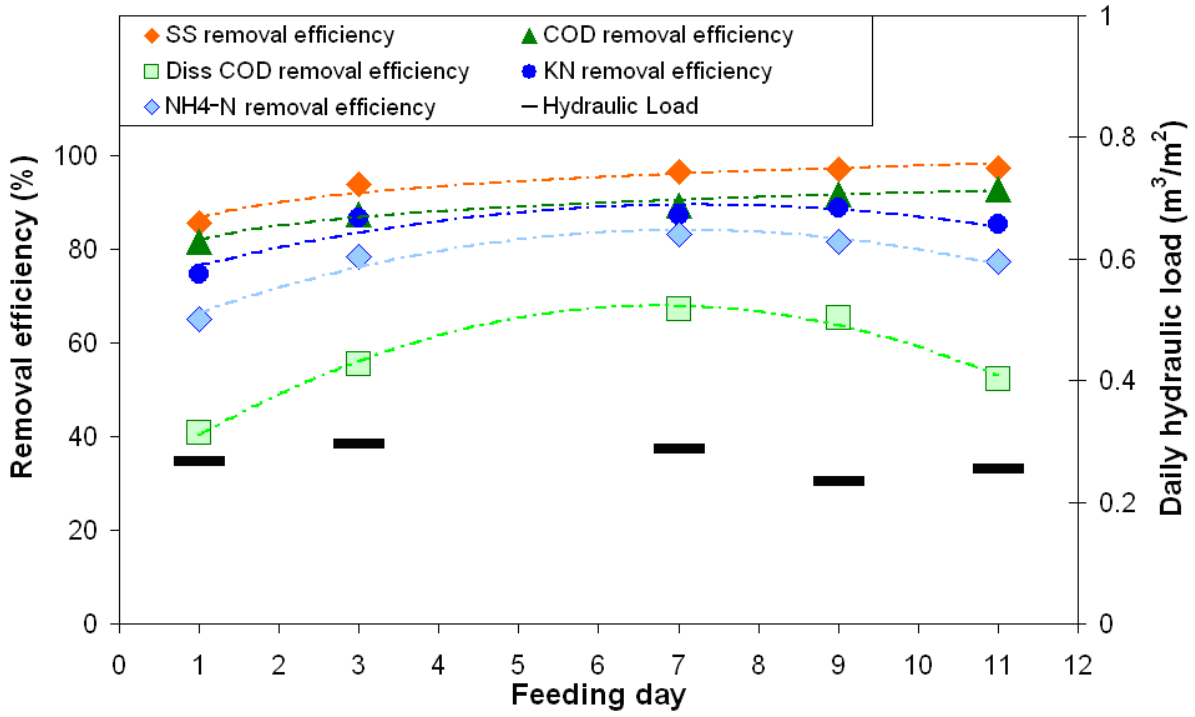

Figure 114: First-stage removal rates according to feeding day

Figure 114 shows how removal performances for SS and total COD increased with feeding days, due to progressive clogging of the filter surface which increases solid filtration and water retention time. If the higher oxygen contents into the porous media are observed at the beginning of the feeding period, the dissolved COD and NH_4-N removal performances increase with feeding days. This performance pattern can be discussed in relation to various factors :

- The NH_4-N removal rates of the first stage increase with feeding days, rising from 65% to over 80%. This increase can be linked to two phenomena: First, after one week of rest, nitrifying bacteria start to regrow during the first feeding days, driving a gradual increase in nitrification activity. Second, the low sludge deposit (2 cm) means water distribution improves with time. The water distribution front progressed about 3.31 m from a feeding point at each m^3 applied per m^2 of filter. Consequently, KN load applied onto the effective infiltration surface is very high at the beginning (144 $gKN/m^2/d$ during the first day) but decreases with time. KN removal efficiency is improved by better water distribution as feeding progresses (as for dissolved COD) and higher nitrifying biomass content.

- Oxygen content within the porous media evolves over time. On the first days, oxygen content is high in almost all the filter and so does not limit the nitrification and organic matter degradation process (Figure 116). However, as wet surface increases to covering all the filter, the oxygen content begins to become alter, which could ultimately alter nitrification and/or organic matter degradation.

To better understand nitrogen dynamics during the feeding period, Figure 115 (*top*) shows the inlet loads and outlet fluxes for the different nitrogen forms in for the first stage of filer.

Outlet NO_x-N fluxes decrease with feeding days from about 71% to 34% of inlet KN, showing the high release (over the first few days) of nitrogen produced during the rest period.

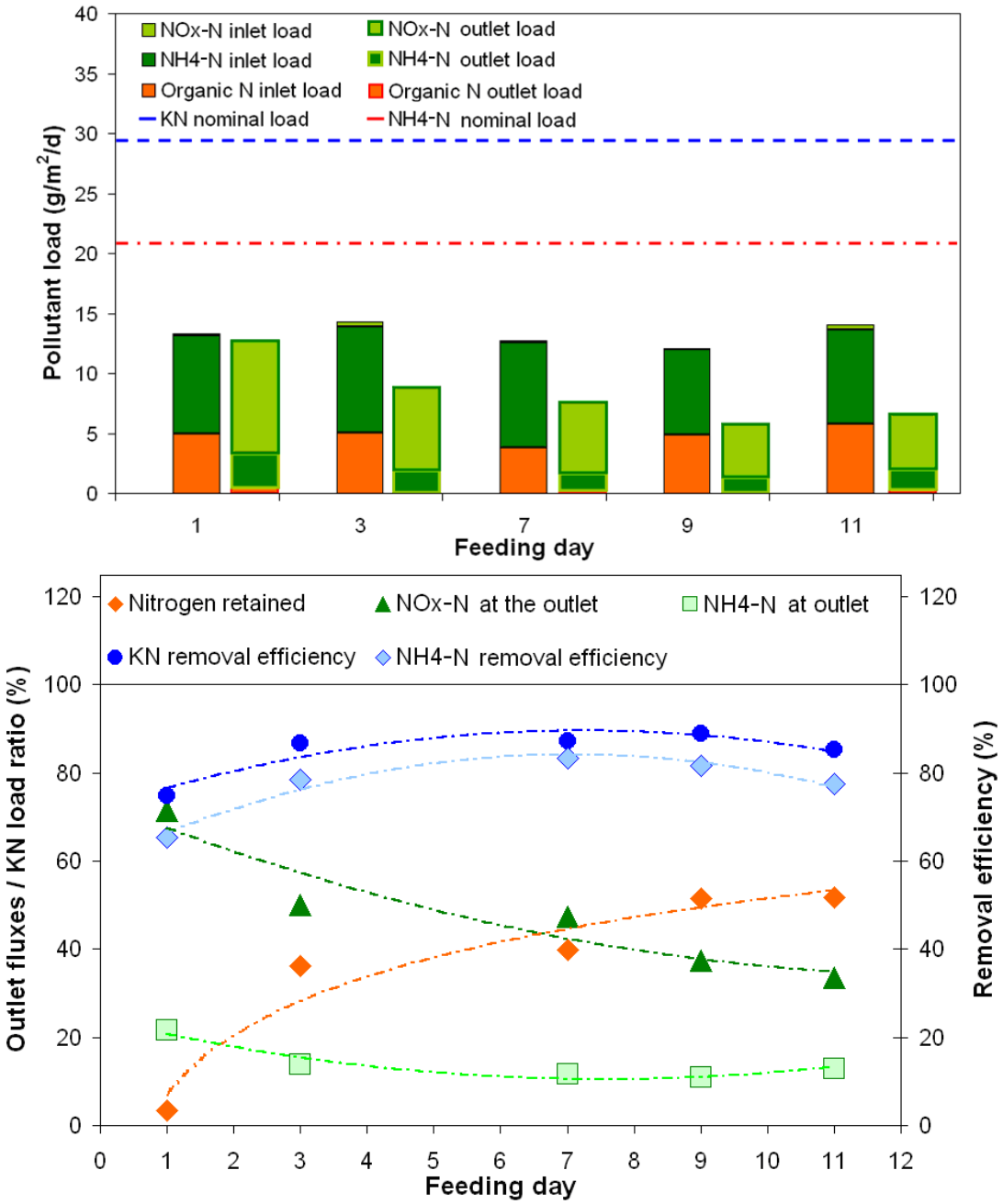

Figure 115: First-stage inlet/outlet nitrogen form loads (*top*), outlet fluxes/KN ratio, and KN and NH_4-N removal efficiency (*bottom*) according to feeding day

Despite the decreasing outlet NO_x-N fluxes, KN and NH_4-N removal rates increased over time (Figure 115, *bottom*). This reveals the buffering capacity of the filter for ammonium adsorption and organic nitrogen filtration. In addition, the time-course evolution of water retention time as showed the tracing campaigns (*see section 4.1.3*) could influence nitrogen retention. A mass balance of Figure 115 (*bottom*) gives an idea of the N forms retained on-filter, rising from 3% to over 52% of inlet KN, and stabilizing at the 9th feeding day, a fact that could explain the decrease in KN and NH_4-N removal rates at the end of feeding period.

Figure 116 charts the time-course evolution of oxygen content profile according to distance to a feeding point (from 0 m to 4.8 m). Oxygen profiles also measure oxygen content according to depth from surface.

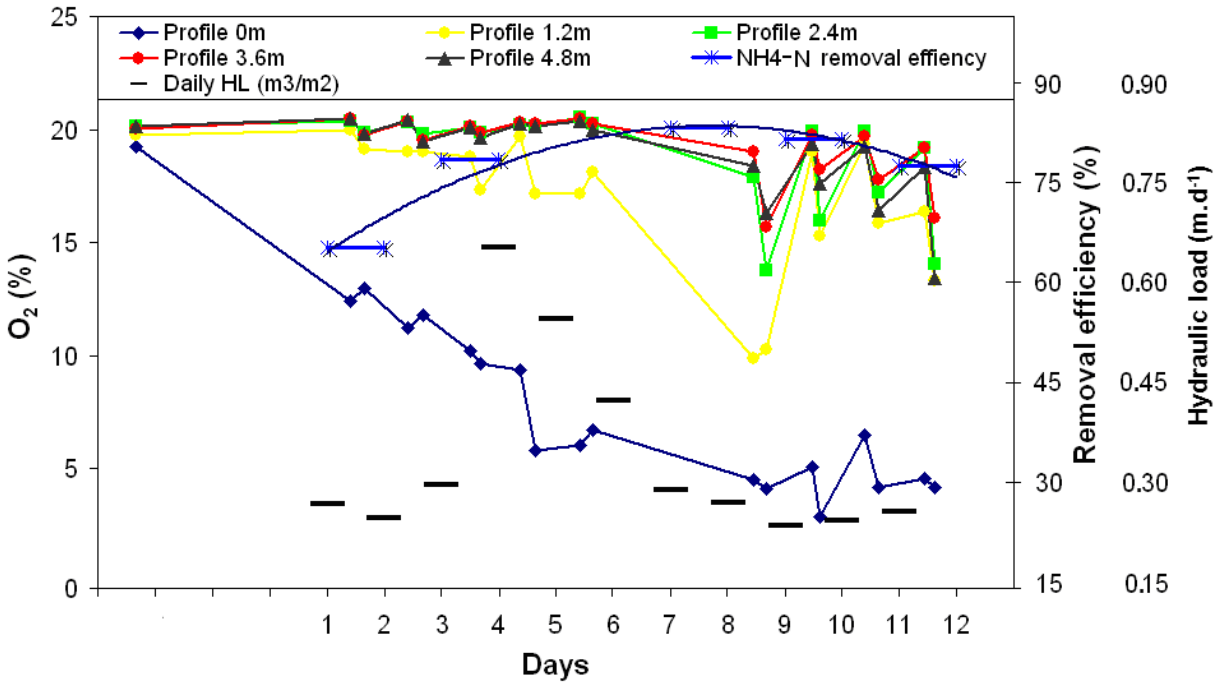

Figure 116: Patterns of oxygen content and NH_4-N removal in a feeding period

For almost all profiles, oxygen content gets higher as measurement point gets closer to the surface. According to the distance from feeding point, oxygen content decreases once water moistens the filter. This oxygen depletion also affects nitrification (Figure 116). Over the course of the feeding period, most of profiles show oxygen content (about 20%) near to air saturation. At the beginning of the feeding period, only the profile near the feeding point receives wastewater, at very high local loads, producing a decrease in oxygen content (13%). This initially abrupt decrease then tends to stabilize as long as surface water distribution improves. After the rain event (day 4), we can see that profile 2 also follows an oxygen content depletion pattern. From the 8th day of feeding, oxygen content is affected at all measurement points after a cumulative hydraulic load of 2.99 m^3/m^2 and an organic load of 1.11 $CODkg/m^2$ and 113 KNg/m^2. All profiles show significant oxygen content variations over the course of the day, with higher contents in morning measurements due to the longer night-time between-batch interval that promotes oxygen renewal. The load applied on effective surface area at day 8 was 13.98 $g/m^2/d$ KN.

The relatively low loads applied during the dry-weather flow result in good NH_4-N removal efficiencies, even over long feeding periods, due to the buffering effect of the filter. Nevertheless, as oxygen content patterns are linked to both organic and hydraulic loads, it is easy to understand how rain events can influence the system. In this campaign, a 0.65 $m^3/m^2/d$ hydraulic load produced by the rain event did not affect filter performances, although the oxygen content did not recover to highly oxygenated conditions in the two profiles near to a feeding point.

Data recorded during the continuous motoring of NH_4-N concentrations at the inlet/outlet of first stage and NO_x-N at the first-stage outlet can be used to chart nitrogen dynamics at one-minute time-steps. Figure 117 shows the evolution of NH_4-N entering the filter.

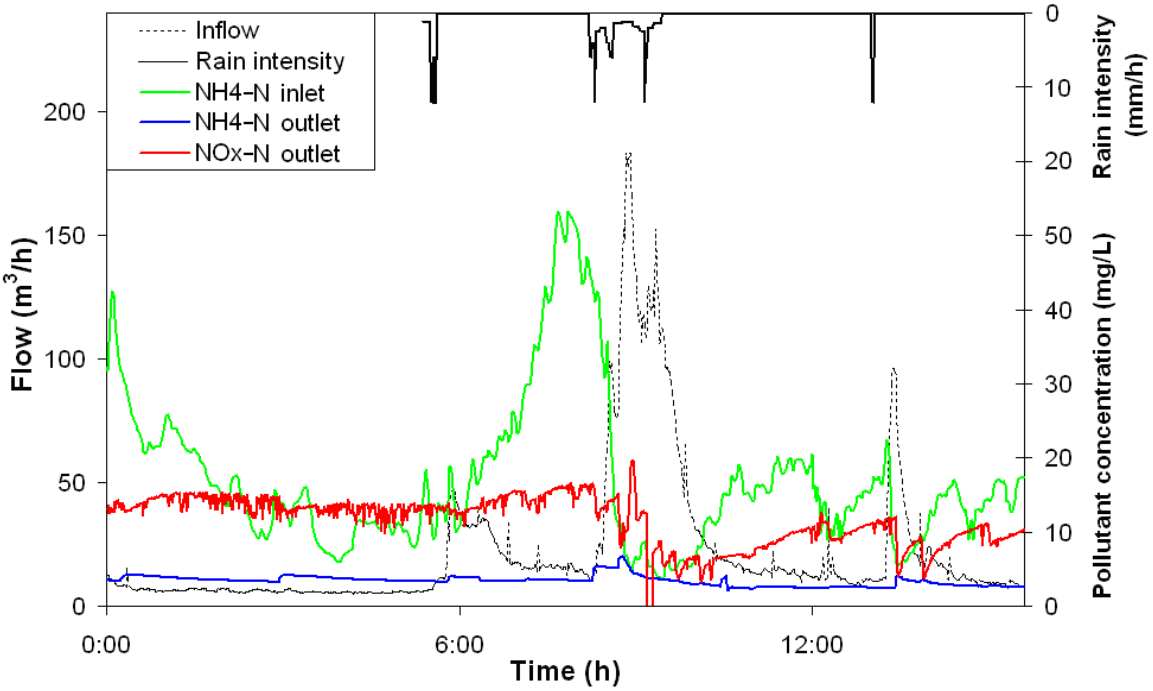

Figure 117: Continuous pollutant concentration monitoring, first-stage inlet/outlet NH_4-N concentrations and first-stage outlet NO_x-N concentrations at the 5th feeding day.

Concentrations were low before morning-time activity in domestic residences. Outlet ammonium and NO_x-N concentrations remain stable even during the peak of inlet ammonium concentration, demonstrating the buffer capacity of the filter. The adsorbed ammonium is nitrified with time, and when inlet ammonium concentration decrease (during the night), there is a constant NO_x-N release as outlet concentrations stay stable. The rain event dilutes inlet concentration and produces a decrease of NO_x-N concentrations at the outlet. Nevertheless, low NO_x-N outlet concentrations do not necessarily mean a nitrification dysfunction caused by the rain event, which may simply be due to a dilution effect. Indeed, just after the rain event, NO_x-N release recovers quickly. Figure 118 charts first-stage filter performances on the last feeding day (11th).

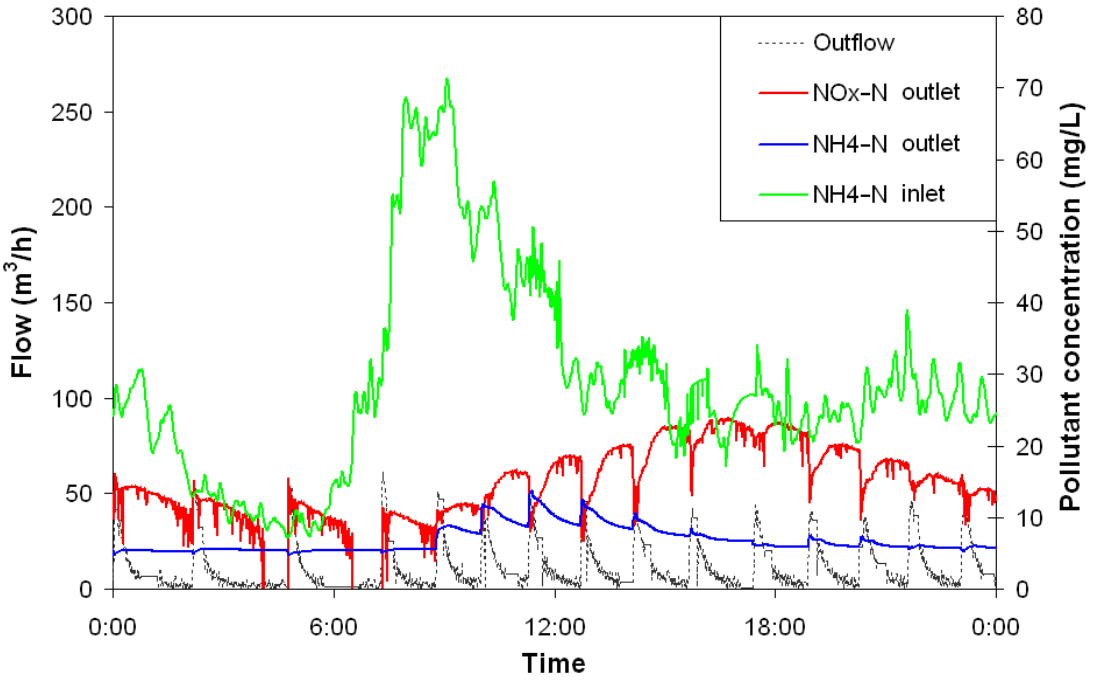

Figure 118: Continuous pollutant concentration monitoring, first-stage inlet/outlet NH_4-N concentrations and first-stage outlet NO_x-N concentrations at the 11th feeding day.

Peak NH_4-N flows are less retained than early-day flows. The outlet NH_4-N remains substantially stable, increasing from 5 mg/L to 13 mg/L by the inlet peak. However, the NH_4-N retained is visibly nitrified over the rest of the day. Indeed, there is a lag between the inlet peak load and the increase in nitrate concentration. These results show that under extreme feeding conditions, with HL variations, oxygen content stays high on the filter, and nitrification is relatively unaffected.

5.5. Continuous monitoring by S::CAN probe

In order to analyse filter dynamics under different hydraulic overloads, outlet NO_x-N concentrations, as provided by the S::CAN probe, were analysed for several rainfall events. Only the highest hydraulic loads are presented. Nitrogen concentrations are essential for gauging filter inlet performances. However, we did not have continuous measurements of NH_4-N concentrations by the VARiON®Plus probes during the full 2-year monitoring campaign. Consequently, to estimate nitrogen, we established an inlet-KN-concentration/inlet-HL relationship from treatment performance campaigns. According to Lee & Bang (2000), for low-residence watersheds equipped with a combined sewer system, as is the case at Challex, the KN concentrations released in response to a rainfall event range from 0.5 mg/L to 24.7 mg/L (SD: 11.5). Thus, an average value for rainfall contribution is hard to determine on such stochastic phenomena. Consequently, the simplest relationship we can state is to assume that KN fluxes produced by rainfall events are negligible compared to domestic WW (80 KNmg/L in dry-weather flow). Consequently, inlet KN concentration would only be affected by dilution during rain events. Figure 119 shows the different inlet KN concentrations of dry-weather and rainfall events (transposed to a 24-hr basis) and the dilution relationship.

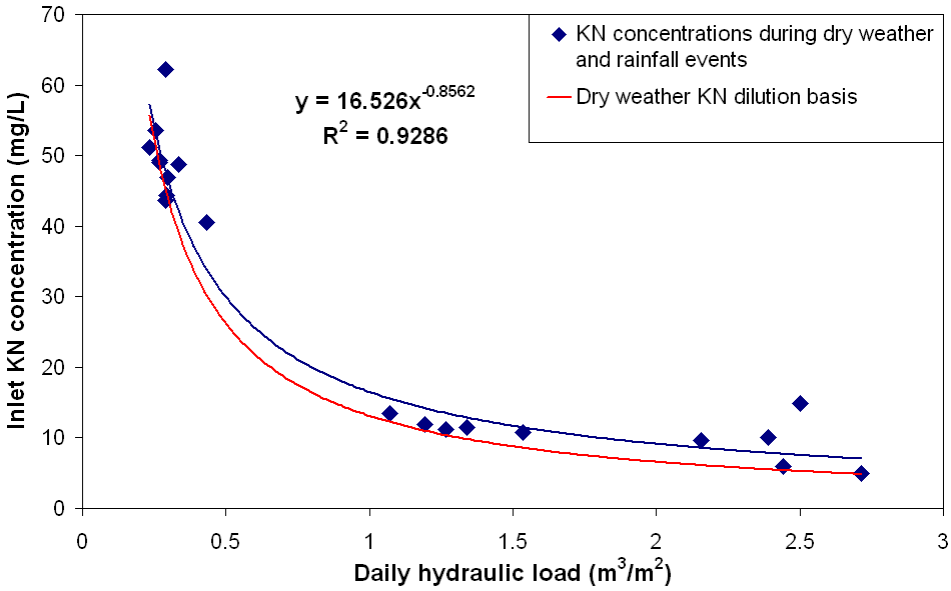

Figure 119: Inlet KN concentrations according to hydraulic load and dry-weather dilution basis

The dilution relationship thus plotted is not so false. Rain event contributions would be about 3 mg/L under HL over 1 m²/m³/d. The KN relationship and the continuously-measured first-stage outlet NO_x-N concentrations were used to analyse different hydraulic overloads and identify the limits of hydraulic load acceptance without treatment dysfunctions. The events studied included an extreme hydraulic overload period in the winter season (Figure 120) where the feeding period of each filter was limited to 100 batches in order protect the filter from hydraulic overloads and test whether short rest periods were enough to guarantee filter performances under high HL. Figure 120 shows the inlet KN and first-stage outlet NO_x-N concentrations for the extreme hydraulic load period from 30th December 2011 to 7th January 2012.

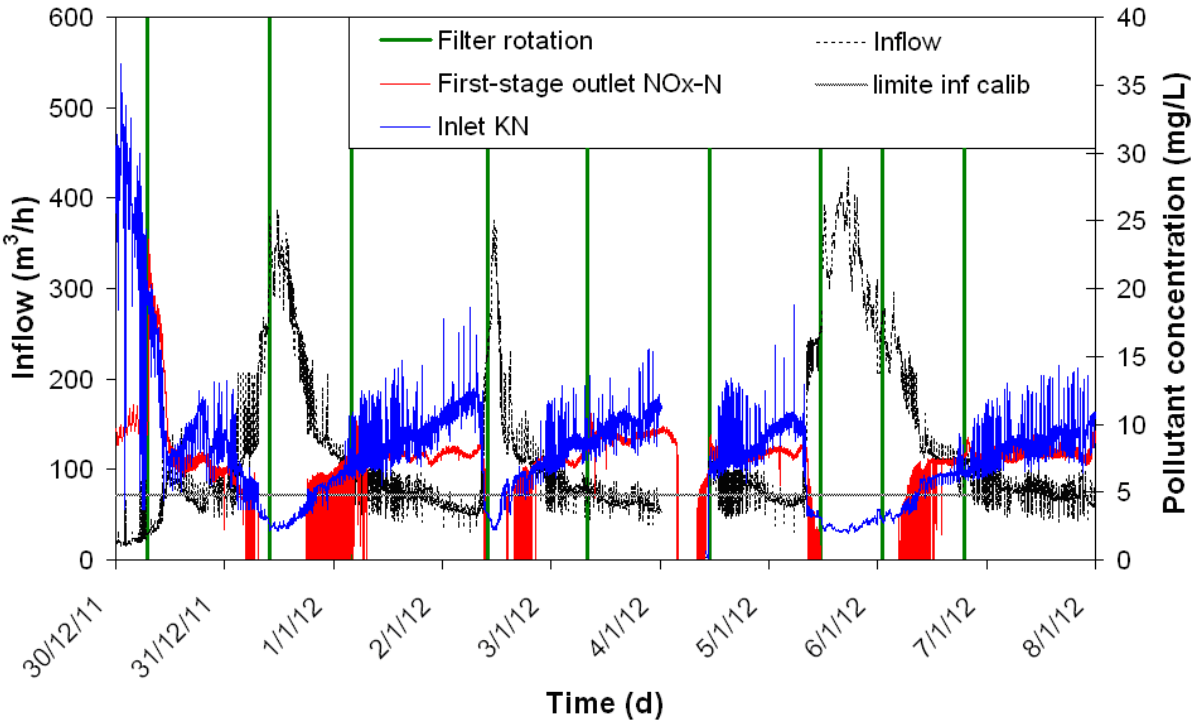

Figure 120: First-stage outlet NO_x-N concentrations according to inlet KN concentrations in an extreme hydraulic overload period (30st December 2011 to 7th January 2012)

As discussed previously, high inflow rates generate a stung dilution of KN arriving at the treatment plant, thus the NO_x-N at the first-stage outlet is also diluted, following the same trend as inlet KN concentrations. Nitrate outlet concentrations are low a during rain event but soon recover to normal levels once the rain event stops. This shows that nitrification is not necessarily affected by these HL (up to 3 $m^3/m^2/d$ on the same filter).

Note that inlet KN concentrations under 5 mg/L promote low outlet NO_x-N concentrations that are under the PLS calibration thresholds (5-56 mg/L), which makes measurements difficult. As the rainfall event distribution system did not automatically change the filter to be fed, in this hydraulic overload period, the flows coming from rain weather distribution system were always spread on filter 3 of the first stage, differing when the dry-weather system rotated to the other filters. However, the global results of this period demonstrate the robustness of the system under hydraulic loads and short rest periods. For security reasons, the HL of 6th January is not taken into account as there were absolutely no NO_x-N measurements available.

Figures 121 and 122 show other individual events reaching peak hydraulic loads into the filter in different seasons and feeding days.

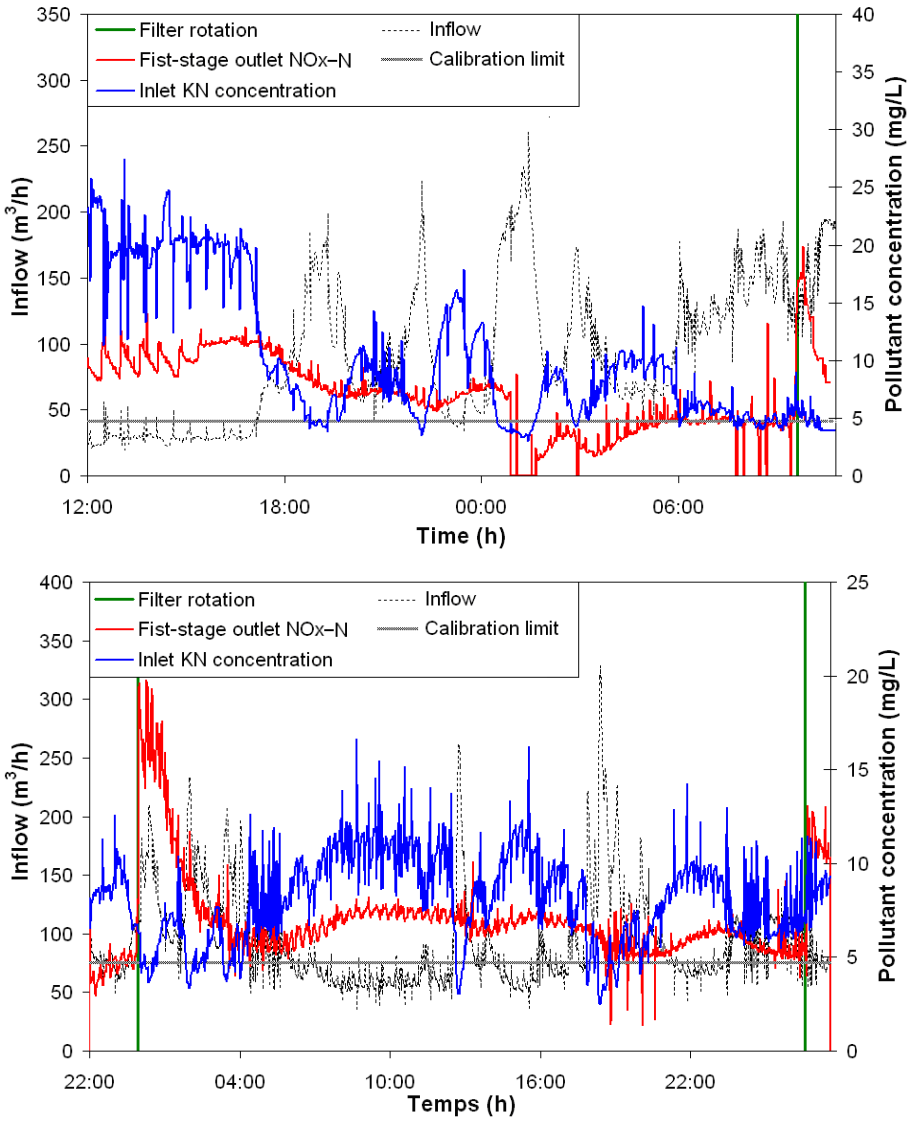

Figure 121: First-stage outlet NO_x-N concentrations according to inlet KN concentrations for 24th April 2012 (*top*) and 21st January 2012 (*bottom*)

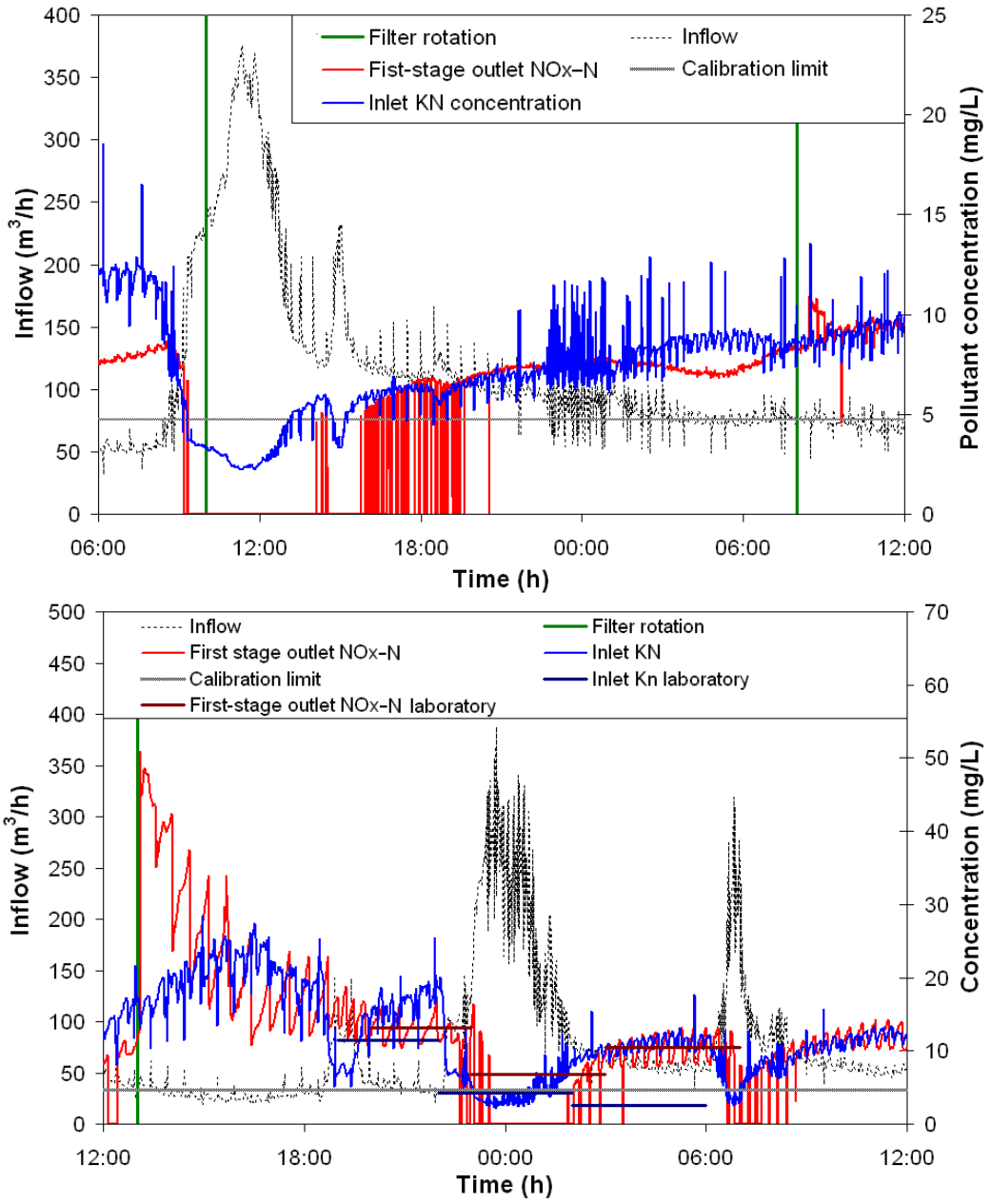

Figure 122: First-stage outlet NO_x-N concentrations according to inlet KN concentrations for 3rd January 2012 (*top*) and 12th June 2012 (*bottom*)

None of these events produced nitrification-related dysfunctions. The filter was always able to recover in the wake of intense flow rates. A 24-hr composite campaign carried out for the event of 12th June 2012 demonstrated that continuous monitoring values for NO_x were consistent with in-lab concentrations before and after rainfall events. During rainfall events, lab data were near the calibration limit, and the S::CAN probe is unable to measure smaller values.

These results demonstrate that the filter can accept hydraulic loads, especially the event of 3rd January 2012, of up to 3 $m^3/m^2/d$ in the winter season (the most hydraulically limiting season) without jeopardizing the treatment performance of the filter. HL intensity visibly has a stronger impact on NO_x-N concentrations (as the 3rd January and 12th June 2012 events show), than duration of hydraulic overload (as the 24th April and 21st January 2012 events show).

Ponding during these events was analysed to establish the “dysfunction alerts” used in the modelling part of the study.

5.6. Alerts criteria / biological limits

In order to link the simplified hydraulic VFCW model to the treatment performance limits of the filter, “dysfunction alerts” were introduced into the model. The objective of the alerts is to connect the hydraulics of the system (HO duration and intensity) to ponding time and then to treatment performances limits. We assume that nitrification is the first process affected by ponding, as ponding slows oxygen renewal into the porous media. Under these conditions, oxygen-dependent treatment processes, such as nitrification, are affected. To evaluate the duration and intensity of HO, the dysfunction alerts are based on :

- Maximal 24-hr cumulative ponding time (to evaluate HO duration)
- Maximal consecutive ponding time (to evaluate HO intensity)

Over these maximal values, we can consider that system is exposed to a biological dysfunction. These alerts were established based on the results of treatment performance campaigns and continuous monitoring (hydraulics and pollutant concentrations).

5.6.1. Establishing the dysfunction alerts

As it was not possible to determine biological limits based on the 24-h composite sample campaigns, we decided to analyze the online monitoring of the highest hydraulic load events. The aim was to determine the ponding time of each rain event (consecutive and cumulative) and link it to nitrification dysfunction. As discussed above, we did not observe any nitrification dysfunction. Nitrate release always returned to normal concentrations just after a rain event. The decrease observed during rain events is due to wastewater dilution. Consequently, the biological limits determined with our data represent secured limits.

Ultrasonic probes cannot accurately determine ponding time due to the uneven planarity of the first-stage surface. The ultrasonic probes measure local water ponding depth when ponding is low. Consequently, these probes are used to give an order of magnitude validating the simplified model (see section 3.2.2.1), after which this chapter calculates ponding time using the simplified hydraulic model. Figures 123 and 124 give some examples of ponding that did not affect nitrification.

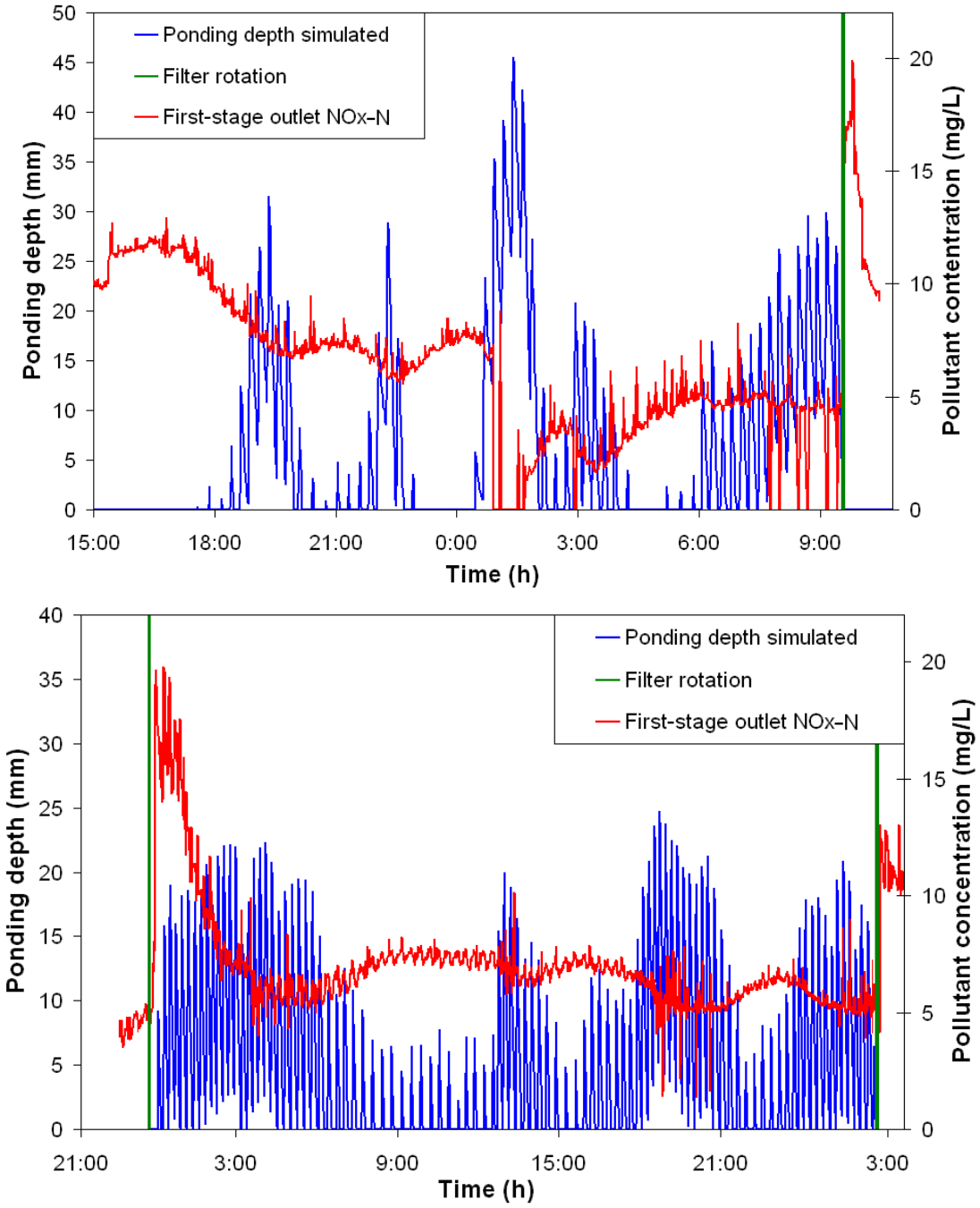

Figure 123: First-stage outlet NOx-N concentrations according to inlet KN concentrations at 24th April 2012 (*top*) and 21st January 2012 (*bottom*)

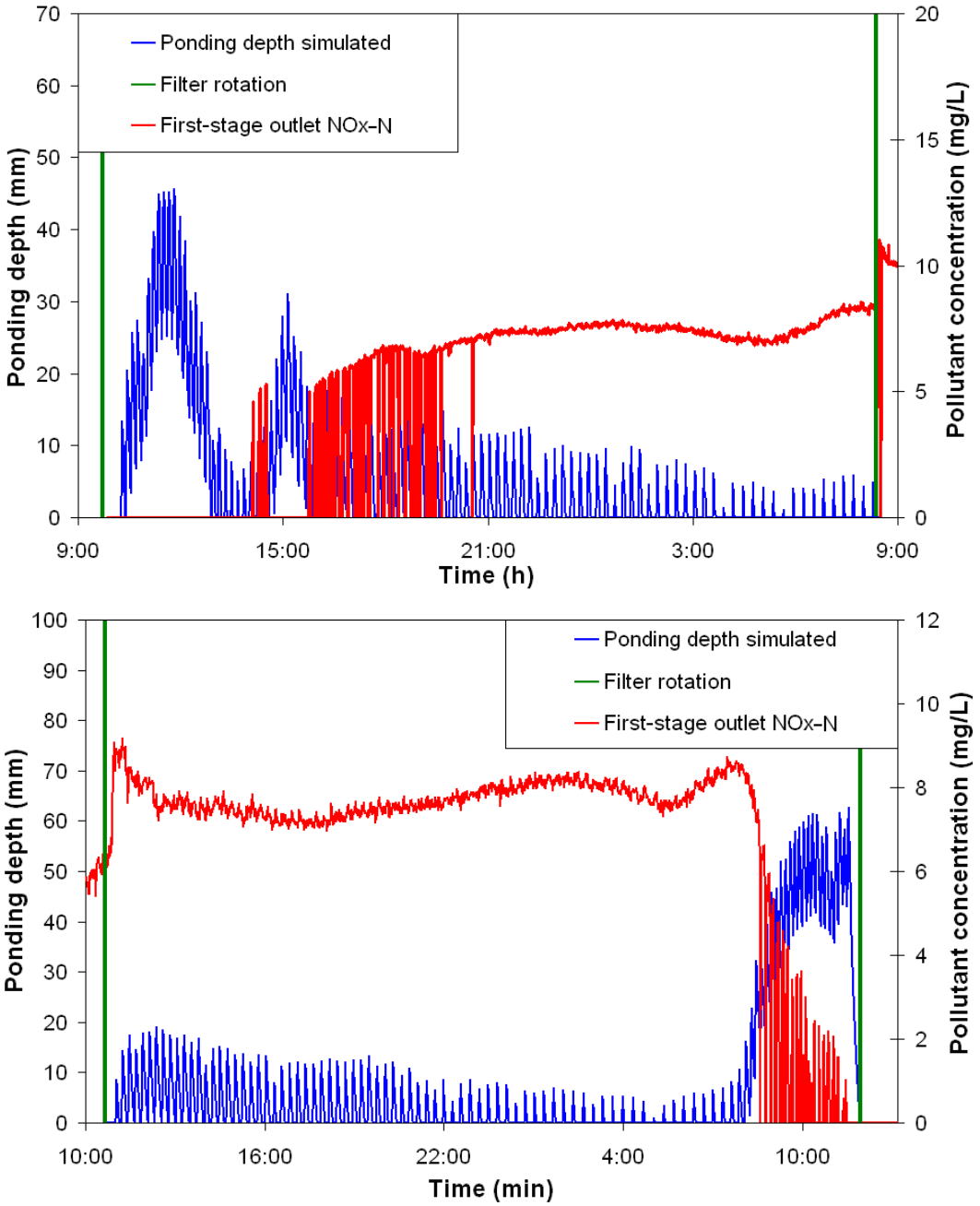

Figure 124: First-stage outlet NOx-N concentrations according to inlet KN concentrations at 3rd January 2012 (*top*) and 5th January 2012 (*bottom*)

As shown in Figures 123 and 124, most of the missing NO_x-N concentration measurements due to dilution are consistent with long on-filter ponding times. Our modelling of the most hydraulically-loaded events enabled us to establish a "cumulative ponding alert" and get an idea of the "consecutive ponding" of the filter. Table 19 shows that events with long ponding times are found in the winter season, which is consistent with the low infiltration rates measured in that season (see section 4.2.1), which promote deeper and longer ponding.

Table 19: Cumulative and consecutive ponding times from the highest hydraulic load events

Event date	Feeding day	Average time between batches (min)	Minimum time between batches (min)	HL ($m.d^{-1}$)	Times the NHL	Ultrasonic probes with ponding measurement	Ponding time (h)	
							Cumulative	*Consecutive*
24/04/2012	2	16	14	2.68	7.68	1	13.57	1.58
15/04/2012	2	19	13	1.67	4.81	0	1.02	0.07
02/01/2012	1	18	10	1.75	5.02	2	5.61	0.13
05/01/2012	1	15	8	2.36	6.76	3	12.61	**3.42**
21/01/2012	1	16	12	2.07	5.95	3	**15.55**	2.63
31/12/2011	1	17	10	2.17	6.24	1	11.25	2.62
03/01/2012	1	13	9	**3.02**	8.68	1	9.86	2.50
12/06/2012	1	21	13	1.91	5.48	0	2.77	1.80

The minimum time observed between batches is 8 minutes, which produced the highest consecutive ponding time of all events analysed. The hydraulic load acceptance of 3 $m^3/m^2/d$ is coherent with the first safeguard of 3.5 $m^3/m^2/d$ established by Molle *et al.* (2006). According to Molle *et al.* (2006), ponding surface has to stay free at least 12 hours per day to ensure a long-enough oxygenation period to maintain aerobic conditions. In our study, the maximal cumulative ponding time observed without causing treatment problems was 15.5 h per day, which increases the threshold of HL acceptance on VFCWs.

Looking at the consecutive ponding values, the highest value recorded here (3.42 hours) did not induce any biological dysfunction. This value can thus be used as a security, but it seems low compared to other studies and could drastically limit the hydraulic acceptance capacity in response to rain events. One of the main reasons for this low value is the specificity of the Challex treatment plant that limits the number of batches on a feeding period. Consequently, during high rain events, there is a more frequent rotation between filters that limits the consecutive ponding time.

In a rain event treatment study, Woźniak *et al.*(2007) investigated hydraulic overloads and oxygen content on a retention soil filter (similar to a VFCW) in a laboratory pilot. The VFCW had similar characteristics to a French system (intermediate feeding, aeration pipes, etc.). Woźniak *et al.*(2007) showed that once a 1 meter of ponding depth has drained through the filter, the oxygen content of the pore volume is completely used up. Consequently, to transpose this result to our study, we needed to calculate how much time it takes the filter to drain 1 m of water. The infiltration rates obtained on the experimental site by *in situ* ponding depth measurements could not be used to estimate the consecutive ponding time because they were mostly recorded in winter-season conditions and were therefore not sufficiently representative of year-round performance. Therefore, the *ICP* parameter of the simplified model was used to estimate the average infiltration rate over the seasons. As the maximal ponding depth calculated on HO events was approximately 50 mm, we used this ponding depth value to obtain the average infiltration rate (3.89E-05 m.s.). According to this infiltration rate, the consecutive ponding time estimate for this 1 m ponding depth was 7.15 hr.

Thus, the dysfunction alerts parameters established were set at :

- 15.5 hours per 24-hr cumulative ponding time
- 7 hours of consecutive ponding time in a feeding period

These alerts provide the link connecting filter hydraulics to treatment performances, and were used in the long-term modelling (see section 6). When the simulated ponding time exceeds one of these dysfunction alerts, we assumed the filter was exposed to a treatment failure due to oxygen deprivation. These dysfunction alerts are important to the modelling, since the objective of long-term modelling is to study the impact of different local contexts on operational filter function and adapt the design to avoid any dysfunction.

6. Long term modelling (rainfall time-series)

The long-term modelling based on the 4-year rainfall time-series set out to analyse the impact of local context and filter design on a filter's ability to accept hydraulic overload (HO). This objective has been reached using the previously established filter dysfunction alerts (see chapter 5.6.1) and first-stage discharge bypasses. This chapter therefore turns to evaluate the ability of the VFCW design to increase HO acceptance, minimize only half-treated discharges to the receiving water body, and guarantee treatment performances.

6.1. Three-component model

As described in section 3.2.4, the long-term modelling is built on three components :

(i) The "watershed/sewer system" component, which tests the influence of local context on inflow to the treatment plant. The principal variables tested, as stated in section 3.2.4, were watershed/sewer system slope and impervious surface coefficient. All these parameters impact treatment plant inflow volume and dynamics. The inputs/outputs of the model were :

Inputs :
- 4-year rainfall time-series
- 4-year dry weather time-series

Output :
- 4-year inflows to the treatment plant

(ii) The "simplified hydraulic model" described in section 3.2.2 simulates water infiltration and ponding on young and mature VFCWs. The *ICP* parameters retained from fitting over seasons are presented in Table 20 for young and mature filters.

Table 20: Month-by-month infiltration parameter values and filter age

Month	Infiltration parameter (*ICP*) value	
	Young filter (s^{-1})	Mature filter (s^{-1})
January	3.35E-04	2.68E
February	2.81E-04	2.68E
March	7.86E-04	2.68E
April	1.03E-03	4.97E
May	1.01E	4.97E
June	1.01E	4.97E
July	1.01E	4.97E
August	1.01E	4.97E
September	1.01E	4.97E
October	1.01E	2.68E
November	1.01E	2.68E
December	1.01E	2.68E

Several HO acceptance-related parameters have been analysed, including filter surface, ponding height, and presence or not of an overflow structure at the inlet of the treatment plant. The inputs/outputs of this component were :

Input :
Inflow to the treatment plant

Outputs :
First-stage ponding time and height,
First-stage outflow,
First-stage bypassed flow

(iii) The "dysfunction alert" component, modelled on R software, calculates number of dysfunction alerts, bypassed discharges at the filter surface, and daily ponding time and height. The inputs/outputs of this component were :

Input :
First-stage ponding time and height

Outputs :
Number of cumulative ponding time alerts
Number of consecutive ponding time alerts
Daily ponding time and average height
Number of bypassed discharges and duration

These model components are the core tools for long-term modelling. We analysed the sensitivity of sewer characteristics and filter design parameters on the model for different rainfall time-series.

6.2. Sensitivity analysis

The sensitivity analysis had two primary objectives: (i) to proportionate the most influential local-context parameters shaping VFCW inflows. The aim was to alert designers to the most problematic scenario based on ponding time alerts and bypass discharges. Then, based on these "most problematic scenarios", (ii) the second objective was to test the design characteristics of the filter itself to minimize the number of bypass discharges and dysfunction alerts occurring.

These two principal objectives were tackled in separate steps :

- Local context influence
  - Influence of sewer characteristics on VFCW inflows and ponding time alerts.
  - Influence of CSO structures at the WWTP inlet.

- Filter design influence
  - Influence of filter surface and bypass height on filter ponding time alerts and bypass discharges.
  - Influence of age of VFCW, filter surface and bypass height on filter ponding time alerts and bypass discharges.

6.2.1. Local context influence on filter (flow and ponding)

According to section 3.2.6, the local context parameters used for the sensitivity analysis were reduced to those parameters that most heavily influenced the flow produced. To not have to study all the watershed surface areas potentially found in small communities, we used the Challex watershed area/population equivalent ratio. Consequently, the main parameters tested were :

- *Impervious surface coefficient (ImC)*, with each value coupled with the imperviousness of the surface directly connected to the sewer system (established at half of *ImC*)

- *Slope (S)* of the watershed coupled with slope of the sewer system.

- *Climate* of two regions presenting different rainfall characteristics, Bretagne (*Br*) and Rhône-Alpes (*R*). 4-year rainfall time-series were used for each climate (see section 3.2.6.2).

As the imperviousness coefficients, like the slopes, were coupled, we obtained 16 tested parameter-sets for each climate type (Bretagne and Rhône-Alpes), i.e. a total of 32 different scenarios for the first sensitivity analysis (Table 21). For each scenario, lag-times were calculated according to the modified Desbordes equation (1974) used in CANOE software for peri-urban watersheds. The rationale was that most small communities where VFCW are installed are peri-urban-like.

Table 21: Set of parameters tested for each rainfall time-series

Scenario	Imperviousness coefficient	Impervious surface directly connected to sewer system	Slope watershed	Sewer system slope	Lag-time
	(%)	*(%)*	*(%)*	*(%)*	*(min)*
ImC10% -S1%	**10**	5	**1%**	0.2%	91.8
ImC10% -S4%	**10**	5	**4%**	0.4%	52.7
ImC10% -S7%	**10**	5	**7%**	1.0%	42.1
ImC10% -S10%	**10**	5	**10%**	2.0%	36.5
ImC17% -S1%	**17**	9	**1%**	0.2%	70.0
ImC17% -S4%	**17**	9	**4%**	0.4%	40.1
ImC17% -S7%	**17**	9	**7%**	1.0%	32.1
ImC17% -S10%	**17**	9	**10%**	2.0%	27.8
ImC23% -S1%	**23**	12	**1%**	0.2%	59.9
ImC23% -S4%	**23**	12	**4%**	0.4%	34.4
ImC23% -S7%	**23**	12	**7%**	1.0%	27.5
ImC23% -S10%	**23**	12	**10%**	2.0%	23.8
ImC30% -S1%	**30**	15	**1%**	0.2%	52.3
ImC30% -S4%	**30**	15	**4%**	0.4%	30.0
ImC30% -S7%	**30**	15	**7%**	1.0%	24.0
ImC30% -S10%	**30**	15	**10%**	2.0%	20.8

Figure 125 presents the hydraulic load a filter would receive (designed for 1.2 m²/p.e.) according to sewer characteristics for different climatic conditions. Note that climate has a

prominent influence on hydraulic load. The Bretagne climate globally produces more HL higher than NHL than the Rhône-Alpes climate. However, the Rhône-Alpes climate shows the highest flows at the sewer system outlet. The Bretagne region has longer-lasting periods of rainfall (see section 3.2.6.2), which are important to analyze when designing a VFCW.

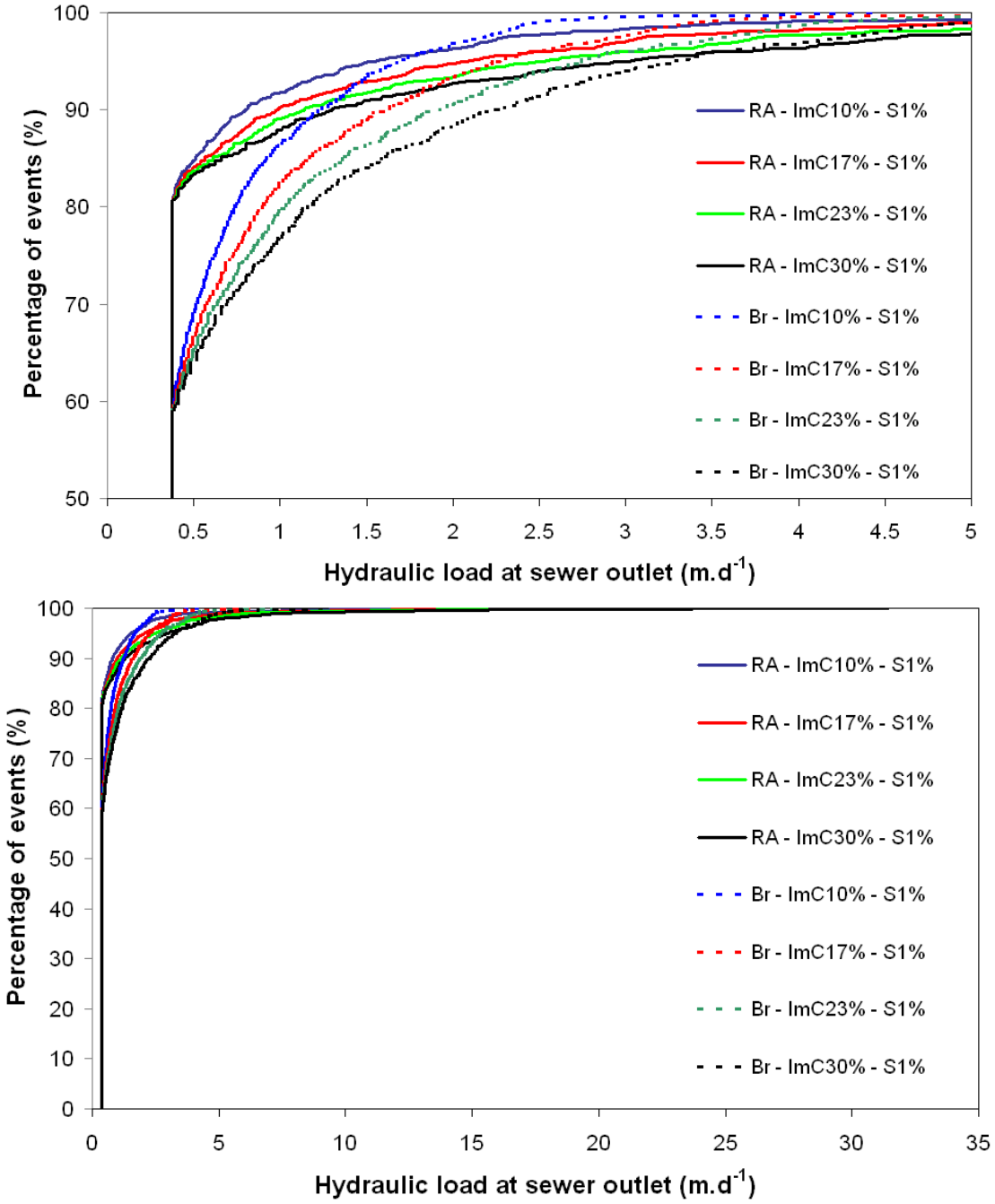

Figure 125: Detail (*top*) and full (*bottom*) daily hydraulic load at sewer system outlet according to imperviousness coefficient at 1% slope in Bretagne (Br) and Rhône-Alpes (RA) climates on a 1.2 m²/p.e. filter surface

Table 22 charts hydraulic loads according to imperviousness coefficient. In this test, watershed slope was set to 1%.

Table 22: Maximal and average HL according to the different imperviousness coefficients tested at 1% slope, for Bretagne and Rhône-Alpes climates (HL calculated from first-stage surface at 1.2 m²/p.e.)

	ImC 10% - S1%		ImC 17% - S1%		ImC 23% - S1%		ImC 30% - S1%	
	Br	*RA*	*Br*	*RA*	*Br*	*RA*	*Br*	*RA*
Max HL ($m.d^{-1}$)	4.47	22.27	6.15	25.58	7.52	28.32	9.03	31.45
Average HL ($m.d^{-1}$)	0.61	0.59	0.72	0.67	0.80	0.74	0.89	0.81
SD	0.49	1.06	0.71	1.34	0.88	1.58	1.07	1.84

Imperviousness coefficient logically influences predicted HL on a receiving filter, whether for average or peak loads. Figure 125 highlights the role of imperviousness coefficient on rainfall drainage by the watershed. The increase of extreme hydraulic loads can be observed mainly from twice dry-weather flow (0.7 $m.d^{-1}$) until 10-fold dry-weather flow (3.5 $m.d^{-1}$). Outside this range, impervious coefficient has little impact on the load received by the filters. Beyond 10-fold nominal hydraulic load, the impervious coefficient (from 10 to 30%) only increases the % of events from 0.21% to 3.56% in a Bretagne climate and from 1.03% to 3.90% in a Rhône-Alpes climate.

The HL obtained in the different scenarios were introduced into the simplified VFCW model in order to analyse filter response in terms of ponding time and alerts. The tests were carried out without CSO limitation to not add another influential factor to the results. Climate and imperviousness coefficient were the factors that demonstrates the strongest influence on filter ponding time, as shown in Figure 126.

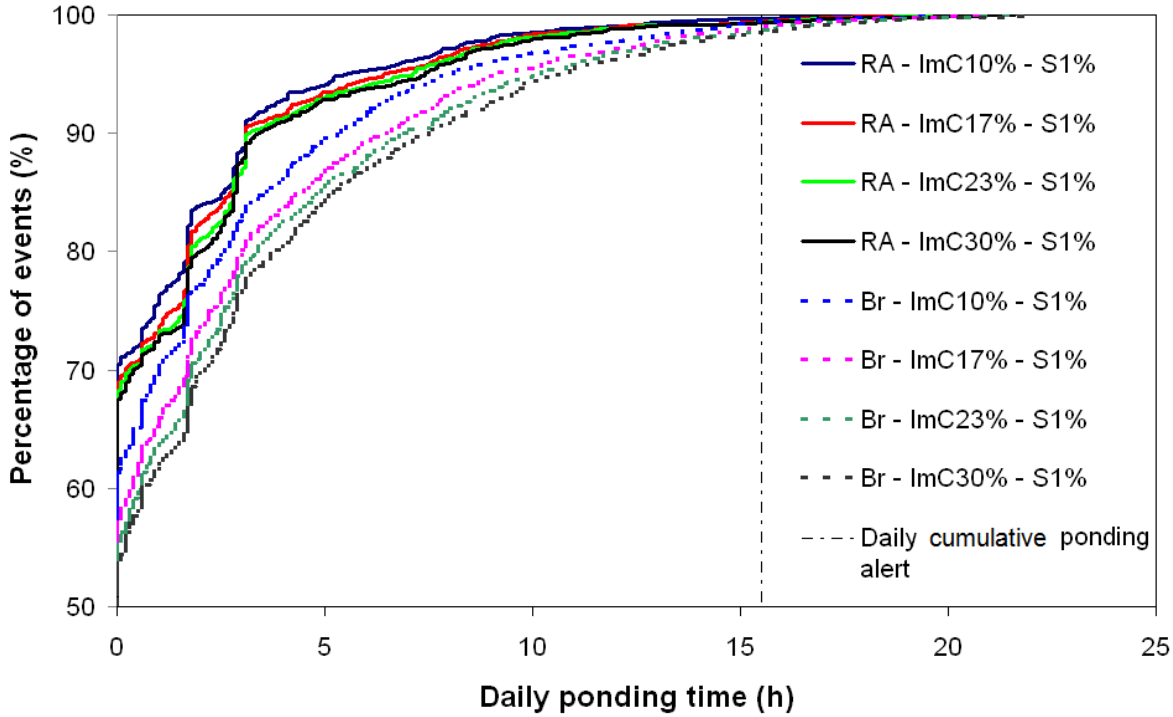

Figure 126: Daily ponding time according to imperviousness coefficient at 1% slope in Bretagne (Br) and Rhône-Alpes (RA) climates on a 1.2 m²/p.e. filter surface.

Figure 126 shows that a Bretagne climate induces longer daily ponding periods than a Rhône-Alpes climate. Furthermore, the effect of imperviousness coefficients, which lead to longer daily ponding periods when high, is stronger under longer low-intensity rain events found in

the Bretagne climate. Rain characteristics and imperviousness coefficients are key factors for VFCW design.

As expected, slope mostly impacts the distribution of HL arriving at the treatment plant, thus affecting ponding time on VFCWs. Although a low slope affects on-filter ponding time, it has less impact than imperviousness and rainfall characteristics, as shown in Figure 127.

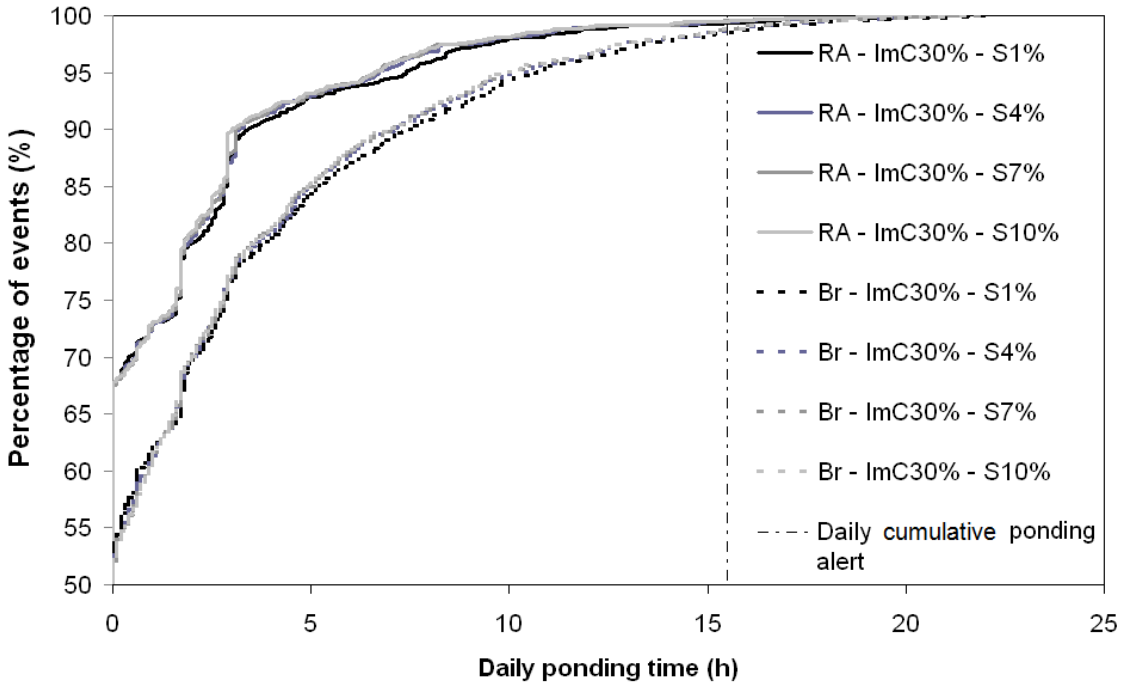

Figure 127: Daily ponding time according to watershed slope at an imperviousness coefficient of 30% Bretagne (Br) and Rhône-Alpes (RA) climates on a 1.2 m²/p.e. filter surface.

The influence of imperviousness coefficient on the system can be confirmed through the number of consecutive ponding alerts obtained per year (Figure 128).

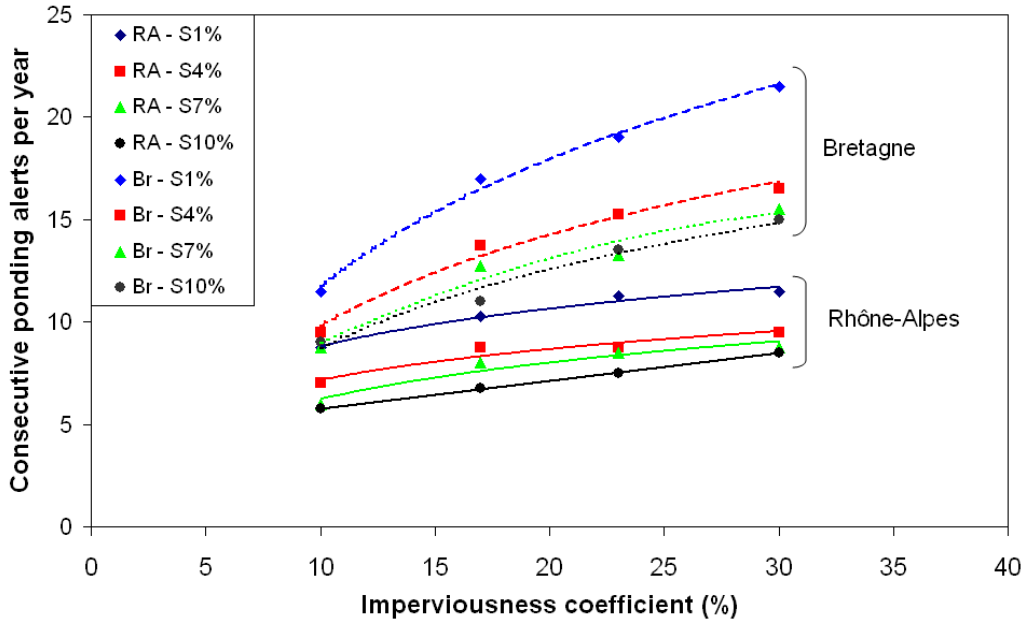

Figure 128: Number consecutive alerts per year according to imperviousness coefficiente and watershed slope in Bretagne (Br) and Rhône-Alpes (RA) climates on a 1.2 m²/p.e. filter surface.

The rainfall characteristics of the Bretagne climate result in up to twice as many alerts compared to the Rhône-Alpes climate, and the alerts increase according to imperviousness coefficient and slope. Although slope has a relatively mild influence on daily ponding time, the distribution of rainfall flow over time strongly influences the number of alerts.

The more dominant influence of imperviousness coefficient over slope is clearly visible in the Bretagne climate. The impact of imperviousness coefficient can be measured by percentage increase of additional consecutive alerts (according to the *ImC* 10% scenario), as shown in Figure 129.

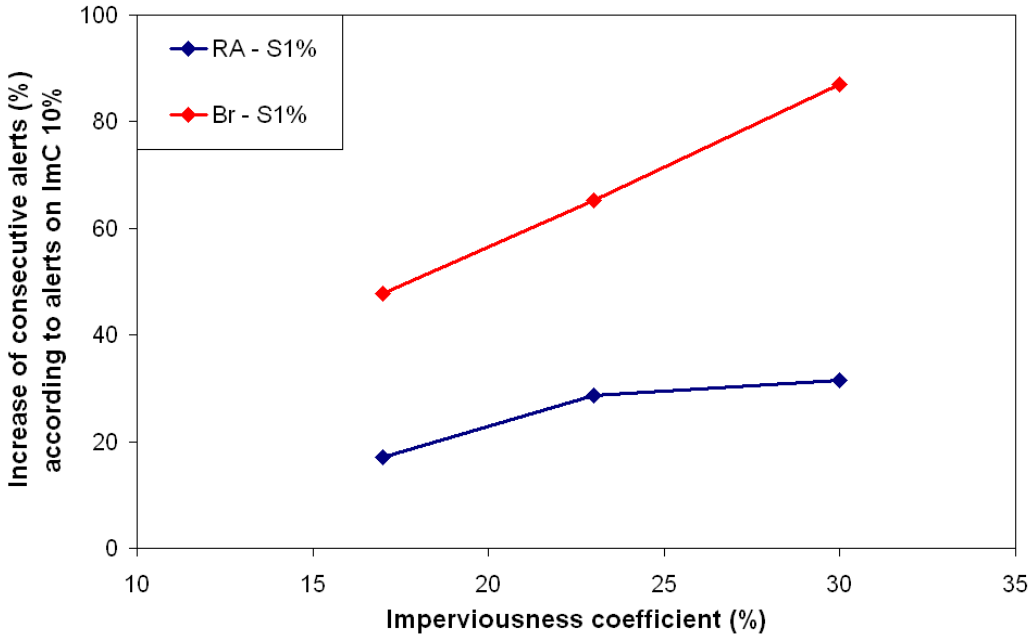

Figure 129: Increase of consecutive ponding time alerts according to imperviousness coefficient at a 1% slope in Bretagne (Br) and Rhône-Alpes (RA) climates on a 1.2 m²/p.e. filter surface.

Figure 129 shows that number of alerts starts to stabilize from ImC 23% and increases up to 35% for an ImC 30% scenario in the Rhône-Alpes climate, whereas in the Bretagne climate the increase in alerts rises linearly, reaching up to 87% for an ImC 30% scenario.

Figure 130 shows that for high slopes, the number of consecutive ponding time alerts can decrease down to 30%. Both climates follow the same tendency to decrease with slope increment. However, it can be seen that the filter is more sensitive under Bretagne climate conditions. This fact highlights that the filter is more sensitive to rainfall duration than rainfall intensity.

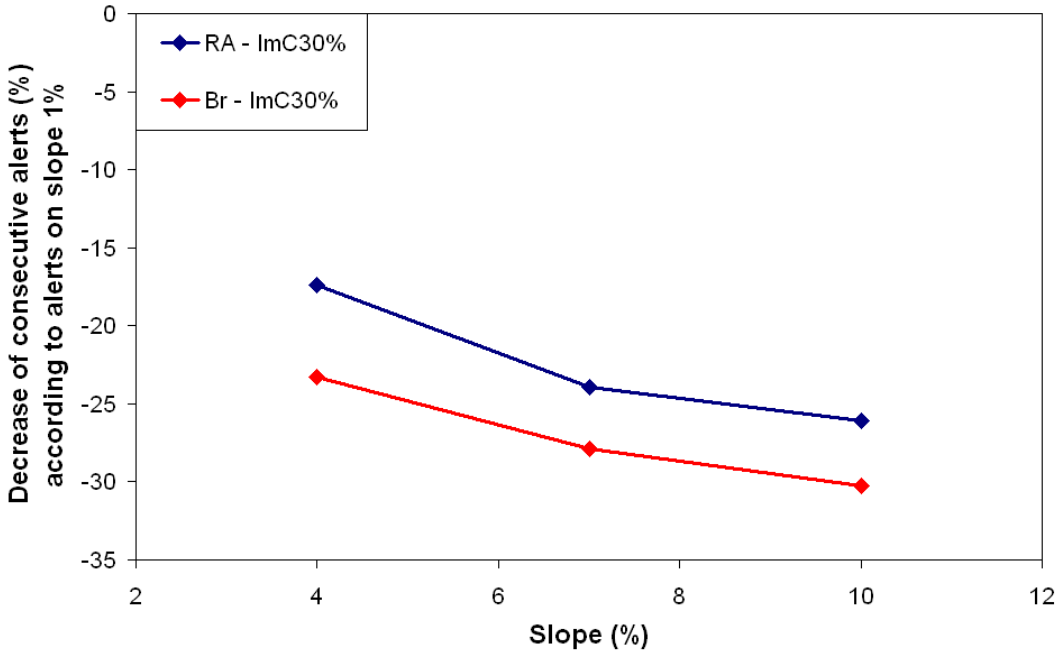

Figure 130: Decrease in consecutive ponding time alerts according to slope at 1% and ImC 30%, in Bretagne (Br) and Rhône-Alpes (RA) climates on a 1.2 m²/p.e. filter surface.

As the scenario of a 30% imperviousness coefficient and a 1% slope is the most problematic in terms of consecutive and cumulative ponding alerts for both climates, this parameter set was taken as a baseline in the rest of this chapter to test the effects of filter design characteristics on number of alerts in unfavourable conditions.

6.2.2. Plant inlet bypass level and discharge

In a move to limit the amount of untreated stormwater discharge to the receiving water body (Urban Waste-Water Treatment Directive 91/271/EEC), Article R2224-17 of the French *Code général des collectivités territoriales* [legislative code governing local community authorities] requires that water entering a sewer system must undergo treatment before being discharged into the natural environment, except in exceptional events. To achieve this objective, new regulation is under construction and, as of 19 March 2013, is expected to set the following treatment objectives :

1. A maximum 20 days of overflow per year at the inlet bypass (averaged on a 5-year period).

or

2. Total overflow volume of 2% (2027 limit date to be respected).

We thus chose to work with these values to illustrate the following part of the study. Based on the different scenarios provided by the local context parameter-sets, Figure 131 highlights the CSO threshold necessary to stay within 20 discharges per year. Due to the similar characteristics between the scenarios with slopes of 7% and 10%, only a 10% scenario was kept for the analysis.

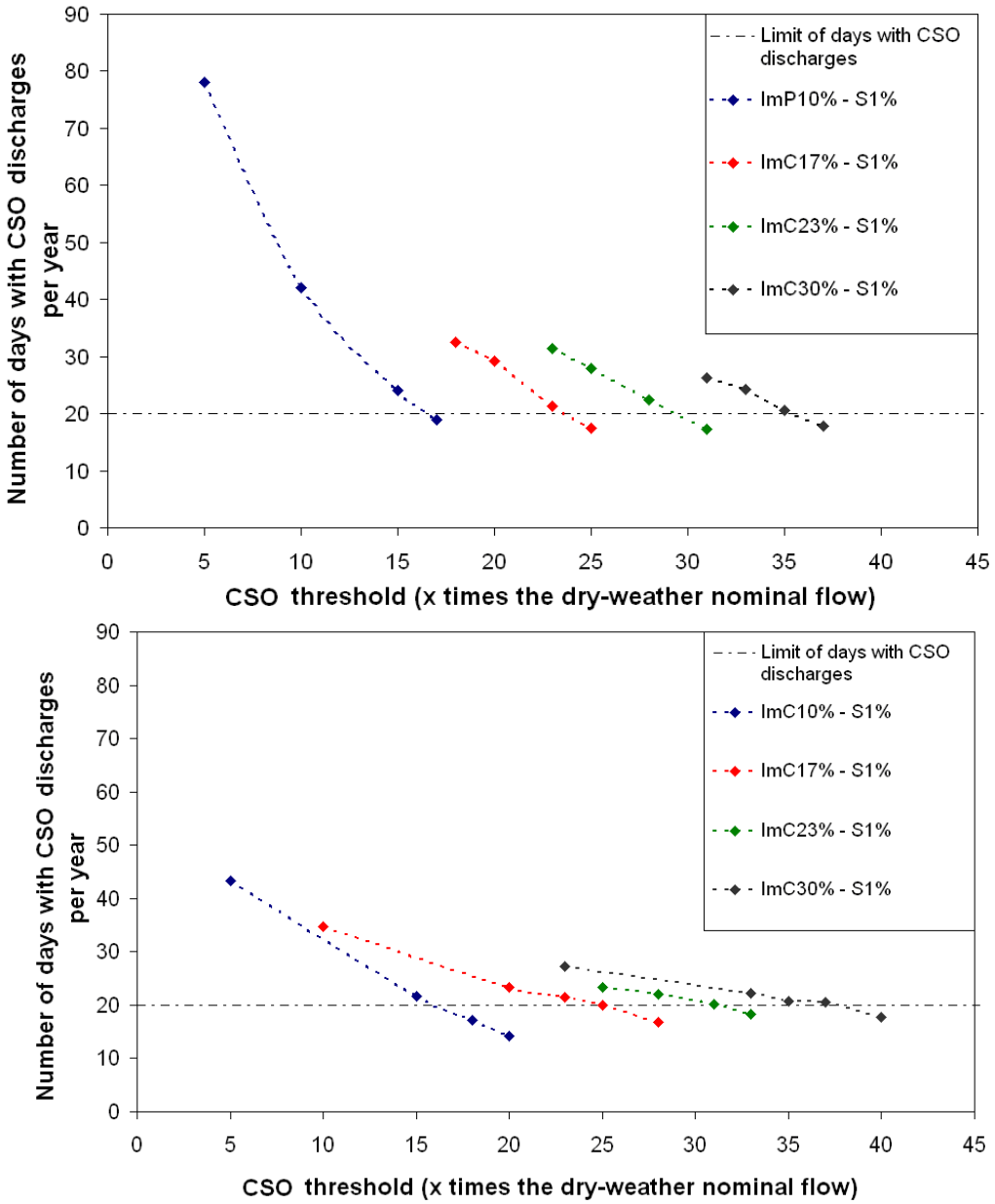

Figure 131: Number of days with CSO discharges according to CSO threshold for Bretagne (*top*) and Rhône-Alpes climates (*bottom*)

Note that as imperviousness coefficient increases, CSO threshold also has to increase to stay within 20 discharges per year. Climate has little impact on the CSO threshold that has to be set to respect the limit of discharges for each ImC, although the difference in number of overflows according to CSO threshold was lower in the Rhône-Alpes climate, probably as rainfalls are less frequent (less CSO discharges) but more intense (higher HL) than in the Bretagne climate. Figure 131 shows that for a low imperviousness coefficient, a CSO threshold of 18-20 times the average dry-weather nominal flow can respect the limit, up to roughly 40 times the average dry-weather nominal flow on a 30% imperviousness coefficient.

Figure 132 shows the percentage of volume discharged to the receiving water body through the CSO according to CSO threshold for both climates (Bretagne and Rhône-Alpes).

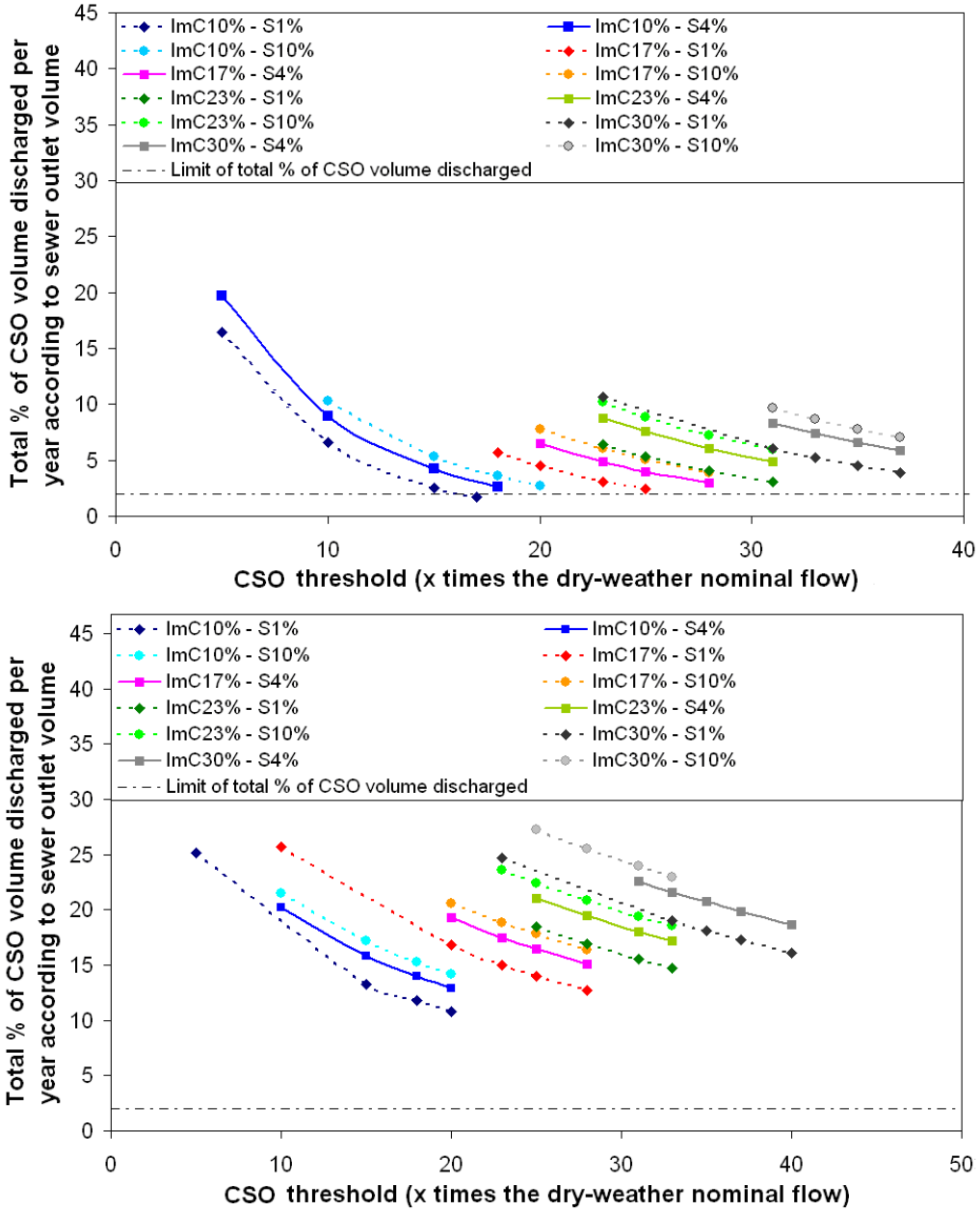

Figure 132: Percentage of volume discharged to the receiving water body through CSO according CSO threshold for Bretagne (*top*) and Rhône-Alpes climate (*bottom*)

Note that rainfall intensity heavily impacts the volume bypassed at the inlet overflow structure. The Rhône-Alpes climate produces a high discharge volume of between 12% and 25% of total annual volume. For the Bretagne climate, when CSO respects the capped number of annual discharges, the percentage of volume discharged ranges from 2% to 9%. Contrary to ponding time, overflow discharge is affected by a short lag-time between the rain event and the flow at the outlet of the sewer. Consequently, high slopes, producing less distributed flow with higher peak rates, affect the volume discharged at the CSO structure.

6.2.3. Influence of CSO threshold on ponding time alerts and bypass discharges

As seen in section 6.2.1, the most problematic local context parameter-set (ImC 30% & slope 1%) was adopted for subsequent filter modelling. The influence of CSO on filter performance was studied through five different thresholds :

- 5-times the dry-weather nominal flow
- 12-times the dry-weather nominal flow
- 20-times the dry-weather nominal flow
- 40-times the dry-weather nominal flow
- No CSO limit

where a 5-fold dry-weather nominal flow (DWNF) was used to refer to actual minimal guidelines in terms of rain event acceptance, a 40-fold DWNF is the threshold value needed to respect the maximum number of discharge days per year, and 12 and 20-fold DWNF were used as intermediate points. No CSO limit scenarios were used to chart the hydraulic limits of VFCW.

As discharges are not clearly defined in the regulations, we established that a CSO discharge has to be superior to 1 hour to be considered as an event. This assumption is not really problematic as it does not induce a lot of difference when compared to number of days with discharges (Figure 133).

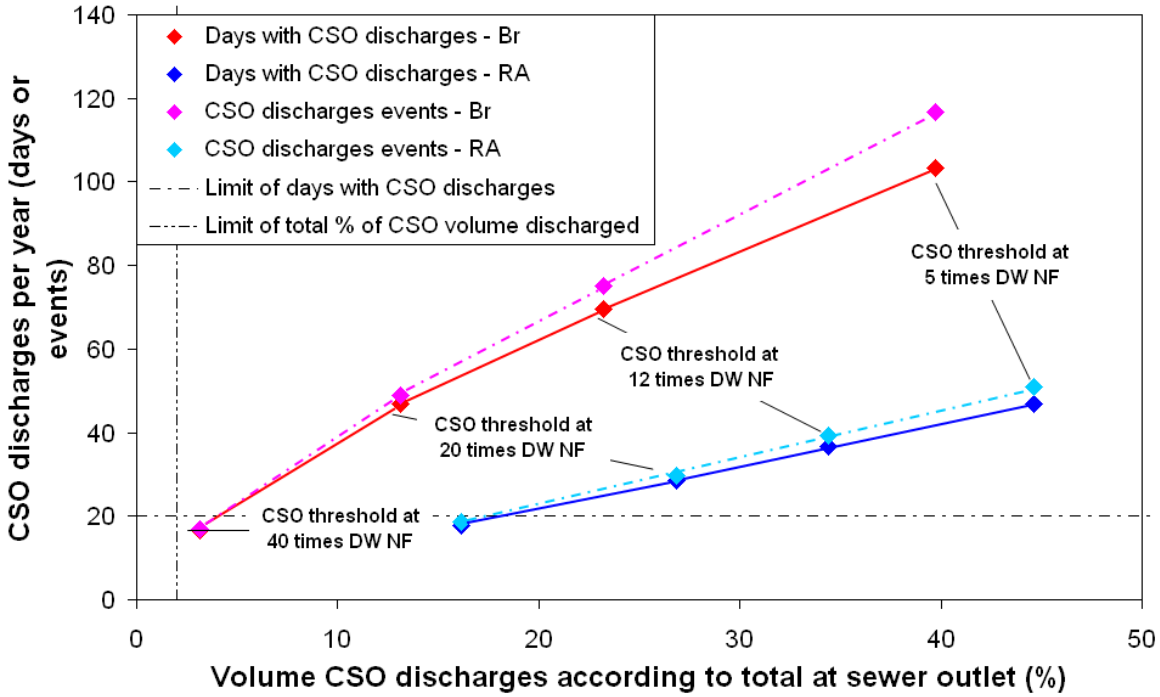

Figure 133: Days with CSO discharges and CSO discharge events per year according to percentage of volume discharged for different CSO thresholds on ImC 30%, S 1% under Bretagne and Rhône-Alpes climates

Figure 134 shows that according to average duration of CSO discharge events, the Rhône-Alpes climate has longer discharges, and that the duration decreases according to CSO threshold in both climates, up to roughly 2 hours per event.

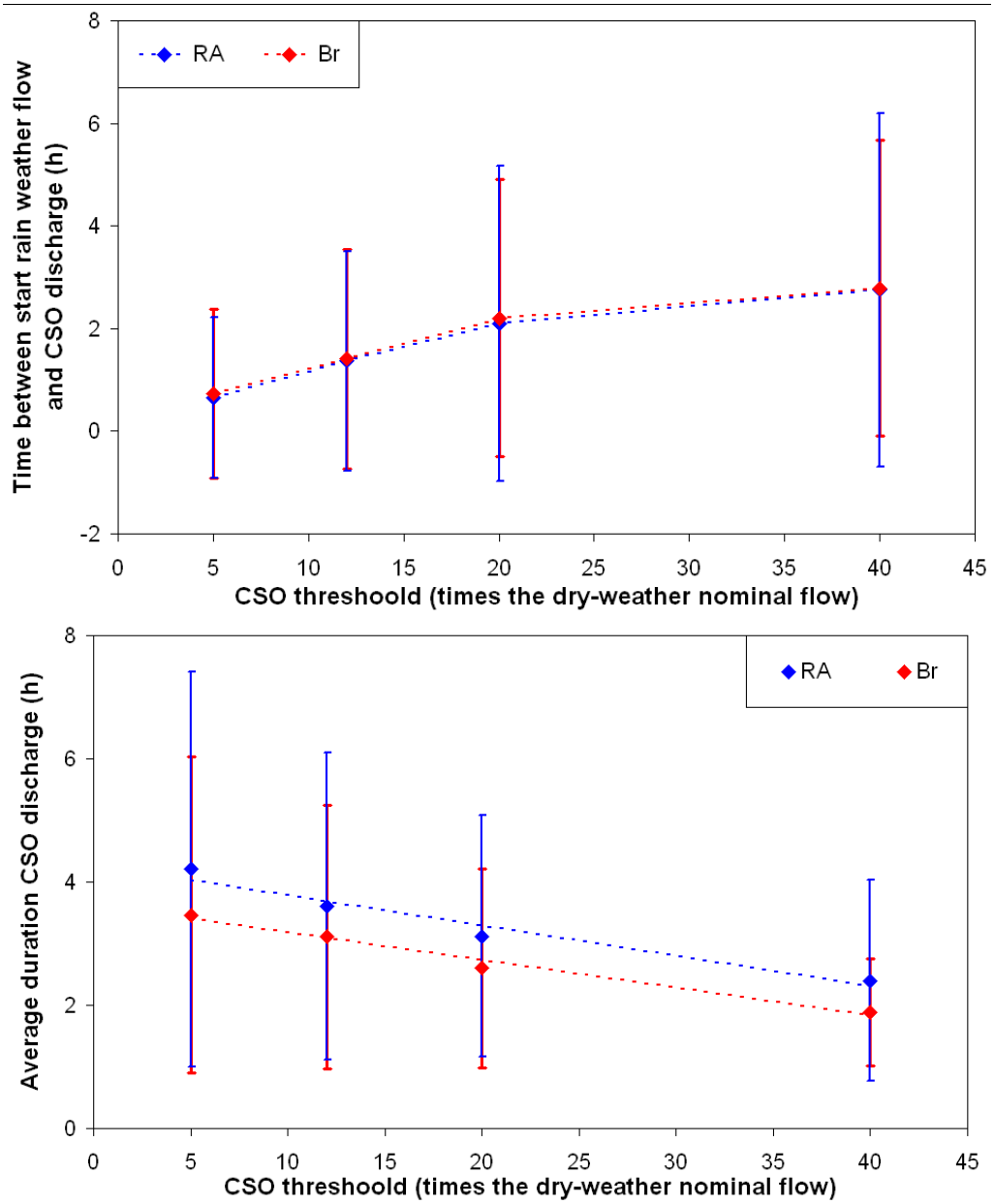

Figure 134: Average duration of CSO discharge (*top*) and time between start of rainfall flow and CSO discharge (*bottom*) according to CSO threshold, for the Bretagne and Rhône-Alpes climates

Obviously, the time between the beginning of a rainfall event (exceeding peak dry-weather flow in this case) and CSO discharge increases with CSO threshold. This gives us a picture of the importance of threshold CSO value when the first hours of rain event have to be treated.

Figure 135 charts cumulative HL distribution due to rain events on a filter with a 1.2 m²/p.e. surface and ImC 30% and slope 1% as sewer characteristics, and presents the HL entering the treatment plant according to CSO threshold.

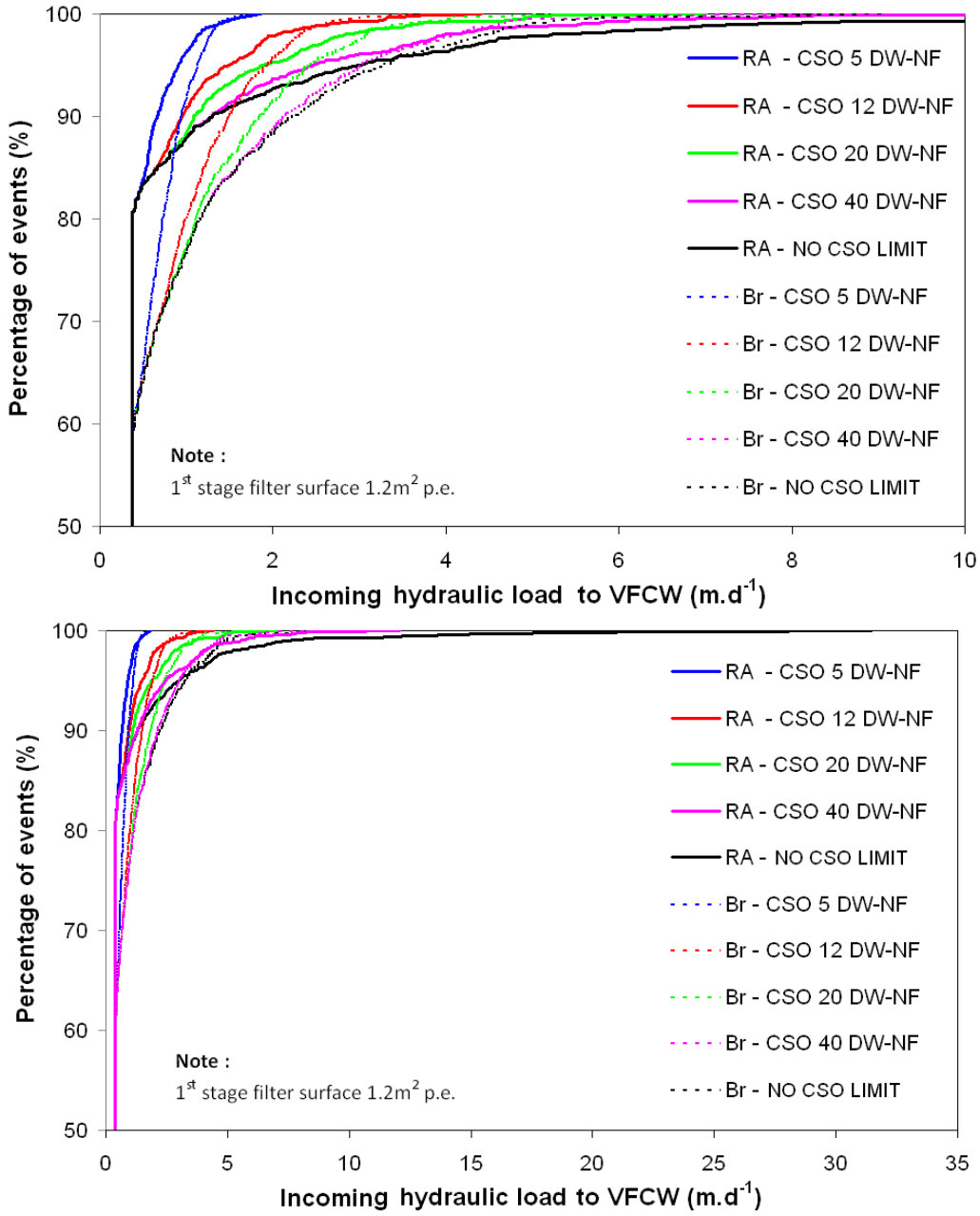

Figure 135: Zoom (*top*) and complete (*bottom*) graphic of daily hydraulic load at entering to VFCW according to CSO threshold in Bretagne (Br) and Rhône-Alpes (RA) climates on a 1.2 m²/p.e. filter surface. DW-NF = Dry-weather nominal flow

To respect 20 discharges a year, the VFCW would have to accept HL of 8.1 $m.d^{-1}$ and 12 $m.d^{-1}$ for Bretagne and Rhône-Alpes climates, respectively (at CSO set up to 40-fold DWNF). In a scenario with no CSO limit, the maximal HL entering the treatment plant is 9 $m.d^{-1}$ and 31.5 $m.d^{-1}$ for Bretagne and Rhône-Alpes, respectively. These high HL levels raise the question of ponding times and bypasses liable to occur at the filter surface.

We tested the impacts of CSO on VFCW on a conventional filter surface (1.2 m²/p.e.) by implementing two different filter scenarios :

- **Young VFCW**
  where the simplified hydraulic model used *ICP* values from the Challex WWTP. First-stage bypass height was set at 0.5 m (0 m sludge deposit).

- **Mature VFCW**

  where the simplified hydraulic model used *ICP* values from Evieu WWTP. First stage bypass height was set at 0.3 m due to 0.2 m of sludge deposit developed on a mature VFCW.

Figure 136 charts ponding time on a 1.2 m²/p.e. filter and an available bypass height of 0.5 m.

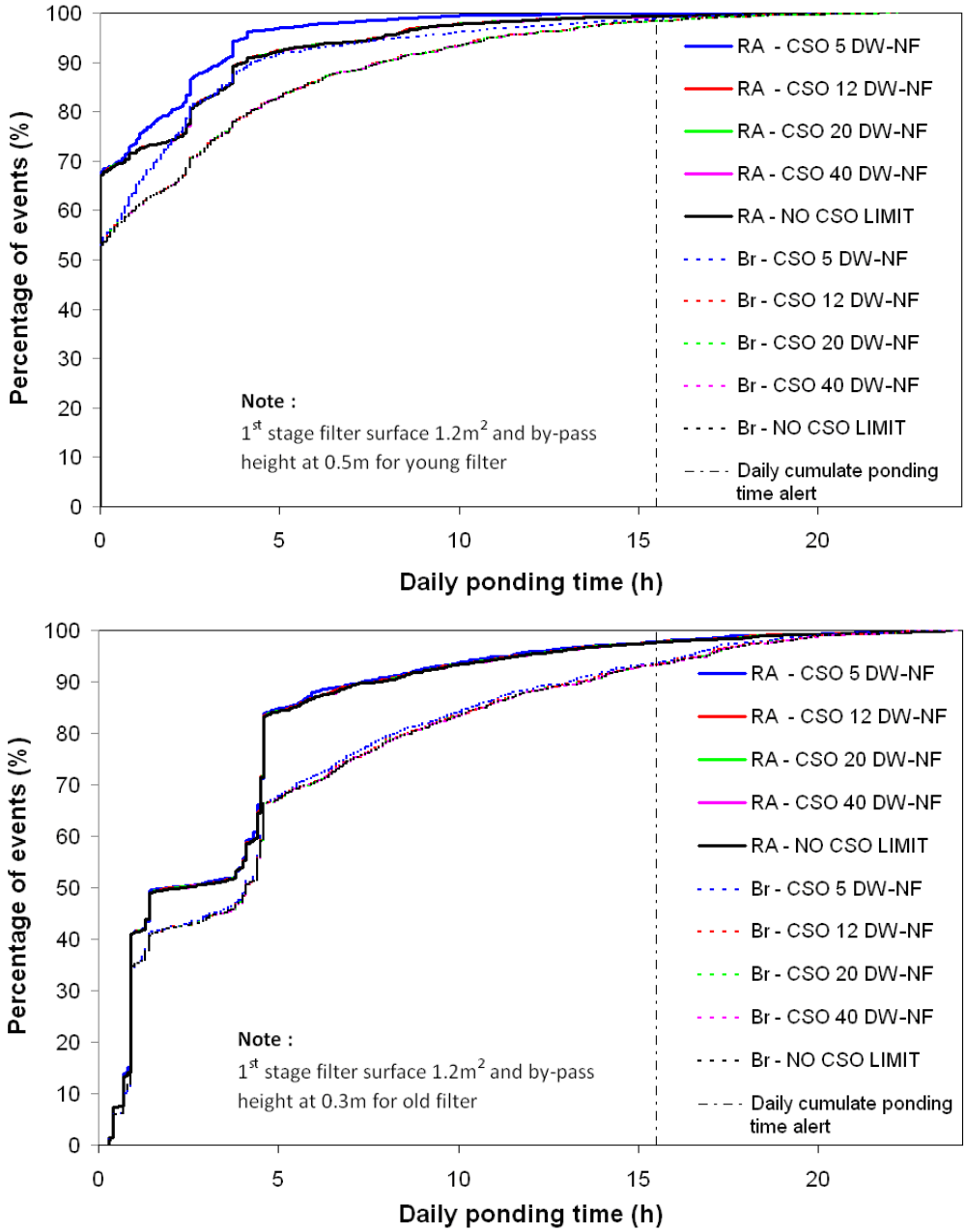

Figure 136: Daily ponding time according to CSO threshold in Bretagne (Br) and Rhône-Alpes (RA) climates for young (*top*) and mature (*bottom*) VFCWs

Limiting the HL entering the filter at 5-fold DWNF is the only way to make a prominent difference on daily ponding time on young filters, as the other thresholds did not show significant differences to the No CSO limit scenario. As the other CSO thresholds could generate HLs reaching the filter holding capacity, the first-stage by-pass could regulate ponding time on the filter.

Figure 137 shows the by-passed events and consecutive and cumulative ponding time alerts according to CSO thresholds on a 1.2 m²/p.e. surface and an available bypass height of 0.5 m (young filter) and 0.3 m (mature filter).

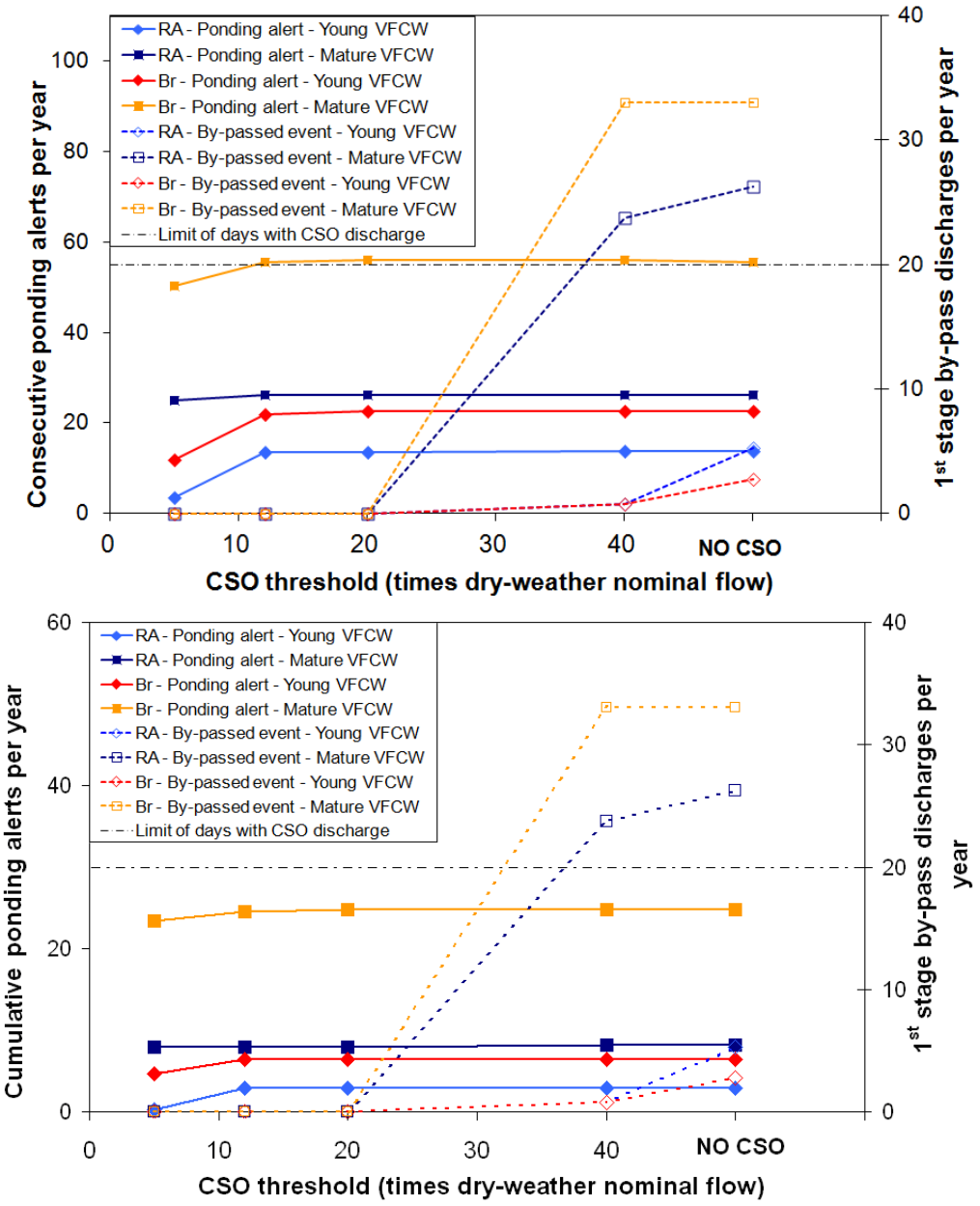

Figure 137: First-stage bypass discharges and consecutive (*top*) and cumulative (*bottom*) ponding time alerts per year according to CSO threshold in Bretagne (Br) and Rhône-Alpes (RA) climates for young and mature VFCW

In terms of filter dysfunctions, Figure 137 shows that cumulative ponding time alerts are lower at a 5 DWNF CSO threshold and stay stable for other scenarios. However, even when ponding alerts remain constant, first-stage bypass discharges still increase, appearing from the 40 DWNF CSO threshold. This pattern highlights that even if cumulative alerts stay stable, the volume stored on the filter surface increases without considerably hampering filter function. As the filter matures, cumulative ponding time alerts get almost 3 and 4 times higher and consecutive ponding times get 2 and 2.5 times higher under Rhône-Alpes and Bretagne climates, respectively, compared to a young filter. According to first-stage bypass discharges,

the differences were more substantial, reaching 5 to 11 times higher values on Rhône-Alpes and Bretagne climates, respectively, and exceeding the discharges limit in the process.

Nevertheless, even if the number of alerts stays constant, the HL entering the filter increases with CSO threshold. This can be seen in the average ponding depth during the cumulate ponding alerts (Figure 138). Figure 138 shows the average ponding depth on days with cumulative alerts according to CSO thresholds on a 1.2 m²/p.e. surface and an available bypass height of 0.5 m (young filter) and 0.3 m (mature filter).

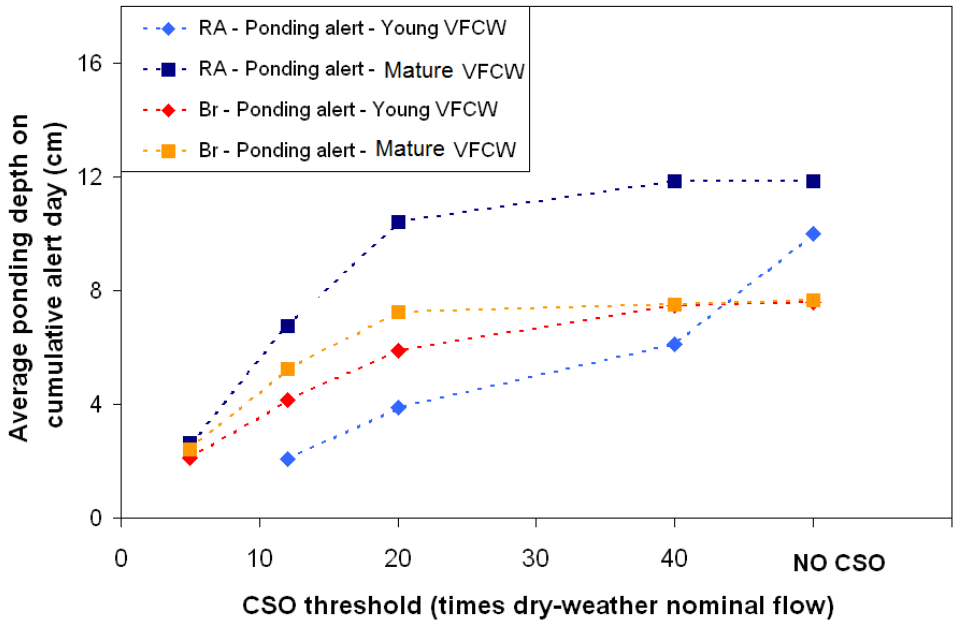

Figure 138: Average ponding depth on cumulative ponding alert days according to CSO threshold in Bretagne (Br) and Rhône-Alpes (RA) climates for young and mature VFCWs

Water storage capacity on the filter surface becomes more stable as the filter matures and loses permeability, especially under the Rhône-Alpes climate where the filter tended to stay within its maximum capacity.

While the filter did not show a significant increase in dysfunction according to CSO threshold, there is still a need to reduce the number of discharges following out into the receiving water body. We saw that even if we configure the CSO to not exceed 20 days with discharges per year, the HL entering the VFCW can produce first-stage bypass discharges that, combined with CSO discharges, will exceed the limit. If we can profit from solids sedimentation on the filter surface, the impact on receiving water bodies should be evaluated. Nevertheless, it seems more useful to limit the acceptable HL by virtue of filter design (surface and water storage) as water storage at the filter surface can buffer hydraulic peaks during rain events, making it possible to accept more water and limit water discharges. In order to protect the filter and inlet structures (screening, siphon or pumps …) from very intense rain events, it is necessary to fix a limit to the CSO structure. The CSO discharges produced in extreme rainfall cases will be tolerated according to the order project.

To test filter design parameters in the most unfavourable conditions, we chose a 30% imperviousness coefficient and 1% slope for the work presented in the following chapters. Furthermore, to test the feasibility of managing discharge at the filter surface bypass, the “no limit” configuration for CSO was used to model the filter design parameters.

6.2.4. Influence of filter surface and bypass height on ponding time alerts and bypass discharges

Once it was decided to increase CSO limit to allow the totality of HL to enter the treatment plant (our "No CSO limit" scenario), the next step was to study the influence of filter surface and bypass height on dysfunction alerts and bypass discharges. The principal objective was to reduce the number of discharges without incrementing the ponding time alerts. The filter surface and bypass height configurations were first tested on a young VFCW. The scenarios are presented in Table 23.

Table 23: Scenarios tested according to filter surface (surface of the 3 filters of the first stage) and first-stage bypass height under Bretagne and Rhône-Alpes climates

Scenarios	
first-stage filter surface (m^2/p.e.)	**first-stage bypass height (m)**
0.9	0.5
1	0.5
1.2	0.5
1.5	0.5
1.2	0.1
1.2	0.3
1.2	0.5
1.2	0.7

The filter surfaces tested were selected according to French guidelines (1.2–1.5 m^2/p.e) and some low surfaces found on French VFCW in tropical climates. These filter surfaces were tested with a 0.5 m bypass height as observed in the Challex VFCW. For bypass height, the values were distributed around Challex values and tested with the minimum surface recommended by French guidelines (0.3 m). Figure 139 shows the daily ponding time on a young filter according to percentage of events for different filter surfaces at an available bypass height of 0.5 m.

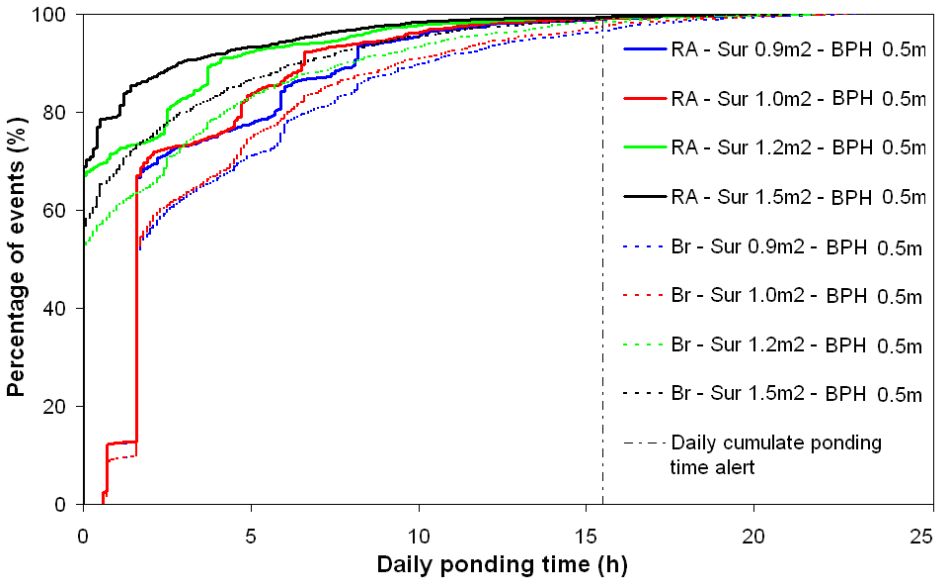

Figure 139: Daily ponding time according to first-stage surface at 0.5 m bypass height under Bretagne and Rhône-Alpes climates

Figure 139 demonstrates that according to daily ponding time, surfaces as low as 0.9 m²/p.e. and 1 m²/p.e. give the highest ponding times and ponded every day, contrary to the recommended surfaces (1.2–1.5 m²/p.e). Figure 140 presents the days with bypass discharges and the cumulative and consecutive ponding time alerts for different filter surfaces.

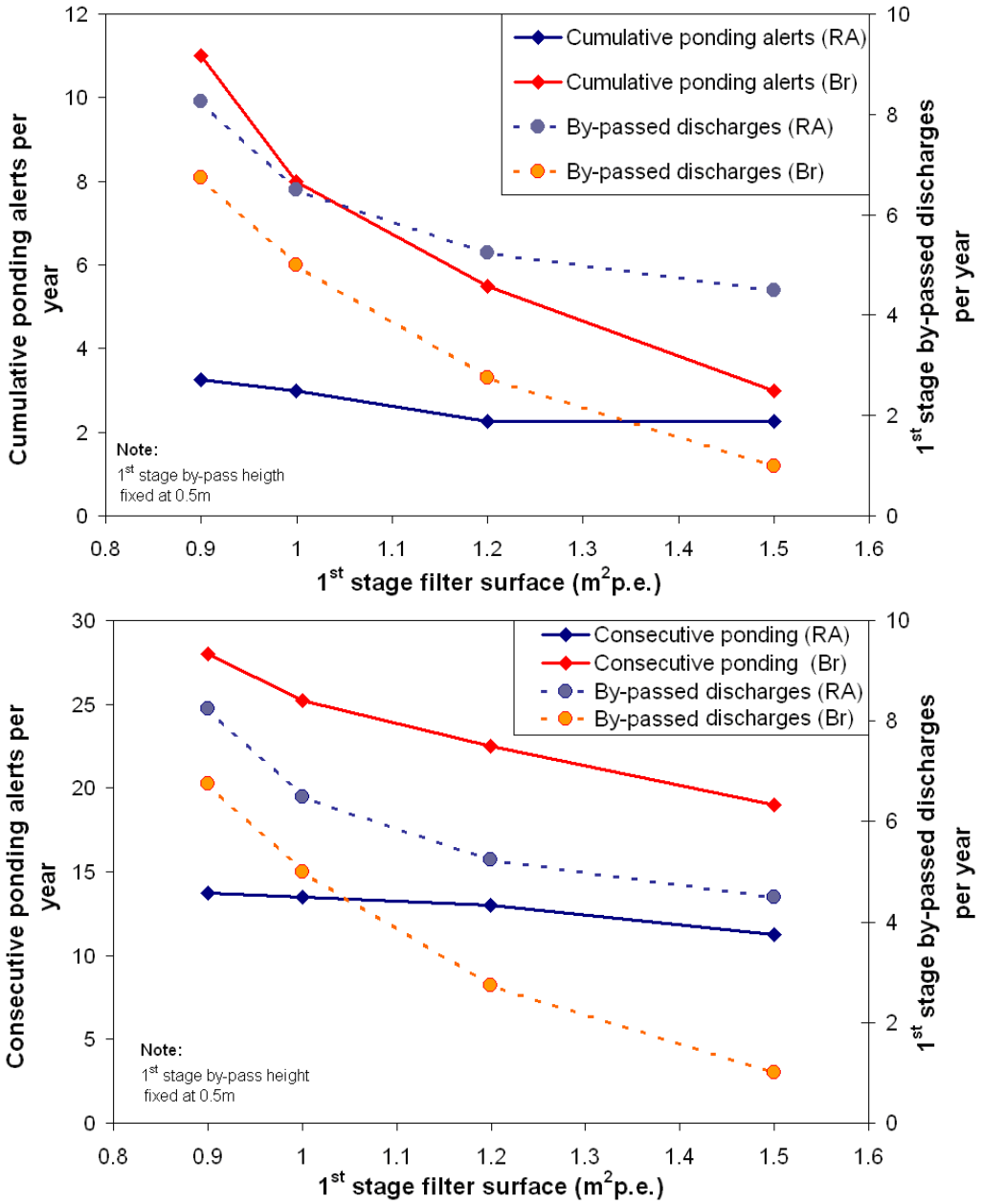

Figure 140: First-stage bypassed events and cumulative (*top*) and consecutive (*bottom*) ponding time alerts according to first-stage surface at 0.5 m bypass height for Bretagne and Rhône-Alpes climates

Obviously, the increase in filter surface decreases the number of ponding time alerts. Cumulative ponding time alerts remained stable from 1.2 m²/p.e under a Rhône-Alpes climate but decreased sharply under a Bretagne climate (where rainfall events are more frequent). For both climates, the cumulative alerts stay lower than 6 per year on a young VFCW with regular French dimensions. Figure 140 also shows that bypass discharges decrease considerably with higher filter surfaces, especially under a Bretagne climate.

Figure 141 shows the days with bypass discharges and consecutive and cumulative ponding time alerts according to first-stage bypass height.

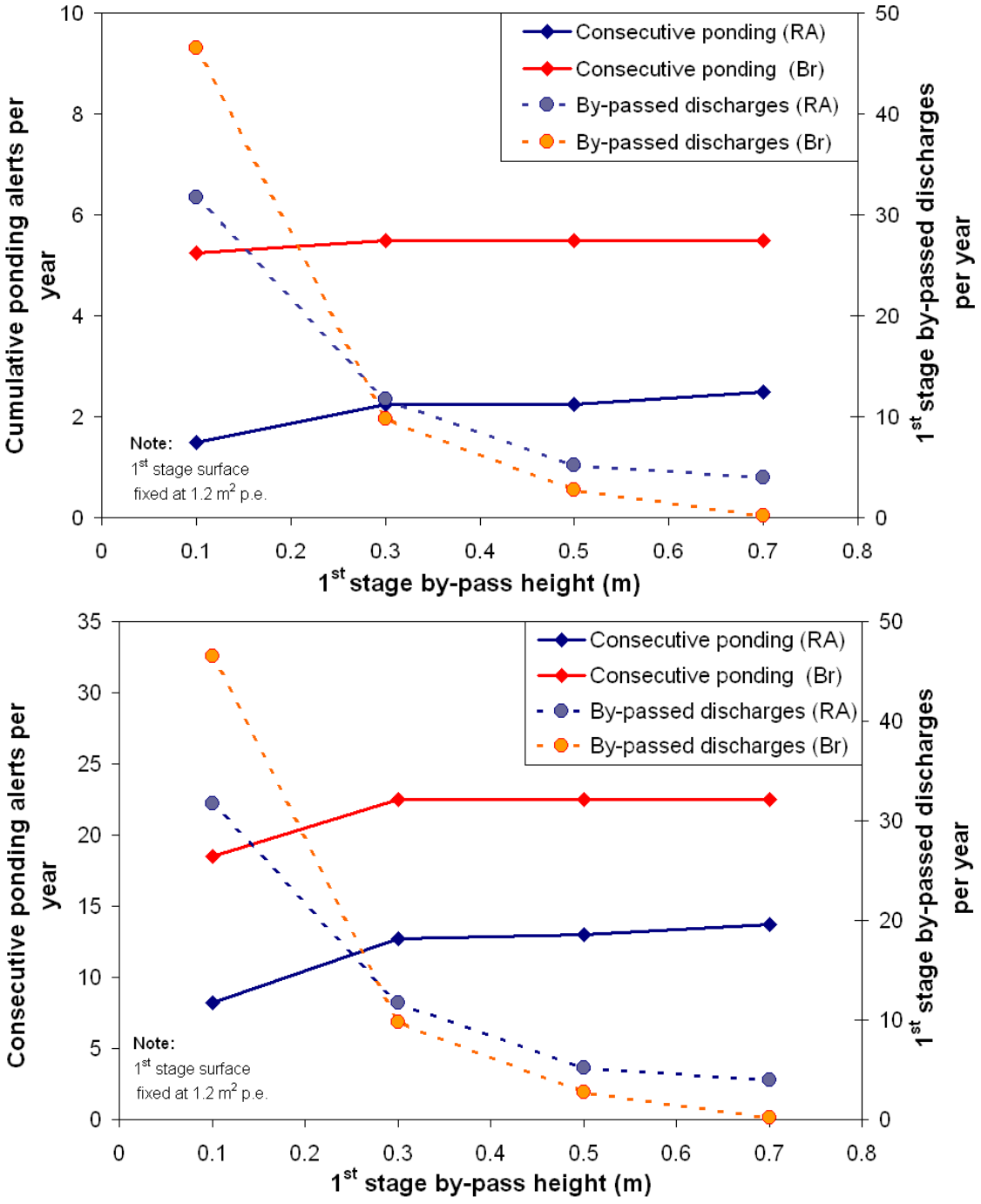

Figure 141: Days of bypass discharges and cumulative (*top*) and consecutive (*bottom*) ponding time alerts according to first-stage bypass height at a 1.2m²/p.e. filter surface under Bretagne and Rhône-Alpes climates

Bypass discharges significantly decrease as first-stage bypass height increases, reaching a minimum of 0.25 and 4 discharges per year for Bretagne and Rhône-Alpes, respectively. On the other hand, the ponding time alerts (cumulative and consecutive) stay essentially stable from 0.3 m to 0.7 m of bypass height in both climates. Thus, increasing bypass height from 0.3 to 0.7 limits the number of discharges without jeopardizing filter function.

These results show that increasing the filter surface cuts the number of ponding time alerts and bypass discharges, while high bypass heights also help decrease discharges without increasing the number of dysfunctions. For both climates, on a young VFCW the bypass discharges were far lower than the expected limit. However, on an aged VFCW, discharges increase considerably as sludge deposits accumulate. For these reasons, the next step was focused on analysing the impact of filter ageing on HL acceptance.

6.2.5. Influence of filter surface, bypass height and filter age on ponding time alerts and bypass discharges

In this part of the modelling effort, we first tested filter responses in two different local contexts, one presenting "normal" imperviousness coefficient and slope values and the other presenting the "most problematic scenario" values used for the previous modelling. In addition, different filter surfaces were tested to see the response of system. Table 24 recaps the scenarios tested in this step.

Table 24: Scenarios tested according to filter surface and local context under Bretagne and Rhône-Alpes climates

Scenarios				
First-stage filter surface (m^2/p.e.)	First-stage bypass height (m)	Filter age	Local context	
			Imperviousness coefficient (%)	Slope (%)
0.9	0.3 (0.5)	Mature	10	4
1	0.3 (0.5)	Mature	10	4
1.2	0.3 (0.5)	Mature	10	4
1.5	0.3 (0.5)	Mature	10	4
0.9	0.3 (0.5)	Mature	30	1
1	0.3 (0.5)	Mature	30	1
1.2	0.3 (0.5)	Mature	30	1
1.5	0.3 (0.5)	Mature	30	1

To better set the key filter design parameters, it is first necessary to set the number of annual cumulative alerts. We worked to the assumption that more than two cumulative ponding alerts per month could be "problematic" for the system (24 alerts per year). This "alert limit" is just a reference to ensure the system can run properly, allowing for the fact that continuous monitoring showed that the filter can recover rapidly after a long time of ponding.

Figure 142 and 143 show the days with bypass discharges and cumulative ponding time alerts on a mature VFCW with different filter surfaces for the two different local contexts, under Rhône-Alpes (Figure 142) and Bretagne (Figure 143) climates.

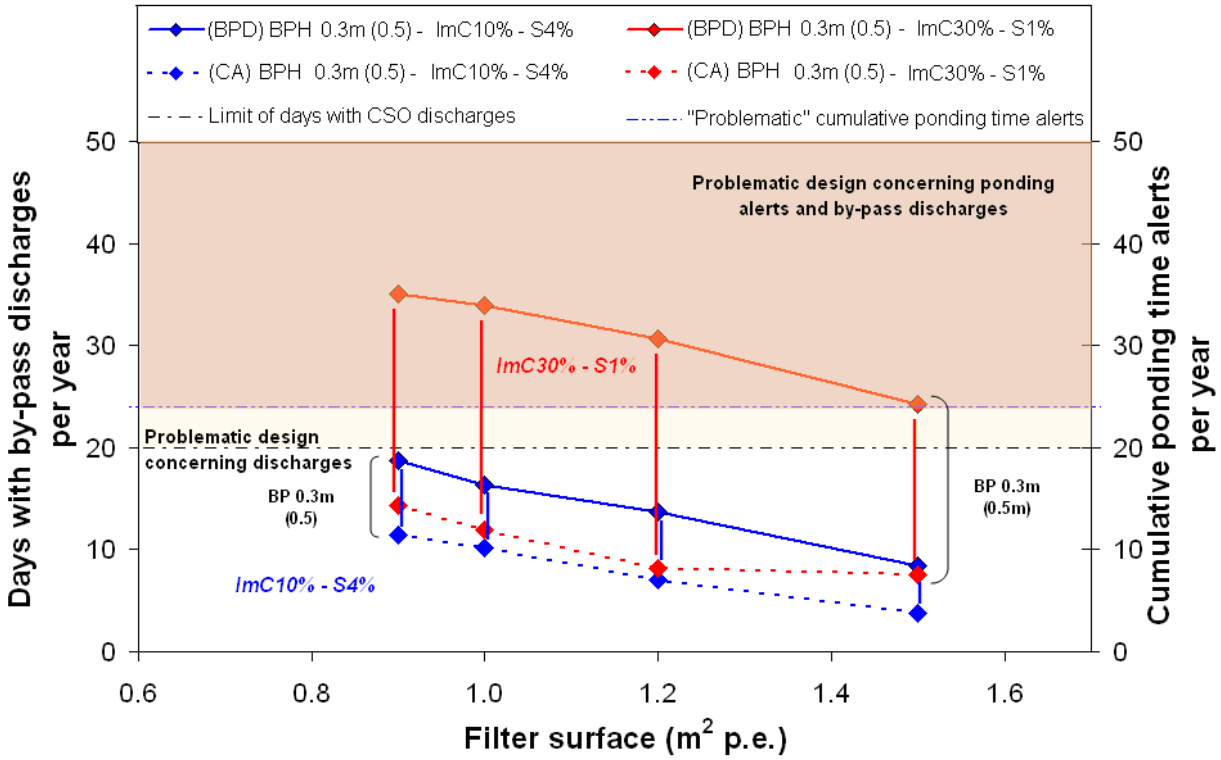

Figure 142: Cumulative ponding time alerts and days with bypass discharges according to first-stage filter surface, for a mature VFCW, in a local context of ImC 30% –S1% and ImC10%-S4%, for Rhône-Alpes climate *with (BP) = bypass discharge, (CA)= cumulative ponding time alerts and BPH = bypass height

Figure 142 (Rhône-Alpes climate) shows that in a "normal" local context scenario (ImC10%-S4%), all the filter surfaces can accept hydraulic overloads without exceeding the limit on cumulative ponding alerts and bypass discharges.

On the other hand, for the "most problematic" local context scenario (ImC30%-S1%), no filter surface was able to comply with the bypass discharge limit (only the cumulative ponding alerts limit was complied with). In contexts presenting very problematic catchment area characteristics (ImC, slope), 0.3 m of available height for water storage seems insufficient once the filters are mature.

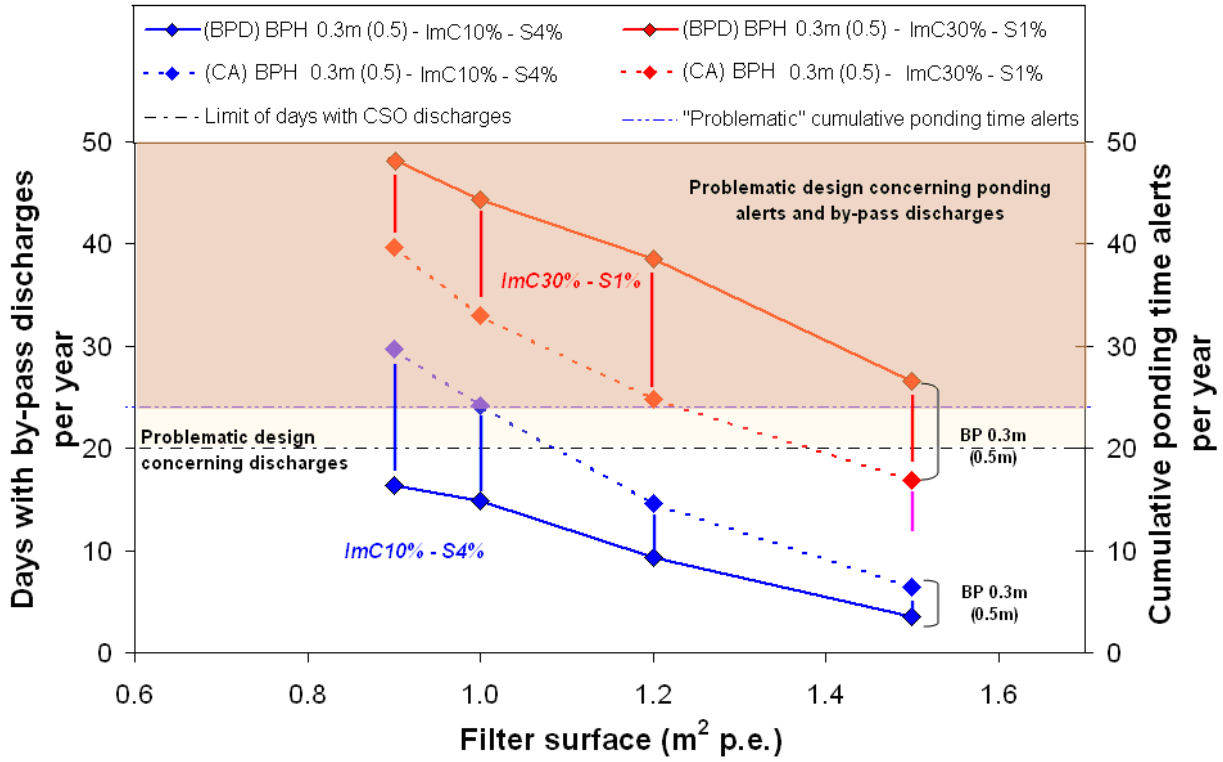

Figure 143: Cumulative ponding time alerts and days with bypass discharges according to first-stage filter surface, for a mature VFCW, in a local context of ImC 30% –S1% and ImC10%-S4%, for Bretagne climate *with (BP) = bypass discharge, (CA)= cumulative ponding time alerts and BPH = bypass height

For the Bretagne climate, under a "normal" local context scenario, cumulative ponding alerts are problematic for a low surface per p.e. Thus, only the filter surfaces of 1.2 and 1.5 m²/p.e respect the ponding thresholds. As with the Rhône-Alpes climate, for the "most problematic" local context, no filter surface was able to accept hydraulic overloads respecting the limits.

In order to test filter robustness, the "most problematic" local context scenario was selected for the next simulation step, which aims to adapt filter configuration to accept a maximum of hydraulic overloads while at the same time respecting the discharge and ponding alerts limits. As show in section 6.2.4 and 6.2.5, the filter configurations achieving less by-pass discharges were tested on young and mature VFCW. Table 25 summarizes the scenarios simulated :

Table 25: Scenarios tested according to filter surface, first-stage bypass height and filter age under Bretagne and Rhône-Alpes climates

Scenarios		
First-stage filter surface (m²/p.e.)	**First-stage bypass height (m)**	**Filter age**
1.2	0.5	Young
1.2	0.7	Young
1.5	0.5	Young
1.5	0.7	Young
1.2	0.3 (0.5)	Mature
1.2	0.5 (0.7)	Mature
1.5	0.3 (0.5)	Mature
1.5	0.5 (0.7)	Mature

Earlier we saw that on mature VFCW, a 0.2 m height of sludge deposit has to be subtracted from the total first-stage bypass height. Table 25 presents the available height for water

storage and, in brackets, the initial available height. Figure 144 shows the days of first-stage bypass discharges and cumulative ponding time alerts according to filter surface and available height for water storage, for young and mature VFCWs.

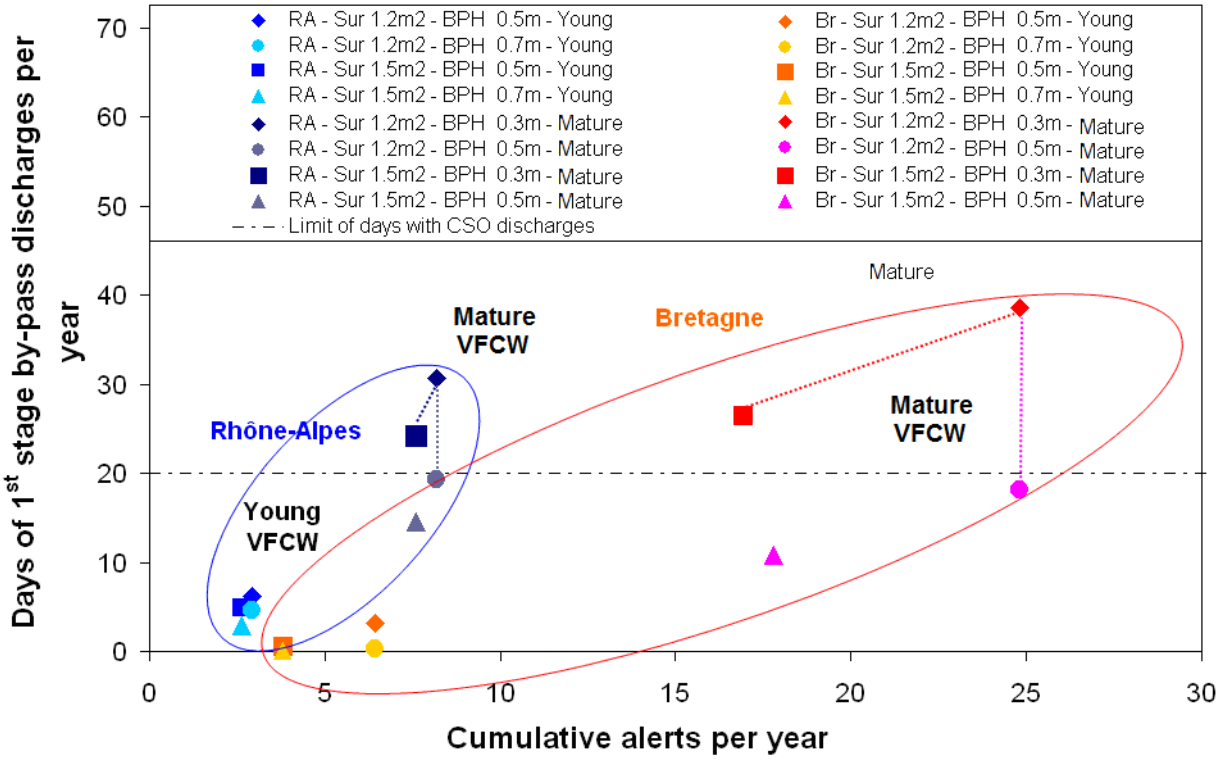

Figure 144: Days of first-stage bypass discharges and cumulative ponding time alerts according to filter surface and bypass height for young and mature VFCW under Bretagne (Br) and Rhône-Alpes (RA) climates *with Sur = filter surface, BPH = bypass height

For young VFCW, whatever the filter configuration and climate, the number of first-stage bypass discharges was always well below the CSO discharge limit, at a maximum 6.5 cumulative ponding time alerts per year. This result shows that the filter delivers good hydraulic performances in its first years of operation. However, on mature VFCWs, the permeability of the filter surface decreases due to the accumulation of organic matter onto and within the porous media, inducing an increase in bypass discharges and ponding time alerts.

Under both climates and filter surface configurations (1.2 and 1.5 m²/p.e), a bypass height of 0.3 m overshoots the limit on number of discharges. Note that increasing filter surface leads to a sharper decrease in discharges and ponding alerts under the Bretagne climate. However, increasing bypass height to 0.5 m (0.7 m on a young VFCW) will only decrease the number of bypass discharges to within the threshold limit on both surfaces studied. Figure 145 charting fraction of discharge (%) to the receiving water body shows the fraction of first-stage bypass discharge and cumulative ponding time alerts according to filter surface and available bypass height for young and mature VFCW.

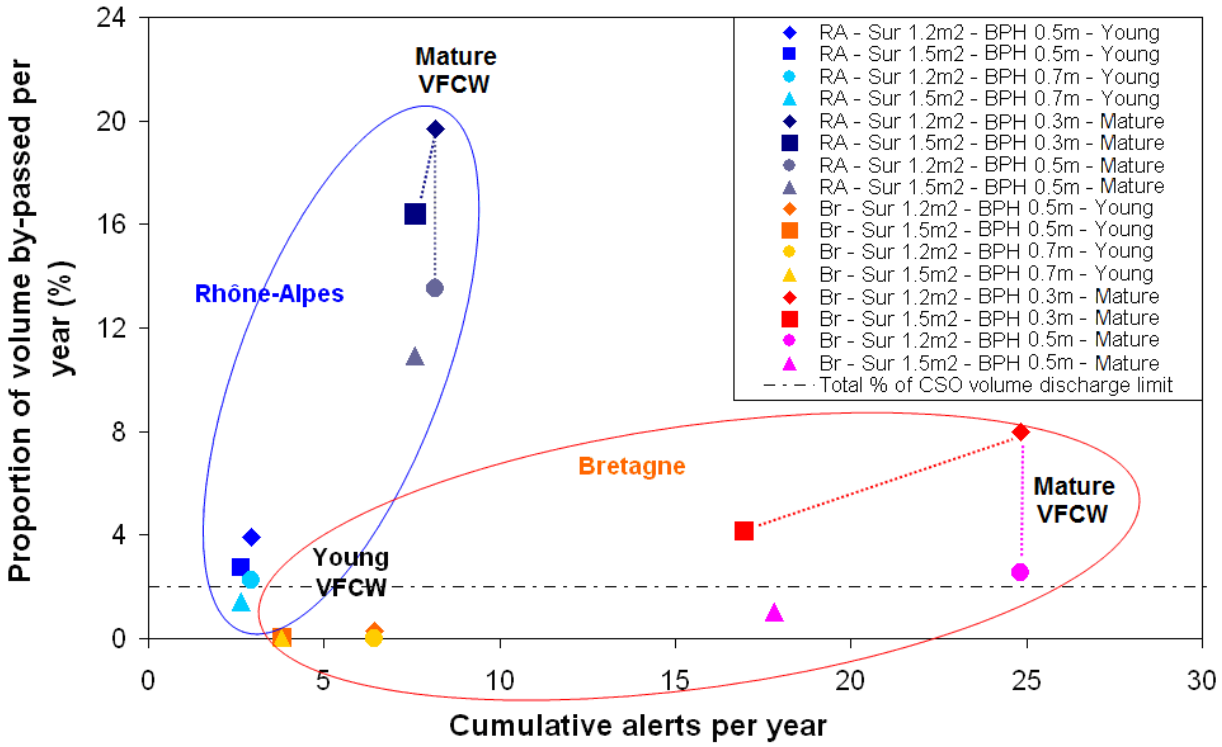

Figure 145: Proportion of volume bypass discharged and cumulative ponding time alerts according to filter surface and bypass height, for young and mature VFCW under Bretagne (Br) and Rhône-Alpes (RA) climates * with Sur = filter surface, BPH = bypass height

Clearly, the 2% limit is unachievable under a Rhône-Alpes-type climate with its highly-loaded rainfall events – just one type of configuration can respect this limit, and only with a young filter that produces a minimum 11% discharge when the filter has matured. On the other hand, for Bretagne-type climates, this fraction limit can be respected whatever the filter age, but only with the 1.5 m²/p.e – 0.5 m available by-pass height configuration.

For the Rhône-Alpes climate, Figure 146 shows the days and fraction of first-stage bypass discharge and cumulative ponding time alerts according to filter surface and available bypass height for young and mature VFCW.

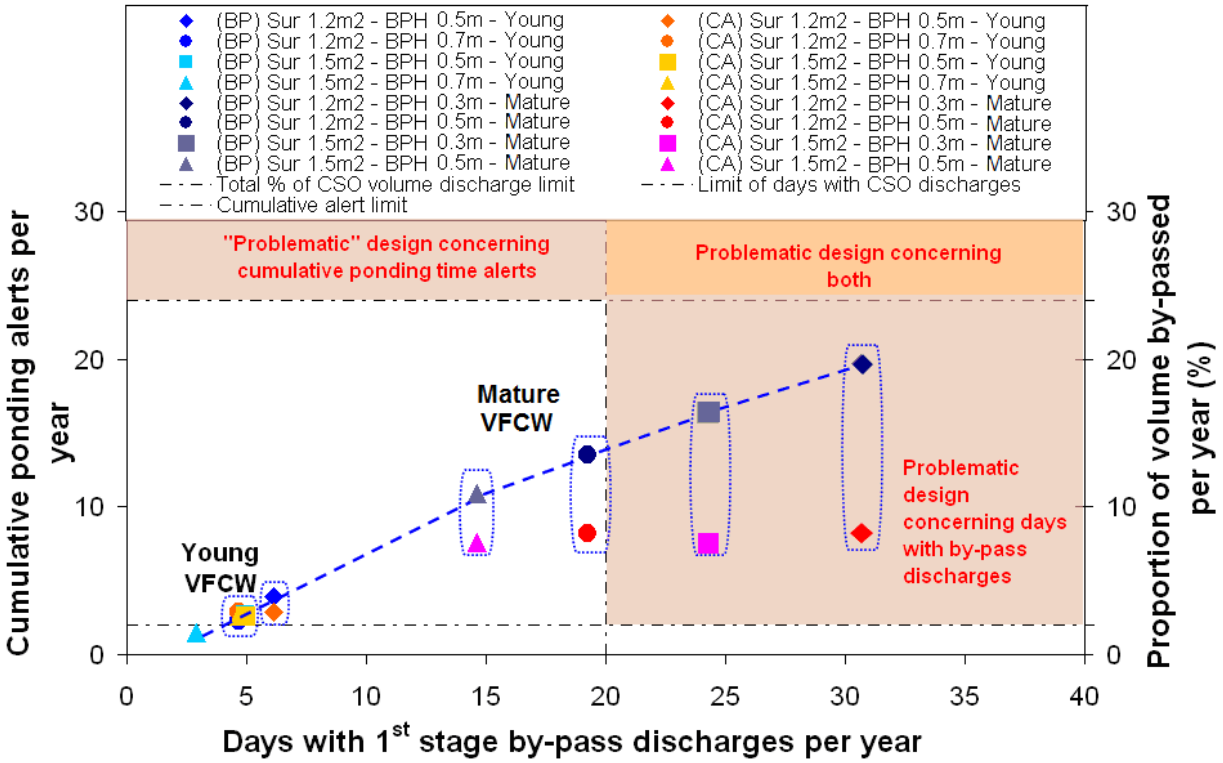

Figure 146: Cumulate ponding time alerts and proportion of volume bypass discharged according to days with first-stage bypass discharges, for young and mature VFCW, under a Rhône-Alpes climate, *with (BP) = bypass discharge, (CA)= cumulate ponding time alerts, Sur = filter surface, BPH = bypass height

None of the configurations showed cumulative ponding time alert problems, even on mature filters. As it was impossible to respect the 2% discharges cap, the design will be focus on reducing the days of bypass discharges in order to work towards the objective of respecting the limit of days with CSO discharges. If configurations with an available by-pass height (water storage height) of 0.5 m respect the limit of discharges when the filter is young, it means that for old systems we will need to increase total storage height by 0.2 m to 0.7 m to include a maximum of 20 cm of sludge deposit.

Note that for the minimal design that respects the limits (1.2 m²/p.e–0.7 m), the number of successive cumulative ponding alerts was only of 1 per year on old VFCWs. For young filters, about 1.75 feeding periods per year present two or more consecutive ponding alerts, whereas with mature filters the number of feeding periods with two or more consecutive ponding alerts can rise to 3.75. These successive cumulative and consecutive alerts should not affect overall performances as they remain extremely rare and the filters quickly recover from ponding. Note that these values decrease with a filter surface of 1.5 m²/p.e. Figure 147 presents the results for the Bretagne climate.

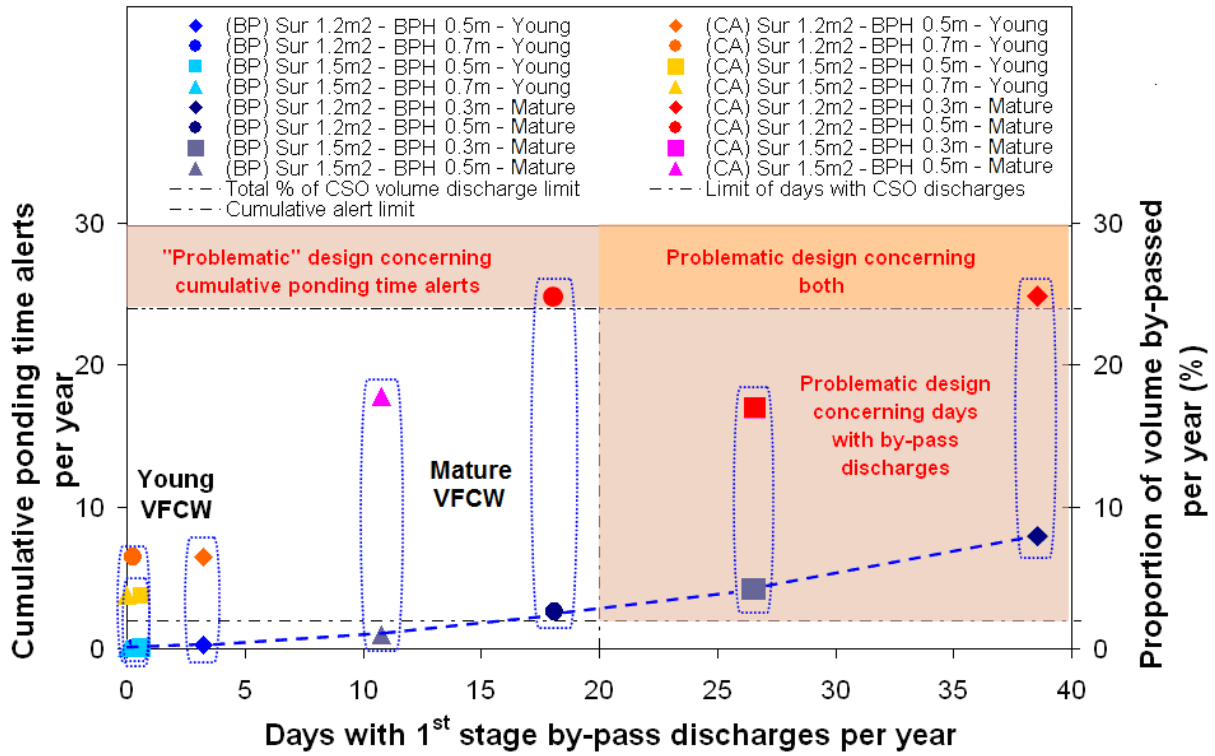

Figure 147: Cumulate ponding time alerts and proportion of volume bypass discharged according to days with first-stage bypass discharges, for young and mature VFCW, under a Bretage climate *with (BP) = bypass discharge, (CA)= cumulative ponding time alerts, Sur = filter surface, BPH = bypass height

Contrary to the Rhône-Alpes climate, data on mature filters under a Bretagne climate show that both surface configurations exceed the discharge limit for an available by-pass height of 0.3 m. In addition, with this filter surface bypass height, the smaller filter surface (1.2 m²/p.e.) presents “problems” in terms of cumulative ponding time alerts. Thus, increasing bypass height may reduce discharges, but cumulate ponding alerts are still over the “limit” (conf. 1.2 m²/p.e–0.5 m). Consequently, increasing the filter surface to 1.5 m²/p.e, and keeping available by-pass height at 0.5 m is a necessary requisite to cutting alerts and discharges down to acceptable levels.

Note that for the configuration that respects the limits (1.5 m²/p.e–0.7 m), the number of successive cumulative ponding alerts was only 0.5 and 2 per year for young and mature VFCW, respectively. Concerning consecutive ponding alerts, 3.25 and 12.25 feeding periods per year presented two or more consecutive ponding alerts on young and mature VFCW, respectively, which should not trouble performances as they are exceptional events. Consecutive ponding alerts should not affect filter performances given that the filters have proven able to recover rapidly.

6.3. Characteristics of alerts and discharges in VFCW configurations that respect the limits

First-stage bypass discharges and ponding time alerts were analysed on the minimal filter configurations that respect the limits. Figure 148 shows that most ponding time alerts occur in the winter season, particularly in November and December in both climates when the filter is mature. For young filters, under a Rhône-Alpes climate, filters show a constant trend of low

numbers of alerts, under a Bretagne climate, the coldest months (January and February) produce more ponding alerts. Remember that the simplified model for young VFCW works with more infiltration capacity parameter (ICP) values — that vary according to season and thus have a stronger influence on ponding alerts — than the mature VFCW model that has only two ICPs.

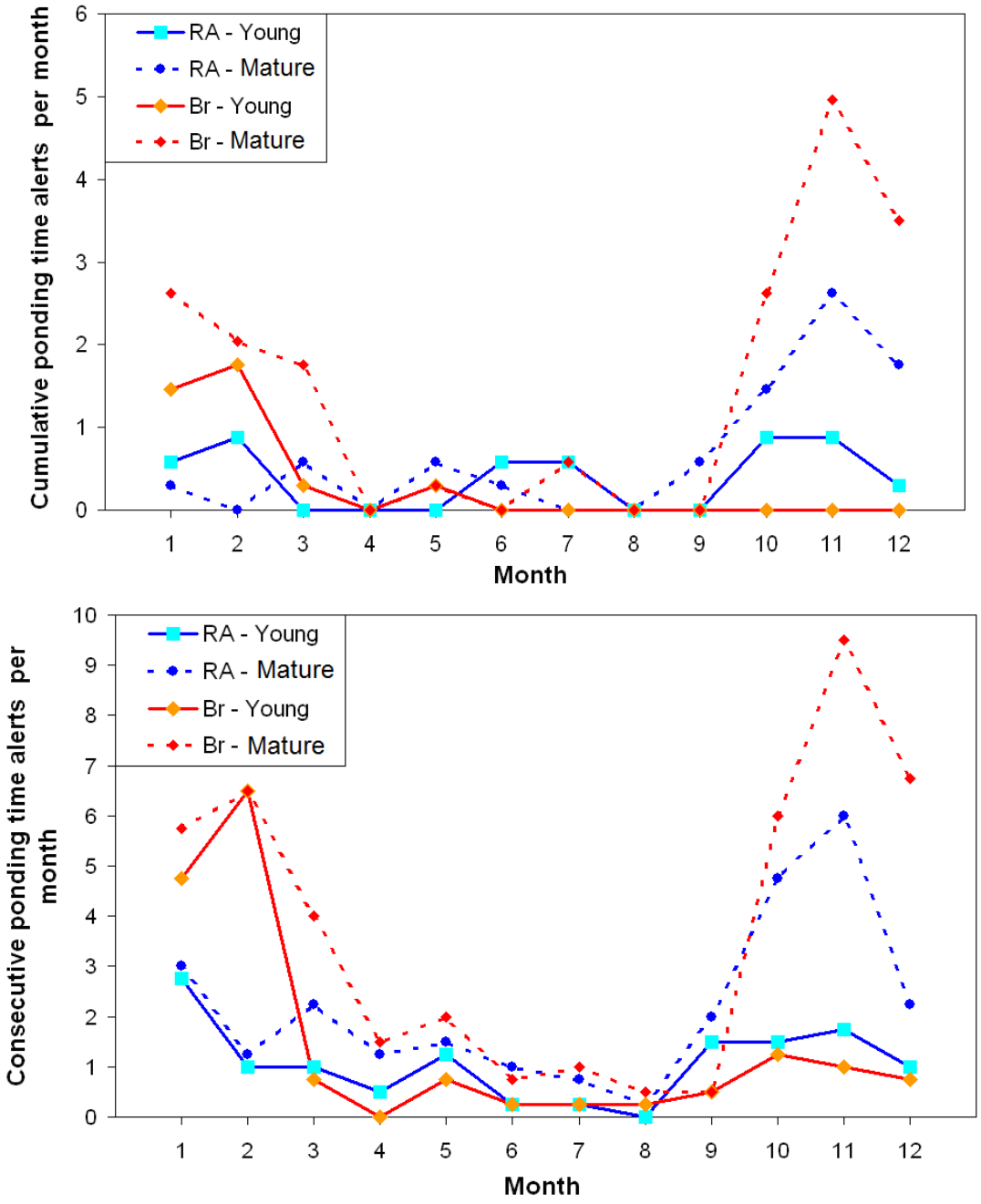

Figure 148: Cumulative (*top*) and consecutive (*bottom*) ponding time alerts distributed over the year, for young and mature VFCW, according to minimum dimensions that respect the limits. Bretagne (Sur 1.5 m^2 p.e, BPH 0.7 m) and Rhône-Alpes (Sur 1.2 m^2 p.e, BPH 0.7 m) climates.

This ponding variation over the season can be translated in terms of bypass frequency (see Figure 149).

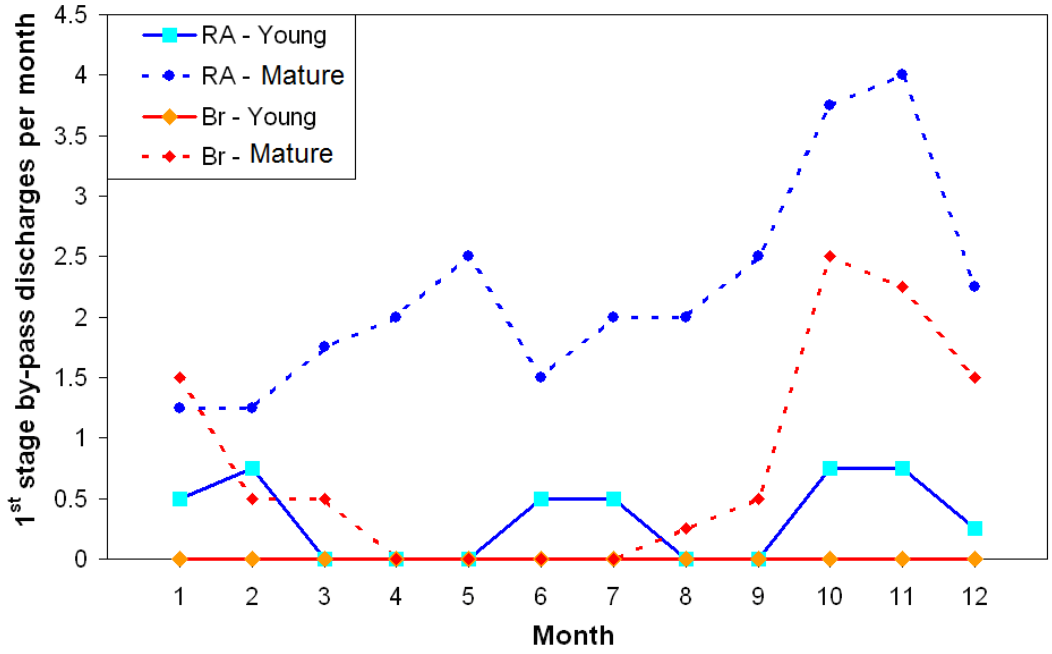

Figure 149: First-stage bypass discharges distributed over the year, for young and mature VFCW, according to the minimum dimensions that respect the limits. Bretagne (Sur 1.5 m²/p.e, BPH 0.7 m) *vs* Rhône-Alpes (Sur 1.2 m²/p.e, BPH 0.7m)

It is difficult to establish a relationship between hydraulic load and ponding time due to the variation of infiltrations rates with season (months) and system age. Table 26 summarizes the characteristics of cumulative ponding time alerts in filter configurations respecting the limits according to climate for young and mature VFCW.

Table 26: Characteristics of cumulative ponding time alerts in filter configurations respecting the limits according to climate and VFCW age (ImC: 30%, slope: 1%)

	Bretagne (1.5 m²/p.e. - 0.7m)				**Rhône-Alpes (1.2 m²/p.e. - 0.7m)**			
	Young filter		*Mature filter*		*Young filter*		*Mature filter*	
Alerts per year	3.8		17.8		2.9		8.2	
	HL ($m.d^{-1}$)	**Daily ponding time (h)**	**HL ($m.d^{-1}$)**	**Daily ponding time (h)**	**HL ($m.d^{-1}$)**	**Daily ponding time (h)**	**HL ($m.d^{-1}$)**	**Daily ponding time (h)**
Max	5.24	21.3	6.59	23.5	31.45	21.7	31.45	23.7
Average	3.10	17.8	2.70	17.7	12.26	18.1	7.31	19.3
Min	1.52	15.8	0.90	15.6	3.87	16	1.76	15.6
SD	1.17	1.83	1.23	2.1	9.11	2.0	6.90	2.4

A HL accepted in the summer season can produce an alert in the winter season, as well as on an old filter (Table 26). For example, for a mature VFCW under a Bretagne climate, the HL that produced an alert was 6.59 $m.d^{-1}$ whereas this same HL did not produce an alert in a young VFCW. Furthermore, cumulative ponding time alerts can be longer on older filters, with maximal values practically covering the entire daytime under both climates.

For consecutive ponding alerts, Table 27 summarizes the characteristics according to climate for young and mature VFCW.

Table 27: Characteristics of consecutive ponding time alerts in filter configurations respecting the limits, according to climate and VFCW age

	Bretagne (1.5 m²/p.e. - 0.7m)		Rhône-Alpes (1.2 m²/p.e. - 0.7m)	
	Young filter	*Mature filter*	*Young filter*	*Mature filter*
Alerts per year	17	44.7	12.7	26.2
	Ponding time (h)	**Ponding time (h)**	**Ponding time (h)**	**Ponding time (h)**
Max	19.5	32.6	26.4	33.9
Average	10.2	11.5	10.4	12.5
Min	7.1	7.1	7.1	7.1
SD	2.9	4.3	3.9	5.3

This table shows that consecutive ponding times are similar under both climate. The maximal consecutive ponding time can exceed the daytime for mature filters under both climates (and young filters under a Rhône-Alpes climate). In these extreme ponding conditions, a more frequent filter rotation during rainfall is recommended as a measure to protect the system, as on Challex plant.

As the concept of "CSO discharge" is not well defined in current regulations, we tried to characterize first-stage bypass discharges in filter configurations respecting the limits according to climate and VFCW age (Table 28).

Table 28: Characteristics of 1st stage by-pass discharges on filter configurations that respect the limits, according to climate and VFCW age*Note: no discharges in the Bretagne-climate young-filter configuration.

	Bretagne (1.5 m²/p.e. - 0.7m)				Rhône-Alpes (1.2 m²/p.e. - 0.7m)			
	Young filter		*Mature filter*		*Young filter*		*Mature filter*	
Discharges per year	0		9.2		4		26.7	
Discharges per day (according to days of discharges)	-		1		1		1.6	
Discharges per year >1h			2.7		2.5		17.7	
	HL ($m.d^{-1}$)	**Discharge duration (h)**	**HL ($m.d^{-1}$)**	**Discharge duration (h)**	**HL ($m.d^{-1}$)**	**Discharge duration (h)**	**HL ($m.d^{-1}$)**	**Discharge duration (h)**
Max	-	-	6.59	5.00	31.45	3.70	31.45	11.30
Average	-	-	3.26	0.96	10.99	1.31	4.65	2.38
Min	-	-	0.41	0.10	1.76	0.20	1.19	0.10
SD	-	-	1.30	0.97	8.29	1.00	4.45	2.18

Table 28 shows that a day with bypass discharges normally features just one discharge, but in the Rhône-Alpes climate and on mature filters, there can be multiple discharges in the same day. Concerning duration, just 35% to 60% of discharges are longer than 1 h. However, again, the regulations are not clear on the definition of a minimal duration that qualifies a discharge. We consequently included all discharges, independently of duration, in the simplified model

in order to provide a more secure configuration. Note that discharge durations are more than two-fold higher under the Rhône-Alpes climate, reaching extreme discharge events lasting a half-day on more mature filters. The high permeability on young filters means higher HLs are needed before a bypass discharge is generated, as shown in Table 28.

6.4. Possible design recommendations

All previous modelling were carried out on a classic feeding period (3.5 days). However, to better protect the filters, it should be possible to reconfigure the feeding periods rotation on a day-to-day basis for dry-weather flows (every 3.5 days) or for hydraulic loads during rain events (every 100 batches) as in the Challex plant. The filter would thus function in a classic way in dry-weather periods and alternate faster during rainfall events. This rapid-switch alternation will protect the filter against long ponding periods and, as shown in section 5.5, enable fast enough recovery after these short rest periods (about 2 days) to maintain high aerobic performances.

Therefore, small community populations looking for a stormwater treatment solution that also enables compliance with the regulatory-set CSO discharge limits can apply a French VFCW to treat both stormwater and dry weather flows. Adopting this solution would mean there is no need to spend resources on a treatment plant exclusively for stormwater or CSO discharges, and no need to separate old sewer systems. According to our modelling results, it appears more useful to manage the rain event discharge by the filter's bypass rather than limiting the inlet water volumes by a CSO structure. In this solution, the first-stage filters play a retention basin role, decreasing the discharges without jeopardizing the filter's biological functioning. Note that first-stage bypass discharges are at minimum treated by solids sedimentation.

The simplified model developed here proved useful for adapting filter design to local context (watershed characteristics and rainfalls). While classical watershed characteristics only need a classically-designed filter (1.2 m²/p.e. and 0.5 m of by-pass height for young filters), the design issue gets more problematic in some unfavourable contexts. Consequently, we now turn to discuss how filter design can deal with negative watershed characteristics, such as :

- Imperviousness coefficient of about 30%
- Low watershed slope (1%)
- No CSO limit
- Combined sewer system

Depending on climate type, the following filter characteristics should be adopted :

- For climates with less frequent but more intense rainfall events, exemplified here under the Rhône-Alpes climate, we can recommend :
    - A minimum filter surface of 1.2 m²/p.e up to 1.5 m²/p.e. for high ImC
    - First-stage bypass height set at a fixed of 0. 7m

  For this type of climate, there are relatively few ponding alerts, but the bypass discharges are the main problem to solve. An increase in bypass height will reduce discharges without compromising filter performances.

- For climates with more frequent but less intense rainfall events, exemplified here under the Bretagne climate, we can recommend :
    - A minimum filter surface of 1.5 m²/p.e
    - First-stage bypass height set at a fixed 0.7 m

  Increasing the filter surface attenuates the hydraulic load on the filter, consequently reducing constant ponding times.

These filter configurations are designed to ensure compliance with the soon-to-be-introduced regulatory limit on days with "CSO" discharge, even for mature VFCWs, without affecting filter treatment performances.

6.5. Short guide for the designer

In order to guide designers as they look to find the filter configuration best adapted to their local situation that complies with the CSO discharge limits without jeopardizing filter functioning, we have produced keynotes on our findings. Only the cases studied here are presented, and consequently this short guide just contains :

- One imperviousness coefficient at 30%
- One watershed slope at 1%
- Two type of climates, Bretagne and Rhône-Alpes

However, as these imperviousness coefficient and slope values represent the most problematic scenario given the local contexts, the filter configurations adapted for this context should provide a secure solution for other scenarios with lower values.

First step, *defining the CSO threshold*

First of all, the CSO threshold has to be defined. As shown in Figure 131, a minimal threshold of 40-fold dry-weather nominal flow is needed in order to stay within the 'regulatory' CSO discharge limits (20 days with CSO discharge per year). To increase the hydraulic acceptance of the filter and use the hydraulic buffer that a filter can produce as it retains water at the top surface, we propose to manage the discharge at the filter surface rather than at the treatment plant inlet. Nevertheless, a CSO is still needed to shield the system from extreme rain events. For that, advise setting a fixed a set CSO to avoid any solid re-suspension at the top surface of the filter. This can be achieved by capping inlet flow at 1.5 m³/h per m² of filter surface, as is done in primary settlement (FNDAE 22, 1998) to ensure solid sedimentation. This value corresponds to 96 and 120 times the average dry-weather flow for a filter surface of 1.2 and 1.5 m²/p.e. respectively.

As the siphon (or pumps) distributes wastewater at a flow rate of 0.5 m/h, it means that higher flows during rain events have to be spread over the filter surface by a channel overflow, as in the Challex plant (see section 3.1.2.1). Consequently, management of the rain event will focus on accepting the flow onto the first stage of filters, using them as water discharge regulators playing at least a sedimentation role.

Second step, *defining the first-stage filter surface and bypass height*

While a young VFCW presents few days with discharges and ponding time alerts, this does not last as the filter matures and ages. This makes it important for design to integrate the impact of sludge deposits on hydraulic permeability over time. Thus, the principal factors to consider for design are :

- Age of filter
  Permeability decreases according to age of VFCW, thus increasing discharges and ponding times.

- Type of climate
  The characteristics of rainfall events influence the hydraulic loads entering the treatment plant, and consequently ponding times and number and volume of discharges.

- First-stage bypass discharges
  Look to stay under a fixed limit of days with CSO discharges.

- Cumulative ponding time alerts
  Look to stay under the pre-set limit (≈ 24 per year) to guarantee good performances.

By addressing these factors, the filter design can be established using the simplified model developed in this work :

- Minimum first-stage surface
  Permits to better decrease hydraulic load on the filter when high loads are received, thus also decreasing ponding times and discharges.
- First-stage filter bypass height
  Principally limits the number of discharges and ponding alerts.

The simplified model makes it possible to test different local contexts. We propose some graphical case studies to illustrate the idea behind the proposed procedure.

- For a VFCW treating rainfall events under a Bretagne-type climate :

  Figure 150 shows cumulative ponding time alerts per year and days with bypass discharges according to first-stage filter surface and bypass height, for young *vs* mature VFCW.

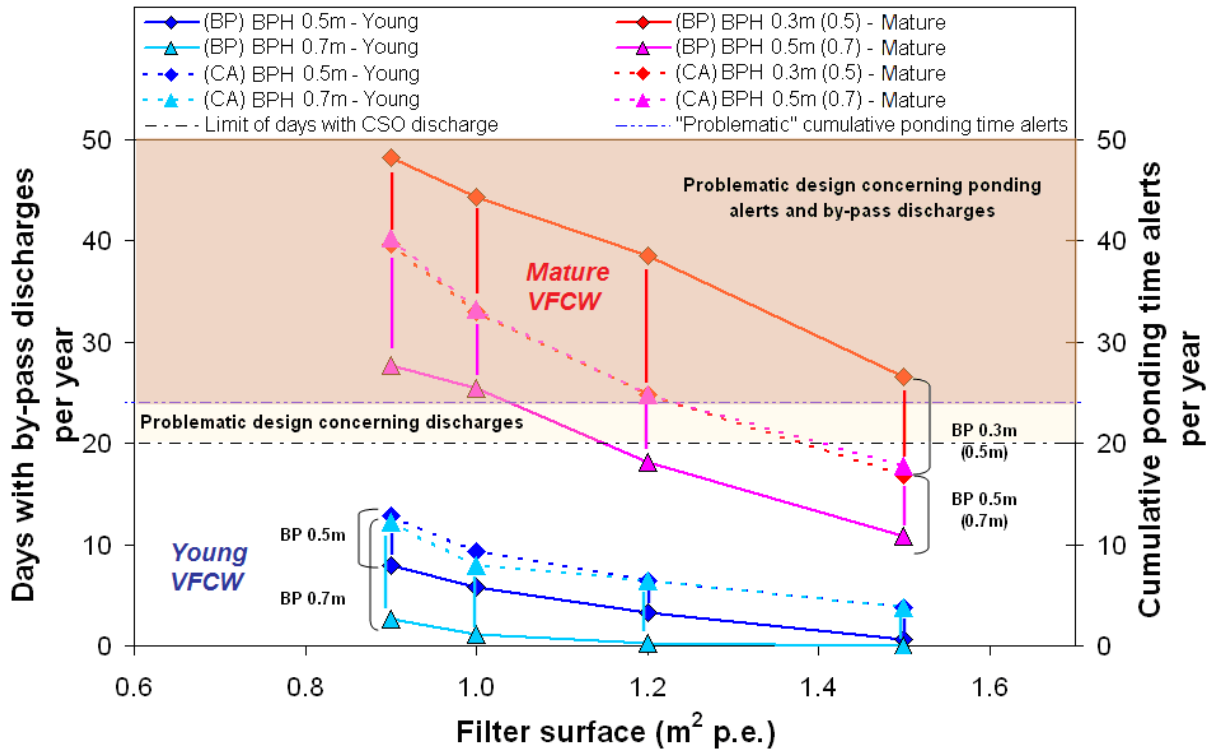

Figure 150: Cumulative ponding time alerts and days with bypass discharges according to first-stage filter surface and bypass height, for young *vs* old VFCW, under a Bretage climate *with (BP) = bypass discharge, (CA)= cumulativee ponding time alerts, and BPH = bypass height

Figure 150 compares number of days with bypass discharges and cumulative ponding time alerts per year, according to filter surface, bypass height and its evolution as the filters mature. It can be seen that low filter surfaces (0.9 and 1 m²/p.e) are not adapted when the filter ages, presenting days of discharges beyond the regulatory limit and cumulative ponding alerts that could be problematic for good filter performance. Thus, the classic filter surface of 1.2 m²/p.e, even with a bypass height of 0.7 m, tends to produce repeating ponding time alerts. The best VFCW solution for this type of climate is the configuration of a 1.5 m²/p.e surface with a 0.7 m bypass height.

- For a VFCW treating rainfall events under a Rhône-Alpes-type climate :

  Figure 151 shows the cumulative ponding time alerts and days with bypass discharges according to first-stage filter surface and bypass height, for young *vs* mature VFCW.

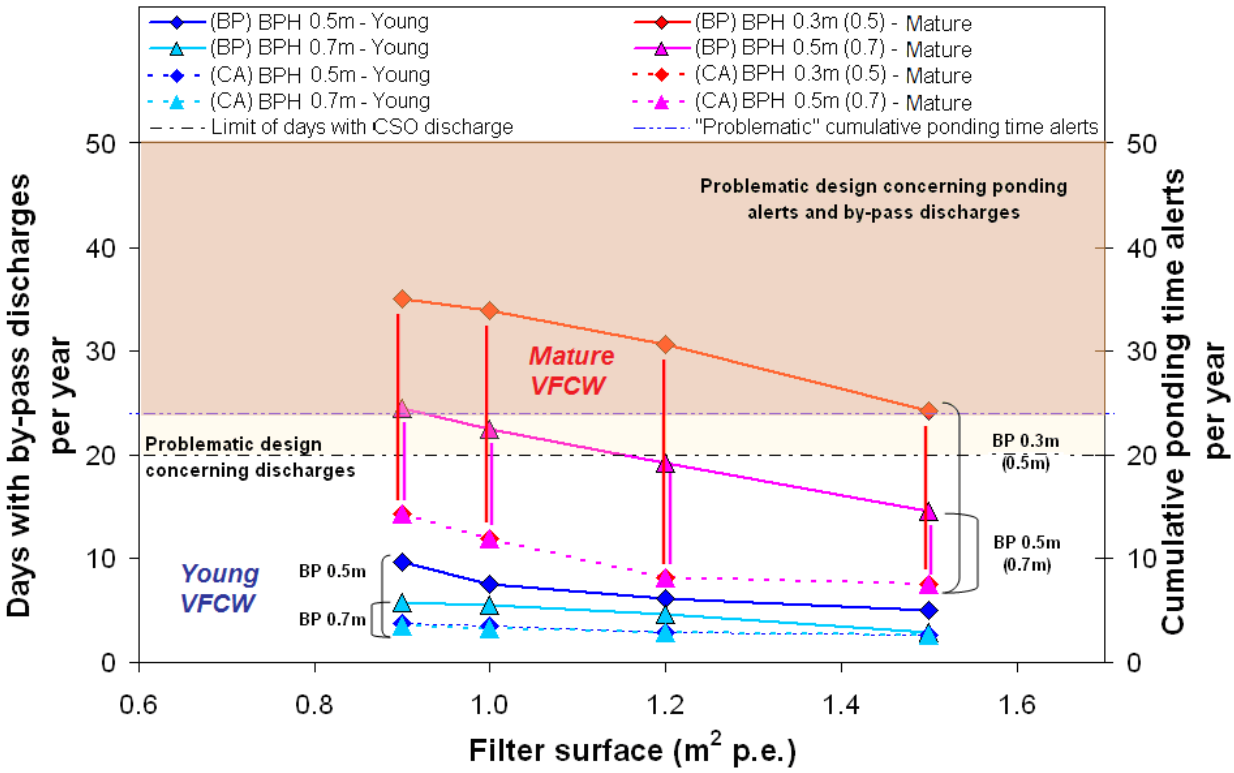

Figure 151: Cumulative ponding time alerts and days with bypass discharges according to first-stage filter surface and bypass height, for young *vs* old VFCW, under a Rhônes-Alpes climate *with (BP) = bypass discharge, (CA)= cumulativee ponding time alerts, and BPH = bypass height

Under a Rhône-Alpes climate, there are fewer ponding time alerts than under a Bretagne climate, producing no problems, even on the mature VFCW. Like in the Bretagne climate, low filter surfaces (0.9 and 1 m²/p.e) are not adapted when the filters age, presenting days of discharges beyond the regulatory limit. In this type of climate, the classic filter surfaces of 1.2 and 1.5 m²/p.e allow to respect the discharges limit, but only when the bypass is set at a height of 0.7 m. Consequently, a filter configuration of a 1.2 m²/p.e surface with a 0.7 m bypass height can be applied and is expected to stay under the discharges limit without compromising filter performances. However, as the number of days with discharges is still close to the limit, a filter surface of 1.5 m²/p.e could be a safer option.

7. Conclusions

7.1. Bibliography

The different designs and uses of VFCWs make it difficult to find any consensus on hydraulic limits in the literature. However, the maximal hydraulic loads applied have been measured in a French system (Molle *et al.* 2006) where the treatment plant (in operation for 9 years) showed no infiltration problems after episodic hydraulic overloads up to 4 $m.day^{-1}$ (>10 times dry-weather HL). Based on these results, a first set of hydraulic limits has been established to 3.5 $m.day^{-1}$ and 1.80 $m.day^{-1}$ for young and mature filters, respectively.

Moreover, the periodicity of rainfall events is just presented in terms of months, and the biological response has not been precisely defined. VFCW hydraulic limitations depend on a host of factors including age of the system, season, sewer characteristics and, of course, climate conditions (the dynamics and duration of storm events). The filter has to be designed not only to accept hydraulic overload but also minimize surface ponding to ensure sufficient oxygen renewal for treatment. Dynamic models thus emerge as valuable tools for describing system hydraulics in response to this high number of influencing factors. Modelling emerges as the key way forward to a better understanding of filter hydraulics and better filter design.

Most numerical models of CW are geared to horizontal flow, and the few projects studying VFCW dynamics mainly rely on mechanistic models. However, while mechanistic models are powerful tools for gaining an in-depth description of on-filter processes, they were originally designed and used for research purposes and are consequently difficult to handle for non-expert users. The choice between detailed description and easy handling will depend on the modelling aims. If the aim is a global design, simplified models offer a good alternative. However, if the number of mechanistic hydraulic models geared to studying VFCW dynamics are limited, the simplified models are extremely reduced, and focused exclusively on CSO treatment. Consequently, there is a pressing need for a large-scale simplified hydraulic VFCW model that, coupled to filter treatment performance data, would be a valuable aid for global design purposes.

7.2. Methods

In addition to assessing the hydraulic limits of a French VFCW, this PhD thesis work focused on developing a simplified hydraulic model of VFCW to guide designers through the process of adapting VFCW systems to treat domestic wastewater in both dry and rain events. We developed a specific methodology to achieve these objectives. First, we worked on a full-scale 2,000-p.e. plant specifically designed to accept rain events and equipped for monitoring. It has been monitored over two years with :

- On-line hydraulic measurements (inlet and outlet flows of each stage, infiltration rates, water content within the media, climate conditions)
- Regular sampling campaigns to assess treatment performances.

- Specific campaigns with on-line pollutant measurements to determine the biological limits under hydraulic overloads

This monitoring effort enabled us to build a simplified hydraulic model that has been fitted on data measurements and compared against a mechanistic model to give more confidence in the results. Moving forward, work on dynamic simulation, mixing sewer simulation and filter simulation made it possible to detail how the VFCW can be adapted to treat rain events. As age of the system is a major driver of hydraulic acceptance, the fitting of the simplified model and the dynamic simulation was also done using previous data collected on a mature filter.

7.3. Large-scale VFCW hydraulics

On a young VFCW like Challex, the high infiltration rates of the first-stage can accept a hydraulic load up to 5.32 $m.d^{-1}$ (15 times the nominal hydraulic load) through rapid filter rotation under extreme HL without inducing bypass discharges. Over the two-year monitoring period, about 51% of treated hydraulic loads were below the nominal load and less than 1% of observed events were 10 times over the nominal hydraulic load (3.48 $m.d^{-1}$).

TDR campaigns highlighted that water distribution onto the filter was not homogenous when the filter is young due to a lack of the deposit layer that improves flow distribution. The net result is that a large fraction of the filter surface stays inactive. Hydraulic load and seasons influence water distribution, which is improved in winter periods due to the lack of reed growth and low infiltration rates. Infiltration rate measurements at Challex plant confirm the mechanical effect of reeds. Winter is the most sensitive period and is liable to deplete oxygen levels in the media. Observations showed that feeding days are ultimately not significant for infiltration rates given the broad variation observed over the seasons.

7.4. Treatment performances

The classical treatment campaigns demonstrate that even on high hydraulic loads up to 2.26 $m.d^{-1}$ (6.5-times the NHL), the entire system did not show any treatment problems. SS and COD removal efficiencies were similar whatever the hydraulic load, despite the high pollutant load variations produced by runoff. This demonstrates the capacity of the system to treat a wide range of hydraulic loads. KN removal was more sensitive to hydraulic load. KN removal performances varied during rainfall events. However, the first stage showed COD, SS and KN outlet concentrations more or less aligned to the total treatment objectives for Challex plant, demonstrating the robustness of the system. The trends of total treatment plant removal rates were 98%, 93% and 91% for SS, COD and KN, respectively. The buffering effect of filter could explain these high removal rates. Efficiency levels of the first and second stages were comparable to those observed in more than 80 different French systems (Molle *et al.* 2005a).

The intensive campaign showed that SS and total COD removal rates increased with feeding day. This is due to the progress of wet filter surface that tends to retain SS retention and a higher contact surface for COD degradation on its particular form. Dissolved COD, KN and NH_4-N removal rates increase as feeding period progresses. This increase of NH_4-N removal

can be linked to two phenomena. First, after one week of rest, nitrification bacteria start to regrow in the first few feeding days, thus driving a gradual increase in nitrification activity. Second, the low level of sludge deposit (2 cm) means that water distribution improves with time. KN removal efficiency improves due to better water distribution as feeding progresses (as was the case with dissolved COD) and higher nitrifying biomass content. Oxygen content within the porous media also evolved over time. In the first few days, the oxygen content is high in almost all the filter and so does not limit the nitrification and organic matter degradation process. However, as water distribution starts to cover the entire filter, oxygen content begins to change and can eventually affect nitrification or organic matter degradation.

High inflow rates substantially dilute the KN arriving at the treatment plant, and consequently NO_x-N at the first-stage outlet is also diluted, following the same trend as inlet KN concentrations. While nitrate outlet concentrations are low during a rain event, they recover to normal concentrations once the rain event stops. This shows that nitrification is not necessarily affected by these HL (up to 3 $m.d^{-1}$ on the same filer). These results are in accordance with Molle *et al.*(2006), demonstrating that the filter can accept hydraulic overloads up to 3 $m.d^{-1}$ (8.7-times NHL) in winter, which is the most hydraulically limiting season, without jeopardizing the on-filter treatment process.

Field trials showed that a faster feeding rotation (each 100 batches on rainfall events) can protect the filter from long ponding periods. The filter showed rapid recovery after the shorter resting period (2 days) caused by this faster feeding rotation, and kept good outlet levels.

The winter events showed more ponding time on filter, consistently with the low infiltration rates specific to this season. Consequently, to ensure an oxygenation period that maintains good aerobic conditions on a VFCW, two ponding time limits were established: (i) a maximal cumulative daily ponding time of 15.5h, which is higher than the 12 h limit proposed by Molle *et al.* (2006); (ii) a maximal consecutive ponding time of 7 h, based on calculations from Woźniak *et al.*(2007) as this limitation has not been reached at the Challex plant. In Challex, during high rain events, the alternation between filters is more frequent and thus limits the consecutive ponding time. These alerts were the link between filter hydraulics and treatment performances used for the long-term modelling.

7.5. Modelling results

The modelling effort made it possible to propose a simplified hydraulic model for French VFCW that has been fitted on 2-year monitoring data on a young filter and spot measurement campaigns on a mature filter. The reliability of this simplified model has been tested by comparison against a mechanistic model (Hydrus-1D). The simplified model can be easily used for designers to adapt filter design to different local contexts. It simulates filter hydraulics in terms of ponding time and first-stage bypass discharges at different periods of the year. The infiltration capacity parameter (*ICP*) of the model evolves according to season in response to reed growth and organic matter degradation patterns. Its use for designing adapted filters has been linked to defined biological alerts (ponding time) that ensure the requisite aerobic conditions within the media.

Moreover, we ran a long-term simulation for two different kinds of rain characteristics (Bretagne region conditions and Rhône-Alpes region conditions) to determine how local

characteristics (sewer characteristics, climate) and filter characteristics shape the ability of the system to accept rain events. It emerged that local context and climate are critical shapers of VFCW performance. A Bretagne-type climate induces longer daily ponding periods than a Rhône-Alpes-type climate. In addition, higher imperviousness coefficients promote higher hydraulic loads arriving at the treatment plant, and consequently longer daily ponding periods. This influence is stronger under a Bretagne climate. Slope has less impact than imperviousness coefficient and climate. Its role was mostly visible in distributing HL arriving at the treatment plant, barely affecting ponding time. However, the flow distribution over time of a high HL strongly influences the number of biological alerts, with more alerts occurring as slope gets lower. Consequently, the most problematic scenario remains a high imperviousness coefficient with low slope under a Bretagne-type climate, demonstrating that the filter is more sensitive to periodicity than intensity of rainfall events.

We then discussed how design can be adapted to limit days with CSO discharges. It appeared that limiting the inlet flow by a CSO structure fails to achieve full compliance with a fixed discharge limit (20 days with discharges per year here), and instead it is better to increase the hydraulic acceptance of the plant and use the hydraulic buffer that a filter can produce as it stores water at the top surface. In this case, discharge is managed at the filter surface, at least allowing particle sedimentation at the top surface. Nevertheless, a CSO is needed to protect the system from extreme rain events. For this purpose, we propose setting a fixed-height CSO to avoid any solid re-suspension at the top surface of the filter, and limiting inlet flow to 1.5 m^3/h per m^2 of filter surface, as is done in primary settlement (FNDAE 22, 1998). This leads to set CSO to 96 and 120-times the average dry-weather flow for a filter surface of 1.2 and 1.5 m^2/p.e., respectively, without jeopardizing biological functioning of the filter. This option will allow discharge only in extreme events that cannot realistically be treated.

Consequently, the proposed approach aims to manage HO at the first-stage step, adapting the size and/or available ponding height (by-pass height) of filters. The HL that cannot be treated will be by-passed, after a sedimentation step, at the maximal ponding height allowed by design. We analysed the impact of design on discharge and ponding alerts under different climates, sewer characteristics and watershed configurations. While increasing the filter surface can decrease the HL, the ponding alerts and the discharges, increase the available ponding height only serve to reduce the discharges. Consequently, designers have to adapt the design as a trade-off between filter surface (that increases footprint and cost) and available ponding height that only impacts discharges. We spotlighted some problematic cases (high imperviousness coefficient, low slope) for both types of climate. Ponding time alerts remained stable from 1.2 m^2/p.e under a Rhône-Alpes climate but continued to decrease with increasing filter surface under a Bretagne climate. High bypass heights also help decrease bypass discharges without increasing the number of dysfunction alerts. We analysed the occurrence and frequency of ponding alerts. Again, type of climate impacted the occurrence of ponding alerts. In Rhône-Alpes climates, alerts are more constant over the year than under the Bretagne climate where winter time is more problematic.

The issue of ageing filters (losing permeability due to the accumulation of organic matter) obviously induces an increase in first-stage bypass discharges and ponding time alerts. On mature filters in Rhône-Alpes and Bretagne climates, compared to a young filter, cumulative ponding time alerts were almost 3 and 4 times higher and consecutive ponding time alerts were 2 and 2.5 times higher, respectively. Looking at first-stage bypass discharges, the difference were more substantial, ranging from 5 to 11 times higher under Rhône-Alpes and Bretagne climates, respectively.

While a filter in a classical watershed can be designed with classical parameters (1.2 m²/p.e. and 0.5 m of available ponding height for young filters), filter design can prove problematic in some unfavourable contexts. Consequently, in an unfavourable context, the simplified model provides designers with useful guidance on choosing design parameters. We presented some proposed designs for a 30% imperviousness coefficient and a 1% slope to comply with a limit of 20 days of discharges per year while still delivering good filter performances. We issued a series of recommendations according to type of climate, as presented below :

- For climates with less frequent but more intense rainfall events, typically a Rhône-Alpes climate, we recommend :
    - A minimum filter surface of 1.2 m²/p.e up to 1.5 m²/p.e. for high *ImC*
    - First-stage available ponding height set at a fixed 0.7 m

  For this type of climate, ponding alerts remain low.

- For climates with more frequent but less intense rainfall events, typically a Bretagne climate, we recommend :
    - A filter surface of 1.5 m²/p.e
    - First-stage available ponding height set at a fixed 0.7 m

  This increase in filter surface reduces hydraulic loads on the filter, consequently also reducing the ponding time.

These filter configurations are expected to stay within the threshold limit of days with “CSO” discharge that could soon be ushered in under regulatory standards, even for old VFCWs, without affecting the filter’s treatment performances.

Thus, the French VFCW is an adapted solution for small populations to treat stormwater and dry-weather flow from a combined sewer system. The VFCW can limit days with CSO discharges to under 20 per year without jeopardizing filter performances, thus eliminating the need to spend community resources on a treatment plant exclusively for stormwater or CSO discharges and eliminating the need for a separate sewer system.

The simplified hydraulic model developed though this research work requires few input data from VFCWs to be fitted (filter inflow and outflow) and can use the most basic local context information (imperviousness coefficient, slope, rainfall time-series). This level of simplicity makes it an easy model–tool for designers to use.

8. Perspectives

The work carried out during this PhD thesis brings new information and tools to guide engineers designing filters to treat both dry-weather and rainfall-event flows, but there are some study limitations to underline to help orient future research.

First, the ponding alerts were determined on a young system that, due to its low organic matter content, allows higher oxygen renewal. Moreover, a consecutive ponding alert threshold has never been reached at the Challex plant, and the threshold used in the simplified model is a calculation drawn from other studies. Consequently, it would be necessary to re-determine these ponding alerts for older filters. A more in-depth study on nitrogen breakdowns and the filter's buffer effect would require continuous monitoring (including continuously measurements of NH_4-N, NO_x-N at the first-stage inlet/outlet and oxygen content in the filter).

The model has been fitted on the little data available for mature treatment plants, which are more sensitive to hydraulic overload. Consequently, it seems necessary to validate the simplified model on a bigger sample of mature VFCWs in order to gain more reliability.

To extend the dimensioning and scaling guide for designers, it would be necessary to include propagation of uncertainties in the proposed design. In the same way, working with different types of climate would make it possible to further adapt design recommendations to different contexts.

All the components of the simplified model (rainfall/flow production, VFCW hydraulic model and discharge/ponding alerts calculation) will need to be reconfigured on a unified tool to give designers the option of obtaining custom-produced results tailored to their own local contexts and climate data.

References

AFNOR (1991). Sols: reconnaissance et essais — Détermination de la masse volumique des particules solides des sols, Méthode du pycnomètre à eau. In: *Norme française NF P 94-054*, Paris.

Aji S., Tavolaro S., Lantz F. and Faraj A. (2003). Contribution of bootstrap techniques to PLS regression: application to the prediction model of gas-oil quality control. *Oil & Gas Science and Technology* 58(5), 599-608.

APHA (2005). *Standard Methods for the Examination of Water & Wastewater*. American Public Health Association.

Arias C. A. and Brix H. (2005). Phosphorus removal in constructed wetlands: Can suitable alternative media be identified? *Water Science & Technology* 51(9), 267-73.

Armstrong W., Armstrong J. and Beckett M. (1990). *Measurement and modelling of oxygent release from roots of Phragmites australis*. Cooper and B.C. Findlater, Pergamon, London.

Avila C., Salas J. J., Martín I., Aragón C. and García J. (2013). Integrated treatment of combined sewer wastewater and stormwater in a hybrid constructed wetland system in southern Spain and its further reuse. *Ecological Engineering* 50, 13-20.

Barko J. W., Gunnison D. and Carpenter S. R. (1991). SEDIMENT INTERACTIONS WITH SUBMERSED MACROPHYTE GROWTH AND COMMUNITY DYNAMICS. *Aquatic Botany* 41(1-3), 41-65.

Beach D. N. H., McCray J. E., Lowe K. S. and Siegrist R. L. (2005). Temporal changes in hydraulic conductivity of sand porous media biofilters during wastewater infiltration due to biomat formation. *Journal of Hydrology* 311(1-4), 230-43.

Binning P. (1994). *Modeling unsaturated zone flow and contaminant transport in the air and water phases.* . Ph.D., Princeton University, Princeton.

Bolomey G. (2006). *Optimisation de sytèmes de filtres plantés à écoulement vertical et d'infiltratio-percolation par analyse de gaz*. M.Sc., Université de Genève, Geneva.

Brix H. (1990). Gas exchange through the soil-atmosphere interphase and through dead culms of Phragmites australis in a constructed reed bed receiving domestic sewage. *Water Research* 24(2), 259-66.

Brix H. (1994a). *Constructed wetlands for municipal wastewater treatment in Europe*. Elsevier Science.

Brix H. (1994b). Functions of macrophytes in constructed wetlands. *Water Science and Technology* 29(4), 71-8.

Brix H. (1997). Do macrophytes play a role in constructed treatment wetlands? . *Water Science & Technology* 35(5), 11-7.

Brix H. and Arias C. A. (2005). The use of vertical flow constructed wetlands for on-site treatment of domestic wastewater: New Danish guidelines. *Ecological Engineering* 25(5), 491-500.

Carman P. C. (1937). Fluid flow through granular beds. *Trans. Inst. Chem. Eng.* 15, 150-66.

Carman P. C. (1956). *Flow of Gases Through Porous Media*, London.

Caselles-Osorio A., Puigagut J., Segú E., Vaello N., Granés F., García D. and García J. (2007). Solids accumulation in six full-scale subsurface flow constructed wetlands. *Water Research* 41(6), 1388-98.

Chapuis R. P. (2004). Predicting the saturated hydraulic conductivity of sand and gravel using effective diameter and void ratio. *Canadian Geotechnical Journal* 41(5), 787-95.

Chazarenc F. and Merlin G. (2005). Influence of surface layer on hydrology and biology of gravel bed vertical flow constructed wetlands. *Water Science and Technology* 51(9), 91-7.

Chocat B. (1997). *Encyclopédie hydrologie urbaine et assainissement*.

Cooper P. (2003). Sizing vertical flow and hybrid constructed wetland systems. In: *First International Seminar on the Use of Aquatic Macrophytes for Wastewater Treatment in Constructed Wetlands,*, Lisbon, Portugal, pp. 195-218.

Cooper P. (2005). The performance of vertical flow constructed wetland systems with special reference to the significance of oxygen transfer and hydraulic loading rates. *Water Science and Technology* 51(9), 81-90.

Cooper P. (2009). What can we learn from old wetlands? Lessons that have been learned and some that may have been forgotten over the past 20 years. *Desalination* 246(1-3), 11-26.

Cooper P. and Green B. (1995). Reed bed treatment systems for sewage treatment in the United Kingdom - The first 10 years' experience. *Water Science and Technology* 32(3), 317-27.

Cooper P., Job G., Green M. B. and Shutes R. (1996). *Reed beds and constructed wetlands for wastewater treatment*. WRc, UK.

Coupe-Canu E. (2005). *Adaptation de la filiére filtres plantés de roseaux aux réseaux unitaires*. Ingenieur ENGEES, Ecole National du Génie de l'Eau et de l'Environnement de Stragbourg, Strasbourg, France.

De Bénédittis J. and Bertrand-Krajewski J. (2006). Measurement of TSS and COD concentrations in wastewater by UV/visible spectrometry. *La Houille Blanche* 4, 136-42.

De Vries J. (1972). Soil filtration of wastewater effluent and the mechanism of pore clogging. *Journal of the Water Pollution Control Federation* 44(4), 565-73.

Desbordes M. (1974). *Réflexions sur les méthodes de calcul des réseaux urbains d'assainissement pluvial*. PhD, Université Montpellier II, Montpellier, France

Drungil C. E. C., Abt K. and Gish T. J. (1989). Soil moisture determination in gravelly soils with time domain reflectometry. *Transactions of the American Society of Agricultural Engineers* 32(1), 177-80.

Durable C. G. a. D. (2011). Le service d'assainissement en France : principales données 2008. In, Chiffres et statistiques p. 8.

FNDAE-22 (1998). Filtres plantés de roseaux adaptées aux petites colectivités. In, Ministère de l'Agriculture et de la Pêche.

Fonder N. and Headley T. (2013). The taxonomy of treatment wetlands: A proposed classification and nomenclature system. *Ecological Engineering* 51, 203-11.

Forquet N. (2009). *Two-phase flow modelling of vertical-flow filters for wastewater treatment*. PhD, ENGEES, Strasbourg.

Forquet N., Wanko A., Mosé R. and Sadowski A. G. (2009). Diphasic modelling of vertical flow filter. *Ecological Engineering* 35(1), 47-56.

Freire F. G., Davies L. C., Vacas A. M., Novais J. M. and Martins-Dias S. (2009). Influence of operating conditions on the degradation kinetics of an azo-dye in a vertical flow constructed wetland using a simple mechanistic model. *Ecological Engineering* 35(10), 1379-86.

García J., Chiva J., Aguirre P., Álvarez E., Sierra J. P. and Mujeriego R. (2004). Hydraulic behaviour of horizontal subsurface flow constructed wetlands with different aspect ratio and granular medium size. *Ecological Engineering* 23(3), 177-87.

Giraldi D., de'Michieli Vitturi M., Zaramella M., Marion A. and Iannelli R. (2009). Hydrodynamics of vertical subsurface flow constructed wetlands: Tracer tests with rhodamine WT and numerical modelling. *Ecological Engineering* 35(2), 265-73.

Giraldi D., de Michieli Vitturi M. and Iannelli R. (2010). FITOVERT: A dynamic numerical model of subsurface vertical flow constructed wetlands. *Environmental Modelling and Software* 25(5), 633-40.

Grant W. D. and Long P. E. (1981). *Environmental microbiology*, Glasgow.

Gromaire M. C., Garnaud S., Saad M. and Chebbo G. (2001). Contribution of different sources to the pollution of wet weather flows in combined sewers. *Water Research* 35(2), 521-33.

Hammer D. A. (1989). Constructed wetlands for wastewater treatment. *Constructed wetlands for wastewater treatment*.

Harouiya N., Prost-Boucle S., Morlay C., Esser D., Ruel S. M. and Molle P. (2011). Performance evaluation of phosphorus removal by apatite in constructed wetlands treating domestic wastewater: column and pilot experiments. *International Journal of Environmental Analytical Chemistry* 91(7-8), 740-52.

Hazen A. (1911). Discussion of "Dams on sand formations" *A.C. Koenig. Transactions of the American Society of Civil Engineers*
73, 199-203.

Heimovaara T. J. (1993). Design of triple-wire time domain reflectometry probes in practice and theory. *Soil Science Society of America Journal* 57(6), 1410-7.

IWA (2000). Constructed Wetlands for Pollution Control: Processes, Performance, Design and Operation.

Iwema A., Raby D., Lesavre J., Boutin C., Dodane P., Liénard A., Molle P., Beck C., Sadowski G., Merlin G., Dap S., Ohresser C., Poulet J., Reeb G., Werckmann M. and Esser D. (2005). *Epuration des eaux ussées doméstiques par filtres plantés de macrophytes: Recommandations techniques pour la conception et la réalisation*. Agence de l'eau Rhône, Méditeranée et Corse.

Jacobsen O. H. and Schjonning P. (1993). A Laboratory Calibration of Time-Domain Reflectometry for Soil-Water Measurement Including Effects of Bulk-Density and Texture. *Journal of Hydrology* 151(2-4), 147-57.

Kadlec R. H. (1999). Chemical, physical and biological cycles in treatment wetlands. *Water Science & Technology* 40(3), 37-44.

Kadlec R. H. (2000). The inadequacy of first-order treatment wetland models. *Ecological Engineering* 15(1-2), 105-19.

Kadlec R. H., Tanner C. C., Hally V. M. and Gibbs M. M. (2005). Nitrogen spiraling in subsurface-flow constructed wetlands: Implications for treatment response. *Ecological Engineering* 25(4), 365-81.

Kadlec R. H. and Wallace S. D. (2009). *Treatment wetlands*, Boca Raton, Florida.

Kayser K. and Kunst S. (2005). Processes in vertical-flow reed beds: nitrification, oxygen transfer and soil clogging. *Water Science & Technology* 51(9), 177-84.

Khatiwada N. R. and Polprasert C. (1999). Assessment of effective specific surface area for free water surface constructed wetlands. *Water Science & Technology* 40(3), 83-9.

Knowles P., Dotro G., Nivala J. and García J. (2011). Clogging in subsurface-flow treatment wetlands: Occurrence and contributing factors. *Ecological Engineering* 37(2), 99-112.

Kozeny J. (1927). Über kapillare Leitung des Wassers im Boden. *Sitzungsber. Akad. Wiss. Wien* 136(2 A), 271-306.

Langergraber G., Fleischmann N. and Hofstädter F. (2003a). A multivariate calibration procedure for UV/VIS spectrometric quantification of organic matter and nitrate in wastewater. *Water Science and Technology* 47(2), 63-71.

Langergraber G., Giraldi D., Mena J., Meyer D., Peña M., Toscano A., Brovelli A. and Korkusuz E. A. (2009). Recent developments in numerical modelling of subsurface flow constructed wetlands. *Science of the Total Environment* 407(13), 3931-43.

Langergraber G., Haberl R., Laber J. and Pressl A. (2003b). Evaluation of substrate clogging processes in vertical flow constructed wetlands. *Water Science and Technology* 48(5), 25-34.

Langergraber G. and Šimůnek J. (2005). Modeling variably saturated water flow and multicomponent reactive transport in constructed wetlands. *Vadose Zone Journal* 4(4), 924-38.

Lee Y. and Bang K. (2000). Characterization of urban stormwater runoff. *Water Research* 34(6), 8.

Liénard A. (1987). Domestic wastewater treatment in tanks with emergent hydrophytes: Latest results of a recent plant in France. *Water Science and Technology* 19(12), 373-5.

Liénard A., Boutin C. and Esser D. (1998). France. In: *Constructed Wetlands for Wastewater Treatment in Europe* Vymazal J BH, Cooper PF, Green MB, Haberl R, (ed.), Backhuys Publishers, Leiden, The Netherlands, pp. 153-67.

Liénard A., Boutin, C. and Esser, D. (1990). Domestic wastewater treatment with emergent hydrophyte beds in France. In: *Constructed Wetlands in Water Pollution Control*, Adv. Wat. Pollut. Control no 11.

Maier U., DeBiase C., Baeder-Bederski O. and Bayer P. (2009). Calibration of hydraulic parameters for large-scale vertical flow constructed wetlands. *Journal of Hydrology* 369(3-4), 260-73.

Malicki M. A., Plagge R. and Roth C. H. (1996). Improving the calibration of dielectric TDR soil moisture determination taking into account the solid soil. *European Journal of Soil Science* 47(3), 357-66.

Małoszewski P., Wachniew P. and Czupryński P. (2006). Study of hydraulic parameters in heterogeneous gravel beds: Constructed wetland in Nowa Słupia (Poland). *Journal of Hydrology* 331(3-4), 630-42.

Marsalek J. (1998). Challenges in urban drainage. In: *Hydroinformatics tools for planning, design, operation and rehabilitation of sewer systems*, Environment NAS (ed.), Kluwer Academic Publishers, Dordrecht/Boston/London,, pp. 1-23.

Marsalek J. and Chocat B. (2002). International Report: Stormwater management. *Water Science and Technology*.

Mays D. C. and Hunt J. R. (2005). Hydrodynamic aspects of particle clogging in porous media. *Environmental Science and Technology* 39(2), 577-84.

McGechan M. B., Moir S. E., Castle K. and Smit I. P. J. (2005a). Modelling oxygen transport in a reedbed-constructed wetland purification system for dilute effluents. *Biosystems Engineering* 91(2), 191-200.

McGechan M. B., Moir S. E., Sym G. and Castle K. (2005b). Estimating inorganic and organic nitrogen transformation rates in a model of a constructed wetland purification system for dilute farm effluents. *Biosystems Engineering* 91(1), 61-75.

Metcalf and Eddy (1998). *Wastewater Engineering, Treatment, Disposal, and Reuse*. McGraw-Hill, New York.

Mevik B. H. and Wehrens R. (2007). The pls package: Principal component and partial least squares regression in R. *Journal of Statistical Software* 18(2), 1-23.

Meyer D., Schmitt T., Woźniak G. R., Sommer T. and Hagen H. (2008). Results of long-term pollution-load simulations of lab-scale constructed wetlands for CSO treatment. In: *11th International Conference on Wetland Systems for Water Pollution Control*, Indore, India, p. 7.

Molle P. (2003). *Filtres plantés de roseaux: Limites hydrauliques et retention du phosphore*. Docteur, Energétique, génie de procédés, Montpellier II, Montpellier, France.
Molle P. (2012). Des végétaux pour traiter les eaux usées. In: *Biofutur* pp. 28-30.
Molle P., Liénard A., Boutin C., Merlin G. and Iwema A. (2005a). How to treat raw sewage with constructed wetlands: an overview of the French systems. *Water Science & Technology* 51(9), 10.
Molle P., Liénard A., Grasmick A. and Iwema A. (2006). Effect of reeds and feeding operations on hydraulic behaviour of vertical flow constructed wetlands under hydraulic overloads. *Water Research* 40(3), 606-12.
Molle P., Liénard A., Grasmick A., Iwema A. and Kabbabi A. (2005b). Apatite as an interesting seed to remove phosphorus from wastewater in constructed wetlands. *Water Science & Technology* 51(9), 193-203.
Molle P., Martin S., Esser D., Besnault S., Morlay C. and Harouiya N. (2011). Phosphorus removal by the use of apatite in constructed wetlands: Design recommendations. *Water Practice and Technology* 6(3).
Molle P., Prost-Boucle S. and Liénard A. (2008). Potential for total nitrogen removal by combining vertical flow and horizontal flow constructed wetlands: A full-scale experiment study. *Ecological Engineering* 34(1), 23-9.
Morvannou A. (2012). *Dynamic modelling of nitrification in vertical flow constructed wetlands.* PhD, Agronomic sciences and biologic engineering speciality, Louvain, Belgium Catholic University of Louvain.
Morvannou A., Forquet N., Vanclooster M. and Molle P. (2012). Which Hydraulic Model To Use In Vertical Flow Constructed Wetlands? In: *13th International Conference on Wetland Systems for Water Pollution Control* IWA (ed.), Perth, Australia, p. 9.
Mualem Y. (1976). New model for predicting hydraulic conductivity fo unsaturated porous-media. *Water Resources Research* 12(3), 513-22.
Musy A. and Soutter M. (1991). *Physique du sol*.
Nguyen L. M. (2000). Organic matter composition, microbial biomass and microbial activity in gravel-bed constructed wetlands treating farm dairy wastewaters. *Ecological Engineering* 16(2), 199-221.
Nivala J., Wallace S., Headley T., Kassa K., Brix H., van Afferden M. and Müller R. Oxygen transfer and consumption in subsurface flow treatment wetlands. *Ecological Engineering*(0).
Paing J. and Voisin J. (2005). Vertical flow constructed wetlands for municipal wastewater and septage treatment in French rural area. *Water Science and Technology* 51(9), 145-55.
Pastor R., Benqlilou C., Paz D., Cardenas G., Espuña A. and Puigjaner L. (2003). Design optimisation of constructed wetlands for wastewater treatment. *Resources, Conservation and Recycling* 37(3), 193-204.
Platzer C. (1999). Design recommendations for subsurface flow constructed wetlands for nitrification and denitrification. *Water Science and Technology* 40(3), 257-63.
Platzer C. and Mauch K. (1997). Soil clogging tin vertical flow reed beds - Mechanisms, parameters, consequences and.....solutions? *Water Science & Technology* 35(5), 175-81.
Prochaska C. A. and Zouboulis A. I. (2006). Removal of phosphates by pilot vertical-flow constructed wetlands using a mixture of sand and dolomite as substrate. *Ecological Engineering* 26(3), 293-303.
Prochaska C. A., Zouboulis A. I. and Eskridge K. M. (2007). Performance of pilot-scale vertical-flow constructed wetlands, as affected by season, substrate, hydraulic load and

frequency of application of simulated urban sewage. *Ecological Engineering* 31(1), 57-66.

Provost C. (2010). *Analyse multiparamétrique dans les eaux usées par sonde spectrométrique UV/Visible : traitement du spectre et limites de la méthode*. Engineer Ecole Nationale Supérieure de Chimie de Paris, Paris.

Richard G., Sillon J. F. and Marloie O. (2001). Comparison of inverse and direct evaporation methods for estimating soil hydraulic properties under different tillage practices. *Soil Science Society of America Journal* 65(1), 215-24.

Rieger L., Langergraber G., Thomann M., Fleischmann N. and Siegrist H. (2004). Spectral in-situ analysis of NO2, NO3, COD, DOC and TSS in the effluent of a WWTP. *Water Science and Technology* 50(11), 143-52.

Ritter A., Hupet F., Muñoz-Carpena R., Lambot S. and Vanclooster M. (2003). Using inverse methods for estimating soil hydraulic properties from field data as an alternative to direct methods. *Agricultural Water Management* 59(2), 77-96.

Ross A., Lipeme-Kouyi G., Fletcher T., Molle P., Chocat B., Calla M., Daly E. and Deletic A. (2011). Hydraulic modelling of constructed reed-bed wetlands for stormwater treatment. In: *12th International Conference on Urban Drainage*, Porto Alegre, Brazi, p. 8.

Rousseau D. P. L., Vanrolleghem P. A. and De Pauw N. (2004). Constructed wetlands in Flanders: a performance analysis. *Ecological Engineering* 23, 151-63.

SAFEGE (2008). Mise à jours du schéma directeur d'assenissaiment In, Challex, p. 30.

Schaap M. G., deLange L. and Heimovaara T. J. (1997). TDR calibration of organic forest floor media. *Soil Technology* 11(2), 205-17.

Schwager A. and Boller M. (1997). Transport phenomena in intermittent filters. *Water Science & Technology* 35(6), 13-20.

Schwartzmann A. (2007). Plan local d'urbanisme de la Commune de Challex. In, p. 59.

SCIRPE (2010). *Realisation d'une station d'epuration à lits plantés de roseaux*.

Šimůnek J., Šejna M., Saito H., Sakai M. and Van Genuchten M. T. (2009). The HYDRUS-1D Software Package for Simulating the One-Dimensional Movement of Water, Heat, and Multiple Solutes in Variably-Saturated Media. In: *Technical manual, version 4.08* PC-Progress (ed.), Prague, Czech Republic p. 332.

Šimůnek J., Šejna M. and Van Genuchten M. T. (2006). The HYDRUS code for simulating the one-dimensional movement of water, heat, and multiple solutes in variably-saturated media. In: *Technical manual, version 1.0* PC-Progress (ed.), Prague, Czech Republic p. 241.

Sorrell B. K. and Boon P. I. (1992). Biogeochemistry of billabong sediments. II. Seasonal variations in methane production. *Freshwater Biology* 27(3), 435-45.

Stackman W. P., Valk G. A. and Horst G. G. (1969). *Determination of soil moisture retention. Sand box apparatus, range pF0 - pF2.7* Wageningen.

Stottmeister U., Wießner A., Kuschk P., Kappelmeyer U., Kästner M., Bederski O., Müller R. A. and Moormann H. (2003). Effects of plants and microorganisms in constructed wetlands for wastewater treatment. *Biotechnology Advances* 22(1-2), 93-117.

Tanner C. C., Sukias J. P. S. and Upsdell M. P. (1998). Organic matter accumulation during maturation of gravel-bed constructed wetlands treating farm dairy wastewaters. *Water Research* 32(10), 3046-54.

Tietz A., Kirschner A., Langergraber G., Sleytr K. and Haberl R. (2007). Characterisation of microbial biocoenosis in vertical subsurface flow constructed wetlands. *Science of the Total Environment* 380(1-3), 163-72.

Tomenko V., Ahmed S. and Popov V. (2007). Modelling constructed wetland treatment system performance. *Ecological Modelling* 205(3-4), 355-64.

Topp G. C., Davis J. L. and Annan A. P. (1980). Electromagnetic determination of soil water content: measurements in coaxial transmission lines. *Water Resources Research* 16(3), 574-82.

Torrens A., Molle P., Boutin C. and Salgot M. (2009). Impact of design and operation variables on the performance of vertical-flow constructed wetlands and intermittent sand filters treating pond effluent. *Water Research* 43(7), 1851-8.

Van Genuchten M. T. (1980). A closed-form equation for predicting the hydraulic conductivity of unsaturated soils. *Soil Science Society of America Journal* 44(5), 892-8.

Vincent J. (2011). *Les lits de séchage de boue plantés de roseaux pour le traitement des boues activées et les matières de vidange : adapter la stratégie de gestion pour optimiser les performances*. PhD, Génie de procédés Université Montpellier II, Montpellier

Vincent J., Forquet N., Molle P. and Wisniewski C. (2012). Mechanical and hydraulic properties of sludge deposit on sludge drying reed beds (SDRBs): Influence of sludge characteristics and loading rates. *Bioresource Technology* 116, 161-9.

Vohla C., Koiv M., Bavor H. J., Chazarenc F. and Mander U. (2011). Filter materials for phosphorus removal from wastewater in treatment wetlands-A review. *Ecological Engineering* 37(1), 70-89.

Vymazal J. (2005). Horizontal sub-surface flow and hybrid constructed wetlands systems for wastewater treatment. *Ecological Engineering* 25(5), 478-90.

Vymazal J. (2007). Removal of nutrients in various types of constructed wetlands. *Science of the Total Environment* 380(1-3), 48-65.

Vymazal J. (2011). Constructed wetlands for wastewater treatment: Five decades of experience. *Environmental Science and Technology* 45(1), 61-9.

Wanko A., Mose R., Carrayrou J. and Sadowski A. G. (2006). Simulation of biodegradation in infiltration seepage - Model development and hydrodynamic calibration. *Water, Air, and Soil Pollution* 177(1-4), 19-43.

Wessolek G., Plagge R., Leij F. J. and Van Genuchten M. T. (1994). Analysing problems in describing field and laboratory measured soil hydraulic properties. . *Geoderma* 64(1-2), 93-110.

Woźniak R., Dittmer U. and Welker A. (2007). Interaction of oxygen concentration and retention of pollutants in vertical flow constructed wetlands for CSO treatment. *Water Science & Technology* 56(3), 31-8.